

Ministry of Education, Science of Ukraine
Odesa National Polytechnic University

**ODES'KYI POLITECHNICHNYI
UNIVERSYTET**

Pratsi

Scientific, science and technology collected
articles

Publication Frequency: 3 issues per year
Established in February 1996

Issue 2(49), 2016

Odesa
2016

Odes'kyi Politechnichniy Universytet. Pratsi: Scientific, science and technology collected articles. — Odesa, 2016. — Issue 2(46). — 128 p. — Language: ENG-UKR.

EDITORIAL BOARD

G.A. Oborsky (Odesa) — chief editor, *S.A. Andronati* (Odesa),
B.I. Basok (Kyiv), *I.I. Bobok* — responsible secretary,
Margaret Beyli (USA, New York), *E.V. Bodyansky* (Kharkiv),
R.A. Boun' (Lviv), *S.M. Vasil'yev* (Russia, Moscow), *A.S. Vereshchaka* (Russia, Moscow),
V.A. Vlasenko (Poland, Opole), *A.S. Garkavenko* (Germany, Kornwestheim),
V.D. Gogounsky (Odesa), *V.T. Grinchenko* (Kyiv), *P. Dasic* (Republic of Serbia, Trstenik),
A.F. Dashchenko (Odesa), *A.V. Yefimov* (Kharkiv), *V.F. Zinchenko* (Odesa),
K.-H. Wehking (Germany, Stuttgart), *A.A. Klyouchnikov* (Kiyiv),
G.V. Kostrova (Odesa) — deputy chief editor, *B.V. Kounshenko* (Odesa),
V.M. Kountsevich (Kyiv), *S.V. Lenkov* (Kyiv), *L.L. Litvinsky* (Kyiv),
L.M. Lyoubchik (Kharkiv), *A.L. Maystrenko* (Kyiv),
M.V. Maksimov (Odesa) — deputy chief editor, *Y.S. Mysak* (Lviv),
V.A. Mokrytsky (Odesa), *I.M. Neklyoudov* (Kharkiv), *V.R. Nikoulshin* (Odesa),
B.S. Prister (Kyiv), *V.I. Slisenko* (Kyiv),
V.A. Strizhalo (Kyiv), *I.M. Tkachenko Górski* (Spain, Valencia),
A.V. Usov (Odesa), *N.M. Fialko* (Kyiv),
H.-E. Schurk (Germany, Augsburg),
S.E. Shcheklein (Russia, Yekaterinburg), *M.A. Yastrebenetsky* (Kharkiv)

Recommended for publication by the Scientific Council
of the Odesa National Polytechnic University,
minutes No. 1, September 6, 2016

Free online access to printed materials at:
<http://www.pratsi.opu.ua>

ISSN 2076-2429 (print)
ISSN 2223-3814 (online)

© — Odesa National Polytechnic University, 2016

Міністерство освіти і науки України
Одеський національний політехнічний університет

Праці
ОДЕСЬКОГО ПОЛІТЕХНІЧНОГО
УНІВЕРСИТЕТУ

Науковий та науково-виробничий
збірник

Виходить три рази на рік
Заснований у лютому 1996 року

Вип. 2(49). 2016

Одеса
2016

Праці Одеського політехнічного університету: Науковий та науково-виробничий збірник. — Одеса, 2016. — Вип. 2(49). — 128 с. — Мова англ., укр.

РЕДАКЦІЙНА РАДА

Г.О. Оборський (Одеса) — головний редактор, *С.А. Андронаті* (Одеса),
Б.І. Басок (Київ), *М. Бейлі* (США, Нью-Йорк),
І.І. Бобок (Одеса) — відповідальний секретар,
Є.В. Бодянський (Харків), *Р.А. Бунь* (Львів), *С.М. Васильєв* (Росія, Москва),
А.С. Верещака (Росія, Москва), *В.О. Власенко* (Польща, Ополе),
О.С. Гаркавенко (Німеччина, Корнвестхайм), *В.Д. Гогунський* (Одеса),
В.Т. Гринченко (Київ), *П. Дашич* (Республіка Сербія, Трстеник),
О.Ф. Дащенко (Одеса), *О.В. Єфімов* (Харків), *В.Ф. Зінченко* (Одеса),
К.-Г. Векінг (Німеччина, Штутгарт), *О.О. Ключников* (Київ),
Г.В. Кострова (Одеса) — заступник головного редактора,
Б.В. Кунієнко (Одеса), *В.М. Кунцевич* (Київ), *С.В. Ленков* (Київ),
Л.Л. Литвинський (Київ), *Л.М. Любчик* (Харків), *А.Л. Майстренко* (Київ),
М.В. Максимов (Одеса) — заступник головного редактора,
Й.С. Мисак (Львів), *В.А. Мокрицький* (Одеса), *І.М. Неклюдов* (Харків),
В.Р. Нікульшин (Одеса), *Б.С. Прістер* (Київ),
В.І. Слієнко (Київ), *В.О. Стрижало* (Київ), *І.М. Ткаченко-Горський* (Іспанія, Валенсія),
А.В. Усов (Одеса), *Н.М. Фіалко* (Київ), *Х.-Е. Шурк* (Німеччина, Аугсбург),
С.Є. Щеклеїн (Росія, Єкатеринбург), *М.О. Ястребенецький* (Харків)

Рекомендується до друку вченою радою
Одеського національного політехнічного університету,
протокол № 1 від 06.09.2016 р.

Комп'ютерна версія опублікованих матеріалів за адресою:
<http://www.pratsi.opu.ua>

ISSN 2076-2429 (print)
ISSN 2223-3814 (online)

© — Одеський національний політехнічний університет, 2016

CONTENTS

MACHINE BUILDING PROCESS METALLURGY MATERIALS SCIENCE

<i>S.O. Koshel, G.V. Koshel.</i> Analysis of fourth-grade flat machines with movable close-cycle formed by the rods and two complex links.....	9
<i>D.V. Mikhaylovskiy, D.M. Matyuschenko.</i> Numerical researches of DGRP-type experimental frames using the finite elements method	14
<i>V.G. Lebedev, A.V. Bespalova, O.P. Dashkovskaya.</i> Regularities of dust formation during stone cutting for construction works	24
<i>Ahmad Rahbar-Ranji.</i> Modal analysis of a box shaped girder by numerical method	31
<i>N.S. Remez, T.A. Osipova.</i> Prediction of strain state of landfill considering soil foundation and angle of slope.....	40

ENERGETICS HEAT ENGINEERING ELECTRICAL ENGINEERING

<i>V.P. Kravchenko, S.V. Surkov, Hussam Ghanem.</i> Modelling and optimization of seawater desalination process using mechanical vapour compression	47
<i>V.G. Ahrameev.</i> Research of the sediment formation intensity at the run-around cooling systems equipment with water cooling towers	56

COMPUTER AND INFORMATION NETWORKS AND SYSTEMS. MANUFACTURING AUTOMATION

<i>A.A. Kobozeva, S.M. Grigorenko.</i> New approach development for solution of cloning results detection problem in lossy saved digital image.....	62
<i>S.A. Nesterenko, J.S. Nesterenko.</i> Costs evaluation methodic of energy efficient computer network reengineering	70
<i>O.V. Kostyrka.</i> Throughput increase of the covert communication channel organized by the stable steganography algorithm using spatial domain of the image	76
<i>V.V. Zorilo, Ye.Yu. Lebedeva, M.O. Kozina, D.S. Belush.</i> Method of photomontage detection under conditions of limitations absence for photos falsification	84

**ELECTRONICS
RADIO ENGINEERING
TELECOMMUNICATION FACILITIES**

I.V. Yatsenko. Improvement of surface layers properties of precision engineering elements of optical ceramics by preliminary electron-beam surfacing 88

FUNDAMENTAL AND APPLIED SCIENCES PROBLEMS

O.B. Kozin, O.B. Papkovskaya, M.O. Kozina. Modelling and solution of contact problem for infinite plate and cross-shaped embedment..... 97

O.A. Mikulich, V.I. Shvab'yuk. Interaction of weak shock waves with rectangular meshes in plate 104

**CHEMISTRY
CHEMICAL ENGINEERING**

M.A. Oliynyk, A.B. Shestozub. Research of calcium oxide hydration in calcium nitrate solutions 111

A.O. Maizelis, B.I. Bairachniy, G.G. Tul'skiy. Formation of the organic-inorganic proton exchange membrane 117

E.O. Mikhailova, V.O. Panasenko, N.B. Markova. Calcium carbonate synthesis with prescribed properties based on liquid waste of soda production..... 122

ЗМІСТ

МАШИНОБУДУВАННЯ ТЕХНОЛОГІЯ МЕТАЛІВ МАТЕРІАЛОЗНАВСТВО

<i>С.О. Кошель, Г.В. Кошель.</i> Аналіз плоских механізмів четвертого класу з рухомим замкненим контуром, утвореним шатунами і двома складними ланками	9
<i>Д.В. Михайловський, Д.М. Матюченко.</i> Чисельні дослідження експериментальних рам типу ДГРП за допомогою методу скінченних елементів	14
<i>В.Г. Лебедев, А.В. Беспалова, О.П. Дашковська.</i> Закономірності пилоутворення при розрізанні каменю для будівельних робіт	24
<i>Ахмад Рахбар-Ранжі.</i> Модальний аналіз коробчастої балки за допомогою чисельних методів.....	31
<i>Н.С. Ремез, Т.А. Осіпова.</i> Прогнозування деформованого стану полігона твердих побутових відходів з врахуванням ґрунтової основи і кута нахилу схилу	40

ЕНЕРГЕТИКА ТЕПЛОТЕХНІКА ЕЛЕКТРОТЕХНІКА

<i>В.П. Кравченко, С.В. Сурков, Хуссам Ганем.</i> Моделювання й оптимізація процесу опріснення морської води в установках з механічним стисненням пари.....	47
<i>В.Г. Ахрамєєв.</i> Дослідження інтенсивності утворення відкладень на обладнанні оборотних систем охолодження з градирнями	56

КОМП'ЮТЕРНІ Й ІНФОРМАЦІЙНІ МЕРЕЖІ І СИСТЕМИ. АВТОМАТИЗАЦІЯ ВИРОБНИЦТВА

<i>А.А. Кобозєва, С.М. Григоренко.</i> Розвиток нового підходу до вирішення питання виявлення результатів клонування в цифровому зображенні, збереженому із втратами.....	62
<i>С.А. Нестеренко, Ю.С. Нестеренко.</i> Методика вартісної оцінки енергоефективного реінжинірингу комп'ютерної мережі	70
<i>О.В. Костицька.</i> Підвищення пропускної спроможності прихованого каналу зв'язку, організованого стійким стеганоалгоритмом, що використовує просторову область зображення.....	76
<i>В.В. Зоріло, О.Ю. Лебедева, М.О. Козіна, Д.С. Бєлуш.</i> Метод виявлення фотомонтажу в умовах відсутності обмежень на використовувані при фальсифікації фотознімки	84

**ЕЛЕКТРОНІКА
РАДІОТЕХНІКА
ЗАСОБИ ТЕЛЕКОМУНІКАЦІЙ**

І.В. Яценко. Покращення властивостей поверхневих шарів елементів точного приладобудування з оптичних керамік шляхом попередньої електронно-променевої обробки їх поверхонь 88

ПРОБЛЕМИ ФУНДАМЕНТАЛЬНИХ І ПРИКЛАДНИХ НАУК

О.Б. Козін, О.Б. Папковська, М.О. Козіна. Моделювання і розв'язання контактної задачі для нескінченної пластини і хрестоподібного включення 97

О.А. Мікуліч, В.І. Шваб'юк. Взаємодія слабких ударних хвиль з прямокутними отворами у пластинці 104

**ХІМІЯ
ХІМТЕХНОЛОГІЯ**

М.А. Олійник, А.Б. Шестозуб. Дослідження процесу гідратації оксиду кальцію в розчинах кальцій нітрату 111

А.О. Майзеліс, Б.І. Байрачний, Г.Г. Тульський. Формування органо-неорганічної протон-обмінної мембрани 117

Є.О. Михайлова, В.О. Панасенко, Н.Б. Маркова. Синтез карбонату кальцію із заданими властивостями на основі рідинних відходів содового виробництва 122

MACHINE BUILDING. PROCESS METALLURGY. MATERIALS SCIENCE

МАШИНОБУДУВАННЯ. ТЕХНОЛОГІЯ МЕТАЛІВ. МАТЕРІАЛОЗНАВСТВО

UDC 621.01

S.O. Koshel, PhD, Assoc.Prof.,

G.V. Koshel, PhD, Assoc.Prof.

Kyiv National University of Technologies and Design, 2 Nemirovich-Danchenko Str., 01011 Kyiv, Ukraine; e-mail: a_koshel@ukr.net

ANALYSIS OF FOURTH-GRADE FLAT MACHINES WITH MOVABLE CLOSE-CYCLE FORMED BY THE RODS AND TWO COMPLEX LINKS

S.O. Koshel, G.V. Koshel. Аналіз плоских механізмів четвертого класу з рухомим замкненим контуром, утвореним шатунами і двома складними ланками. Складні багатоланкові плоскі механізми все частіше застосовуються в технологічному обладнанні легкої промисловості. Відсутність універсального способу кінематичного дослідження таких механізмів зумовлює актуальність робіт з кінематичного аналізу багатоланкових механізмів. **Мета:** Метою роботи є розробка алгоритму кінематичного дослідження швидкостей точок, що співпадають з геометричними центрами кінематичних пар структурної групи четвертого класу третього порядку з рухомим замкненим контуром, утвореним шатунами і двома складними ланками. **Матеріали і методи:** Для досягнення мети дослідження використано графоаналітичний метод кінематичного дослідження. Розробка алгоритму базується на положеннях теорії механізмів і машин про властивість механізмів вищих класів змінювати клас в залежності від умовно обраного іншого можливого початкового механізму, що входить до складу ведених структурних груп ланок механізму, і положеннях теоретичної механіки щодо миттєвого центра швидкостей. **Результати:** Визначено вектори швидкостей точок ланок групи Ассура 4-го класу 3-го порядку складного плоского механізму графоаналітичним методом, в якому умовно змінено початковий механізм, що привело до зменшення класу механізму і дозволило дослідити його. На відміну від відомого методу помилкових положень, який застосовується для дослідження структурних груп 3-го класу, запропонований алгоритм кінематичного аналізу дозволяє дослідити механізми 4-го класу без необхідності перебудовування плану, який був побудований в невизначеному масштабі, з подальшим розрахунком дійсного масштабного параметра виконаної графічної побудови.

Ключові слова: механізм; кінематичне дослідження; вектор швидкості; план швидкостей.

S.O. Koshel, G.V. Koshel. Analysis of fourth-grade flat machines with movable close-cycle formed by the rods and two complex links. Complex multielement mechanisms are increasingly used in the technical equipment of consumer industry. The lack of a universal method of kinematic research of these mechanisms asserts the relevance of work on the kinematic analysis of multielement mechanisms. **Aim:** The aim of this research is to develop an algorithm kinetic research of velocities of the points that coincide with geometric centers kinematic pairs of structure group of the 4th class and 3rd order with movable close-cycle formed by connecting rod and two complex links. **Materials and Methods:** The graphic-analytical method of a kinematic research will be used to achieve the goals of research. Development of an algorithm is based on provisions of the theory of mechanisms and engines about property of high classes mechanisms to change its class depending on another possible initial mechanism chosen conditionally which comes to structure of the conducted structural groups of the mechanism links and provisions of theoretical mechanics relatively to instantaneous center of speeds. **Results:** Velocity vectors of points of Assur group links of the 4th class and 3rd order of the composite flat mechanism are determined by a graphic-analytical method, where the initial mechanism speeds that led to decrease of a class of the mechanism and allowed to investigate it. Unlike the known erroneous statements method which is applied to research the structural groups of the 3rd class, the offered algorithm of the kinematic analysis allows to investigate mechanisms of the 4th class without need to rebuild the plan which was constructed in a uncertain scale, with the subsequent calculation of the real scale parameter of provided plotting of a graph.

Keywords: mechanism, kinematic research, velocity vector, plan of the velocity vectors.

Introduction. Improving of existing technology equipment of light industry and design of new machines connected with efficiency of existing analysis methods for structural group of planar mecha-

DOI 10.15276/opu.2.49.2016.03

© 2016 The Authors. This is an open access article under the CC BY license (<http://creativecommons.org/licenses/by/4.0/>).

nisms links, of which the last composed. The methods of investigation of dyads are the most effective today. Enough known the analyze methods of structural group to which four links enter. They form the 3rd class and 3rd order groups or 4th class and 2nd order groups, on the base of which you can structural synthesize the mechanisms of the relevant class.

On the one hand the structural group with six structural links have used or have significant prospects of application in machinery of technological equipment in light industry, on the other – the appropriateness (effectiveness) of their use is not theoretically justified because there is no known method for their kinematic and dynamic researches. This is due to the variety of structural groups that may be formed by six links and nine kinematic pairs.

Imperfection in methods of analysis of such structural groups is a factor of deterrence of their use in technological equipment.

Last decades significant number of publications devoted to the practical use of planar complex mechanisms, which class is at least four, a well as the questions of theoretical research of structural, kinematic and dynamic parameters.

Application of multilink structural groups in specific mechanisms is protected by patents for utility model [1...3]. The issue of a theoretical analysis of the upper class mechanisms, including mechanisms for light industry equipment, there are several works dedicated [5...9].

Tasks of kinematic research of complex flat mechanisms remain relevant because in each case, according to the class of mechanism, it is necessary to develop a new algorithm which combines several methods of kinematic analysis. Universal way to research of such complex mechanisms of fourth and higher classes does not exist at present time.

The aim of this research is to develop an algorithm kinetic research of velocities of the points that coincide with geometric centers kinematic pairs of structure group of the 4th class and 3rd order with movable close-cycle formed by connecting rod and two complex links.

Materials and Methods. The graphic-analytical method of a kinematic research will be used to achieve the goals of research. Development of an algorithm is based on provisions of the theory of mechanisms and engines about property of high classes mechanisms to change its class depending on another possible initial mechanism chosen conditionally which comes to structure of the conducted structural groups of the mechanism links and provisions of theoretical mechanics relatively to instantaneous center of velocity (ICV).

Let us consider the complex plane joint-lever mechanism of fourth class (Fig. 1).

The initial mechanism (links 0, 1) with Assur group of the 4th class and 3rd order, which includes the set of six links 2...7 ($n = 6$) with nine kinematic pairs of 5th class – A, B, C, D, E, L, K, M, N ($p_5 = 9$) – forming the mechanism of the 4th class with degree of freedom 1 by Chebyshev formula (mechanism with a driving crank):

$$W = 3n - 2p_5 - p_4.$$

Structure formula of the complex mechanism that examines is

$$1^{\text{st}} \text{ class (links 0, 1)} \rightarrow 4^{\text{th}} \text{ class } 3^{\text{rd}} \text{ order (links 2...7)}.$$

The structural feature of the mechanism is the presence of variable form closed circuit, formed by four connecting rods BD, BC, DE, the EC, two of which – BD and EC – located opposite each other and have the form of complex links, forming with other parts three kinematic pairs, but rod 5 bears the four elements of kinematic pairs.

To perform the kinematic analysis of the mechanism using known methods of study of 3rd class complex mechanisms by graphic-analytical method is not possible. This is due to the fact that the connecting rod 2 which is directly connected to the crank 1 on the other side there are two rods 3, 4 attached, and their kinematic parameters and trajectory points are unknown.

Input parameters for kinematic study of the mechanism is the angular velocity of the crank 1 ($\omega_1 = \text{const}, s^{-1}$) and the scale of the length (Kl, m/mm) of the mechanism kinematic scheme.

In [10] it was shown that the mechanisms of the upper classes have a structural property to change (decrease) the class provided by the replacement of primary mechanism for other possible first class mechanism.

If review the set of links 0, 7 as initial, the mechanism takes the form of 3rd class with structure formula

1st class (links 0, 7) → 2nd class 2nd order 1st type (links 5, 6) → 3rd class 3rd order (links 1...4).

If another possible initial mechanism is choose as a first class mechanism such as set of links 0, 6 then general view of the structure formula remains unchanged, and links 5, 7 will form the Assur group of the 2nd class in the formula.

Conventionally on the size and direction we set the angular velocity ω_7 of rocker 7 as a link, which, according to the formula of mechanism structure is the second conventionally possible leading link of the mechanism. On the plan of the mechanism velocity vector draw $\vec{P}l$ vector of any length along perpendicular to the line ML. For definiteness the direction of angular velocity ω_7 we set clockwise. Compose a system of vector equations for determining of point K velocity:

$$\begin{cases} \vec{V}_K = \vec{V}_L + \vec{V}_{K:L} \\ \vec{V}_K = \vec{V}_N + \vec{V}_{K:N} \end{cases} \quad (1)$$

Let solve a system of equations and indicate $\vec{P}k$ vector on the plan. In case of origin of L, K, C, E points to a complex link 5 and according to the theorem of similarity determine the position of points e, c and velocity vectors \vec{V}_E , \vec{V}_C on the plane of velocity.

Note that to simplify the calculations, we can assume that the points L, K, C, E belonging to one link 5, which moves planar. The direction of the velocity vectors of points K, L is given by the kinematic scheme of the mechanism therefore vectors \vec{V}_K , \vec{V}_L directed along perpendiculars to the NK and ML directions respectively.

Based on these conditions we determine the position of the P_5 —ICV of rod 5 as the point of intersection of continued axial lines of NK and ML links.

According to the theorem of determining the velocity points of the body, which has a planar movement we set on the velocity plan the length of one point velocity vector (for example, point L).

The velocity vectors of the other three points are proportional to the distance from them to the point P_5 . Vectors of L, K, C, E points directed perpendicularly to the segments that connecting them with ICV of links 5. In fact, the instantaneous angular velocity of the connecting rod 5 around ICV of this link can be set conventionally.

A further solution is to choose the length of the velocity vector \vec{V}_A of point A such that satisfies the condition of arbitrarily assumed value of the angular velocity of the connecting rod 5. Velocity $\vec{V}_A \perp OA$ directed toward the direction given angular velocity ω_1 of mechanism link 1 and line of possible real a point positions on velocity plan is the line that drawn through the pole P in a direction perpendicular to the crank OA.

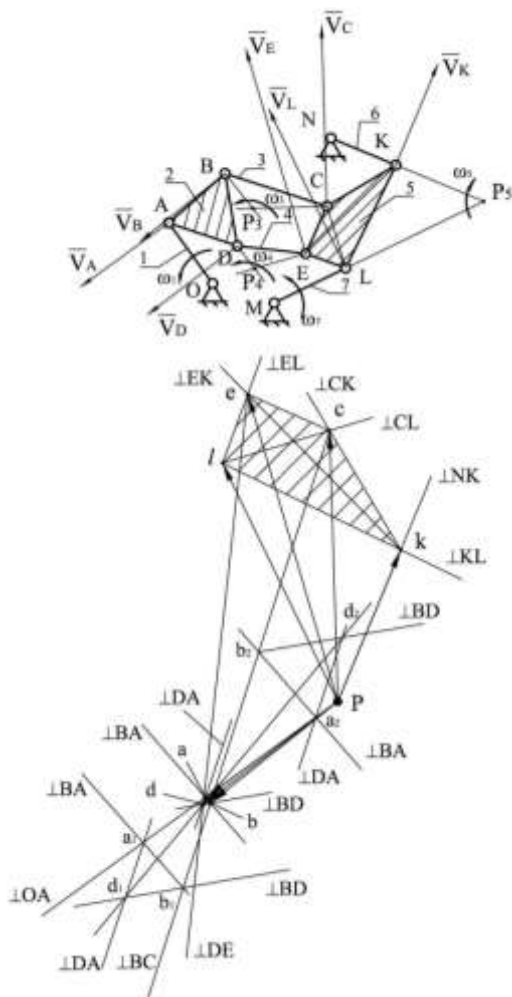


Fig. 1. Kinematic scheme and plan of the velocity vectors of the 4th class mechanism:
0 — riser, 1 — host link, 2...5 — rods,
6, 7 — rocker

Set possible position of the point a_1 and solve a system of vector equations for determining the position of the other two points b_1 and d_1 on the plan:

$$\left\{ \begin{array}{l} \vec{V}_B = \vec{V}_C + \vec{V}_{B;C}; \vec{V}_B = \vec{V}_A + \vec{V}_{B;A}; \\ \vec{V}_D = \vec{V}_A + \vec{V}_{D;A}; \vec{V}_D = \vec{V}_B + \vec{V}_{D;B}, \end{array} \right\} \quad (2)$$

where relative velocities vectors are perpendicular to respective instantaneous radii rotation.

Analysis of the position of the d_1 allows stating that the position of point a_1 on the plan was not chosen correctly, because the received position of the d_1 does not match the vector equation

$$\vec{V}_D = \vec{V}_E + \vec{V}_{D;E}, \quad (3)$$

from which point d_1 must be on the line, which is drawn through the point e perpendicularly to the segment DE.

Similarly, define the position of the d_2 for another arbitrarily selected point a_2 on the plan.

As in the previous case, the position of the a_2 defined incorrectly. The actual position of the point a is on crossing the line, based on the plan according to the vector equation (3) and lines d_1d_2 . Under the system of vector equations (2) determine the actual position of the points b and d on the plan.

Results. The resulting plan of velocity is a graphic display of velocity vectors of linear point velocities of fourth class mechanism, constructed from the pole in an uncertain scale. In case of specified size of links and the angular velocity of the actual leading link to calculate the scale is easy.

Note, that unlike the known erroneous statements method which is applied to research the structural groups of the 3rd class, the offered algorithm of the kinematic analysis allows to investigate mechanisms of the 4th class without need to rebuild the plan which was constructed in a uncertain scale, with the subsequent calculation of the real scale parameter of provided plotting of a graph.

Conclusions. It was developed the algorithm for kinematic study of points velocities of the fourth class mechanism with the mobile closed circuit that formed by connecting rods and two complex links that is based on structural properties of higher class mechanisms to reduce class on the condition of other possible initial mechanism choice.

The proposed algorithm allows perform the kinematic analysis of complex mechanism on condition of graphic scale optimization of research constructions. In addition, the algorithm of kinematic analysis can be recommended for similar studies of complex planar mechanisms fourth and upper classes.

Література

1. Пат. 2201348 Российская Федерация, МПК В30В 1/06, F16Н 21/00. Кривошипно-ползунный механизм пресса / Дворников Л.Т., Чужиков О.С., Стариков С.П.; патентообладатель Сибирский государственный индустриальный университет. — № 2001120227/02; заявл. 18.07.2001; опубл. 27.03.2003.
2. Пат. 2303699 Российская Федерация, МПК E21D 23/00. Секция механизированной крепи / Дворников Л.Т., Князев А.С., Стариков С.П.; патентообладатель Сибирский государственный индустриальный университет. — № 2005141748/03; заявл. 30.12.2005; опубл. 27.07.2007.
3. Пат. 2332260 Российская Федерация, МПК В02С 1/04. Двухщечковая дробильная машина / Дворников Л.Т., Стариков С.П.; патентообладатель Сибирский государственный индустриальный университет. — № 2007101108/03; заявл. 09.01.2007; опубл. 27.08.2008.
4. Кикин, А.Б. Аналитико-оптимизационный синтез шестизвенного механизма с выстоем / А.Б. Кикин, Э.Е. Пейсах // Изв. ВУЗов. Технология текстильной промышленности. — 2008. — № 5(311). — С. 79–83.
5. Дворников, Л.Т. Исследование кинематики и кинестатики плоской шарнирной шестизвенной группы Ассура с четырехугольным замкнутым изменяемым контуром / Л.Т. Дворников, С.П. Стариков // Изв. ВУЗов. Машиностроение. — 2008. — № 4(595). — С. 3–10.
6. Чашников, Д.О. Кинематическое исследование плоского восьмизвенного механизма шестого класса с поступательной парой / Д.О. Чашников, В.В. Горяшин, Л.Т. Дворников // Успехи современного естествознания. — 2011. — № 7. — С. 231–232.

7. Чашников, Д.О. Кинематическое исследование плоского восьмизвенного механизма шестого класса с поступательной парой аналитическим методом / Д.О. Чашников, В.В. Горяшин // Успехи современного естествознания. — 2012. — № 6. — С. 158–159.
8. Гебель, Е.С. Моделирование кинематики механизма игл основовязальной машины / Е.С. Гебель, Е.В. Солонин // Сб. мат. X междунар. науч.-практ. конф. «Теоретические знания в практические дела»: в 2 ч. — Омск, 2009. — Ч. 2. — С. 211–215.
9. Кикин, А.Б. Синтез рычажных механизмов для привода нитераскладчика мотальной машины / А.Б. Кикин // Изв. ВУЗов. Технология текстильной промышленности. — 2005. — № 1(282). — С. 115–119.
10. Кошель, С.О. Структурний аналіз складних плоских механізмів четвертого класу / С.О. Кошель, Г.В. Кошель // Вісник Хмельницького національного університету. Технічні науки. — 2015. — № 1. — С. 72–78.

References

1. Sibirskij Gosudarstvennyj Industrial'nyj Universitet. (2001). *Crank-Slider Mechanism of the Press*. Russian Federation Patent: RU 2201348.
2. Sibirskij Gosudarstvennyj Industrial'nyj Universitet. (2005). *Powered Support Section*. Russian Federation Patent: RU 2303699.
3. Sibirskij Gosudarstvennyj Industrial'nyj Universitet. (2007). *Double Jaw Crushing Machine*. Russian Federation Patent: RU 2332260.
4. Kikin, A.B., & Peisakh, E.E. (2008). Analytical-optimizational synthesis of six-linking mechanism with dwell. *Proceedings of Higher Education Institutions: Textile Industry Technology*, 5, 79–83.
5. Dvornikov, L.T., & Starikov, S.P. (2008). The study of kinematics and kinetostatics of the flat six-section group of Assur of the fourth class with quadrangular closed changeable contour. *Proceedings of Higher Educational Institutions: Machine Building*, 4, 3–10.
6. Chashnikov, D.O., & Garyashin, V.V. (2011). Kinematic study of eight-link planar mechanism of sixth class with sliding pair. *Advances in Current Natural Sciences*, 7, 231–232.
7. Chashnikov, D.O., & Garyashin, V.V. (2012). Kinematic study of eight-link planar mechanism of sixth class with sliding pair by analytical method. *Advances in Current Natural Sciences*, 6, 158–159.
8. Gebel, E.S., & Solonin, E.V. (2009). Kinematics modeling of needle mechanism of warp-knitting machine. In *Proceedings of 10th International Scientific and Practical Conference "Theoretical Knowledge — into Practice"* (Vol. 2, pp. 211–215). Omsk: MSUTM named after K.G. Razumovsky.
9. Kikin, A.B. (2005). Linkages synthesis to drive of the thread spreading for a winding machine. *Proceedings of Higher Education Institutions: Textile Industry Technology*, 1, 115–119.
10. Koshel, S.O., & Koshel, A.V. (2015). Structural analysis of complex flat mechanisms fourth class. *Herald of Khmelnytskyi National University: Technical Sciences*, 221(1), 72–78.

Received April 19, 2016

Accepted June 10, 2016

UDC [624.072.33:624.011.1]:512.547.2

D.V. Mikhaylovskiy¹, PhD, Assoc.Prof.,
D.M. Matyushenko², Senior Engineer¹ Kyiv National University of Construction and Architecture, 31 Povitroflotsky Ave., 03680 Kyiv, Ukraine² JSC "Ukrbudproekt", 5-B Aviakonstruktora Antonova Str., 03031 Kyiv, Ukraine; e-mail: matyushenko.ubp@gmail.com

NUMERICAL RESEARCHES OF DGRP-TYPE EXPERIMENTAL FRAMES USING THE FINITE ELEMENTS METHOD

Д.В. Михайловський, Д.М. Матющенко. Чисельні дослідження експериментальних рам типу ДГРП за допомогою методу скінченних елементів. Одним з найрозповсюдженіших типів конструкцій з клеєної деревини є гнукотесні рами. З використанням гнукотесних рам побудовано багато споруд промислового і громадського призначення. Використання таких рам в спорудах з агресивним середовищем показало велику надійність. Однак, при всіх перевагах гнукотесних рам з клеєної деревини їх застосування стримується недосконалістю методик розрахунку напружень, які базуються на принципах розрахунку конструкцій з цільної деревини. Потреба ретельного дослідження і удосконалення методик розрахунку гнукотесних рам обумовлює актуальність теми дослідження. **Мета:** Метою роботи є чисельні дослідження експериментальних рам з подальшим вдосконаленням методик розрахунку напружень в карнизних вузлах гнукотесних рам. **Матеріали і методи:** Для досягнення поставленої мети було проведено теоретичне визначення переміщень і компонент напруженого стану з використанням експериментальних пружних характеристик матеріалу рам. Клеєна деревина в порівнянні з цільною ближча до трансропної розрахункової схеми симетрії, згідно з якою механічні і пружні властивості будівельного матеріалу в площинах, перпендикулярних напрямку вздовж волокон деревини, є еквівалентними. Для достовірного визначення параметрів напружено-деформованого стану в елементах будь-якого обрису, отримання якісної картини розподілу напружень по всій довжині рами і встановлення закономірності зміни напружень у складі всієї конструкції було використано програмний комплекс ЛІРА-САПР, в якому було реалізовано модель ортогональної анізотропії (ортотропії) в пластинчастих скінченних елементах. **Результати:** Аналізуючи отримані результати, можна зробити висновок, що в цілому збіг між теоретичними і експериментальними даними є задовільним. Можна стверджувати, що деформований стан рам, отриманий теоретичним розрахунком з врахуванням дійсних фізико-механічних характеристик матеріалу експериментальних конструкцій, є достовірним. Враховуючи те, що в стиснуто-згинальних елементах додатковий згинальний момент від нормальної сили є функцією переміщень, можна вважати, що даний розрахунок за методом скінченних елементів в ПК ЛІРА-САПР дозволяє цілком задовільно визначати напруження з врахуванням деформованої схеми рам і анізотропії фізико-механічних властивостей клеєної деревини.

Ключові слова: гнукотесна рама, клеєна деревина, карнизний вузол, напружено-деформований стан, метод скінченних елементів.

D.V. Mikhaylovskiy, D.M. Matyushenko. Numerical researches of DGRP-type experimental frames using the finite elements method. One of the most common types of structures made of glulam beams is curved frames. A lot of industrial plants and public buildings are built using curved frames. The using of such frames in buildings with an aggressive environment showed their great reliability. However, with all the advantages of curved frames with glulam beams their using is constrained by imperfect methods of stress analysis based on the principles of calculation of structures with solid wood. The need for careful study and improvement of methods of calculation of Curved frames determines the relevance of researched topic. **Aim:** The aim of this research is to study the numerous researches of pilot frame for further improving of methods of stress analysis in the cornice nodes of curved frames. **Materials and Methods:** In order to achieve this goal the theoretical displacements and component stress state were determined using experimental elastic characteristics of the frames material. Glulam beams compared to a solid closer to trans tropic design scheme of symmetry, according to which the mechanical and elastic properties of building materials in planes perpendicular direction along the wood fibers are equivalent. For reliable determination of the parameters of the stress-strain state in the elements of any shape, getting of quality pictures of stress distribution along the length of the frame and establishing patterns of changes in stress in the composition of the assembly, the software system LIRA-CAD has been used, where a model of orthogonal anisotropy (orthotropy) in the plate finite elements has been realized. **Results:** Analyzing the results, we can conclude that the overall coincidence between theoretical and experimental data is satisfactory. Arguably, the strained state of frames obtained by theoretical calculation with taking into account the real physical and mechanical characteristics of the experimental designs material is significant. Given that in the compressed-bending elements the additional bending moment on the normal force is a function of movement, we can assume that this calculation method of finite elements in LIRA-CAD allows satisfactorily determine the tension in view of the deformed circuit frames and anisotropy of physical and mechanical properties of glulam beams.

Keywords: curved frame, glulam beams, cornice node, stress-strain state, finite elements method.

Introduction. Experimental studies and operating experience of Curved frames with glulam beams show that cornice node is the most dangerous place in the frame and the reliability of whole construction depends on its reliability[1...4].

DOI 10.15276/opu.2.49.2016.04

© 2016 The Authors. This is an open access article under the CC BY license (<http://creativecommons.org/licenses/by/4.0/>).

To ensure the reliability of frame structures with glulam beams is important to have a precise method of determining of stresses component of the stress state. Given that glulam beams are anisotropic materials, the problem of determining the stress component of the stress state is extremely important.

Existing methods of stress analysis are different and are inaccurate. So important is the development of precision engineering techniques of stress analysis, which will to formulate the conditions under which the compatible component actions of the stress state will be considered.

Methods of stress analysis that occur in the cornice nodes of curved frames somewhat limited. In the regulations [5, 6] and publications [7...9] there are methods and recommendations proposed that can make certain assumptions about the a stressful state in cornice nodes of curved frames, but they do not take into account the distribution of stress in height section of curved frames and questionable about the legality of their use for these types of frames.

The aim of this research is to study the numerous researches of pilot frame for further improving of methods of stress analysis in the cornice nodes of curved frames.

Materials and Methods. To achieve this purpose it was the theoretical determination of displacements and component of stress state (normal stresses along the grain σ_x , normal stresses across the grain σ_y and pinned stress τ_{xy}).

For reliable determination of the parameters of the stress-strain state in the elements of any shape, getting of quality pictures of stress distribution along the length of the frame and establishing patterns of changes in stress in the composition of the assembly, the software system LIRA-CAD has been used, where a model of orthogonal anisotropy (orthotropy) in the plate finite elements has been realized.

Hereinafter, we conducted the comparison of the theoretical results with experimental data of tests of curved frames with rack-cornice block presented in [10].

It was introduced the following elastic constants: elastic modulus parallel to grain E_0 , modulus of elasticity across the grain E_{90} , shear modulus G_0 , Poisson coefficient $\mu_{90,0}$, $\mu_{0,90}$, which are determined on specimens made of glulam beams of frames after the test.

When calculating the problems in mechanics of solid deformable anisotropic body an important issue is the choice of the calculation model of environment that establishes the nature of the change of elastic and strength characteristics depending on the direction of the major axes of symmetry.

Well known that for the glulam beams the scheme of orthogonal anisotropy, i.e. the presence of three mutually perpendicular planes of symmetry [11...13] is characterized. This structural symmetry planes are the planes perpendicular to the normal direction along the fiber, the radial and tangential directions across the fibers.

Properties of solid wood are determined by its structure, namely the different orientation of annual layers for radial and normal directions, as well as the width and content of medullar rays, but building elements of considerable size, made of wood, characterize the random orientation of annual layers in relation to their faces and not coincides with the radial and normal directions.

The structure of glulam beams compared to solid wood is more order. Therefore for building structures made of glulam beams the anisotropy even more strong than for the solid. As glulam beams components made of a set of boards that have a random orientation of the annual layers relative to the side surfaces, the elastic properties of glulam beams in the direction perpendicular to the axis of the glulam package is averaged, and can be considered as equivalent.

So on the basis of [12...15] Considering the above, we can conclude that glulam beams compared to solid wood closer to trans tropic calculation scheme of symmetry, according to which the mechanical and elastic properties of building materials in planes perpendicular direction along the fiber wood are equivalent.

For the calculation of the experiment in program complex LIRA-CAD a model of orthogonal anisotropy (orthotropy) in the plate finite elements was implemented. This allows reliably determine the parameters of the stress-strain state in the elements of any shape, get a good picture of stress distribution along the length of the frame and install the patterns of stress changes in the composition of the whole structure.

When calculating the following assumptions have been taken:

- 1) Work timber is considered only in elastic deformation stage;
- 2) The functional relationship between stresses and deformations described by generalized Hooke's law for transtropic body;
- 3) Stress-strain state is subject to the hypothesis planar sections;
- 4) Finite elements are rectangles.

The geometry of the studied frames described by coordinates of mesh nodes for external and internal contours in the direction of both axes X and Z . Discretization of construction by altitude is automatically performed after setting the number of required partitions.

Calculated loading is applied was concentrated forces acting on objects of research in grid nodes under the partition. Calculated loading and location of meshes performed by scheme of testing installation described in [10] in detail. Calculated cross sections for which tensions were determined shown in Fig. 1.

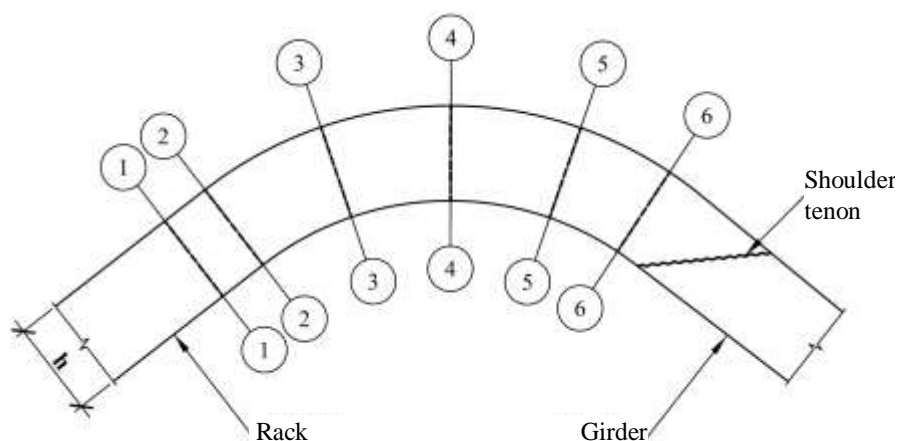


Fig. 1. Scheme of calculation sections location in the cornice node of curved frames DGRP-5 and DGRP-6

The calculation was has been made using plate-type elements 41 and 44 according classifier LIRA-SAPR 2013. Parameters of glue seam are adopted identical to wood and regarded as components of finite elements. The influence of elastic-plastic properties can be ignored. The maximum size of the finite element in calculation schemes of experimental frames is not exceeding 16×8 mm in the front, 8×8 mm in curved part and 8×5 mm in rectilinear girders. Thus, each layer (lamella) has a thickness of 8 mm in rack-cornice block and 5 mm in comb-shaped node.

Finite elements were provided with orthogonally anisotropic (orthotropic) properties with the following experimental parameters: modulus of elasticity along the fiber $E_x = 1407930.683$ t/m², modulus of elasticity across the fibers $E_z = 57675.841$ t/m², Poisson coefficient $\mu_{zx} = 0.429$, $\mu_{xz} = 0.017$, density of wood $\rho = 0.52$ t/m³.

The supporting node of the frames simulated with plate elements of the same type as the frame, but with isotropic properties of materials (steel and plywood). For steel, elastic modulus $E = 2.1 \cdot 10^7$ t/m², Poisson coefficient $\mu = 0.3$, density $\rho = 7.85$ t/m³; for plywood pad, elastic modulus $E = 6 \cdot 10^4$ t/m², Poisson coefficient $\mu = 0.065$, density $\rho = 0.7$ t/m³.

When modeling of supporting and comb-shaped nodes construction the basic principle was to ensure hinge properties to order thereby to approximate the design scheme to testing installation. In supporting node there was supporting metal plate modeled with thickness of 8 mm, which is fixed by the central script on axes Z and Y . There has been modeled the plywood pad of size 80×20 mm, through which thrust (axial load) was passed.

To ensure hinge properties in the comb-shaped node the metal part was modeled, on which the transverse force operates and providing free turn of crossbar ends. In purlins fastening places it was set ties along the axis Y .

For modeling of loading which is applied gradually in increments of 25 % from the estimated loading according to [16] there was used the subsystem of LIRA-CAD program "Installation Plus". This made it possible to take into account the deformation of calculation scheme under the influence of its own weight with equipment placed on it. For conventional zero of displacement there was adopted their own frame weight with test equipment.

One of the criteria of reliability of using the method calculation of curved frames considering geometric nonlinearity is the coincidence of theoretical and experimental forms of curved axes. Shown in Fig. 2 and 3 the curves of deformed frames axes built for two series and show their identity forms. Identified theoretical value of movements for most sections are slightly larger than the experimental.

Comparison of values (Fig. 2 and 3) for frames of series DGRP-5 and DGRP-6 showed that their difference is within 6 %, excluding the reduction of local movements in the area to comb-shaped node for frame of series DGRP-6.

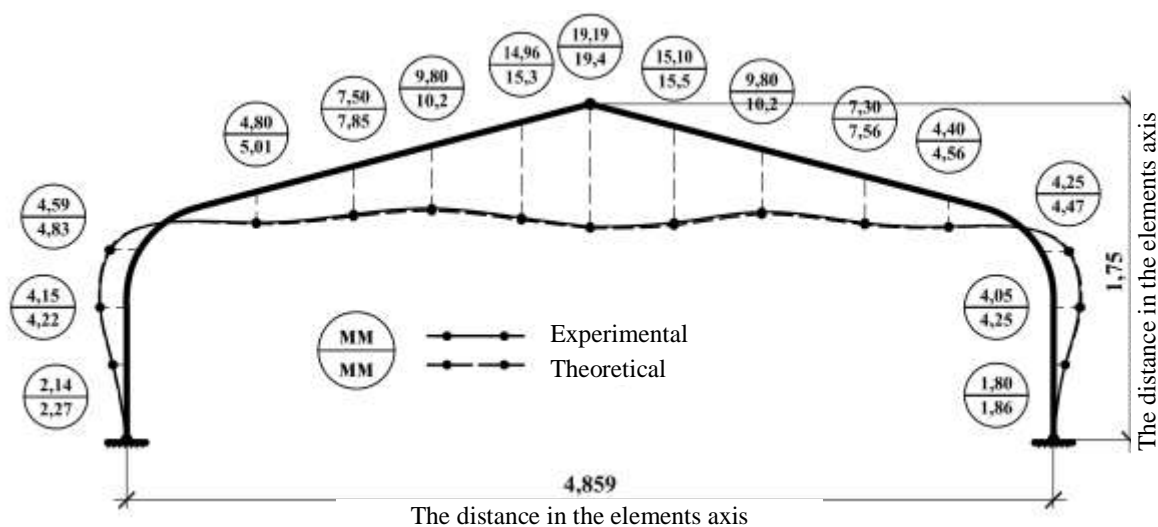


Fig. 2. Theoretical and experimental displacements of frames DGRP-5

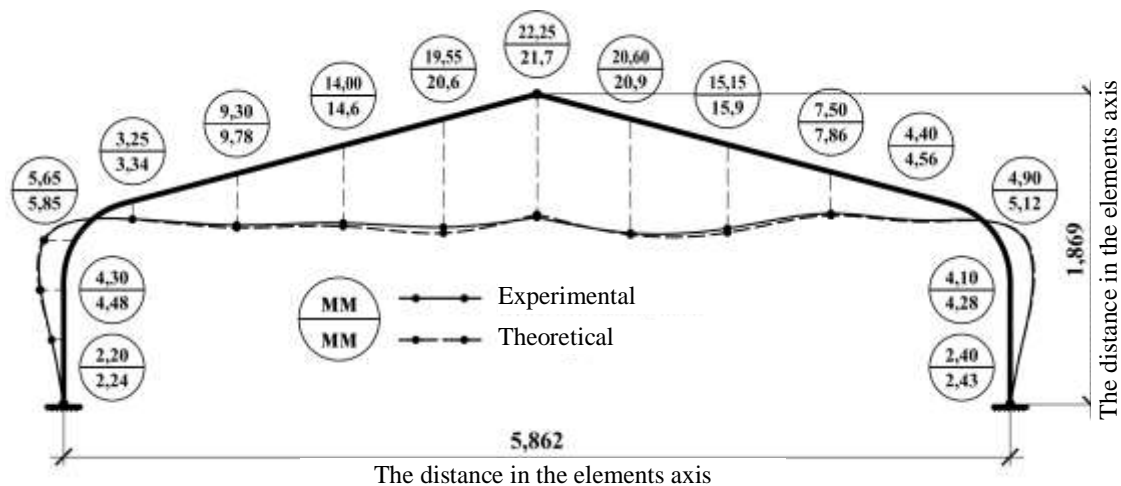


Fig. 3. Theoretical and experimental displacements of frames DGRP-6

Fig. 4...9 show the diagrams of tension σ_x , σ_y and τ_{xy} in curved (5, 4, 3) and transient (6, 2, 1) areas of cornice node.

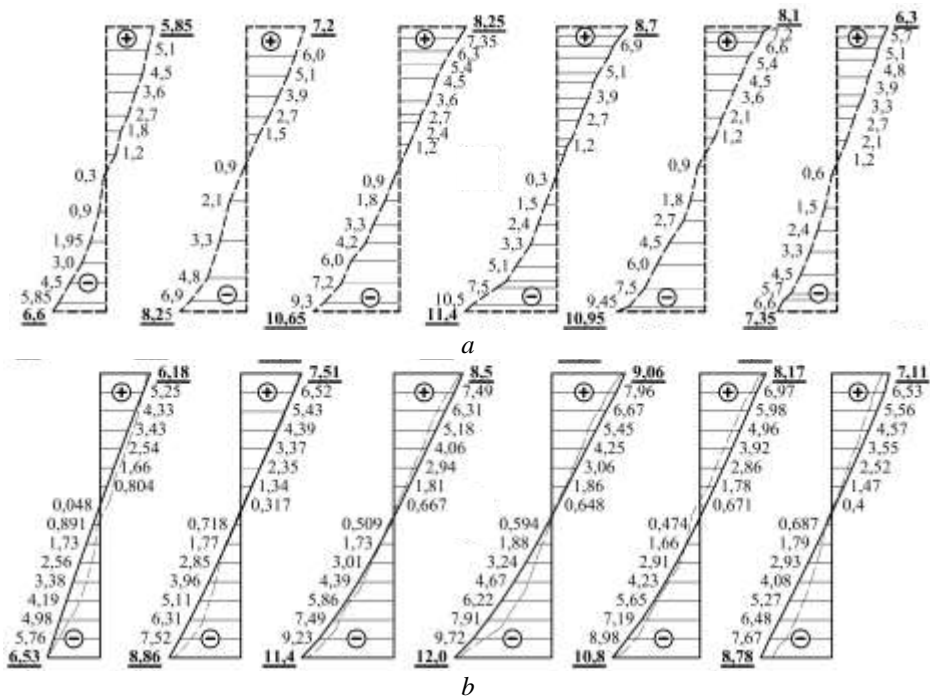


Fig. 4. Diagrams of normal tensions along the fibers σ_x in a rack-cornice block for frame DGRP 5: a — experimental; b — theoretical

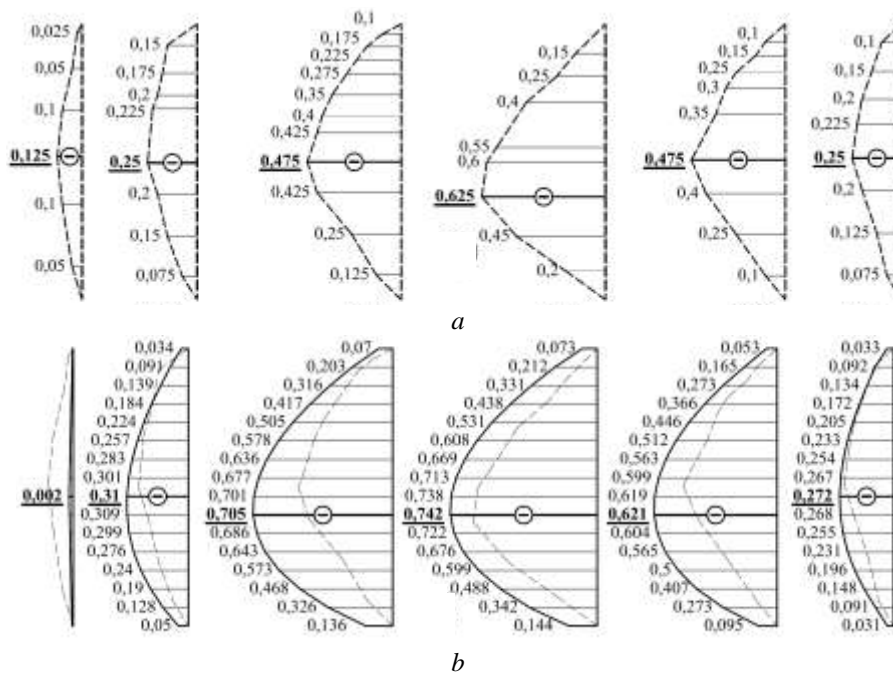


Fig. 5. Diagrams of normal tensions across the fibers σ_y in a rack-cornice block for frame DGRP 5: a — experimental; b — theoretical

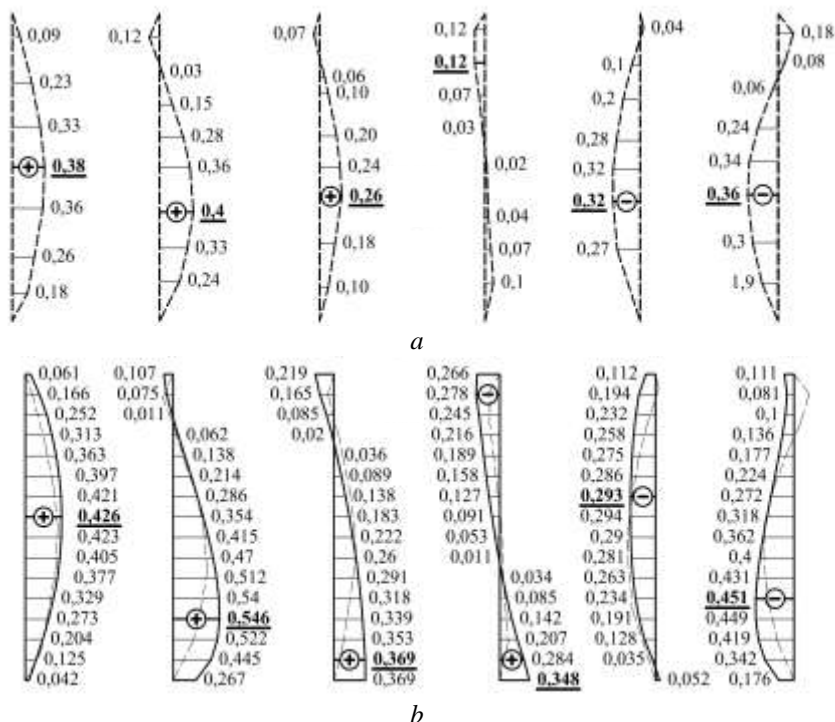


Fig. 6. Diagrams of pinned tension τ_{xy} in a rack-cornice block for frame DGRP-5:
a — experimental; b — theoretical

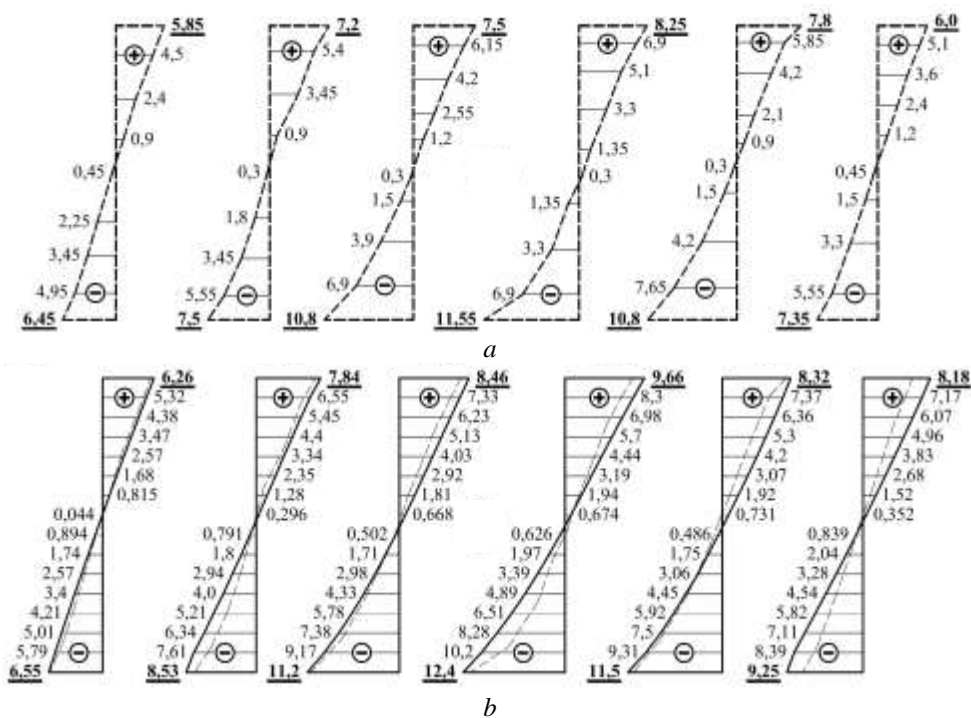


Fig. 7. Diagrams of normal tensions along the fibers σ_x in a rack-cornice block for frame DGRP-6:
a — experimental; b — theoretical

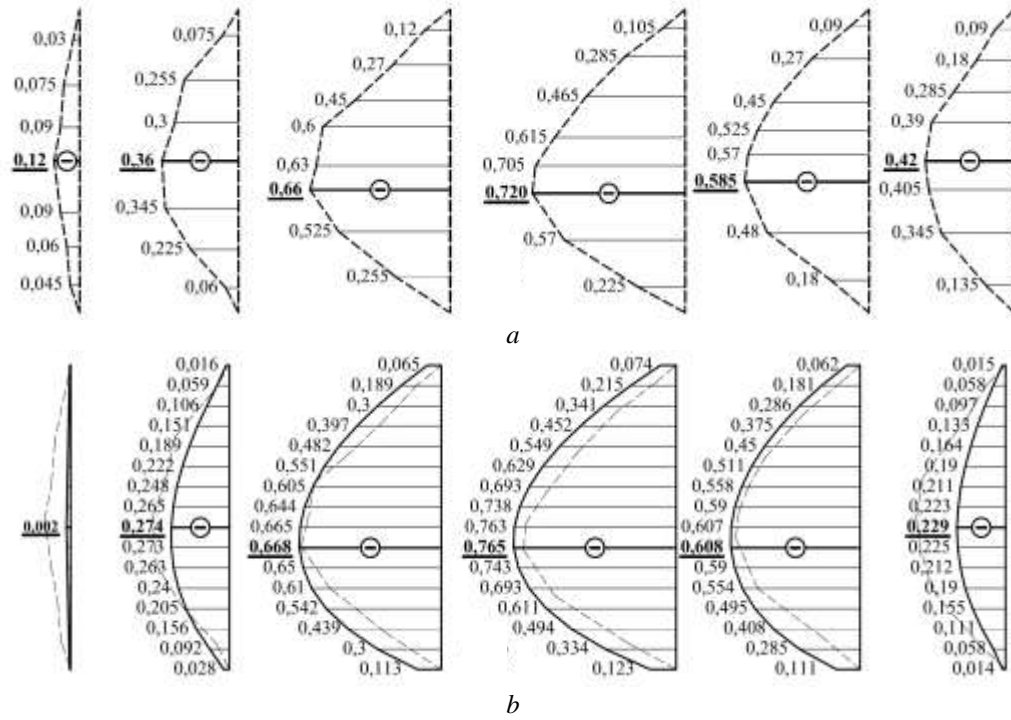


Fig. 8. Diagrams of normal tensions across the fibers σ_y in a rack-cornice block for frame DGRP-6:
a — experimental; b — theoretical

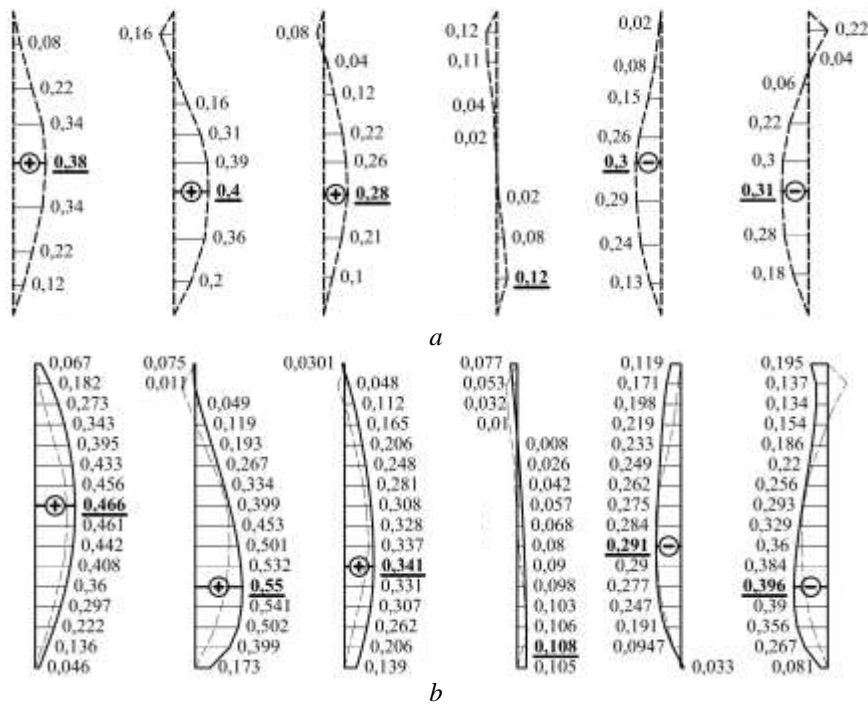


Fig. 9. Diagrams of pinned tensions τ_{xy} in a rack-cornice block for frame DGRP-6:
a — theoretical; b — experimental

The local increase of displacement in frame DGRP-6 in the comb-shaped node may be associated with a possible shift of the supporting and comb-shaped hinges and plywood pad, which perceives the spacing in the supporting node.

Analyzing all the presented results we can conclude that the overall coincidence between theoretical and experimental movement is satisfactory. We can therefore say that the strained state of frames obtained by theoretical calculation and taking into account the real physical and mechanical characteristics of the material experimental designs is significant.

Given that in the compressed-bending elements the additional bending moment from normal force is a function of movement, we can assume that this calculation method of finite elements in program complex LIRA-CAD allows satisfactorily determine the tension in view of the deformed scheme of frames and anisotropy of physical and mechanical properties of glulam beams.

Comparison of theoretical and experimental values of tensions was performed by comparing the stress diagram σ_x , σ_y and τ_{xy} in sections, which were equipped with strain gauges.

In experimental diagrams at some points local breaks were observed that are caused by local wood defects or local defects, come to the surface, cut fibers, loose wood core and other wood structure homogeneities.

Comparison of theoretical and experimental curves (Fig. 4...9) distribution of all three components of plane stressed state both in length and height section indicates that they are close enough.

The magnitude of the theoretical values σ_x were slightly higher experimental. On the stretched edge a difference is 1...17 %, and compressed — 1...14 %. At points in height section also were observed some differences (mainly in the compressed area of curved areas) not exceeding 0.17 h , where h is height section.

From the stress analysis the most intense stress fibers boundary zone section, compressed and stretched zone are identified. Theoretical value σ_y slightly higher the experimental also. The difference between them is 1...19 %, the biggest difference is observed in transitional areas of cornice node that can be attributed to strong heterogeneity and anisotropy of physical and mechanical properties of wood.

As for tangential stresses τ_{xy} the theoretical data exceeding over the experimental within 5...20% also and only in some points of section 1, 2, 4, where diagrams are alternating in nature preferably, the experimental values are increasing compared to theoretical. It should be noted that the heterogeneity structure of the adhesive package significantly affects on difference of experimental data from theoretical as well as that the angle of displacement of glulam beams γ_{xy} is variable, depending on the degree of fluctuations in the values and ε_0 and ε_{90} .

Particular attention attracts the fact that malfunctioning of supporting hinge placement and plywood pad in experimental frames that perceive and vertical anchors effort affect on the magnitude of stress significantly.

Conclusions. Analyzing the results of a comparison of experimental and theoretical data we noted that in general, in the examined constructions full quality compliance experimental and theoretical pictures of stress strain state is observed.

This allow to apply the new design principles [17] of glulam beams structures, the main of which is the principle of a precise definition of stress along the grain, across the grain and tangents in view of anisotropy of physical and mechanical properties of materials and joint action of all existing stresses in a dangerous place. This approach, according to the authors, will ensure reliability and safety of curved frames in general as a form of building structures.

Література

1. Богданова, Е.Н. Анализ причин обрушения зданий и сооружений методы усиления конструкций: обзор.-аналит. докл. / Е.Н. Богданова. — М.: ВНИИТПИ, 2004. — 96 с.

2. Matiuschenko, D.M. Experimental and numerical investigations of glulam frames of glued wood / D.M. Matiuschenko // Чернігівський науковий часопис. Серія 2, Техніка і природа. — 2012. — № 1(3). — С. 92–99.
3. Кліменко, В.З. Вітчизняний досвід впровадження в капітальному будівництві конструкцій з клеєної деревини. Здобутки і проблеми / В.З. Кліменко // Будівництво України. — 2009. — № 5. — С. 17–21.
4. Михайловський, Д.М. Напружений стан гнукоткесених рам з врахуванням анізотропії фізико-механічних властивостей клеєної деревини / Д.В. Михайловський, Д.М. Матющенко // Строительство, материаловедение, машиностроение. — 2015. — Вып. 81. — С. 124–129.
5. ДБН В.2.6-161:2010. Конструкції будинків і споруд. Дерев'яні конструкції. Основні положення. — Чинний від 2011-09-01. — К.: Мінрегіонбуд України, 2011. — 102 с.
6. EN 1995-1-1:2004. Eurocode 5: Design of timber structures — Part 1-1: General — Common rules and rules for buildings. — Approved: April 16, 2004. — Brussels: European Committee for Standardization, 2004. — 121 p.
7. Найчук, А.Я. Некоторые особенности расчета клееных деревянных конструкций / А.Я. Найчук, Е.Н. Серов, И.Ф. Захаркевич // Сб. науч. тр. Междунар. симпозиума «Современные металлические и деревянные конструкции (нормирование, проектирование и строительство)», 15–18 июня 2009 г., Брест, Беларусь. — Брест: ОАО «Брестская типография», 2009. — С. 205–211.
8. Ormarsson, S. Moisture-induced stresses in glulam frames / S. Ormarsson, Ó.V. Gíslason // European Journal of Wood and Wood Products. — 2016. — Vol. 74, Issue 3. — PP. 307–318.
9. Study of stress distribution and stress concentration factor in notched wood pieces with cohesive surfaces / J.R. Aira, T. Descamps, L. Van Parys, L. Léoskool // European Journal of Wood and Wood Products. — 2015. — Vol. 73, Issue 3. — PP. 325–334.
10. Проектирование конструкций из дерева и пластмасс / С.В. Поветкин, А.А. Сморгчов, В.А. Кабанов, С.Ю. Табунов. — Курск: КПИ, 1993. — 93 с.
11. Smardzewski, J. Furniture design / J. Smardzewski. — Cham, Switzerland: Springer, 2015. — 649 p.
12. Ашкенази, Е.К. Анизотропия древесины и древесных материалов / Е.К. Ашкенази. — М.: Лесная промышленность, 1978. — 224 с.
13. Wood composites / ed. by M.P. Ansell. — Cambridge: Woodhead Publishing, 2015. — 437 p.
14. Ашкенази, Е.К. Анизотропия конструкционных материалов / Е.К. Ашкенази, Э.В. Ганов. — 2-е изд., перераб. и доп. — Л.: Машиностроение, 1980. — 248 с.
15. Светозарова, Е.И. Определение упругих констант клееной древесины / Е.И. Светозарова, А.В. Хапин // Изв. ВУЗов. Лесной журнал. — 1982. — № 3. — С. 63–66.
16. ГОСТ 16483.29-73. Древесина. Метод определения коэффициентов поперечной деформации. — Введ. 01.01.1975. — М.: Изд-во стандартов, 1974. — 7 с.
17. Проектирование современных конструкций из клееной древесины на принципах новой концепции / В.З. Клименко, А.Я. Найчук, В.В. Фурсов, Д.В. Михайловский. — К.: Вид-во «Сталь», 2010. — 24 с.

References

1. Bogdanova, E.N. (2004). *Analysis of the Causes of Building Collapse. Reinforcing Construction Methods* (Analytical Report). Moscow: VNIINTPI.
2. Matiuschenko, D.M. Experimental and numerical investigations of glulam frames of glued wood. *Scientific e-Journal of Chernihiv State Institute of Economics and Management. Series 2, Technique and Nature*, 1, 92–99.
3. Klimenko, V.Z. (2009). The domestic experience of implementing the plywood structures into capital construction. Achievements and Problems. *Budivnytstvo Ukrainy*, 5, 17–21.
4. Mikhaylovskiy, D.V., & Matyushchenko, D.N. (2015). Stress state bent frames, taking into account the anisotropy of the physical and mechanical properties of laminated wood. *Construction, Materials Science, Mechanical Engineering*, 81, 124–129.
5. SE “State Research Institute of Building Constructions”. (2011). *The constructions of buildings and structures. Design of timber structures. Common rules* (DBN V.2.6-161:2010). Kyiv: Ministry for Regional Development, Building and Housing of Ukraine.
6. European Committee for Standardization. (2004). *Eurocode 5: Design of Timber Structures*. Brussels: BSI.

7. Naichuk, A.Ya., Serov, E.N., & Zakharevich, I.F. (2009). Some features of the calculation of glued wooden structures. In *Proceedings of the International Symposium "Modern Metal and Wooden Structures: Standardization, Design, and Construction"* (pp. 205–211). Brest: JSC "Brest Typography".
8. Ormarsson, S., & Gislason, Ó.V. (2016). Moisture-induced stresses in glulam frames. *European Journal of Wood and Wood Products*, 74(3), 307–318. DOI:10.1007/s00107-016-1006-5
9. Aira, J.R., Descamps, T., Van Parys, L., & Léoskool, L. (2015). Study of stress distribution and stress concentration factor in notched wood pieces with cohesive surfaces. *European Journal of Wood and Wood Products*, 73(3), 325–334. DOI:10.1007/s00107-015-0891-3
10. Povetkin, S.V., Smorchkov, A.A., Kabanov, V.A., & Tabunov, S.Yu. (1993). *Designing the Constructions of Wood and Plastic*. Kursk: KPI.
11. Smardzewski, J. (2015). *Furniture Design*. Cham, Switzerland: Springer.
12. Ashkenazi, E.K. (1978). *Anisotropy of Timber and Wood-Based Materials*. Moscow: Les. Prom.
13. Ansell, M.P. (Ed.). (2015). *Wood Composites*. Cambridge: Woodhead Publishing.
14. Ashkenazi, E.K., & Ganov, E.V. *Anisotropy of Construction Materials* (2nd Ed.). Leningrad: Mashinostroenie.
15. Svetozarova, E.I., & Khapin, A.V. (1982). Calculation of the elastic constants of glued wooden structures. *Bulletin of Higher Educational Institutions: Lesnoy Zhurnal*, 3, 63–66.
16. Ministry of Forest Industry of the USSR. (1974). *Wood. Method for determination of factors of cross-sectional deformation* (GOST 16483.29-73). Moscow: Standards Publishing House.
17. Klimenko, V.Z., Naichuk, A.Ya., Fursov, V.V., & Mikhaylovskiy, D.V. (2010). *Designing the Modern Constructions of Plywood Based on a New Concept*. Kyiv: Stal'.

Received May 4, 2016

Accepted June 21, 2016

UDC [621.91:624.12]+628.511.123

V.G. Lebedev¹, DSc, Prof.,A.V. Bespalova², PhD, Assoc.Prof.,O.P. Dashkovskaya², PhD, Assoc.Prof.¹ Odessa National Polytechnic University, 1 Shevchenko Ave., 65044 Odessa, Ukraine; e-mail: wlebedev29@rambler.ru² Odessa State Academy of Civil Engineering and Architecture, 1 Koval'ska Str., 65029 Odessa, Ukraine

REGULARITIES OF DUST FORMATION DURING STONE CUTTING FOR CONSTRUCTION WORKS

В.Г. Лебедєв, А.В. Беспалова, О.П. Дашковська. **Закономірності пилоутворення при розрізанні каменю для будівельних робіт.** При різанні каменю виділяється велика кількість пилу, яка є сумішшю дрібних, здебільшого гострих, мінеральних частинок. Дрібний сухий пил при попаданні в дихальні шляхи викликає в органах ті ж патологічні зміни, що є наслідком проникнення в них гострих і твердих частинок. Незважаючи на важливість зазначеної проблеми, практично не розглянутими залишаються питання генерації пилу при різних робочих процесах і його розподіл по фракціях, від чого залежить час перебування пилу в повітрі і його негативний вплив на людину. **Мета:** Метою роботи є дослідження процесу пилоутворення при розрізанні каменю і закономірностей розподілу пилу по фракціях, а також визначення кількісних показників процесу пилоутворення з метою вдосконалення виробничого обладнання, індивідуальних і колективних засобів захисту персоналу. **Матеріали і методи:** Безліч видів різання можна умовно поділити на дві групи — різання «всуху» і різання з використанням мастильно-охолоджувальної рідини. Пил при різанні «всуху» являє собою сукупність мікростружок, які зрізаються абразивними зернами. Розміри таких стружок досить невеликі: від долей мікрметра до декількох мікрметрів. Таким чином, розміри стружок обумовлюють можливість створення пилової суспензії, швидкість осідання якої мала, і яка в робочому просторі знаходиться у великих концентраціях. **Результати:** В результаті проведеного дослідження було отримано такі характеристичні залежності: залежність часу осідання пилу від розміру пилинок, розмірів пилинок від хвилинної подачі і зернистості круга, питомої кількості пилинок від номера зернистості абразивного круга і температури пилинок від подачі на оберт круга. Показано, що розподіл стружок (пилинок) за розмірами підпорядковується нормальному закону. Розміри стружок при розрізанні знаходяться в діапазоні 0,4...6 мкм. Так утворюється пилова суспензія, час осідання частинок якої досягає декількох годин, що створює значні хвилинні концентрації пилу — в межах $0,28 \cdot 10^8 \dots 1,68 \cdot 10^8$ одиниць/м³.

Ключові слова: розрізувальний круг, величина зерна, швидкість різання, величина мікростружки.

V.G. Lebedev, A.V. Bespalova, O.P. Dashkovskaya. **Regularities of dust formation during stone cutting for construction works.** When cutting stone, a large amount of dust release, which is a mixture of small, mostly sharp, mineral particles. Shallow dry dust with inhalation causes the pathological changes in organs that are a consequence of infiltration of acute and solids particles. Despite the importance of this problem, the questions of dust generation during the various working processes and its fractions distribution are practically not considered. This determines the time of dust standing in the air and its negative impact on a person. **Aim:** The aim of this research is to study the process of dusting during stones cutting and dust distribution on fractions regularities and quantification of dust formation process in order to improve the production equipment, staff individual and collective safety equipment. **Materials and Methods:** Many types of cutting can be divided into two types — a “dry” cutting and cutting with fluid. During “dry” cutting a dust represents a set of micro-chips which are cut off by the abrasive grains. The size of such chips very small: from a micrometer to a few micrometers fraction. Thus, the size of chips causes the possibility of creating dust slurry with low fall velocity, and which is located in the working space in large concentrations. **Results:** The following characteristic dependences were obtained as a result of research: dependence of the dust fall from the size of the dust particles, size of dust particles from minute feeding and grain range wheel, the specific amount of dust from the number of grit abrasive wheel and the temperature of the dust particles from the feeding at wheel turnover. It was shown that the distribution of chips (dust) by size will be a normal distribution law. Dimensions of chips during cut are in the range of 0.4...6 μm. Thus, dust slurry is formed with time of particles fall of several hours. This creates considerable minute dust concentration — within $0.28 \cdot 10^8 \dots 1.68 \cdot 10^8$ units/m³.

Keywords: cutting wheel, grain size, cutting speed, microchip dimension.

Introduction. Varieties of stone building materials of natural origin form a wide range of products derived from rocks. Stone artificial origin construction materials such as ceramics made from natural clays, as well as mixtures thereof with organic and mineral supplements by shaping, drying and firing. Because of the wide distribution of such materials inevitably arises the question of their shaping, which is performed by cutting them. In most cases the cutting carried with disk diamond wheels, speed of rotation of which as well as the material cutting speed is 35...50 m/s [1].

Due to the high intensity of the process of cutting and intensive micro chip formation, stone cutting process is accompanied by considerable dust formation. This can be both harmful and dangerous factor in operation.

DOI 10.15276/opu.2.49.2016.05

© 2016 The Authors. This is an open access article under the CC BY license (<http://creativecommons.org/licenses/by/4.0/>).

During cutting stone, a large amount of dust release, which is a mixture of small, mostly sharp, mineral particles. Shallow dry dust with inhalation causes the pathological changes in organs that are a consequence of infiltration of acute and solids particles. The consequence of inhalation of dust may be diseases such as pneumoconiosis, which are associated with the deposition of dust release in the lungs and tissue reaction to its presence.

Recently, much attention is paid to hygiene and sanitary of work conditions that led to the intensification of research on influence of dust release on the human body, as well as clarification of time duration of dust in the atmosphere of the production facilities [2...6].

Despite the importance of these issues, these sources do not consider all aspects of such phenomena as dust in work areas. Almost does not discuss the generation of dust in various work processes and its fractions distribution, which determines the time of dust existing in the air and its negative impact on a person.

This paper discusses the generation of dust when cutting stone and withdrawn the quantitative indicators of dust fractions in the working space of stone-cutting facility.

The aim of this research is to study the process of dusting during stones cutting and dust distribution on fractions regularities and quantification of dust formation process in order to improve the production equipment, staff individual and collective safety equipment.

Materials and Methods. Upon cutting a variety of materials the dustiness of air is much higher than the maximum allowable concentration, and the expanding chips is a source of eye injury. In addition, dust and chips reduce reliability and degrade the efficiency of means of automatics and control systems, as well as the cutting equipment.

Many types of cutting can be divided into two types — a “dry” cutting and cutting with fluid.

From the viewpoint of labor protection the “dry” cutting could be considered as a continuous generator of dangerous production factors — dust, which, depending on the ground material may be of different size, chemical composition, and therefore varying harmfulness.

During “dry” cutting a dust represents a set of micro-chips which are cut off by the abrasive grains. The size of such chips very small: from a micrometer to a few micrometers fraction. Thus, the size of chips causes the possibility of creating dust slurry with low fall velocity, and which is located in the working space in large concentrations.

It should also be noted that under the influence of rising temperature during cutting fine dust particles may be alloyed, welded and coalesce into conglomerates in size to several mm, which is already posed a serious threat to employee (particularly the eyes), because such particles airspeed may be 25...50 m/s.

Dust is a dispersion system. Dust particle with diameter of $\leq 1 \mu\text{m}$ forms with the air aerosol slurry. The settling rate of dust increases with the diameter of the dust particles. For example, settling time of dust particles of $0.05 \mu\text{m}$ diameter from a height of 1 m is 320 hours, $1 \mu\text{m}$ diameter — 3 hours, $100 \mu\text{m}$ diameter — 3 seconds. Therefore, in the inhaled air there are relatively few particles with a diameter

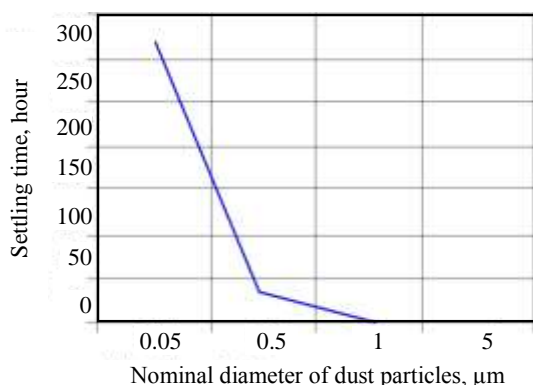


Fig. 1. Dependence of dust fall from the size of the dust particles

greater than 5 microns. Dependence of dust fall from the size of the dust particles is shown in Fig. 1 [2].

Determination of dust size. Distribution law of dust by size. Abrasive and diamond grains are polyhedral. The size and shape of there are different (Fig. 2) [2, 7].

Thus, it can be argued that the abrasive grains are irregular polyhedral, and a cutting element of the abrasive grain has a generally pyramidal shape. The apex angle of the cutting element usually is close to 90° . Each of the cutting elements of abrasive grain has a rounded top, the radius of curvature of the apex depends on the grain size: than abrasive grains is bigger in size, than more its apex radius.

The scheme and shadow projection of the abrasive grains are presented in Fig. 3 and 4 [2, 7].

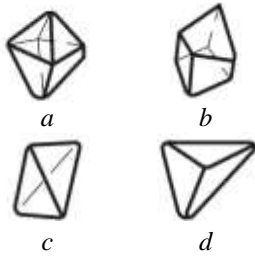


Fig. 2. Shapes of abrasive grains

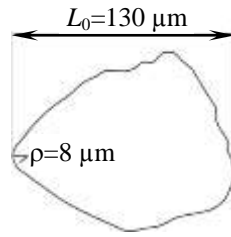


Fig. 3. Scheme of abrasive grain



Fig. 4. Shadow projection of abrasive grain

Fig. 5 shows the process of chip formation, based on the shape of the cutting abrasive grains.

As can be seen from the figure, in order to determine the thickness of the removable chip by cutting grain, you need to know: nose radius R of the cutting grain (depending on the number of grit abrasive wheel); the actual distance between the cutting grains l (in cutting involved only 10...12 % of the grains [4]); specific amount of cutting grains per surface unit of wheel (depending on l), and cutting conditions: V_{rot} — rotational speed of wheel, m/s, V_{min} — minute feeding, m/s, t — feeding at single wheel turnover, mm or m; S — cross feed, mm/rev.

These values were determined by the method involving the use of semi-synthetic micro-thermocouples with electrode diameter of 10 mm, described in [3, 7].

The most significant value in this process is the thickness of chips during cutting, which according to [3, 7] can be described by the expression

$$h = \frac{20tV_{min}l}{V_{rot}\sqrt{Dt}}, \tag{1}$$

where V_{min} — minute feeding,
 V_{rot} — rotational speed of wheel,
 t — feeding at single wheel turnover,
 l — the actual distance between the cutting grains in a wheel,
 D — wheel diameter.

The dependence of size of dust particles from minute feeding is shown in Fig. 6.

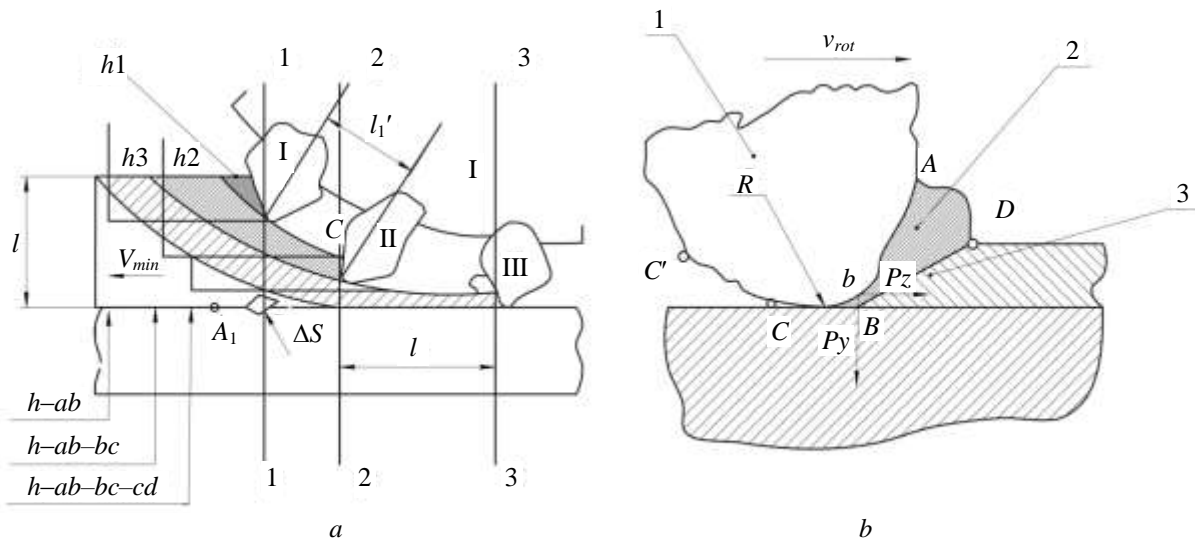


Fig. 5. Scheme of chips formation during grinding: a — trajectory of cutting grains motion: h_1, h_2, h_3 — thickness of the chips, l — actual distance between the cutting grains, t — cutting depth during grinding; b — scheme of chips formation: 1 — cutting grain, 2 — chip formation edge (ADB), 3 — shear plane (BD), R — nose radius of cutting grain

The number of chips (dust particles) formed during one second, obviously, will be

$$n = v_w \cdot S \cdot z, \quad (2)$$

where S — the width of the cutting wheel,

z — specific number of cutting grains per unit of surface of the grinding wheel equal in accordance with [10, 12]

$$z = 117 \cdot 10^6 \cdot N_z^{-1.3} \cdot N_{ctr}^{-0.167}, \quad (3)$$

where N_z — number of grit, reduced to granularity of abrasive wheels;

N_{ctr} — wheel structure number.

The dependence of the specific amount of dust from the number of grit abrasive wheel is shown in Fig. 7.

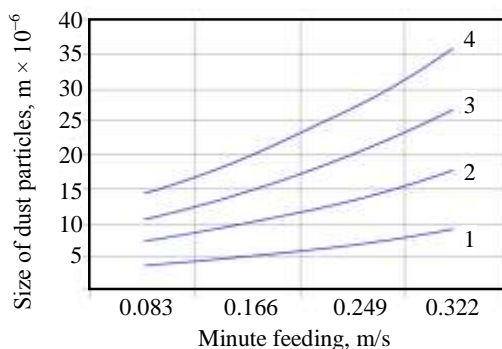


Fig. 6. Dependence of size of dust particles from minute feeding and grain range wheel, $v_w = 35$ m/s, $t = 0.01$ mm: 1 — grain range 6; 2 — grain range 10; 3 — grain range 16; 4 — grain range 25

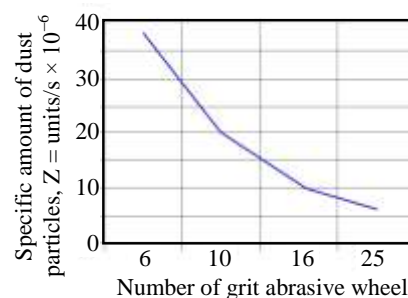


Fig. 7. The dependence of the specific amount of dust from the number of grit abrasive wheel

Minute dust concentrations during grinding with size of the working area $0.5 \times 0.5 \times 0.5$ m is within the $(0.28 \dots 1.68) \cdot 10^8$ units/m³.

There are two important factors that affect to the size of the grains. This is a rotational speed of the cutting wheel V_{rot} and feeding at single wheel turnover t . Analysis of Eq. (1) shows that the size of the grains is inversely proportional to the rotational speed. In regard to the feeding at wheel turnover, the size of the dust particles is directly proportional to the value $t^{0.5}$. Thus, as at speeds less than 30 m/s cutting is not performed then we can expect a decrease in the size of the dust particles in the transition to high-speed cutting (≈ 50 m/s). As result, the dust size range will change from 0.5...3.5 to 0.35...2.1 mm, as shown in Fig. 6.

In regard to the feeding at wheel turnover, during “dry” grinding the feeding at wheel turnover of the value more than 0.03 mm practically do not use. Using this value we can obtain the dust particles with size of 0.86...6 μ m. Thus, during cutting of construction material is produced dust particles of such dimensions that have the greatest pathogenic effects on the human body.

To more accurately determine the size of the grains must take into account the probability distribution of the size of abrasive grains that make up the cutting wheel. Typically, the abrasive grains depending on their size can be divided into three factions — average, small and large. Normally, the proportion of the main fraction is 45 % by weight of the dust, while the small and large fractions amount is 27.5 % both. Dimensions of the large and small fractions grains differ from the dust of the middle fraction by 11.5 % (Table).

Distribution of abrasive grain size is subject to a normal distribution law (Fig. 8).

Note, that larger grains protrude from the bunch more, and thus remove chips greater than smaller ones. Thus, we can say with a high probability that the size of the chips (dust particles) will be subject to the normal law.

Dimensions of the dust fractions formed during grinding, μm

Cutting wheel number N	Minute feeding V_{min} , m/s			
	0.083	0.166	0.249	0.332
6	0.4; 0.45; 0.5	0.448; 0.50; 0.56	0.58; 0.65; 0.724	0.81; 0.9; 1.0
10	0.67; 0.75; 0.84	0.89; 1.0; 1.15	1.25; 1.4; 1.56	1.52; 1.7; 1.9
16	0.98; 1.1; 1.22	1.34; 1.5; 1.67	1.88; 2.1; 2.34	2.06; 2.3; 2.56
25	1.34; 1.5; 1.67	1.79; 2; 2.23	2.33; 2.6; 2.9	3.22; 3.6; 4.0

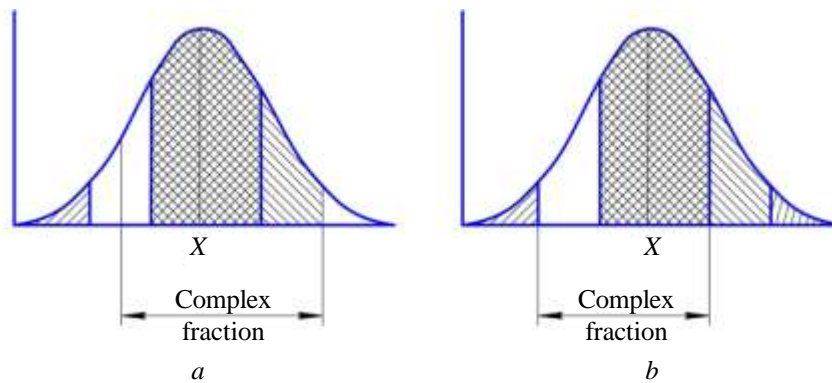






Fig. 8. Distribution law of abrasive grain size:

a — big and medium abrasive grain sizes, b — medium and small abrasive grain sizes.

Fractions:  — small;  — average;  — large;  — boundary value

Analyzing the data presented above, it can be concluded, that even during grinding when feeding at wheel turnover $t = 0.03$ mm, the grains sizes are such that their pathogenic effect on human be maximized and the rate of sedimentation in the air will be a few hours.

Determination of the chemical composition of the dust particles. In the zone of contact the cutting wheel with work piece during grinding substantial amount of heat generated. Part of this heat (approximately 10 %) is transferred to the chip. It is often sufficient to heat the chips to the combustion temperature.

The results of experiments carried out by Maslov [8] showed that sparks during grinding of sufficiently strong materials are melted or glowing fine particles flying at a tangent to that point of a circle of the rotating wheel to which the sample is pressed. Blazing chips or particles of molten material discarded by centrifugal force, not only does not going out because of a sharp differences between their temperature and the ambient temperature, but, flying at high speed in the air are heating even more. This can be explained by the fact that under the influence of oxygen in the air there is intense oxidation (combustion) of chips, which increases its temperature.

Thus formed dust should consist of mineral oxides and from minerals themselves. We define a chip heating temperature.

From Fig. 5, b it is clear that separation of the chips from the processed material is accompanied by friction with the surface of the grain ADB , which can be regarded as the front surface of the cutting element (grain). In this case, the chip temperature can be defined as the temperature of its abrasion with the front surface.

Heat flow produced through friction of chip with front surface of the cutting element (grain) can be calculated as

$$q_1 = P_{zed} V_{rot} k_{ff}, \quad (4)$$

where q_1 — heat flow generated by single cutting grain,

k_{ff} — friction factor taken equal to 0.1.

Specific heat flow during friction we determine based on the assumption that it allocated on square-shaped site with a side h :

$$\bar{q} = \frac{q_1}{h^2}. \quad (5)$$

Chip temperature is determined according to [11], taking into account the fact that only 10 % of heat is passed to the chip

$$T = \frac{1.064\bar{q}}{\lambda} \left(\frac{2\alpha l}{V_{rot}} \right)^{0.5}, \quad (6)$$

where λ — mineral's heat conductivity factor,

α — mineral's thermal diffusivity,

l — length of the abrasion element.

Fig. 9 shows the dependence of the temperature of the dust particles from the feeding at wheel turnover during cutting of complex mineral. Analyzing the dependence, we can conclude that during cutting by wheel with numbers 6...25 and feeding at wheel turnover of about 10...35 μm the chips aren't burnt; in turn, when cutting wheel number is 40 and feeding is 10...15 μm , we can expect to receive the dust consisting of mineral oxides and unburned particles.

Conclusions. The "dry" cutting is characterized by high dust content in the air of the working area. During "dry" cutting a dust represents a set of micro-chips which are cut off by the abrasive grains. Dimensions of chips during cut are in the range of 0.4...6 μm . Thus, dust slurry is formed with time of particles fall of several hours. This creates considerable minute dust concentration — within $0.28 \cdot 10^8 \dots 1.68 \cdot 10^8$ units/ m^3 .

The dust chemical composition depends on the type of material and on the chip heating temperature, which can be above or below the combustion temperature of a particular material. Thus, during cutting the complex stone structures there are various iron oxides and refractory materials such as W, Mo, Ti, Nb, Va and others may be present in the dust.

Knowledge of the laws of the dust formation including the dust particles size, concentration, chemical composition and rate of sedimentation of dust particles makes it possible to determine the degree of harmfulness of the cutting process and to develop the adequate protection of the working system.

Література

1. Чумаченко, Т.В. Фактическое расстояние между режущими зернами в эльборовом круге / Т.В. Чумаченко, В.Г. Лебедев // Проблемы техники. — 2009. — № 2. — С. 124–134.
2. Аль-Аджейлат, С.А. Фактическое расстояние между режущими зернами и удельное число режущих зерен в единице поверхности эльборового круга, радиусы закругления зерен из КНБ и средняя величина стружки, снимаемая режущим зерном / С.А. Аль-Аджейлат, Т.В. Чумаченко, В.Г. Лебедев // Новые и нетрадиционные технологии в ресурсо- и энергосбережении: мат-лы науч.-техн. конф., 9–10 сентября 2010 г., Одесса. — Киев: АТМ Украины, 2010. — С. 6–8.
3. Аль-Аджейлат, С.А. Аналитическое определение сил и температур резания единичным эльборовым зерном / С.А. Аль-Аджейлат, В.Г. Лебедев, А.В. Усов // Вісник ХНТУСГ імені Петра Василенка. — 2009. — Вип. 81 — С. 263–270.
4. Редько, С.Г. Процессы теплообразования при шлифовании металлов / С.Г. Редько. — Саратов: СПИ, 1962. — 231 с.

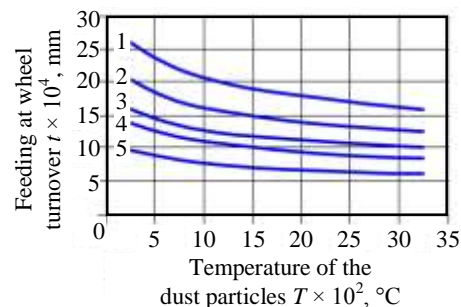


Fig. 9. Dependence of the temperature of the dust particles from the feeding at wheel turnover during grinding by wheels with different cutting numbers; $V_{rot} = 35$ m/s, $V_{min} = 0.166$ m/s; 1 — 40; 2 — 25; 3 — 16; 4 — 12; 5 — 6

5. Respiratory tract responses to dust: Relationships between dust burden, lung injury, alveolar macrophage fibronectin release, and the development of pulmonary fibrosis / K.E. Driscoll, J.K. Maurer, R.C. Lindenschmidt, *et al.* // *Toxicology and Applied Pharmacology*. — 1990. — Vol. 106, Issue 1. — PP. 88–101.
6. Kennedy, F.E. Frictional heating and contact temperatures / F.E. Kennedy // *Modern Tribology Handbook*. Vol. 1: Principles of Tribology / ed. by B. Bhushan. — Boca Raton: CRC Press, 2001. — PP. 235–272.
7. Маслов, Е.Н. Теория шлифования материалов / Е.Н. Маслов. — М.: Машиностроение, 1974. — 319 с.
8. Мущенко, Б.Л. Расчет скорости падения частиц пыли и оценка степени влияния различных сил, действующих на частицу / Б.Л. Мущенко // *Научный вестник Воронежского ГАСУ. Строительство и архитектура*. — 2009. — № 2(14). — С. 58–63.
9. Азаров, В.Н. Теоретические исследования скорости оседания мелкодисперсной пыли в воздушной среде рабочих помещений предприятий машиностроения и стройиндустрии / В.Н. Азаров, О.И. Бессараб, О.В. Кабаев // *Вестник ВолгГАСУ. Сер.: Строительство и архитектура*. — 2010. — Вып. 17(36). — С. 102–105.
10. Dorman, R.G. Dust control and air cleaning / R.G. Dorman. — Oxford: Pergamon, 1974. — 615 p.
11. Балтренас, П.Б. Обеспыливание воздуха на предприятиях стройматериалов / П.Б. Балтренас. — М.: Стройиздат, 1990. — 184 с.
12. Абразивная и алмазная обработка материалов: справочник / под ред. А.Н. Резникова. — М.: Машиностроение, 1977. — 391 с.

References

1. Chumachenko, T.V., & Lebedev, V.G. (2009). Actual distance between cutting grains in Borazon wheel. *Problemy Tekhniki*, 2, 124–134.
2. Al-Adjelat, S.A., Chumachenko, T.V., & Lebedev, V.G. (2010). Actual distance between cutting grains and their specific number per surface unit area of the Borazon wheel, radius of rounding of CBN grains and mid-size of chips removed by abrasive grains. In *Proceedings of Scientific and Technical Conference on Modern and Innovative Technologies of Resource and Energy Saving* (pp. 6–8). Kyiv: ATM Ukrainy.
3. Al-Adjelat, S.A., Lebedev, V.G., & Usov, A.V. (2009). Analytical determination of cutting forces and temperatures of single borazone grain. *Bulletin of Kharkiv Petro Vasylenko National Technical University of Agriculture*, 81, 263–270.
4. Red'ko, S.G. (1962). *Processes of Heat Build-Up while Grinding Metal*. Saratov: GSU.
5. Driscoll, K.E., Maurer, J.K., Lindenschmidt, R.C., Romberger, D., Rennard, S.I., & Crosby, L. (1990). Respiratory tract responses to dust: Relationships between dust burden, lung injury, alveolar macrophage fibronectin release, and the development of pulmonary fibrosis. *Toxicology and Applied Pharmacology*, 106(1), 88–101. DOI:10.1016/0041-008X(90)90109-8
6. Kennedy, F.E. (2001). Frictional heating and contact temperatures. In B. Bhushan (Ed.), *Modern Tribology Handbook* (Vol. 1, pp. 235–272). Boca Raton: CRC Press.
7. Maslov, E.N. (1974). *Theory of Grinding Materials*. Moscow: Mashinostroenie.
8. Muschenko, B.L. (2009). Calculation of speed of falling of the dust particles and estimation of influence of the various forces acting on a particle. *Scientific Herald of the Voronezh State University of Architecture and Civil Engineering: Construction and Architecture*, 2, 58–63.
9. Azarov, V.N., Bessarab, O.I., & Kabayev, O.V. (2010). Theoretical researches of rate of subsidence of the finely divided dust in the air of working rooms of the enterprises of mechanical engineering and building industry. *Bulletin of Volgograd State University of Architecture and Civil Engineering: Civil Engineering and Architecture*, 17, 102–105.
10. Dorman, R.G. (1974). *Dust Control and Air Cleaning*. Oxford: Pergamon.
11. Baltrenas, P.B. (1990). *Dedusting of Air in Enterprises of Building Materials*. Moscow: Stroiizdat.
12. Reznikov, A.N. (Ed.). (1977). *Abrasive and Diamond Processing of Materials*. Moscow: Mashinostroenie.

Received March 24, 2016

Accepted May 19, 2016

UDC [303.725:624.072.7]:512.547.2

Ahmad Rahbar-Ranji, Assoc.Prof.

Amirkabir University of Technology, 424 Hafez Ave., 15914 Tehran, Iran; e-mail: rahbar@aut.ac.ir

MODAL ANALYSIS OF A BOX SHAPED GIRDER BY NUMERICAL METHOD

Ахмад Рахбар-Ранжі. Модальний аналіз коробчастої балки за допомогою чисельних методів. Для розрахунку власних частот і форм коливань виконано модальний аналіз структур. Ці параметри є основною технічною інформацією, необхідною для аналізу і розробки будь-яких структур. Інформація про них додатково необхідна для розуміння і моделювання динамічної поведінки структур. Для прогнозування цих параметрів в простих структурах може бути використаний теоретичний підхід, однак для складних структур необхідно використовувати чисельні методи. Заявлено, що для складних структур аналітичне рішення може бути використано для прогнозування власної частоти моди першого порядку за допомогою спрощення складних структур до простих. У даній роботі проведено чисельні дослідження модального аналізу коробчастої балки, а також проведено порівняльний аналіз з моделлю двоопорної балки, яка має аналогічні характеристики поперечного перерізу. Виявлено, що за допомогою моделі двоопорної балки можна прогнозувати вібрації першого порядку, за умови адекватного врахування граничних умов.

Keywords: модальний аналіз, коробчаста балка, метод скінченних елементів.

Ahmad Rahbar-Ranji. Modal analysis of a box shaped girder by numerical method. Modal analysis of structures is carried-out to calculate natural frequencies and mode shapes. These parameters are the essential technical information required in the analysis and design of any structures. In addition, this information is needed for understanding and simulating dynamic behavior of structures. For simple structures, theoretical approach can be used to predict these parameters, however for complex structures, numerical method should be used. It is claimed that for complex structures, closed form solution can be used to predict natural frequency of first mode by idealization of complex structures to simple one. In this paper, the modal analysis of a box shaped girder is studied numerically and results are compared with simple beam model which has the same cross sectional properties. It is found that simple beam model can predict first mode of vibration, if adequate boundary conditions are considered.

Keywords: modal analysis, box shaped girder, FEM.

Introduction. Noise, malfunction and failure of mechanical systems/structures are caused by excessive dynamic behavior. Increasing demands for the condition assessment, safety and reliability assessment of structures requires needs better understanding of dynamic properties. To determine the dynamic characteristics of existing structures, modal analysis should be performed.

Modal analysis of any structure is carried-out to determine natural frequencies and mode shapes. These parameters are the essential technical information required in engineering analysis and design. For simple structures, such as beams and plates, good analytical predictions using closed form solutions can be easily found in various reference books (for example, [1]). For more complex structures, like multi-storey frames when number of degree of freedoms is limited to two or three, hand calculation still can be used for modal analysis. For higher degree of freedoms the numerical or experimental methods should be used. It is claimed that for these types of structures, simple model based on some idealization still can be used to predict the natural frequency of first mode with some acceptable accuracy.

In recent years, modal analysis has received wide acceptance in structural engineering application particularly for identification of bridges modal properties. Salane and Baldwin [2] have used the test data to determine modal stiffness and damping of single and three span bridges. Fryba and Pirner [3] have used long-term tests to determine natural frequencies and the dynamic impact factors of old bridges for the estimation of their residual life and determination of inspection intervals. Cremona [4] has used modal analysis for health monitoring of a high-speed railway bridge. Rahbar-Ranji [5] has used finite elements method (FEM) to investigate accuracy and applicability of rule-based dynamic magnification factor of a hollow box shaped girder.

Special gantry cranes are used for loading/unloading containers from ship-to-shore, which are called STS cranes. These are large dock side cranes and only seen at the container terminals. The crane

DOI 10.15276/opu.2.49.2016.06

© 2016 The Authors. This is an open access article under the CC BY license (<http://creativecommons.org/licenses/by/4.0/>).

Table 1

Position of Transverse Diaphragms

Stations	X (mm)	Stations	X (mm)
#1	0.00	#14	22961
#2	1104	#15	24879
#3	2957	#16	26797
#4	4810	#17	28715
#5	6663	#18	30633
#6	8516	#19	32551
#7	10369	#20	34469
#8	12222	#21	36464
#9	14075	#22	38459
#10	15928	#23	41115
#11	17781	#24	43771
#12	19634	#25	46427
#13	21043	#26	49047

Table 2

Thickness of plates and stiffeners size

Location	Plate thickness (mm)	Stiffener size (mm)
Top Plate	10 mm (from station 1 to 5, and from station 17 to 26), and 15 mm (from station 5 to 17)	L 150×100×10
Bottom Plate	10 mm (from station 1 to 17, and from station 22 to 26) and 15 mm (from station 17 to 22)	L 150×100×10
Sides	10	L 100×50×6
Diaphragms	10, and 15 mm	FB 150×10

Finite elements model of Boom. The ANSYS v.10 computer software is chosen for modal analysis. First step for finite elements analysis (FEA) is to model structure adequately, which is the most laborious step of the analysis. For global vibration the plates are modeled using Shell63 plane stress elements. This four-node quadrilateral shell element is capable of modeling elastic behavior and can simulate both membrane and flexural behaviors. In addition, it has three rotational and three translational degrees of freedom per node. The stiffeners can be modeled either by beam elements or truss elements (link). If truss elements are used, the bending stiffness, which could create some errors, is ignored. However, the stiffness matrix is smaller and solution is faster. In case of very large structures, like big ships, it is necessary to use this type of elements. Beam44 beam element is used for modeling all longitudinal stiffeners and rings around circular and trapezoidal holes. BEAM44 is an uniaxial element with tension, compression, torsion and bending capabilities. The element has six degrees of freedom at each node: translations in the nodal x, y, and z directions and rotations about the nodal x, y, and z axes. This element allows using different unsymmetrical geometry at each end and permits offsetting of the end nodes from the centroidal axis of the beam. Fig. 3...6 show different parts of FE model of boom.

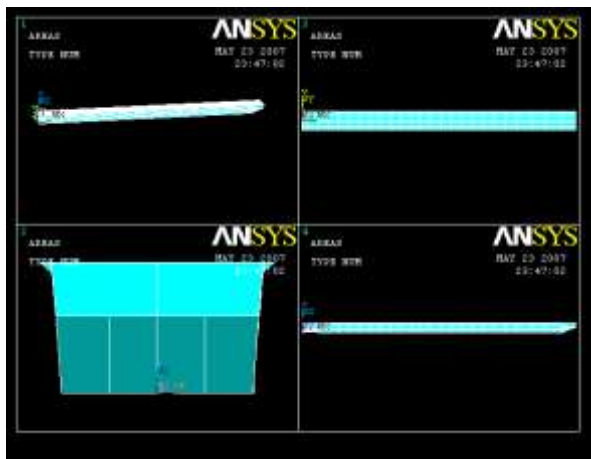


Fig. 3. Structural model of whole boom in ANSYS software

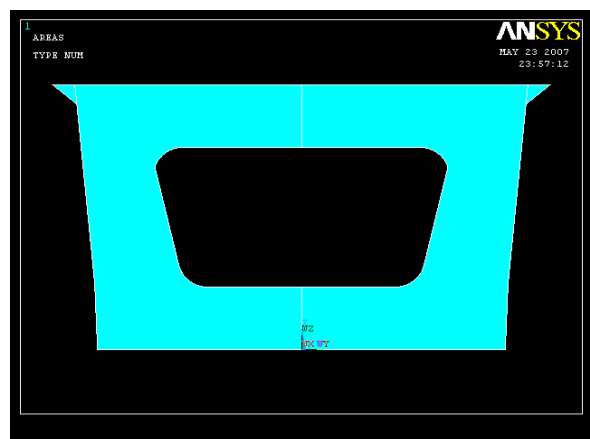


Fig. 4. Structural model of Transverse Diaphragm from station 2 to station 19 and from station 23 to station 25

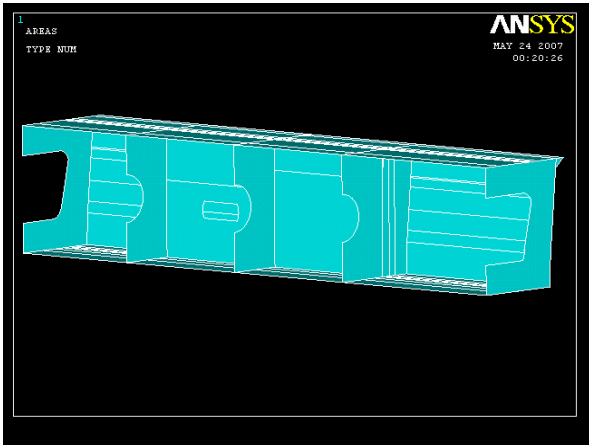


Fig. 5. Structural model of boom from station 19 to station 23

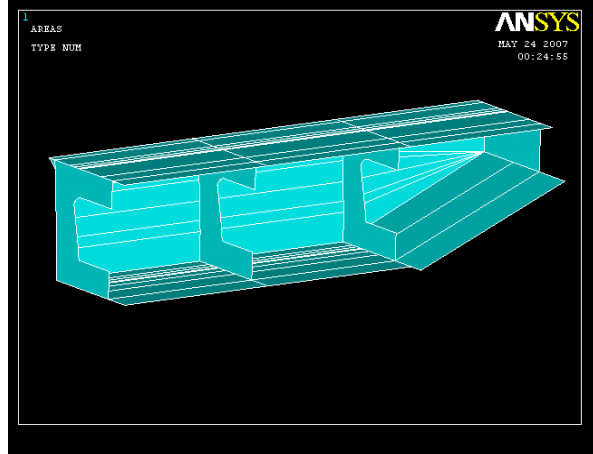


Fig. 6. Structural model of boom from station 23 to station 26

1. *Boundary conditions.* As it can be seen from Fig. 1, the boom is supported by sloped cables connected to eye-plates at the stations 21 to 22, and by a plate from station 1 to 2. Fig. 7 shows the simplified boundary condition model used for the boom. Therefore, following boundary conditions are applied (Fig. 8):

1) From station 1 to station 2, at distance ± 890 mm, and ± 1110 mm from centerline on cover-plate, $U_x = U_y = U_z = 0$.

2) From station 21 to station 22 at distance ± 850 mm, and ± 992.50 mm from centerline, on cover plate, $U_x = U_y = U_z = 0$.

2. *Masses.* In the computation of vibration, the natural frequencies are highly depend on mass distribution, and following masses must be taken into account:

- boom structure,
- equipment,
- cargo (containers).

In the FE techniques, a distinction is drawn between nodal masses and element masses. For the arrangement of structural masses, as well as for the distributable parts of equipment masses, element masses are used. Here, mass of boom and rail are considered automatically by applying density for all elements (7850 kg/m^3 for structural steel).

Nodal masses are concentrated at corresponding nodal points of the FE model. This arrangement of masses is advisable for heavy parts of equipment. The total mass of trolley and container are considered as nodal mass. The trolley has 29.09 tons of weight and weight of container is considered as 50 tons. These masses are applied as concentrated masses at foot-print area of four wheels. In this study these masses are considered as $10+0.679$ m.

3. *Meshing.* After creating the geometry of model and applying boundary conditions and masses, the model is meshed by adequate mesh size. Fig. 9...11 show the meshed model of boom with corresponding elements.



Fig. 7. Boundary conditions of boom

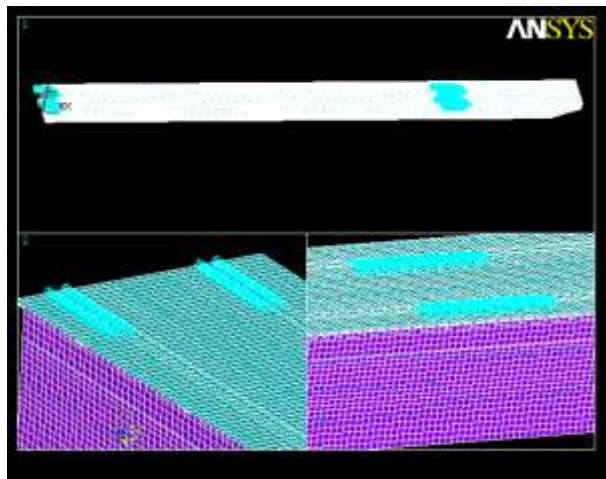


Fig. 8. Boundary conditions of boom

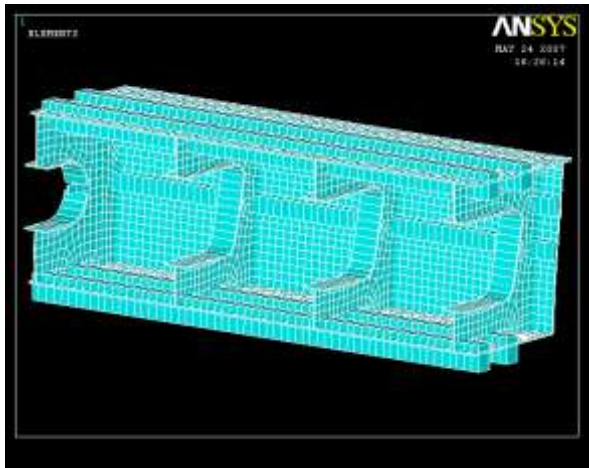


Fig. 9. Shell and beam elements of boom model from station 2 to station 5 (elements are shown by Eshape command)

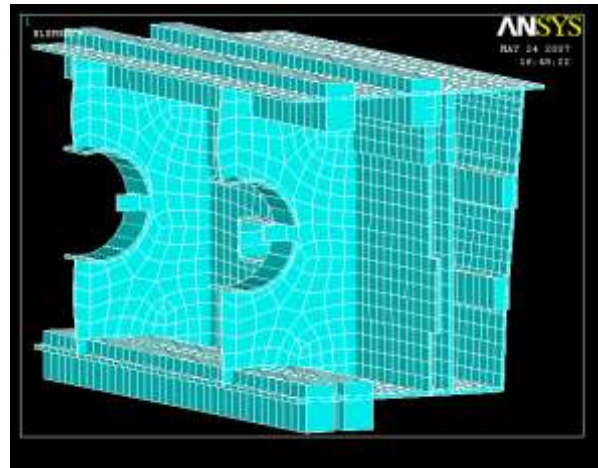


Fig. 10. Shell and beam elements of boom model from station 19 to station 20 (elements are shown by Eshape command)

Results and Discussion.

Finite Elements Model. FE computer software modal analysis is used to determine the natural frequencies and mode shapes of the boom. Modal analysis using the ANSYS products family is a linear analysis. Any nonlinearities, such as plasticity, are ignored even if they are defined. Fig. 12...15 show first four natural frequencies and mode shapes.

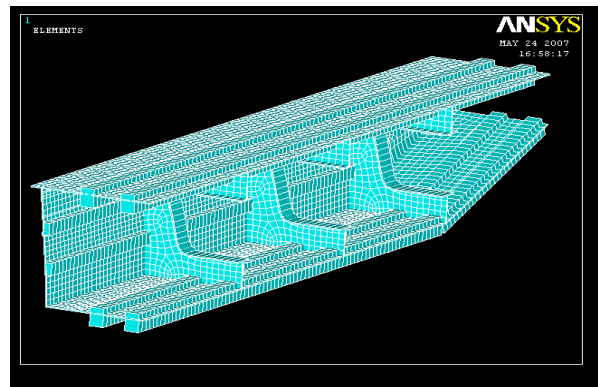


Fig. 11. Shell and beam elements of boom model from station 23 to station 26 (elements are shown by Eshape command)

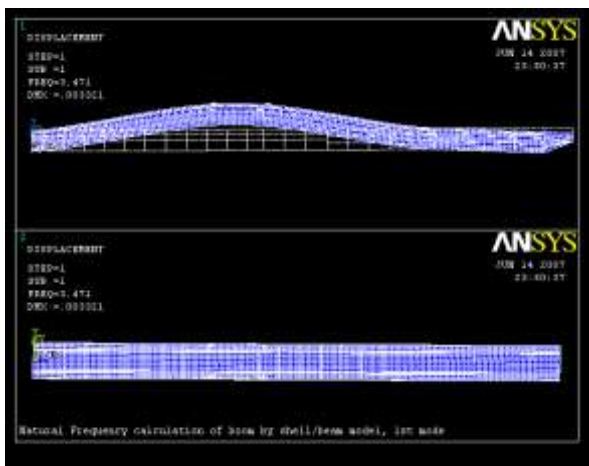


Fig. 12. Mode Shape of boom by shell/beam model, 1st mode

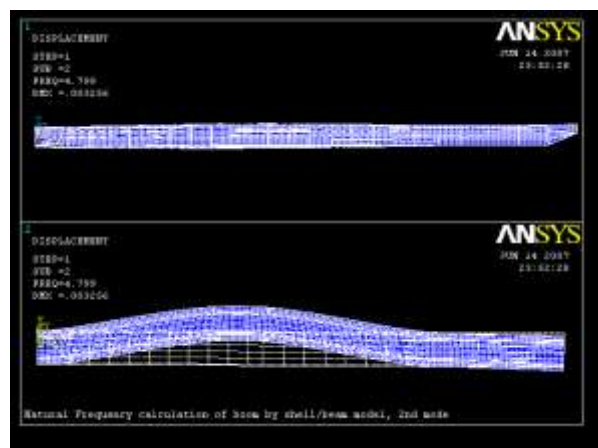


Fig. 13. Mode Shape of boom by shell/beam model, 2nd mode

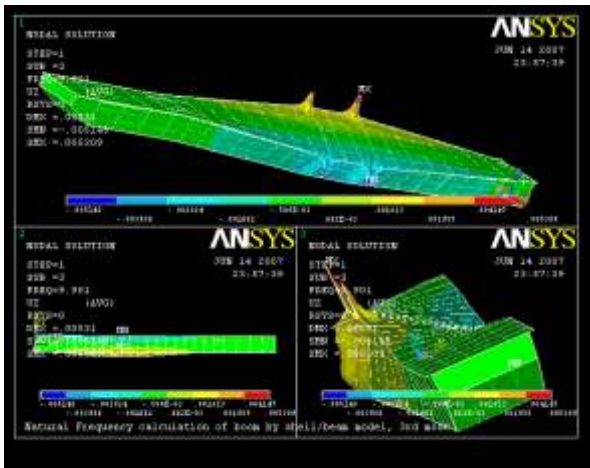


Fig. 14. Mode Shape of boom by shell/beam model, 3rd mode

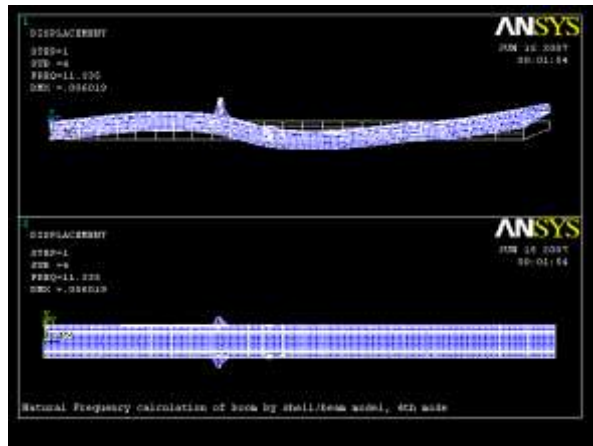


Fig. 15. Mode Shape of boom by shell/beam model, 4th mode

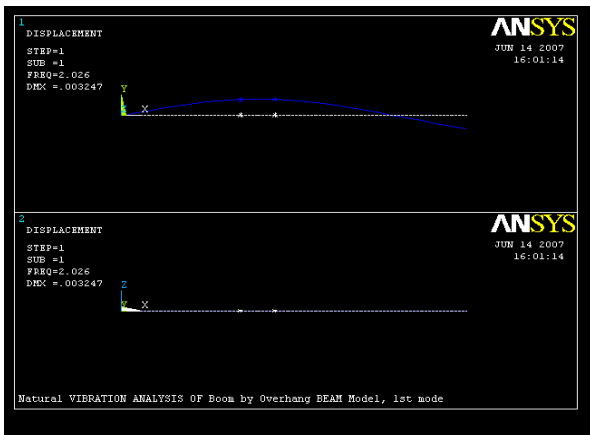


Fig. 16. Mode Shape of boom by beam model, 1st mode

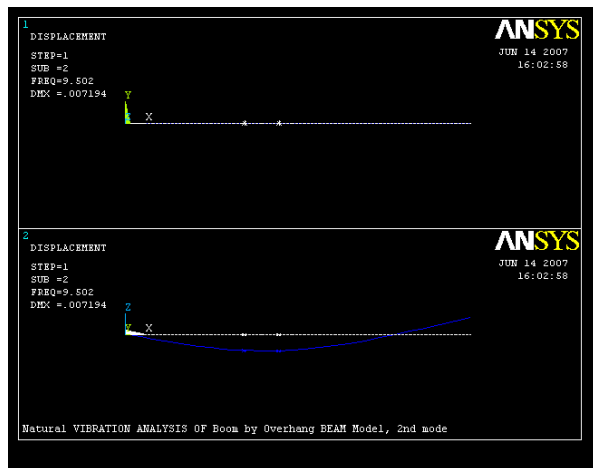


Fig. 17. Mode Shape of boom by beam model, 2nd mode

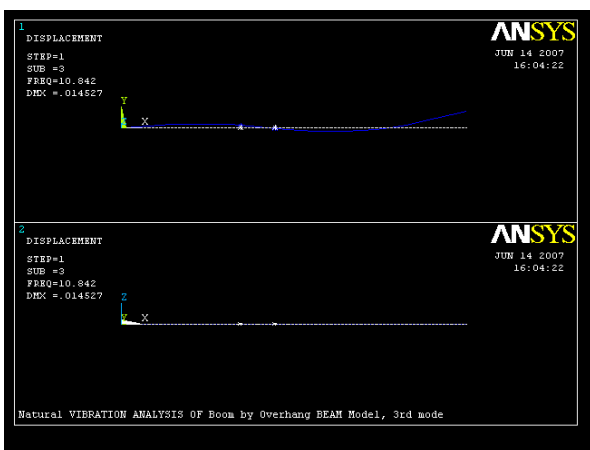


Fig. 18. Mode Shape of boom by beam model, 3rd mode

Beam model with clamped supported boundary condition. The same beam model with clamped boundary condition at station 0.5 (Fig. 19) is considered.

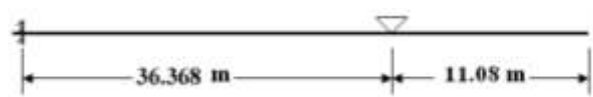


Fig. 19. Beam model with clamped boundary condition

Fig. 20...22 show first three vibration modes and natural frequencies of simple beam model with clamped boundary condition.

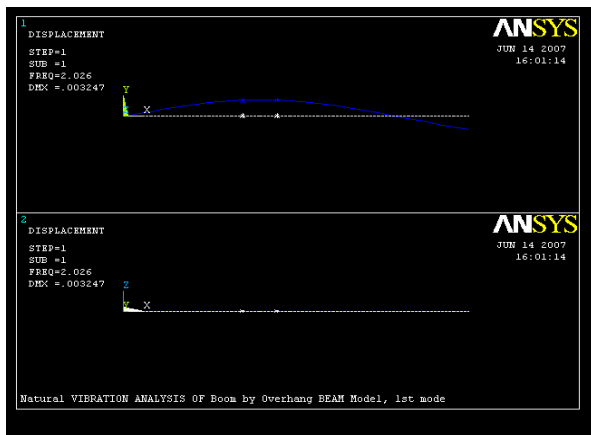


Fig. 20. Mode Shape of boom by beam model, 1st mode

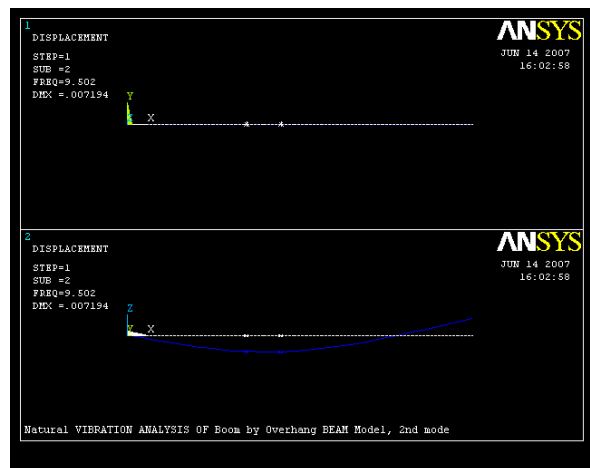


Fig. 21. Mode Shape of boom by beam model, 2nd mode

Table 3 depicts the first 10 frequencies and mode shapes of boom calculated by FEM and compared with the simple beam models.

As it can be seen, beam model with clamped boundary condition has better agreements than beam model with simple support boundary condition. The differences between beam model by clamped boundary conditions and FEM for main global vibration modes are less than 10...15%. This difference could be explained by:

- ignoring transverse diaphragms by beam model,
- applying boundary conditions in beam model at one point,
- applying mass of trolley and container in one node by beam model,
- applying boundary conditions at upper nodes in FEM having full depth in beam model.

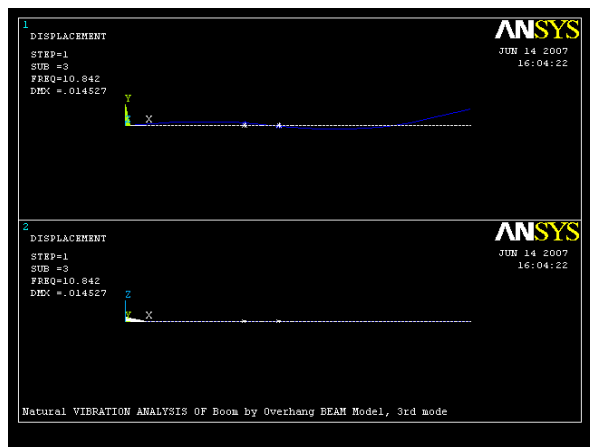


Fig. 22. Mode Shape of boom by beam model, 2nd mode

Table 3

Summary of results for two model of boom

Mode number	Frequency and mode shape by beam model		Frequency and mode shape by FEM
	Simply support	Clamped at station 0.5	
1	2.0260 Vertical Bending, 2 Node	3.0787 Vertical Bending, 2 Node	3.4714 Vertical Bending, 2 Node
2	9.5022 Horizontal Bending, 2 Node	9.5022 Horizontal Bending, 2 Node	4.7994 Horizontal Bending, 2 Node
3	10.842 Vertical Bending, 3 Node	11.543 Vertical Bending, 3 Node	9.9006 Torsion, 2 Node

Mode number	Frequency and mode shape by beam model		Frequency and mode shape by FEM
	Simply support	Clamped at station 0.5	
4	16.488 Longitudinal	16.488 Longitudinal	11.335 Vertical Bending, 3 Node
5	17.441 Vertical Bending, 4 Node	19.460 Vertical Bending, 4 Node	12.618 Local Bending of cover plate
6	26.332 Horizontal Bending, 3 Node	26.332 Horizontal Bending, 3 Node	12.825 Vertical Bending of Fore Part
7	37.028 Vertical Bending, 5 Node	42.649 -	13.167 Local Bending of Cover plate
8	42.649 Vertical Bending, 6 Node	42.752 Vertical Bending, 5 Node	13.712 Local Bending of Cover plate
9	48.363 -	48.530 Horizontal Bending, 4 Node	14.011 Local Bending of Fore part
10	48.530 Horizontal Bending, 4 Node	51.940 Longitudinal	15.901 Local transverse Vibration of plate

As it could also be seen from Table 3 that order of mode shapes changes as boundary condition of beam change. For example, vertical bending mode with five nodes is seventh mode shape for beam with simple supported condition, while it is eighth mode shape in beam with clamped boundary condition. Also it can be observed that local vibration modes and torsional modes can be caught by beam model.

Conclusions. FEM is used for modal analysis of a box shaped girder. Shell elements and beam elements are used for girder modeling. Upon comparison with simple beam model, it is found that if adequate boundary conditions are chosen, simple beam model can be used to estimate some first natural frequencies of a complex structure. The local vibration and torsional vibration modes are missed using this simple model.

Література

1. Chopra, A.K. Dynamics of structures: Theory and applications to earthquake engineering / A.K. Chopra. — Englewood Cliffs: Prentice Hall, 1995. — 729 p.
2. Salane, H. Identification of modal properties of bridges / H. Salane, J. Baldwin, Jr. // *Journal of Structural Engineering*. — 1990. — Vol. 116, Issue 7. — PP. 2008–2021.
3. Frýba, L. Load tests and modal analysis of bridges / L. Frýba, M. Pirner // *Engineering Structures*. — 2001. — Vol. 23, Issue 1. — PP. 102–109.
4. Cremona, C. Dynamic monitoring applied to the detection of structural modifications: A high-speed railway bridge study / C. Cremona // *Progress in Structural Engineering and Materials*. — 2004. — Vol. 6, Issue 3. — PP. 147–161.
5. Rahbar-Ranji, A. Dynamic magnification factor in a box-shape steel girder / A. Rahbar-Ranji // *Journal of The Institution of Engineers (India): Series C*. — 2014. — Vol. 95, Issue 1. — PP. 11–18.

References

1. Chopra, A.K. (1995). *Dynamics of Structures: Theory and Applications to Earthquake Engineering*. Englewood Cliffs, N.J.: Prentice Hall.
2. Salane, H., & Baldwin, J., Jr. (1990). Identification of modal properties of bridges. *Journal of Structural Engineering*, 116(7), 2008–2021. DOI:10.1061/(ASCE)0733-9445(1990)116:7(2008)

3. Frýba, L., & Pirner, M. (2001). Load tests and modal analysis of bridges. *Engineering Structures*, 23(1), 102–109. DOI:10.1016/S0141-0296(00)00026-2
4. Cremona, C. (2004). Dynamic monitoring applied to the detection of structural modifications: A high-speed railway bridge study. *Progress in Structural Engineering and Materials*, 6(3), 147–161. DOI:10.1002/pse.177
5. Rahbar-Ranji, A. (2014). Dynamic magnification factor in a box-shape steel girder. *Journal of The Institution of Engineers (India): Series C*, 95(1), 11–18. DOI:10.1007/s40032-014-0096-2

Received June 8, 2016

Accepted July 22, 2016

UDC 628.4.032+504.062

N.S. Remez, DSc, Prof.,

T.A. Osipova

National Technical University of Ukraine "Kyiv Polytechnic Institute", 37 Peremogy Ave., 03056 Kiev, Ukraine; e-mail: osipova_tetiana@ukr.net

PREDICTION OF STRAIN STATE OF LANDFILL CONSIDERING SOIL FOUNDATION AND ANGLE OF SLOPE

Н.С. Ремез, Т.А. Осіпова. Прогнозування деформованого стану полігона твердих побутових відходів з врахуванням ґрунтової основи і кута нахилу схилу. Сьогодні серйозною проблемою світового масштабу виступає збільшення обсягів накопичення побутових відходів. Україна займає одне з перших місць в світі за кількістю сміття на одиницю населення. В країні вже близько 7 % території знаходиться під твердими побутовими відходами, крім того щороку утворюється понад 52 млн. тонн побутового сміття. У зв'язку з цим гостро постає питання про стійкість полігонів після їх закриття для використання в подальшому як основи для інженерних споруд і конструкцій. **Мета:** Метою роботи є встановлення залежності осідання закритого полігона твердих побутових відходів від властивостей підстельних ґрунтів, а також від кута нахилу схилу полігона для прогнозування можливості використання його як основи споруди. **Матеріали і методи:** Під час дослідження було враховано поетапне навантаження полігона шарами відходів, а також кут його нахилу. Покриваючий і підстельний шари описано моделлю Кулона-Мора. Тіло полігона було змодельовано як слабкий ґрунт з урахуванням його повзучості, для цього використано модель Soft Soil Creep (SSC). Для чисельного розв'язання задачі використано метод скінченних елементів. **Результати:** В роботі вперше побудовано математичну модель осідання полігона твердих побутових відходів з врахуванням геометричних і фізико-механічних параметрів полігона і ґрунтової основи, що дозволить у подальшому прогнозувати можливість використання полігона для будівництва на ньому споруд різного призначення. В результаті досліджень встановлено, що зі зменшенням кута нахилу схилу відбувається значне зменшення осідання полігона. Так, при зменшенні кута з 75° до 30° осідання зменшується на 5...22 % в залежності від типу ґрунтів основи. Найбільше зменшення осідання спостерігається у найменш щільного ґрунту — у піску.

Ключові слова: осідання, тверді побутові відходи, деформація, математичне моделювання.

N.S. Remez, T.A. Osipova. Prediction of strain state of landfill considering soil foundation and angle of slope. Today increase in volumes of accumulation of a household waste acts as a global serious problem. Ukraine occupies one of the first places on the list in the world by garbage quantity per capita. Already about 7 % of the territory in the country are under municipal solid waste, besides more than 52 million tons of household waste are annually formed. In this regard, sharply raises the question of the stability of landfills after their closure for further use as a basis for engineering constructions and designs. **Aim:** The aim of this research is to establish the dependence of settlement of the closed landfill on the properties of the underlying soil, as well as the landfill slope angle to predict the possibility of using it as a basis for construction. **Materials and Methods:** The phased load of landfill by waste layers and angle of inclination were taken into account during the research. The covering and underlying layers are described by Coulomb-Mohr model. The body of landfill was modeled as a weak ground considering its creep. The Soft Soil Creep (SSC) model was applied for this. The finite elements method was used for numerical solution of the problem. **Results:** In this work the mathematical model of sedimentation of municipal solid waste constructed for the first time, taking into account geometrical and physical and mechanical parameters of landfill and soil base, which will allow further prediction the use of landfill for building structures on it for various purposes. As a result of researches was found that with decreasing of inclination angle of the landfill slope there is a significant decrease in settlement. Thus, while reducing the angle from 75° to 30° the settlement is reduced by 5...22% depending on the type of soil foundation. The largest landfill reduction is observed for the least dense soil (sand).

Keywords: landfill, municipal solid waste, strain, mathematical modelling.

Introduction. Today increase in volumes of accumulation of a household waste acts as a global serious problem. Ukraine occupies one of the first places on the list in the world by garbage quantity per capita. Already about 7 % of the territory in the country are under municipal solid waste, besides more than 52 million tons of household waste are annually formed. In this regard, sharply raises the question of the stability of landfills after their closure for further use as a basis for engineering constructions and designs.

Ukraine has about 6 thousand dumps and landfills of 7.4 thousand hectares total area, 32 thousand illegal dumps, 15 sorting lines and only two waste incineration plants. Very often landfills (about 5 %) are overloaded or they do not meet the standards of environmental safety (about 16 %). It should also be noted that in Ukraine, unfortunately, no waste treatment plants, common in economically developed countries [1].

In this connection the question arises about firmness of landfills after their closure for use as a basis for engineering buildings and structures in the future.

DOI 10.15276/opu.2.49.2016.07

© 2016 The Authors. This is an open access article under the CC BY license (<http://creativecommons.org/licenses/by/4.0/>).

To predict the firmness of the landfill is necessary to study its settling considering angle of landfill and stress-strain state of the underlying soil base.

Often, to assess the stability of the landfill the experimental techniques are using, namely the method of inverse analysis, laboratory tests and more. Analysis of the literature showed that the experimental methodology for assessing of the stability of the landfill is financially costly and effective only for specific conditions. For example, the method of inverse analysis is based on consideration of the properties already destroyed landfills. This method is not satisfactory for other landfills due to the difference of waste, environmental conditions, properties of landfill body and underlying soil mass. In turn, through laboratory tests the landfill conditions can't be displayed – to capture in one sample all the layers of waste and take into account the geotechnical, physical and mechanical properties. Therefore, to consider the stress-strain state of the polygon layers and underlying soil mass and its characteristics the mathematical modeling is advisable to apply.

Applied mathematical models for the prediction of settling can be divided into the following classes: rheological; empirical; models based on soil mechanics; models that take into account biodegradation.

Park and Lee [2] proposed a model of settling, taking into account the time-dependent biodegradation of waste: sedimentation rate is expressed through plurality of settlings directly proportional to the amount of solids that decompose; and the process of dissolving of organic materials can be described by equations of the first order kinetics.

Note that the definition of kinetic coefficients and/or hydrolysis constants with the possibility of monitoring of their changes in the environment in a real time is a non-trivial task.

Empirical models predict a total waste behavior by adjusting of empirical parameters for a specific site.

Marques *et al.* [3] have developed the rheological model to account the primary and secondary compression mechanisms that governed by the rheological parameters that is also included in the biodegradation of waste. Note that the primary compression does not depend on time.

The common feature of these and other models [4...7] is that they just adapted to model the behavior and properties of solid waste, ignoring such an important part of the landfill as soils that lie at its core. Exactly the type, strength, geotechnical properties of the underlying soil affect on the stability of the landfill, because the ground has the greatest burden.

Given the fact that some steep slopes of dumps remain stable, we can conclude that the focus in the analysis of the landfill firmness should be given to materials that are the basis of municipal solid waste (MSW). Therefore, to forecast the estimation the landfill firmness in this paper first studied the settling as well as the stress-strain state of the underlying soil base.

The aim of this research is to establish the dependence of settlement of the closed landfill on the properties of the underlying soil, as well as the landfill slope angle to predict the possibility of using it as a basis for construction.

Materials and Methods. During the study we will take into account the phase loading of landfill waste layers and angle of inclination. To predict the settling of closed landfill MSW the following mathematical models were used.

Covering and underlying layers described the Coulomb-Mohr model [8].

The body of landfill was modeled as a weak ground considering its creep for this a model uses Soft Soil Creep (SSC). Currently, this model more fully describes the properties of weak soil as stress-dependent stiffness and compression based secondary creep. It should be noted that the SSC model takes into account both physical and geometric nonlinearity of soil deformation process.

Total volume deformation ε_v , caused by the growth of effective stress from the initial value p'_0 to p' for the period of time T ($T = t_c + t'$) consists of an elastic ε_v^e and viscoplastic ε_v^{vp} components. Viscoplastic component is the amount of deformation during consolidation $\varepsilon_{v_c}^{vp}$ and after consolidation $\varepsilon_{v_{ac}}^{vp}$. Rangeard [9] showed that the relationship between the deformations is expressed as follows:

$$\varepsilon_v = \varepsilon_v^e + \varepsilon_{v_c}^{vp} + \varepsilon_{v_{ac}}^{vp} ,$$

where

$$\varepsilon_v^e = \kappa^* \ln \left(\frac{p'}{p'_0} \right),$$

$$\varepsilon_{v\ c}^{vp} = (\lambda^* - \kappa^*) \ln \left(\frac{p'_{pc}}{p'_0} \right),$$

$$\varepsilon_{v\ ac}^{vp} = \mu^* \ln \left(\frac{\tau_c + t'}{\tau_c} \right),$$

where μ^* — modified creep factor;

τ_c — time of consolidation that depends on the geometry of the sample under study;

t' — time pass from the start of loading of landfill;

κ^* — modified swelling ratio;

λ^* — modified compression ratio;

t_c — completion of primary consolidation;

p'_0 — initial effective stress;

p' — effective stress;

p'_{pc} — effective pre consolidation pressure.

The ratio of model parameters with internationally standardized parameters as follows:

$$\mu^* = \frac{C_\alpha}{2.3(1+e_0)}, \quad \lambda^* = \frac{C_c}{2.3(1+e_0)}, \quad \kappa^* = \frac{2C_s}{2.3(1+e_0)};$$

where C_c — compression ratio;

C_s — swelling ratio;

C_α — creep factor.

As noted above, the underlying soil is described by the Coulomb-Mohr model. Full yield condition of Coulomb-Mohr model consists of six functions (surfaces yield f), which are formed as follows:

$$f_{1a} = \frac{1}{2}(\sigma'_2 - \sigma'_3) + \frac{1}{2}(\sigma'_2 + \sigma'_3) \sin \varphi - c \cos \varphi \leq 0;$$

$$f_{1b} = \frac{1}{2}(\sigma'_3 - \sigma'_2) + \frac{1}{2}(\sigma'_3 + \sigma'_2) \sin \varphi - c \cos \varphi \leq 0;$$

$$f_{2a} = \frac{1}{2}(\sigma'_3 - \sigma'_1) + \frac{1}{2}(\sigma'_3 + \sigma'_1) \sin \varphi - c \cos \varphi \leq 0;$$

$$f_{2b} = \frac{1}{2}(\sigma'_1 - \sigma'_3) + \frac{1}{2}(\sigma'_1 + \sigma'_3) \sin \varphi - c \cos \varphi \leq 0;$$

$$f_{3a} = \frac{1}{2}(\sigma'_1 - \sigma'_2) + \frac{1}{2}(\sigma'_1 + \sigma'_2) \sin \varphi - c \cos \varphi \leq 0;$$

$$f_{3b} = \frac{1}{2}(\sigma'_2 - \sigma'_1) + \frac{1}{2}(\sigma'_2 + \sigma'_1) \sin \varphi - c \cos \varphi \leq 0,$$

where c — clutch;

$\sigma'_1, \sigma'_2, \sigma'_3$ — normal stresses;

φ — angle of internal friction.

In addition to the yield surface a Coulomb-Mohr model presented by six plastic potential functions g :

$$g_{1a} = \frac{1}{2}(\sigma'_2 - \sigma'_3) + \frac{1}{2}(\sigma'_2 + \sigma'_3) \sin \psi;$$

$$g_{1b} = \frac{1}{2}(\sigma'_3 - \sigma'_2) + \frac{1}{2}(\sigma'_3 + \sigma'_2) \sin \psi;$$

$$g_{2a} = \frac{1}{2}(\sigma'_3 - \sigma'_1) + \frac{1}{2}(\sigma'_3 + \sigma'_1) \sin \psi;$$

$$g_{2b} = \frac{1}{2}(\sigma'_1 - \sigma'_3) + \frac{1}{2}(\sigma'_1 + \sigma'_3) \sin \psi;$$

$$g_{3a} = \frac{1}{2}(\sigma'_1 - \sigma'_2) + \frac{1}{2}(\sigma'_1 + \sigma'_2) \sin \psi;$$

$$g_{3b} = \frac{1}{2}(\sigma'_2 - \sigma'_1) + \frac{1}{2}(\sigma'_2 + \sigma'_1) \sin \psi,$$

where ψ — angle of dilation.

Hydrodynamic aspects consist in the account of seepage forces acting on the skeleton of the soil environment and interaction parameters of liquid and solid phases of soil (pressure, tension and porosity) in the process of consolidation. Assuming the vortex seepage flow and distribution of the resistance element evenly over the section we will use the generalized Darcy law and equation of continuity. We assume that the compressibility of the skeleton and pore fluid is low, which leads to a linear dependence of the porosity of the soil pressure.

The interaction of soil skeleton and fluid characterize by volume force which proportional to the pressure gradient.

According to [10], the equation of continuity we supplement with the initial and boundary conditions.

For numerical solution of the problem finite element method was used. Estimated area was divided into 265 finite elements.

Landfill for which was conducted simulation consists of ten layers of waste, thickness of 3 m each. Subsidence was defined based on incremental load of landfill in 30 years after its closure. The basis of Landfill is clay, sand and loam.

Simulations were conducted at three slopes angle of the polygon 30, 60 and 75°. Linear dimensions of polygons with different angles of slopes chosen so that the volume of landfill body remained unchanged. Settings of underlying soils are presented in Table 1. Parameters of waste are presented in Table 2 (Layer №1 — latest, Layer №10 — first of underlying polygon).

Table 1

Physical and mechanical parameters of soils

Parameter	Soils		
	Sand	Loam	Clay
Deformations module E_{ref} , kN / m ³	18000	10000	9000
Poisson's ratio ν , units.	0.34	0.36	0.37
Soil specific weight γ_{unsat} , kN/m ³	18.0	13	19.0
Specific weight of water-saturated soil γ_{sat} , kN/m ³	20.7	14.6	21.8
Filtration coefficient in the horizontal direction k_x , units.	0.5	0.006	0.004
Filtration coefficient in the vertical direction k_y , units.	0.5	0.006	0.004
Module of deformation E , MPa	50	33	28
The specific adhesion c , kPa	3	34	81
The angle of internal friction ϕ , degrees	31	14	13

Table 2

Physical and mechanical parameters of waste

Parameter	Values
Specific weight γ_{unsat} , kN/m ³	7.504
Specific weight of water-saturated soil γ_{sat} , kN/m ³	10.0
The specific adhesion c , kPa	25
The angle of internal friction φ , degrees	20
The initial coefficient of porosity e_0 , units.	0.4268
Compression ratio C_c , units.	0.3987
Swelling ratio C_s , units.	0.0394
Creep factor C_a , units :	
Layer №1	0.0615
Layer №2	0.0474
Layer №3	0.0448
Layer №4	0.0429
Layer №5	0.0414
Layer №6	0.0402
Layer №7	0.0391
Layer №8	0.0382
Layer №9	0.0374
Layer №10	0.0367

Results and Discussion. In [11] the calculations of landfill strain at the slope angle of 75° was conducted. They amounted to 4.95 m for landfill with sand base, with clay base — 3.83 m, with loam base — 4.47 m.

Deformed estimated area of landfill with clay base and with his body angle of 60° shown in Fig. 1. An analysis of numerical calculations shows that vertical deformation of landfill totaled 3.8 m.

As a result of numerical calculation found that at the same angle the maximum vertical deformation was: for landfill of sand — 4.34 m (Fig. 2), with loam — 4.27 m. A comparison of these results shows that the angle of inclination of the landfill body significantly affects the vertical deformation, decreasing the angle from 75° to 60° deformations decreased by 1...12 % depending on the type of soil base.

To establish the impact of slope angle of landfill on its settling the simulations for landfill with angle of 30° was conducted. As a result of studies it was found that with decreasing of slope angle of landfill the impact on the underlying soil subsidence reduced and the difference between the values of deformation decreases.

Thus, if the underlying layer is sand, it can be observed that the vertical deformation reaches 3.94 m (Fig. 3), if the loam — 3.89 m (Fig. 4). If we use clay as underlayment then vertical deformation is the least compared to the previous two versions — 3.63 m (Fig. 5).

Comparing the value of settling showed that decreasing of the angle from 60° to 30° deformity decreased by 5...9 % depending on the type of soil base.

With decreasing of angle from 75° to 30° vertical deformation reduction was greatest for sand (20.4 %), while the same value for loam is 13 % and for clay is 5.22 %.

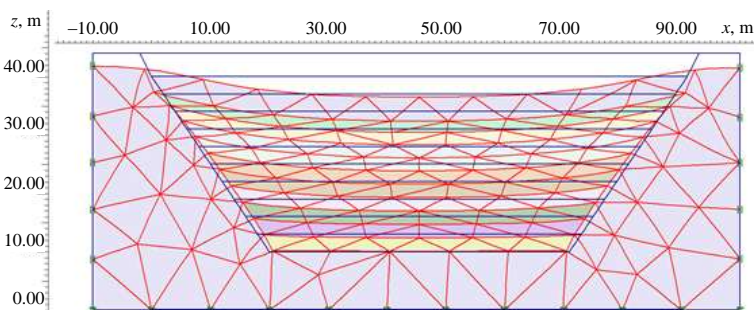


Fig. 1. Deformed calculated area of landfill with clay soil underlying (slope angle of landfill 60°)

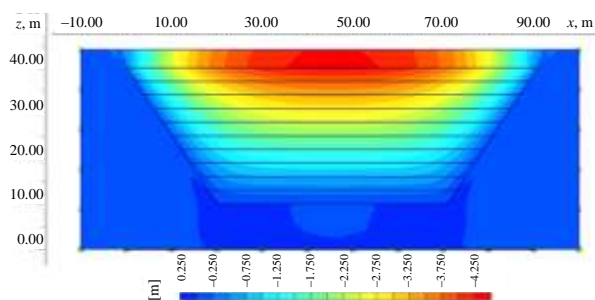


Fig. 2. Vertical deformation of landfill with sandy soil (angle of slope of landfill 60°)

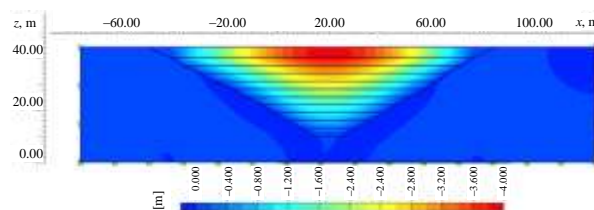


Fig. 3. The vertical deformation of landfill with sandy soil underlying (angle of landfill 30°)

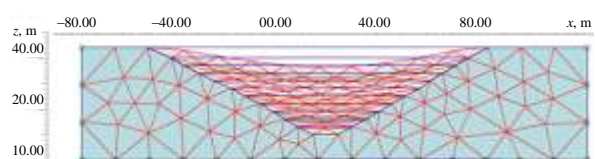


Fig. 4. Deformed calculated area of polygon with loam, as the underlying soil (angle of landfill 30°)

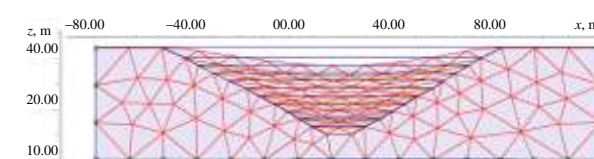


Fig. 5. Deformed calculated area of polygon with clay as underlying soil (angle of landfill 30°)

Fig. 6 shows the dependence of landfill settling from the slope angle of ground for three types of underlying soil.

Conclusions. The modeling of strain state of landfill in view of soil foundations and angle of landfill using finite element method was held. As a result of studies we found that with decreasing of slope angle of landfill the settling is significant reduce. Thus, decreasing the angle from 75° to 30° settling decreases by 5...22 % depending on the type of soil base. The largest decrease is observed in less dense soil — sand.

We have got the dependencies of settling from the angle of slopes for different soil foundations as a second-degree polynomial. They are as follows:

- For clay — $y = -0.07x^2 + 0.18x + 3.72$;
- For loam — $y = -0.09x^2 + 0.07x + 4.49$;
- For sand — $y = 0.105x^2 - 0.925x + 5.77$.

Using these dependences can be defined the settling for intermediate values of slope angles. With decreasing of slope angle the difference between settlings of landfill on different bases is decreasing. The results can be used in predicting of landfill settling with different geometric, physical and mechanical parameters for assessing the possibility of further exploitation of landfill as the foundation structures for various purposes.

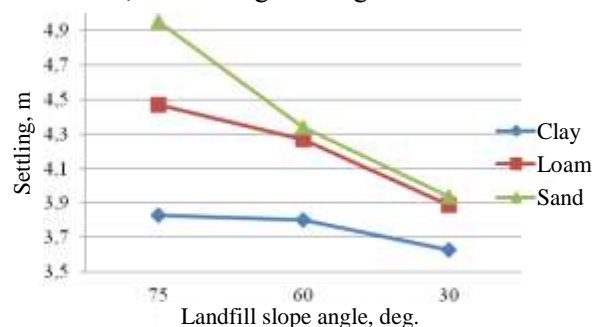


Fig. 6. Dependence of settling from the angle of slopes for MSW landfill

Література

1. Тихенко, В.С. Реалізація національних та наднаціональних проєктів збирання та переробки побутових відходів в Україні / В.С. Тихенко // Вісник Дніпропетровського університету. Сер.: Економіка. — 2014. — Т. 22, Вип. 8(2). — С. 84–88.
2. Park, H.I. Long-term settlement behaviour of landfills with refuse decomposition / H.I. Park, S.R. Lee // Journal of Solid Waste Technology and Management. — 1997. — Vol. 24, Issue 4. — PP. 159–165.

3. Marques, A. Composite compressibility model for municipal solid waste / A. Marques, G. Filz, O. Vilar // *Journal of Geotechnical and Geoenvironmental Engineering*. — 2003. — Vol. 129, Issue 4. — PP. 372–378.
4. Prediction of long-term municipal solid waste landfill settlement using constitutive model / G. Sivakumar Babu, K. Reddy, S. Chouskey, H. Kulkarni // *Practice Periodical of Hazardous, Toxic, and Radioactive Waste Management*. — 2010. — Vol. 14, Issue 2. — PP. 139–150.
5. Sowers, G.F. Settlement of waste disposal fills / G.F. Sowers // *Proceedings of the 8th International Conference on Soil Mechanics and Foundation Engineering*, 6–11 August 1973, Moscow, USSR. — Moscow: Stroiizdat, 1973. — Vol. 2.2. — PP. 207–210.
6. Yen, B.C. Sanitary landfill settlement rates / B.C. Yen, B. Scanlon // *Journal of the Geotechnical Engineering Division*. — 1975. — Vol. 101, Issue 5. — PP. 475–487.
7. Gibson, R.E. A theory of consolidation for soils exhibiting secondary compression / R.E. Gibson, K.Y. Lo // *Norwegian Geotechnical Institute Publication*. — 1961. — № 41. — PP. 1–16.
8. Vermeer, P.A. A soft soil model that accounts for creep / P.A. Vermeer, H.P. Neher // *Proceedings of the International Symposium “Beyond 2000 in Computational Geotechnics — 10 Years of PLAXIS International”*, 18–20 March 1999, Amsterdam, The Netherlands. — Rotterdam: Balkema, 1999. — PP. 249–261.
9. Rangeard, D. Influence of soil model on the analysis of pressuremeter test / D. Rangeard, R. Zentar, N-E. Abriak // *Proceedings of the 9th Symposium on Numerical Models in Geomechanics (NUMOG IX)*, 25–27 August 2004, Ottawa, Canada. — London: Taylor & Francis Group, 2004. — PP. 699–705.
10. Ремез, Н.С. Напряженно-деформированное состояние полигонов твердых бытовых отходов с учетом слоистого грунтового основания / Н.С. Ремез, Т.А. Осипова // *Вісник НТУУ «КПІ». Серія «Гірництво»*. — 2015. — Вип. 28. — С. 11–17.
11. Ремез, Н.С. Прогнозирование использования полигонов ТБО в качестве основания сооружения / Н.С. Ремез, Т.А. Осипова // *ISJ Theoretical & Applied Science*. — 2015. — № 07(27). — С. 34–39.

References

1. Tykhenko, V. (2014). Realization of national and supranational projects on collection and processing of domestic waste in Ukraine. *Herald of the Dnepropetrovsk National University: Economics*, 22(8/2), 84–88.
2. Park, H.I., & Lee, S.R. (1997). Long-term settlement behaviour of landfills with refuse decomposition. *Journal of Solid Waste Technology and Management*, 24(4), 159–165.
3. Marques, A., Filz, G., & Vilar, O. (2003). Composite compressibility model for municipal solid waste. *Journal of Geotechnical and Geoenvironmental Engineering*, 129(4), 372–378. DOI:10.1061/(ASCE)1090-0241(2003)129:4(372)
4. Babu Sivakumar, G., Reddy, K., Chouskey, S., & Kulkarni, H. (2010). Prediction of long-term municipal solid waste landfill settlement using constitutive model. *Practice Periodical of Hazardous, Toxic, and Radioactive Waste Management*, 14(2), 139–150. DOI:10.1061/(ASCE)HZ.1944-8376.0000024
5. Sowers, G.F. (1973). Settlement of waste disposal fills. In N.A. Tsytoich (Ed.), *Proceedings of the 8th International Conference on Soil Mechanics and Foundation Engineering* (Vol. 2.2, pp. 207–210). Moscow: Stroiizdat.
6. Yen, B.C., & Scanlon, B. (1975). Sanitary landfill settlement rates. *Journal of the Geotechnical Engineering Division*, 101(5), 475–487.
7. Gibson, R.E., & Lo, K.Y. (1961). A theory of consolidation for soils exhibiting secondary compression. *Norwegian Geotechnical Institute Publication*, 41, 1–16.
8. Vermeer, P.A., & Neher, H.P. (1999). A soft soil model that accounts for creep. In R.B.J. Brinkgreve (Ed.), *Proceedings of the International Symposium “Beyond 2000 in Computational Geotechnics — 10 Years of PLAXIS International”* (pp. 249–261). Rotterdam: Balkema.
9. Rangeard, D., Zentar, R., & Abriak, N-E. (2004). Influence of soil model on the analysis of pressuremeter test. In G.N. Pande, S. Pietruszczak (Eds.), *Proceedings of the 9th Symposium on Numerical Models in Geomechanics (NUMOG IX)* (pp. 699–705). London: Taylor & Francis Group. DOI:10.1201/9781439833780.ch98
10. Remez, N.S., & Osipova, T.A. (2015). Stress strain state of municipal solid waste landfills considering layered soil foundation. *Herald of the National Technical University of Ukraine “Kyiv Polytechnic Institute”*: *Mining*, 28, 11–17.
11. Remez, N.S., & Osipova, T.A. (2015). The prediction of using MSW landfill as a base of constructions. *ISJ Theoretical & Applied Science*, 7(27), 34–39. DOI:10.15863/TAS.2015.07.27.6

Received April 27, 2016

Accepted June 15, 2016

ENERGETICS. HEAT ENGINEERING. ELECTRICAL ENGINEERING

ЕНЕРГЕТИКА. ТЕПЛОТЕХНІКА.
ЕЛЕКТРОТЕХНІКА

UDC 628.165.048+621.577.4

V.P. Kravchenko, DSc, Prof.,
S.V. Surkov, PhD, Assoc.Prof.,
Hussam Ghanem

Odessa National Polytechnic University, 1 Shevchenko Ave., 65044 Odessa, Ukraine; e-mail: surkov101@mail.ru

MODELLING AND OPTIMIZATION OF SEAWATER DESALINATION PROCESS USING MECHANICAL VAPOUR COMPRESSION

В.П. Кравченко, С.В. Сурков, Хуссам Ганем. Моделювання й оптимізація процесу опріснення морської води в установках з механічним стисненням пари. В умовах глобальних змін клімату нестача прісної води стає актуальною проблемою для все більшої кількості країн. Однією з найбільш перспективних технологій опріснення морської води є механічне стиснення пари (МСП), що забезпечує низьке енергоспоживання завдяки використанню принципу теплового насоса. **Мета:** Метою роботи є виявлення резервів підвищення ефективності опріснювальних систем, заснованих на механічному стисненні пари, шляхом оптимізації схеми і параметрів установок з МСП. **Матеріали і методи:** Запропоновано новий тип опріснювальної установки, головним елементом якої є теплообмінник прихованої теплоти. Морська вода після попереднього нагрівання в теплообмінниках надходить у випарник-конденсатор, де отримує основну кількість теплоти від пари, що конденсується. Частина морської води випаровується, а концентрований розчин солі (розсіл) виходить з випарника і після охолодження скидається назад в море. Пара, що утворюється, стискається за допомогою компресора і надходить у конденсатор. Суттєвою особливістю даної схеми є те, що конденсація відбувається при вищих температурах, ніж випаровування. Завдяки цьому теплота, що виділяється при конденсації пари, використовується для випаровування морської води. **Результати:** Було вирішено наступні питання: модифікована і доповнена математична модель установок з МСП, модифіковано схему включення теплообмінників, досліджено вплив конструктивних параметрів установки на вартість обладнання і електроенергії. Аналіз схем установки і математичної моделі дозволив визначити шляхи зниження енерговитрат. Проаналізовано вплив двох основних параметрів – питомої потужності компресора й питомої площі поверхні випарника-конденсатора – на величину приведених витрат опріснювальної установки. Визначено оптимальне співвідношення цих параметрів.

Ключові слова: опріснення морської води, механічне стиснення пари, чисельне моделювання.

V.P. Kravchenko, S.V. Surkov, Hussam Ghanem. Modelling and optimization of seawater desalination process using mechanical vapour compression. In the conditions of global climate changes shortage of fresh water becomes an urgent problem for an increasing number of the countries. One of the most perspective technologies of a desalting of sea water is the mechanical vapour compression (MVC) providing low energy consumption due to the principle of a heat pump. **Aim:** The aim of this research is to identify the reserves of efficiency increasing of the desalination systems based on mechanical vapour compression by optimization of the scheme and parameters of installations with MVC. **Materials and Methods:** The new type of desalination installation is offered which main element is the heat exchanger of the latent heat. Sea water after preliminary heating in heat exchangers comes to the evaporator-condenser where receives the main amount of heat from the condensed steam. A part of sea water evaporates, and the strong solution of salt (brine) goes out of the evaporator, and after cooling is dumped back in the sea. The formed steam is compressed by the compressor and comes to the condenser. An essential singularity of this scheme is that condensation happens at higher temperature, than evaporation. Thanks to this the heat, which is comes out at devaporation, is used for evaporation of sea water. Thereby, in this class of desalination installations the principle of a heat pump is implemented. **Results:** For achievement of a goal the following tasks were solved: the mathematical model of installations with MVC is modified and supplemented; the scheme of heat exchangers switching is modified; influence of design data of desalination installation on the cost of an inventory and the electric power is investigated. The detailed analysis of the main schemes of installation and mathematical model allowed defining ways of decrease in energy consumption and the possible merit value. Influence of two key parameters — a specific power of the compressor and a specific surface area of the evaporator-condenser — on a value of given expenses of desalination installation is analyzed. The optimum ratio of these parameters is defined.

Keywords: desalting of sea water, mechanical vapour compression, numerical modeling.

Introduction. Now the need for fresh water, both for domestic needs and for the production enterprises, grows in many countries of the world. Especially this problem is particularly acute in the

DOI 10.15276/opu.2.49.2016.08

© 2016 The Authors. This is an open access article under the CC BY license (<http://creativecommons.org/licenses/by/4.0/>).

countries of the Arabian Peninsula and the Persian Gulf. As of 2008 the Persian Gulf countries were producing 58% of the bulk world volume of desalinated water. Global climate changes and population growth do a problem of fresh water more and more urgent for the majority of regions of the Globe [1].

Especially high requirements for the consumed water are placed by heat power production. On nuclear power plants water is used as a working medium and as the coolant. Effectiveness of thermal energy transfer and the its subsequent transformation into a mechanical energy is defined by purity of surfaces of metal contacting with water and steam. According to technical requirements, the quantity of permeates in working water must be no more than $10 \mu\text{g/l}$ [2].

The required quality of water can be reached only by means of technologies of a thermal desalting (distillation) which have several modifications. Multistage installations of instantaneous flashing (MSF) are mainly used in large stationary installations. In the presence of the industrial vapor sources the installations with thermal vapour compression (TVC) are optimum. Far from the industrial vapour sources and in mobile installations the technology of a desalting with mechanical vapour compression (MVC) has the greatest advantages. In this research this technology is chosen for the detailed analysis.

In the works of El-Dessouky [3] and Al-Juwayhel *et al.* [4] the mathematical models of systems with MVC are developed. Further researches were devoted to decrease in prime cost of the water freshened with MVC use. In particular, Lara [5, 6] investigated the prospects of use of high performance gerotor compressors and hydrophobic evaporators-condensers, and Cherkasskiy [7] investigated high-temperature working modes.

The aim of this research is to identify the reserves of efficiency increasing of the desalination systems based on mechanical vapour compression by optimization of the scheme and parameters of installations with MVC.

To achieve the goal, it is necessary to solve the following problems:

- to modify and complete the mathematical model of installations with MVC;
- increase the convergence of iterative methods and the reliability the obtained results;
- to modify the scheme of heat exchangers plug-in;
- to research the influence of design parameters of desalination installation on the cost of an

inventory and the electric power.

Materials and Methods. The scheme of the offered desalination installation is submitted in Fig. 1.

The main element of this installation is a uniform block of the evaporator-condenser, or the latent heat exchanger.

Seawater after preliminary heating in heat exchangers comes to the evaporator-condenser where receives the main heat amount from the condensed vapour. A part of seawater evaporates, and the strong solution of salt (brine) goes out of the evaporator, and after cooling is dumped back in the sea. The formed vapour is compressed by the compressor and comes to the condenser.

The $T(s)$ — chart of process is schematically shown in Fig. 2. Here, the piece 1–2 shows the process of evaporation of seawater; 2–3 — compression of vapour in the compressor which can be considered as adiabatic; 3–4 — isobaric cooling, 4–5 — devaporation.

Essential singularity of this scheme is that condensation takes place at higher temperature, than evaporation. Due to this the heat evolved at devaporation is used for evaporation of seawater. Thereby in this class of desalination installations the principle of a heat pump is implemented.

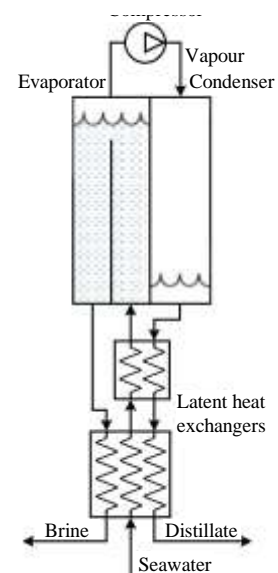


Fig. 1. The scheme of desalination installation with mechanical vapour compression

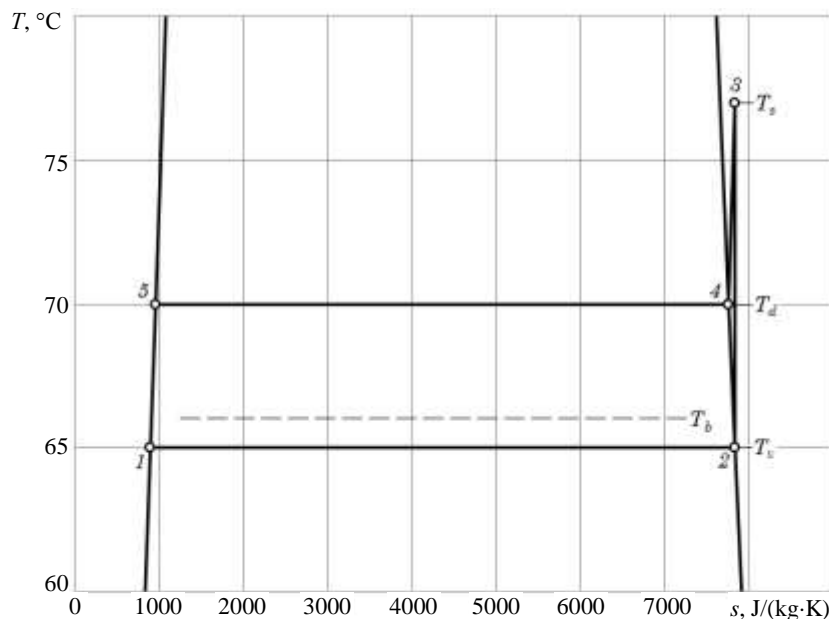


Fig. 2. The $T(s)$ — chart of desalting process with mechanical vapour compression

Now let's write down a weight conservation law for water and for salt respectively:

$$G_f = G_d + G_b, \quad (1)$$

$$G_f X_f = G_b X_b, \quad (2)$$

where G — mass flow of substance (water, salt);
 X — salt concentration.

Here indexes f , d and b belong to the feeding ocean water, the distillate and a brine dumped in the sea respectively.

The energy balance for the device in general is calculated according to the equation

$$h_{cw} G_f + W G_d = h_d G_d + h_b G_b, \quad (3)$$

where h — enthalpy,

W — specific energy, transferred to the steam flow from the compressor.

Using mean specific heat c_p , the equation (3) can be rewritten as

$$W G_d = (G_b + G_d) c_p (T_{out} - T_{cw}),$$

where T_{out} — temperature of the output streams of a brine and distillate,

T_{cw} — temperature of the input seawater.

From here it is possible to obtain

$$T_{out} = T_{cw} + \frac{W G_d}{c_p (G_b + G_d)}. \quad (4)$$

For a numerical example is set that a mass output of distillate is 1 kg/s.

The amount of heat needed to evaporate the second mass of vapour is calculated using the formula

$$Q_2 = G_d r_b, \quad (5)$$

where r_b — latent heat of vaporization at boiling point of a brine.

The quantity of heat Q_2 has to be transmitted to the boiling brine through evaporator-condenser walls.

The temperature of vapour which is formed during salty water boiling can be calculated as

$$T_v = T_b - BPE,$$

where BPE — boiling point elevation, which can be calculated according to [3, 4].

The saturation pressure in an evaporator corresponding to temperature T_v is calculated by the formula

$$p_v = p_s(T_v).$$

For further calculations it is necessary to set first approximation for temperature T_d at which the vapour in the condenser is condensed. Further value of T_d is defined by method of simple iterations

The compressor has to create pressure in the condenser that would be equal to saturated vapor pressure at temperature T_d , i.e.

$$p_d = p_s(T_d).$$

Vapor pressures on the saturation line $p_s(T_d)$ and $p_s(T_b)$ are also calculated according to the ratios given in [4].

Estimation of minimum necessary intensity of vapour compression in the compressor is made according to the equation

$$Cr = p_s(T_d)/p_s(T_b). \quad (6)$$

The specific power consumed by the compressor electric motor according to [7] is calculated using formula

$$W_c = \frac{\gamma}{\gamma-1} \frac{p_v v_v}{\eta} \left[\left(\frac{p_d}{p_v} \right)^{\frac{\gamma-1}{\gamma}} - 1 \right], \quad (7)$$

where v_v — specific volume of a saturated vapour at a temperature T_v ;

γ — heat capacity ratio;

η — compressor efficiency.

Apparently, the following ratio is fair in adiabatic process:

$$\frac{T_s}{T_v} = \left(\frac{p_d}{p_v} \right)^{\frac{\gamma-1}{\gamma}}. \quad (8)$$

From here it is possible to evaluate the temperature of compressed vapor

$$T_s = T_v \left(\frac{p_d}{p_v} \right)^{\frac{\gamma-1}{\gamma}}.$$

The heat amount allocated during devaporation process is calculated according to the ratio

$$Q_1 = G_d [r_d + c_p''(T_s - T_d)], \quad (9)$$

where r_d — latent heat of vaporization at condensation temperature.

As calculations show, this power, as a rule, is more, than Q_2 because of the “excess” values of T_s arising at adiabatic vapour compression in the compressor. Excess of power ($Q_1 - Q_2$) in practice leads to boiling temperature T_b rise, and together with it — the rise of all other specific temperatures.

However, in this work authors assume that excess of power is compensated by a thermolysis to ambient medium, and process can be considered as conservative one.

The heat transfer equation can be written as

$$Q_2 = U_e A_e (T_d - T_b), \quad (10)$$

where U_e — total heat transfer coefficient of the evaporator-condenser;

A_e — area of surface-heat transfer of evaporator-condenser.

At predefined values of A_e and U_e the condensation temperature is determined uniquely

$$T_d = T_b + \frac{Q_1}{U_e A_e}, \quad (11)$$

but, because U_e depends on temperature [3], it is necessary the iterative refinement of T_d .

The loop body containing the equations (6...11) repeats until change of T_d value becomes less than the preset small value. Calculations show that the iterative cycle converges quickly.

Results and Discussion. All calculations were performed for a hypothetical machine which mass yield of distillate is 1 kg/s. Thus, all values of power and areas can be considered as appanage. The heat transfer coefficient was calculated by the integral relations given in [3, 4], and average value of it is 2.45 kW/(m²·K).

In fig. 3 the dependence of power and excess of power of the compressor on a heat exchange surface area is shown.

From Fig. 3 it is evident that the necessary compressor power significantly decreases at increase of a heat exchange surface area of evaporator-condenser. The optimum ratio between these parameters can be found based on the economic calculation.

Specific energy consumption on production of one cubic meter of desalinated water is bound to a specific power with the ratio

$$W = 3.6 \cdot N,$$

where W — specific consumption of the electric power, (kW·h)/m³;

N — specific power, kW/kg.

In Fig. 4 the dependence of specific power consumption of W on temperature of seawater boiling at two various values of heat-transfer coefficient in evaporator-condenser is shown.

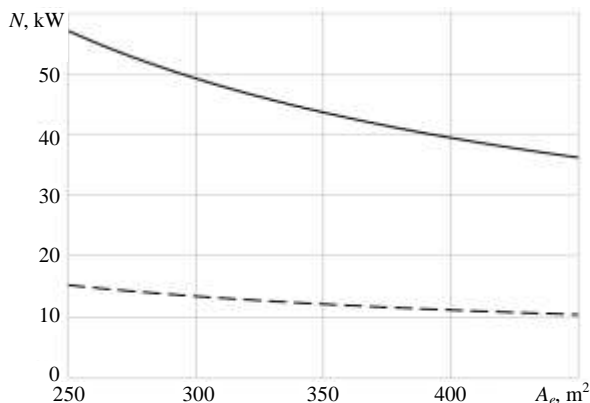


Fig. 3. Dependences of necessary power of the compressor («—») and excess of a thermal power («---») on a surface area of heat exchange of evaporator-condenser

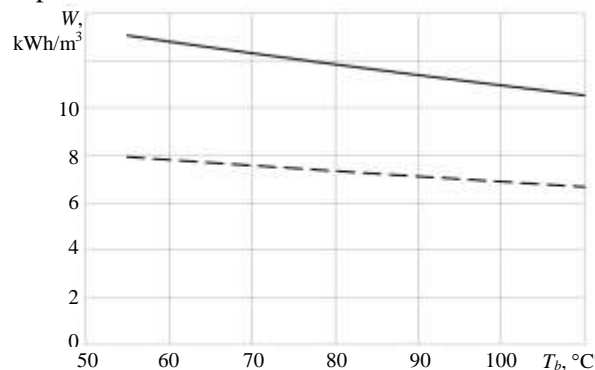


Fig. 4. Dependence of specific power consumption on temperature of seawater boiling at two various values of heat-transfer coefficient in evaporator-condenser:
«—» — $U_e = 2,5 \text{ kW}/(\text{m}^2 \cdot \text{K})$;
«---» — $U_e = 5,0 \text{ kW}/(\text{m}^2 \cdot \text{K})$

From Fig. 4 it is evident that at increasing of boiling temperature the specific energy consumption and the surplus of power lost are simultaneously decrease. However, at increasing of boiling temperature above 70 °C the speed of adjournment of a scum on device walls sharply increases that leads to growth of operational expenses.

The system of preliminary water heating consisting of two heat exchangers is offered.

The energy balance for the smaller heat exchanger utilizing heat of distillate can be calculated from the equation

$$Q_d = G_d c_{p1} (T_d - T_b) = G_f c_{p2} (T_b - T_x); \tag{12}$$

in turn, for the second heat exchanger utilizing heat of a brine and distillate can be calculated from the equation

$$Q_b = G_b c_{p3} (T_b - T_{out}) + G_d c_{p4} (T_b - T_{out}) = G_{cw} c_{p5} (T_x - T_{cw}). \tag{13}$$

The T_x we evaluate of (12)

$$T_x = T_b - (T_d - T_b) \frac{G_d c_{p1}}{G_f c_{p2}}$$

and substitute in (13).

When all temperatures at input and output for each heat exchanger are determined, it is possible to calculate the necessary areas of surfaces of heat exchange. We will calculate log mean temperature pressures according to the following ratios:

$$\Delta T_d^{lm} = \frac{(T_d - T_b) - (T_b - T_x)}{\ln \frac{T_d - T_b}{T_b - T_x}}, \quad \Delta T_b^{lm} = \frac{(T_b - T_x) - (T_{out} - T_{cw})}{\ln \frac{T_b - T_x}{T_{out} - T_{cw}}}. \tag{14}$$

The necessary surfaces areas of heat exchange are calculated by the formulas:

$$A_d = \frac{Q_d}{U_d \Delta T_d^{lm}}, \tag{15}$$

$$A_b = \frac{Q_b}{U_b \Delta T_b^{lm}}. \tag{16}$$

The equations (12...16) give the only solution in whole studied range of temperatures and provide heating of seawater to temperature T_b .

In Fig. 6 the dependence of the necessary surfaces areas of heat exchange on boiling temperature is shown T_b .

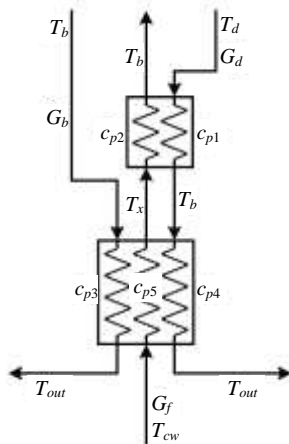


Fig. 5. The scheme of plug-in of heat exchangers of seawater preliminary heating with the indication of temperatures and mass expenses of water

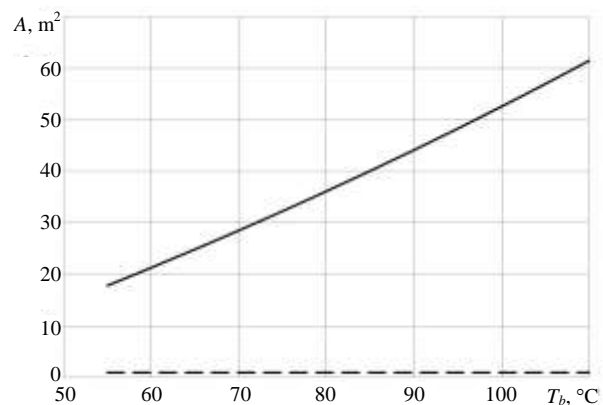


Fig. 6. The necessary surfaces areas of heat exchange for preliminary heaters of seawater:
«—» — A_b ; «---» — A_d

From the plot it is visible that the areas of surfaces A_d for preliminary heat exchangers are 10 times less than the areas of surfaces of evaporator-condenser A_b . The area A_b is greatly rises at rise of boiling temperature T_b . Therefore, in economic calculation the main attention needs to be paid to the cost of evaporator-condenser.

Criterion of technical and economic optimization. As criterion of comparison the annual given costs are accepted [8, 9]:

$$C = e_n C_c + C_{op}, \quad (17)$$

where e_n — normative rate of return (assumed equal to 0.12);

C_c — capitalized expenses;

C_{op} — annual expenditure.

Annual expenditure C_{op} may be calculated by the formula

$$C_{op} = C_{el.} + C_{clean.} + C_{am.} + C_{expl.}, \quad (18)$$

where $C_{el.}$ — annual power expenses;

$C_{clean.}$ — costs of water purification and transfer of salts to a soluble state for prevention of salts loss on the heating surfaces (we accept equal 0.3 USD/m³ of initial water);

$C_{am.}$ — annual costs for depreciation of capital investments and maintenance estimated at 10...20 % of depreciation expense;

$C_{expl.}$ — operating expenses.

Annual energy costs are calculated by the formula:

$$C_{el.} = A_{el.en.} P_{el}, \quad (19)$$

where P_{el} — national electricity cost (for UAE $P_{el} = 0.04$ USD/(kW·h));

$A_{el.en.}$ — annual energy consumption, kWh.

Annual costs on depreciation of capital investment and maintenance calculated by the formula

$$C_{am.} = p_a C_c + C_m = p_a C_c + 0.1 p_a C_c = 1.1 p_a C_c, \quad (20)$$

where p_a — depreciation rate (assumed equal to 0.06).

C_m — maintenance costs.

Maintenance costs are determined according to the ratio

$$C_{expl.} = C_{lab.} + C_{oth.},$$

where $C_{lab.}$ — annual salary of the staff;

$C_{oth.}$ — other manufacturing expenses.

The value of manufacturing expenses $C_{oth.}$ is 20...30 % total costs for depreciation, maintenance works and wages, i.e. operating costs are in accordance with the ratio:

$$C_{expl.} = C_{lab.} + 0.2(p_a C_c + 0.1 p_a C_c + C_{lab.}) = 1.2 C_{lab.} + 0.22 p_a C_c. \quad (21)$$

Substituting the values of all components in the expression (18), we obtain the formula for annual operating costs:

$$C_{op} = C_{el.} + C_{clean.} + 1.1 p_a C_c + 1.2 C_{lab.} + 0.22 p_a C_c = C_{el.} + 1.32 p_a C_c + 1.2 C_{lab.}. \quad (22)$$

The expression for the given expenses can be written as

$$\begin{aligned} C &= e_n C_c + C_{el.} + C_{clean.} + 1.32 p_a C_c + 1.2 C_{lab.} = C_c (e_n + 1.32 p_a) + C_{el.} + C_{clean.} + 1.2 C_{lab.} = \\ &= 0.1992 C_c + C_{el.} + C_{clean.} + 1.2 C_{lab.}. \end{aligned} \quad (23)$$

Then, the final expression for the variable part of given expenses takes the form:

$$C = 0.1992 C_c + C_{el}. \quad (24)$$

The needs for the electric power are determined under condition of installation operating within 22 hours a day and 360 days within a year. During the choice of the equipment was accepted that productivity of installation makes 25 m³ per day.

Capital expenditure consists, mainly, of the cost of evaporator-condenser, preliminary heat exchangers and the compressor.

As evaporator-condenser and preliminary heaters of seawater it is expedient to use the lamellar heat exchangers differing in high coefficient of a heat transfer. The analysis of cost of heat exchangers shows that in approximate calculation it is possible to accept their cost of directly proportional to surface area of heat exchange.

For typical in the studied range heat exchanger Ridan NN 41 the surface area of heat exchange is 217.35 m² at the price of 4806 USD [10]. Then the total cost of heat exchangers can be estimated using the formula

$$C_{h.e.} = 22.11 (A_e + A_b + A_d).$$

Compressor cost $C_{compr.}$ can be averagely set to proportional power of electric engine. According to [11], $C_{compr.} = 645 \cdot N_c$.

Total capital expenditure will be

$$C_c = C_{h.e.} + C_{compr.}$$

The given annual costs (17) have been calculated taking into account the power of the compressor and the areas of heat exchange surfaces obtained higher. Results of calculation of the specified cost for installation with a productivity of 1 kg/s of desalinated water are presented in Fig. 7.

The analysis of the plots shows that the minimum of the given capital expenditure is reached at the specific area of evaporator-condenser of 570 m². The electricity cost continuously drops at increase of surface of heat exchange of evaporator-condenser A_e . Total annual costs decrease up to value $A_e = 1000$ m². But at such great areas the heat exchangers have the large weight and dimensions and therefore A_e needs to be limited accordingly to transportation cost.

Conclusions. Numerical modeling has shown that in systems with adiabatic compression of steam there are losses of power which are 26...29 % of the general expenses of energy. These losses can be reduced when using advanced processes of compression of vapour along the line of saturation, for example — at injection of water in the compressor.

Decrease in prime cost of desalinated water can be reached mainly due to increase of efficiency of the compressor and increase of a heat transfer coefficient of evaporator-condenser.

With the given productivity of desalination installation, the optimum parameters of the compressor (from the economic point of view) and evaporator-condenser can be found.

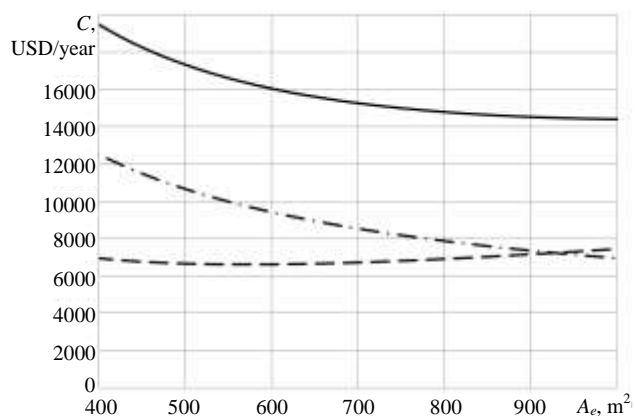


Fig. 7. The given annual costs as function of the surface area of heat exchange of evaporator-condenser:
«—» — total annual costs;
«---» — reduced capital costs;
«-•-» — the annual cost of electricity

Література

1. Escobar, I.C. Sustainable water for the future: Water recycling versus desalination / I.C. Escobar, A.I. Schäfer. — Amsterdam; Boston: Elsevier Science, 2010. — 416 p.
2. Копылов, А.С. Водоподготовка в энергетике / А.С. Копылов, В.М. Лавыгин, В.Ф. Очков. — 2-е изд., стер. — М.: Издат. дом МЭИ, 2006. — 309 с.
3. El-Dessouky, H.T. Fundamentals of salt water desalination / H.T. El-Dessouky, H.M. Ettouney. — Amsterdam: Elsevier Science, 2002. — 670 p.
4. Al-Juwayhel, F. Analysis of single-effect evaporator desalination systems combined with vapor compression heat pumps / F. Al-Juwayhel, H. El-Dessouky, H. Ettouney // *Desalination*. — 1997. — Vol. 114, Issue 3. — PP. 253–275.
5. Lara, J.R. Advanced mechanical vapor-compression desalination system / J.R. Lara, Omorinsola Osunsan, M.T. Holtzaple // *Desalination, Trends and Technologies* / ed. by M. Schorr. — Rijeka: InTech, 2011. — PP. 129–148.
6. Lara, J.R. An investigation of high operating temperatures in mechanical vapor-compression desalination / J.R. Lara, G. Noyes, M.T. Holtzaple // *Desalination*. — 2008. — Vol. 227, Issues 1–3. — PP. 217–232.
7. Черкасский, В.М. Насосы, вентиляторы, компрессоры / В.М. Черкасский. — М.: Энергоатомиздат, 1984. — 416 с.
8. Беренс, В. Руководство по подготовке промышленных технико-экономических исследований: монография / В. Беренс, П.М. Хавранек; пер. с англ. А.О. Гридин и др.; науч.ред. Р.П. Вчерашний и др. - новое перераб. и доп. изд. — М.: Интерэксперт, 1995. — 343 с.
9. Preparation of a Feasibility Study for New Nuclear Power Projects / International Atomic Energy Agency. — Vienna: IAEA, 2014. — 125 p.
10. Типовые цены на Теплообменники пластинчатые [Электронный ресурс] / ТеплоПрофи: Комплексные поставки инженерного оборудования по России и СНГ. — Режим доступа: <http://www.teploprofi.com/ceni/> (Дата звернення: 25.05.2016).
11. Оборудование [Электронный ресурс] / ERSTEVAK Ltd. — Режим доступа: <http://www.erstvak.com/equipment/> (Дата звернення: 24.05.2016).

References

1. Escobar, I.C., & Schäfer, A.I. (2010). *Sustainable Water for the Future: Water Recycling Versus Desalination*. Amsterdam; Boston: Elsevier Science.
2. Kopylov, A.S., Lavygin, V.M., & Ochkov, V.F. (2006). *Water Treatment in Power Engineering* (2nd Ed.). Moscow: MEI.
3. El-Dessouky, H.T., & Ettouney, H.M. (2002). *Fundamentals of Salt Water Desalination*. Amsterdam: Elsevier Science.
4. Al-Juwayhel, F., El-Dessouky, H., & Ettouney, H. (1997). Analysis of single-effect evaporator desalination systems combined with vapor compression heat pumps. *Desalination*, 114(3), 253-275. DOI:10.1016/S0011-9164(98)00017-4
5. Lara, J.R., Omorinsola Osunsan, Holtzaple, M.T. (2011). Advanced mechanical vapor-compression desalination system. In M. Schorr (Ed.), *Desalination, Trends and Technologies* (pp. 129–148). Rijeka: InTech. DOI:10.5772/14711
6. Lara, J.R., Noyes, G., & Holtzaple, M.T. (2008). An investigation of high operating temperatures in mechanical vapor-compression desalination. *Desalination*, 227(1–3), 217–232. DOI:10.1016/j.desal.2007.06.027
7. Cherkassky, V.M. (1985). *Pumps, Fans, Compressors*. Moscow: Mir.
8. Behrens, W., & Hawranek, P.M. (1991). *Manual for the Preparation of Industrial Feasibility Studies*. Vienna: UNIDO.
9. International Atomic Energy Agency. (2014). *Preparation of a Feasibility Study for New Nuclear Power Projects*. Vienna: IAEA.
10. TeploProfi. (n.d.). *Prices for Lamella Heat-Exchangers*. Retrieved from <http://www.teploprofi.com/ceni/>
11. ERSTEVAK Ltd. (n.d.). *Equipment*. Retrieved from <http://www.erstvak.com/equipment/>

Received May 20, 2016

Accepted July 7, 2016

UDC 621.182.11.001.57

V.G. Ahrameev, PhD

Odessa National Polytechnic University, 1 Shevchenko Ave., 65044 Odessa, Ukraine; e-mail: ahvitalchik@mail.ru

RESEARCH OF THE SEDIMENT FORMATION INTENSITY AT THE RUN-AROUND COOLING SYSTEMS EQUIPMENT WITH WATER COOLING TOWERS

В.Г. Ахрамеев. Дослідження інтенсивності утворення відкладень на обладнанні оборотних систем охолодження з градирнями. Для оборотних систем охолодження найбільш небезпечні забруднення твердими мінеральними відкладеннями, що утворюються внаслідок кристалізації малорозчинних неорганічних солей при переході циркуляційної води в пересичений стан. **Мета:** Метою роботи є дослідження інтенсивності відкладень кристалів важкорозчинних солей з пересиченою циркуляційної води на поверхнях нагріву випарного охолодження і конденсаторів в оборотних системах охолодження енергоустановок з градирнями. **Матеріали і методи:** Методика проведених досліджень полягала у вимірюванні маси і величини важкорозчинних кристалів в циркуляційній воді і їх відкладень на теплообмінній поверхні конденсатора і випарній поверхні градирні. Вихідна вода для експерименту була відібрана з р. Стир. Експериментальні дослідження проводилися на масштабній моделі оборотної системи охолодження. Для вивчення характеру процесів взаємодії частинок твердої фази між собою у вихідній і циркуляційній воді було використано метод дисперсійного аналізу частинок грубодисперсної фази в оптично сканованому шарі води. **Результати:** Проведено експериментальне дослідження інтенсивності відкладень кристалів важкорозчинних солей з пересиченою циркуляційної води на поверхнях нагріву випарного охолодження і конденсаторів в оборотних системах охолодження енергоустановок з градирнями. Визначено, що в міру охолодження циркуляційної води при її стиканні вздовж охолоджуючої поверхні і аерації зустрічним потоком пароповітряної маси відбувається збільшення солевмісту потоку і зростання маси кристалів карбонатних солей, що виділилися; в кінцевому підсумку це призводить до утворення пухких відкладень на необігріваних зрошуючих поверхнях градирень. Виділення центрів кристалізації важкорозчинних карбонатних солей при їх нагріванні в теплообмінних трубках конденсатора відбувається за рахунок термічної дисоціації добре розчинних бікарбонатних солей в важкорозчинні карбонатні солі з наступним відкладенням їх на поверхні трубок, що нагрівається.

Ключові слова: циркуляційна вода, оборотна система охолодження, відкладення.

V.G. Ahrameev. Research of the sediment formation intensity at the run-around cooling systems equipment with water cooling towers. For circulating cooling systems, the solid mineral sediments formed as a result of crystallization of sparingly soluble inorganic salts in the transition of circulating water in the supersaturated state are the most dangerous. **Aim:** The aim of this research is to study the intensity of sediments of hardly soluble salts crystals on the surfaces of the heating of evaporative cooling equipment and condensers from supersaturated circulating water in the circulating cooling systems of power plants with water cooling towers. **Materials and Methods:** The methodology of the research was to study the mass and size of the hardly soluble crystals in circulation water and sediments on heat exchange surfaces of the condenser and the evaporator surface of the water cooling tower. Source water for the experiment was selected from Styr river. Experimental studies were carried out at the installation of a scale model of circulation cooling system. To study the nature of the interaction of the solid phase particles with each other in the starting water and the circulating used the method of dispersion analysis of coarse phase particles in the optically scanned water layer. **Results:** The study the intensity of sediments sparingly of soluble salt crystal on the surfaces of the heating of evaporative cooling equipment and condensers from supersaturated circulating water in the circulating cooling systems of power plants with water cooling towers were held. It has been determined that as the circulation water is cooling, with its runoff along the cooling surface and aeration by counter-steam mass flow there are salinity increase and increase the weight of precipitated carbonate salts crystals, which ultimately leads to the formation of loose sediments in the unheated watering surfaces of water cooling towers. Allocation of crystallization centers of sparingly soluble carbonate salt when it is heated in the heat exchange condenser tubes is due to the thermal dissociation of good soluble bicarbonate salts into sparingly soluble carbonate salts and then sediment at the heated tubes surface.

Keywords: circulating water, circulating cooling system, sediments.

Introduction. For circulating cooling systems, the solid mineral sediments formed as a result of crystallization of sparingly soluble inorganic salts in the transition of circulating water in the supersaturated state are the most dangerous. However, a visual inspection of water cooling towers and condensers in Ukrainian power plants shows significant sediments and drifts at the heat exchange surfaces of cooled condensers as well as at the evaporator surfaces of water cooling towers.

Many authors paid attention to the study of the formation sediment process at the heat exchange tubes. Most authors examined the sediments in once-through systems, exploring the water passing through the heat exchanger once [1...5].

DOI 10.15276/opu.2.49.2016.09

© 2016 The Authors. This is an open access article under the CC BY license (<http://creativecommons.org/licenses/by/4.0/>).

Briançon [3] and Andritsos [6] considered mainly the dependence of kinetics and mechanisms of sediments, depending on flow multiplicity of the heat exchange tubes surface, ribbing, and the recycling of the circulating water. Also, Andritsos shows that during formation of sediments on rough surfaces the turbulent transport of particles to the heat surface increases and thus decreases the induction period of the process.

Kishnevsky and Chichenin [7] studied the sediments on heat exchange surfaces by using scale inhibitors and without them.

Sediment formation is a complex process involving water supersaturating for salts with nucleation, their transport to the heat exchange surface with the possible sediment. To date, there is no reliable theory of thermodynamic prediction of carbonate salts sediments process on the heat exchange surface. Therefore, most of the known studies based on observational criteria. They allow calculate the probability of formation of sediment on heat exchange surfaces of condensers, but do not consider other types of heat exchangers [8, 9].

Practically in all previously published studies in the preparation of the material and salt balance of circulating cooling systems, it was assumed that most of the sediments are crystallized at the heat exchange tubes of condensers

In the works of Kishnevskiy [10] and Garrels [11] there is a studying method of water and chemical mode of circulating cooling systems at the scale model, as well as the possible criterion of sediment formation (Δ_{Ca-Alk}) is offered, it is assumed that all the solid phase is deposited on the heat exchange surface condenser.

Chichenin [12] proposed a method of the study of the intensity sediments at the coupons without heating the coolant made from the materials typical for heat exchangers in which the heating of coolant is present. At the same time overlooked the processes occurring in the water cooling tower.

In the literature and in the open press author does not found researches aimed at understanding the mechanisms of calcium carbonate crystals sediments on the cooling surface of the water cooling towers and the pipeline surfaces of the run-around cooling systems.

Drifts and sediments at the evaporator surface reduce the operation efficiency of the cooling towers, and, moreover, with significant sediments threaten by major accidents related to the collapse of the irrigation surface.

Thus, study the intensity of sediments at the evaporation part of the water cooling tower and the distribution ratio of sediments mass between the condenser surface and cooling tower surfaces is actually.

The aim of this research is to study the intensity of sediments of hardly soluble salts crystals on the surfaces of the heating of evaporative cooling equipment and condensers from supersaturated circulating water in the circulating cooling systems of power plants with water cooling towers.

To achieve the aim is needed solve the following problems:

— Improve the methodology of research of intensity of sparingly soluble salts sediments on the surface of the cooling tower and evaporative heating surface of condenser.

— Improve the large scale stand of circulation cooling system.

— Carry out the experimental studies at the laboratory stand of large scale cooling system.

Materials and Methods. Formation of carbonate calcium CaCO_3 sediments in the cooling tower and the condenser takes place in different thermal and hydraulic conditions:

— in a condenser — at heating of circulating water with the release of CaCO_3 on the heated surface;

— in a water cooling tower — during cooling water by increasing the salt content on unheated surface.

Formation of crystallization centers in the circulation water during evaporative cooling in water tower occurs at the “liquid / water-steam mixture” interface.

Allocation of crystallization centers of sparingly soluble carbonate salts during heating of circulating water in the heat exchange tubes of the condenser is due to the thermal decomposition of readily soluble bicarbonate salts with the formation of dense and poorly soluble carbonate salts, and their subsequent sediments onto the heated surface of the tubes.

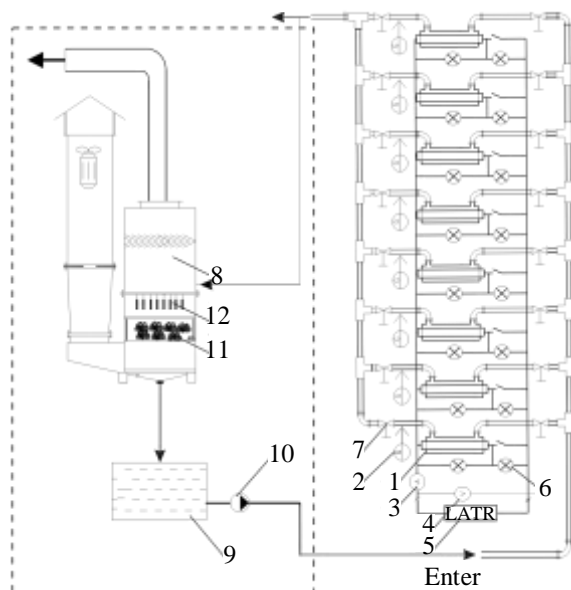


Fig. 1. The model of run-around cooling system:
1 — working cell (heat exchanger with external flow), 2 — flowmeter, 3 — ammeter, 4 — voltmeter, 5 — laboratory transformer (LATR), 6 — indicator, 7 — valve, 8 — water cooling tower, 9 — capacity, 10 — pump, 11 — “crossed wheels” nozzle, 12 — coupons

tower. These elements are designed to compare the growth of sediments in the cooling tower and the condenser on the same materials. Coupons were mounted in the water cooling tower directly under the stream of circulating water dispersed by the nozzle, above the “crossed wheels” nozzle and parallel to air flow.

To control the sediments on the evaporator of the water cooling tower from the nozzle layer were selected and marked 12 elements, connected by a fishing-line.

In operation, the experiment was interrupted after 40 and 100 hours for extraction of nozzle control elements and coupons. Extracted from the installation control elements were placed in a drying oven until dry, then the check weighing held. Detailed sample processing method described in [12].

Control of deposits on the tubes, coupons and cross-disks conducted as weight gain. For elements made of LAMsh, it takes into account the effect of minor corrosion. Kinetics of growth of sediments was investigated in the condenser tubes, coupons and nozzles in a cooling tower.

Characteristics and composition of the source water taken from river Styra the following: pH = 7.4, evaporation rate $K_e = 1$, water alkalinity $A_w = 1 \text{ mgEq/dm}^3$, water hardness $H_w = 1.9 \text{ mgEq/dm}^3$; $[\text{Cl}^-] = 0.7 \text{ mgEq/dm}^3$, $[\text{SO}_4^{2-}] = 0.95 \text{ mgEq/dm}^3$.

In the pilot study the evaporation rate of the circulating water was maintained at 2, and pH = 8.

Every 12 hours there was sampled for the study of physical and chemical composition of water and the amount of sediments on the controlled areas of the experimental installation at given water velocity and air flow. Humidity, temperature of atmosphere air and air at the outlet of the cooling tower controlled using psychrometric analysis.

To study the nature of the interaction processes between the particles of the solid phase in source and circulating water we used the analysis-of-variance method for coarse phase particles in optically scanned water layer, described in detail in [13].

Results. The obtained experimental data for determining the mass of sediment on the coupons, tubes and crossed disks are shown in Tables 1 and 2.

In the process of circulating water cooling in the cooling tower during its run-off along the cooling surface and aeration with counter vapor flow (saturation with CO_2 as result) flow salinity and mass of carbonate salts crystals are increasing. This eventually leads to the formation of loose sediments in the unheated watering surfaces of cooling towers.

The methodology of the research was to study the mass and size of sparingly soluble crystals in circulation water and sediments on heat exchange surfaces of the condenser and the evaporator surface of the water cooling tower. Experimental studies were carried out on a large-scale installation of the run-around cooling systems model (Fig. 1).

Detailed description of the stand is given in [7]. The design of water cooling tower and working cell is shown in [12].

The procedure of the experiment was as follows.

Previously prepared according the procedure described in [12], LAMsh brass tubes installed in the working cell 1 (Fig. 1).

Moreover, the flat elements (coupons) of $70 \times 10 \times 2 \text{ mm}$ size which are made from LAMsh 77-2-0.05 brass material added to the water cooling

Table 1

Characteristics of the heat exchange surfaces

Data	Nozzle	Tubes	Coupons
Quantity, pcs	350	8	3
Area S , m^2	0.4613	0.02512	0.0039

Table 2

Mass of sediment on heat exchange surfaces

Time, hour	Sediments mass, g		
	Nozzles	Tubes	Coupons
40	3.32136	0.7536	0.000288
100	4.1517	1.1304	0.00036
200	6.9195	1.5072	0.00048

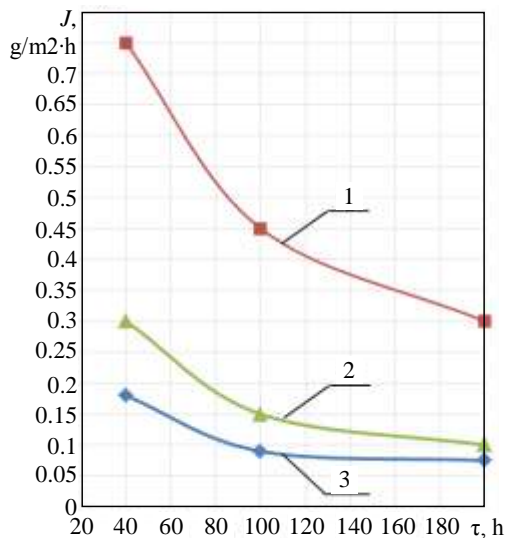


Fig. 2. Dependence of the intensity of sediment on the heat exchange surfaces of water cooling towers and condenser: 1 — LAMsh brass tube, 2 — LAMsh brass coupons, 3 — polyethylene nozzles

Visual inspection shows that the sediments in the water cooling towers are loose; moreover, the adhesion between the sediments and the heat exchange surfaces is flimsy.

Dependences of the intensity of sediments on the heating surfaces of the condenser, nozzles and control coupons considering the density of carbonate salts are shown in Fig. 2.

The intensity of sediments on the heated heat exchanger surface of the condenser tubes was $0.75 \text{ mg}/(\text{m}^2 \cdot \text{h})$ after 40 hours after the start of the experiment, and $0.30 \text{ mg}/(\text{m}^2 \cdot \text{h})$ — after 200 hours. The intensity of sediments on the unheated surface in the water cooling tower for LAMsh brass coupons was 0.30 and $0.10 \text{ mg}/(\text{m}^2 \cdot \text{h})$, respectively.

Thus, the intensity of sediment in the condenser is different from the intensity in the water cooling tower in more than two times, provided that they are made of the same material (LAMsh).

The intensity of sediments on the unheated surface in the water cooling tower on the polyethylene nozzles was $0.170 \text{ mg}/(\text{m}^2 \cdot \text{h})$ at the beginning of the experiment,

and $0.07 \text{ mg}/(\text{m}^2 \cdot \text{h})$ at the end. This is a few less than for LAMsh brass coupons, but the difference is not so significant.

Conclusions. The conducted research lead to the conclusion that the processes of formation of carbonate salt sediments in the water cooling tower and in the condenser determined by the heat-hydraulic conditions.

The obtained experimental data indicate that the intensity of sediments on the heat exchanger surface of the condenser tubes is more than two times higher than on the control coupons of irrigated surface of the water cooling towers made of LAMsh brass. Furthermore, it is shown that the intensity of sediments on unheated surface of LAMsh brass coupons is higher than on the polyethylene nozzles by 30...40 %.

Література

1. Исследование дисперсного состава и характеристик твердофазных частиц в циркуляционной воде оборотных систем охлаждения / А.Б. Гуляенко, Е.В. Кишневский, О.М. Малиновский, В.Ф. Очков // Пр. Одес. політехн. ун-ту. — 2010. — Вип. 1(33)–2(34). — С. 70–75.
2. Кишневский, В.А. Предотвращение коррозии паровых калориферов и их конденсатопроводов / В.А. Кишневский, А.П. Боровский, Б.Н. Шукайло // Пр. Одес. політехн. ун-ту. — 2005. — Вип. 2(24). — С. 90–95.

3. Неведров, А.В. Сравнительный анализ физических методов обработки воды для уменьшения накипеобразования / А.В. Неведров, Г.В. Ушаков // Теплоэнергетика. — 2003. — № 11. — С. 62–64.
4. Calcium carbonate deposit formation under isothermal conditions / N. Andritsos, M. Kontopoulou, A.J. Karabelas, P.G. Koutsoukos // *The Canadian Journal of Chemical Engineering*. — 1996. — Vol. 74, Issue 6. — PP. 911–919.
5. Kazi, S.N. Fouling and fouling mitigation on heated metal surfaces / S.N. Kazi, G.G. Duffy, X.D. Chen // *Desalination*. — 2012. — Vol. 288. — PP. 126–134.
6. Andritsos, N. Morphology and structure of CaCO₃ scale layers formed under isothermal flow conditions / N. Andritsos, A.J. Karabelas, P.G. Koutsoukos // *Langmuir*. — 1997. — Vol. 13, Issue 10. — PP. 2873–2879.
7. Briançon, S. Modelling of crystalline layer growth using kinetic data obtained from suspension crystallization / S. Briançon, D. Colson, J.P. Klein // *Chemical Engineering Journal*. — 1998. — Vol. 70, Issue 1. — PP. 55–64.
8. Kostoglou, M. Comprehensive modeling of precipitation and fouling in turbulent pipe flow / M. Kostoglou, A.J. Karabelas // *Industrial & Engineering Chemistry Research*. — 1998. — Vol. 37, Issue 4. — PP. 1536–1550.
9. Karabelas, A.J. Scale formation in tubular heat exchangers — research priorities / A.J. Karabelas // *International Journal of Thermal Sciences*. — 2002. — Vol. 41, Issue 7. — PP. 682–692.
10. Кишневский, В.А. Исследование процессов карбонатных отложений на теплообменных поверхностях конденсаторов / В.А. Кишневский, В.В. Чиченин // *Восточно-Европейский журнал передовых технологий*. — 2014. — № 3/8 (69). — С. 52–58.
11. Garrels, R.M. Solutions, minerals, and equilibria / R.M. Garrels, C.L. Christ. — Boston: Jones and Bartlett, 1990. — 450 p.
12. Исследование скорости коррозии и накопления отложений при упаривании циркуляционной воды в лабораторных условиях / В.В. Чиченин, В.А. Кишневский, А.С. Грицаенко и др. // *Восточно-Европейский журнал передовых технологий*. — 2015. — № 5/8 (77). — С. 14–20. DOI:10.15587/1729-4061.2015.51205
13. Кишневский, В.А. Методика расчета водно-химического режима комплексной оборотной системы охлаждения с рециркуляцией / В.А. Кишневский, В.В. Чиченин, И.Д. Шуляк // *Восточно-Европейский журнал передовых технологий*. — 2013. — № 6/8 (66). — С. 10–14.

References

1. Guliyenko, A.B., Kishnevsky, E.V., Maleenovsky, O.M., & Ochkov, V.F. (2010). Research of dispersion composition and characteristics of solid-phase particles in circulation water of the circulating systems of cooling. *Odes'kyi Politechnichniy Universytet. Pratsi*, 1–2, 70–75.
2. Kishnevsky, V.A., Borovsky, O.P., & Shukaylo, B.N. (2005). Prevention of corrosion in steam air heaters and their condensate pipes. *Odes'kyi Politechnichniy Universytet. Pratsi*, 2, 90–95.
3. Nevedrov, A.V., & Ushakov, G.V. (2003). A comparative analysis of physical methods for water treatment to reduce scale formation. *Thermal Engineering*, 50(11), 944–947.
4. Andritsos, N., Kontopoulou, M., Karabelas, A.J., & Koutsoukos, P.G. (1996). Calcium carbonate deposit formation under isothermal conditions. *The Canadian Journal of Chemical Engineering*, 74(6), 911–919. DOI:10.1002/cjce.5450740614
5. Kazi, S.N., Duffy, G.G., & Chen, X.D. (2012). Fouling and fouling mitigation on heated metal surfaces. *Desalination*, 288, 126–134. DOI:10.1016/j.desal.2011.12.022
6. Andritsos, N., Karabelas, A.J., & Koutsoukos, P.G. (1997). Morphology and structure of CaCO₃ scale layers formed under isothermal flow conditions. *Langmuir*, 13(10), 2873–2879. DOI:10.1021/la960960s
7. Briançon, S., Colson, D., & Klein, J.P. (1998). Modelling of crystalline layer growth using kinetic data obtained from suspension crystallization. *Chemical Engineering Journal*, 70(1), 55–64. DOI:10.1016/S1385-8947(98)00080-1
8. Kostoglou, M., & Karabelas, A.J. (1998). Comprehensive modeling of precipitation and fouling in turbulent pipe flow. *Industrial & Engineering Chemistry Research*, 37(4), 1536–1550. DOI: 10.1021/ie970559g

9. Karabelas, A.J. (2002). Scale formation in tubular heat exchangers — research priorities. *International Journal of Thermal Sciences*, 41(7), 682–692. DOI:10.1016/S1290-0729(02)01363-7
10. Kishnevsky, V., & Chichenin, V. (2014). Study of carbonate deposits on heat exchange surfaces of condensers. *Eastern-European Journal of Enterprise Technologies*, 3(8), 52–58.
11. Garrels, R.M., & Christ, C.L. (1990). *Solutions, Minerals, and Equilibria*. Boston: Jones and Bartlett.
12. Chichenin, V., Kishnevskiy, V., Hrytsaienko, A., Ahrameev, V., & Shuliak, I. (2015). Study of corrosion rate and accumulation of deposits under circulating water concentration in bench experiments. *Eastern-European Journal of Enterprise Technologies*, 5(8), 14–20. DOI:10.15587/1729-4061.2015.51205
13. Kishnevskiy, V., Chichenin, V., & Shulyak, I. (2013). Method of calculation of water chemistry of the integrated circulation cooling system with recirculation. *Eastern-European Journal of Enterprise Technologies*, 6(8), 10–14.

Received June 10, 2016

Accepted July 22, 2016

COMPUTER AND INFORMATION NETWORKS AND SYSTEMS.

MANUFACTURING AUTOMATION

КОМП'ЮТЕРНІ Й ІНФОРМАЦІЙНІ МЕРЕЖІ І СИСТЕМИ.

АВТОМАТИЗАЦІЯ ВИРОБНИЦТВА

UDC 004.932:004.052.42

A.A. Kobozeva, DSc, Prof.,

S.M. Grigorenko

Odessa National Polytechnic University, 1 Shevchenko Ave., 65044 Odessa, Ukraine; e-mail: alla_kobozeva@ukr.net

NEW APPROACH DEVELOPMENT FOR SOLUTION OF CLONING RESULTS DETECTION PROBLEM IN LOSSY SAVED DIGITAL IMAGE

A.A. Kobozeva, S.M. Grigorenko. Розвиток нового підходу до вирішення питання виявлення результатів клонування в цифровому зображенні, збереженому із втратами. Розглянуто питання виявлення результатів фальсифікації цифрового зображення, здійсненої шляхом клонування — одного з найбільш часто використовуваних програмних інструментів, реалізованого у всіх сучасних графічних редакторах. *Мета:* Метою роботи є подальший розвиток підходу до вирішення питання виявлення клонування в умовах збереження клонованого зображення у форматі із втратами, запропонованому авторами раніше. *Матеріали і методи:* Запропонований підхід засновано на врахуванні малості зміни об'єму циліндричного тіла з твірною, паралельною осі OZ , обмеженого зверху графіком інтерполюючої функції для матриці яскравості аналізованого зображення, знизу — площиною XOY , в процесі стиснення. *Результати:* Проведено адаптацію запропонованого підходу до умов стиснення клонованого зображення з довільним коефіцієнтом якості (коефіцієнтом стиснення). Продемонстровано можливість використання запропонованого підходу в умовах стиснення клонованого зображення відповідно до алгоритмів, що відрізняються від стандарту JPEG: JPEG2000, стиснення з використанням малорангових апроксимацій матриці (блоків матриці) зображення. Наведено результати обчислювального експерименту. Показано, що розроблений підхід може бути використано для виявлення результатів клонування в цифровому відео в умовах подальшого після клонування стиснення із втратами.

Ключові слова: цифрове зображення, виявлення клонування, стиснення з втратами, малорангова апроксимація.

A.A. Kobozeva, S.M. Grigorenko. New approach development for solution of cloning results detection problem in lossy saved digital image. The problem of detection of the digital image falsification results performed by cloning is considered – one of the most often used program tools implemented in all modern graphic editors. *Aim:* The aim of the work is further development of approach to the solution of a cloning detection problem having the cloned image saved in a lossy format, offered by authors earlier. *Materials and Methods:* Further development of a new approach to the solution of a problem of cloning results detection in the digital image is presented. Approach is based on the accounting of small changes of cylindrical body volume with the generatrix, that is parallel to the OZ axis, bounded above by the interpolating function plot for a matrix of brightness of the analyzed image, and bounded below by the XOY plane, during the compression process. *Results:* Adaptation of the offered approach to conditions of the cloned image compression with the arbitrary factor of compression quality is carried out (compression ratio). The approach solvency in the conditions of the cloned image compression according to the algorithms different from the JPEG standard is shown: JPEG2000, compression with use of low-rank approximations of the image matrix (matrix blocks). The results of computational experiment are given. It is shown that the developed approach can be used to detect the results of cloning in digital video in the conditions of lossy compression after cloning process.

Keywords: digital image, cloning detection, lossy compression, low-rank approximation.

Introduction. One of the program tools implemented in all modern graphic editors (Adobe Photoshop, Gimp, etc.) which are most often used for falsifications of the digital images (DI) is the

DOI 10.15276/opu.2.49.2016.10

© 2016 The Authors. This is an open access article under the CC BY license (<http://creativecommons.org/licenses/by/4.0/>).

cloning at which the part of DI called a prototype is copied and moves to another area of the same image, replacing with itself his original part and forming a clone. The cloning is used in case when an “undesirable” object is removed from the image, the existing objects are duplicated, their location changes within the image scene.

Taking into account the modern level of information technologies development, the implemented capabilities of graphic editors the changes on DI, in particular cloning, can be made so qualitatively that their detection is the problem needed for the solution of the attraction of the widest mathematical apparatus, the methods considering various tricks of falsification “authors” for the purposes of masking of the main results of their work, including, post-processing of DI after cloning executed in it.

In spite of the fact that the problem of detection of cloning results in the conditions of post-processing, in particular, of lossy DI compression isn't new [1..4], it is not completely solved. In particular, efficiency of clone/prototype areas detection needs improvement under conditions of lossy compression in case when the cloning aims the hiding of an object (objects) using the prototype which is a part of the DI background area. It is possible to assume that one of the main reasons for this is the widely known approach for the solution of such problems is based on technology of use of characteristic points of the image [2, 5...7] and is effective in case if objects are cloned.

In [8] authors of the work have offered theoretical bases of new approach to the solution of results of cloning detection problem in a digital image saved after change in a lossy format. Approach is based on the considering of a small change of a cylindrical body volume with generatrix during the compression process. That generatrix is parallel to OZ axis and limited from above by the plot of the interpolating function $g(x, y)$ for the image brightness matrix \mathbf{F} , from below — by the XOY plane. Indicator of existence of clone areas of prototype is the proximity of double integrals values from function $g(x, y)$ on the corresponding subareas of definition range of the function which is originally set the initial image.

New approach gives the principle possibility based on it in providing of the effective solution of viewed problem that is irrespective of performed cloning specifics, used during compression algorithm and parameters, that has not been fully provided in [8].

The aim of the work is to further develop of proposed in [8] approach to solve the problem of cloning detection in conditions of lossy saving of the DI.

To accomplish the aims, such problems are solved in this *work*:

1. Adaptation of the approach offered in [8] to conditions of cloned DI compression with any quality offered in [8] (compression ratio);
2. Providing (providing check) a solvency of the offered approach in the conditions of compression of cloned DI according to algorithms other than the JPEG standard.

Materials and Methods. Without limiting of verbal proofs collectivity, to simplify the statement, the DI are further considered in gradation of gray which formal representation is one two-dimensional matrix. In case of the color image, all following verbal proofs can be carried to each of color component separately, participating in its formal representation (RGB scheme), or to a brightness matrix (YUV scheme).

Let \mathbf{F} — $n \times m$ -DI matrix with elements f_{ij} , $i = \overline{1, n}$, $j = \overline{1, m}$. Let set, as in the [8], B_{ij} — $q \times q$ \mathbf{F} matrix block, for which at position (1,1) is situated the element f_{ij} . To each such block, according to [8], we will associate $(n-q+1) \times (m-q+1)$ - $\mathbf{M}^{(i,j)}$ matrix, each element $m_{k,l}^{(i,j)}$, $k = \overline{1, n-q+1}$, $l = \overline{1, m-q+1}$ of it shows the difference of B_{ij} block from B_{kl} block in such sense: $m_{k,l}^{(i,j)} = \sum_{t,p=1}^q r_{tp}$, where r_{tp} , $t, p = \overline{1, q}$, — elements of matrix $\mathbf{R} = |B_{ij} - B_{kl}|$, where the last equality is understood as element-by-element method.

The approach offered in [8] is essentially not connected with the value of DI compression ratio after performed cloning. For the blocks B_{ij} and B_{kl} of clone and the prototype image respectively

shown, that $\min M^{(i,j)} = \min M^{(k,l)}$ and reached in corresponding elements, that correspond to the prototype and clone image. So, if to define $(n-q+1) \times (m-q+1)$ - \mathbf{G} matrix with elements g_{ij} in such way: $g_{ij} = \min M^{(i,j)}$, then for the blocks B_{ij} and B_{kl} of clone and the prototype image the elements $g_{ij} = g_{kl}$, at that in this elements the global minimum of the \mathbf{G} is reached practically certain. At this, the g_{ip} element is called as global minimum of the \mathbf{G} , if $g_{ip} = \min_{1 \leq i \leq n-q+1, 1 \leq j \leq m-q+1} g_{ij}$. Such conclusion was made in [8] allowing for additional perturbation actions, that are applied to DI after cloning process. i.e. lossy saving, cannot be great, because otherwise violation of image perception is possible – artifact appearance. However, in practice the use of low quality factors (high compression ratios) often doesn't lead to appearance of visible artifacts on the compressed image, so such parameters can be essentially used at unauthorized change of DI for the subsequent masking of these changes. Therefore, to eliminate the restrictions of the applicability domain of the developed approach its adaptation is needed to ensure its viability, regardless of the quality factor used during DI compression.

Considerable compression (with low quality factor) will significantly change all elements of DI matrix. Here, the option is essentially possible when change of the DI blocks which weren't coinciding among themselves by values before compression can lead to the fact that their difference after compression will be comparable (or even smaller), than for the corresponding blocks of a clone and prototype image which were originally coinciding on values. However, taking into account the way of formation of blocks B_{ij} of DI matrix, it is obviously, that in small neighborhood of the corresponding blocks of a clone/prototype image their difference among themselves will be the smallest. Thus, at any quality factor used for lossy compression of the cloned image, an indicator of the corresponding blocks of clone and prototype images B_{ij} and B_{kl} will be the coincident elements $g_{ij} = g_{kl}$ of the \mathbf{G} matrix, in which not only the global, but also local minimum of the \mathbf{G} can be reached (in element g_{ip} the local minimum is reached if in the \mathbf{G} matrix such neighborhood $U(g_{ip})$ exist for element g_{ip} , that for any matrix element $g_{ij} \in U(g_{ip})$, $g_{ij} \neq g_{ip}$ the condition $g_{ij} > g_{ip}$ is true). This, as a rule, can be reached, when the cloning is used to remove an object from DI using prototype image, being the part of image background. This conclusion provides the possibility of the new approach using at DI compression with any quality factor.

Illustration for the told is the example given in Fig. 1 where the global minimum of the function which is an interpolation spline for \mathbf{G} matrix elements is reached in the elements of the \mathbf{G} corresponding to the DI blocks different from clone/prototype image blocks. At the same time the areas of a clone and a prototype image correspond to the local minima of the \mathbf{G} coinciding by value, resulting in characteristics of the plot: to existence of comparable in a form cone-shaped surfaces (the neighborhood of clone/prototype image blocks), which z -coordinates of tops have identical values (marked in Fig. 1).

Confirmation of effective recognition of cloning in DI in conditions of considerable compression using the approach [8] which has gained further development in this work, were results of the computing experiment were made with an experimental set of images (ES) which consisted of 300 DI of the NRCS base [9], which is traditional for testing of the algorithms working with images.

During the experiment an original DI was exposed to cloning and then was saved in JPEG format with quality factors $QF \in \{25, 35, 45, 55, 65, 75, 85, 95\}$.

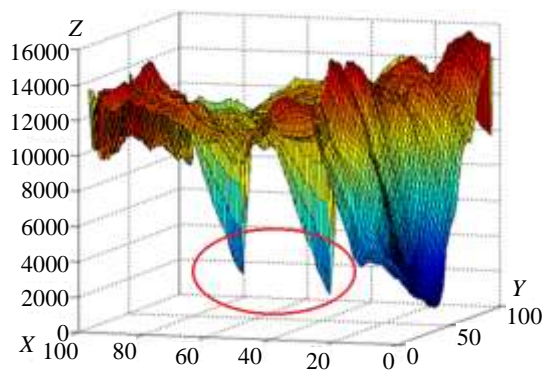


Fig. 1. A plot of function, interpolating the \mathbf{G} matrix elements, for DI after cloning with the subsequent saving using JPEG format with $QF = 25$

Compressed DI were analyzed using the advanced approach: for the received \mathbf{G} matrix ($q \in \{16, 24, 32\}$) the function plot was built, interpolating its elements, which showed the presence of characteristic areas corresponding to the elements of the \mathbf{G} , where its local minima coinciding on values were reached. Expert assessment of characteristic properties of the plot has yielded the positive result for 98.7 % of DI used in experiment: for them the areas of a clone/prototype image corresponding to real have been found. The comparable result (98.1 % of DI) has been received in case when images after cloning were saved in JPEG2000 format with quality factors $QF \in \{25, 35, 45, 55, 65, 75, 85, 95\}$.

As one more option of DI lossy compression implementation we will consider a way which is not the accepted standard, but it is often used during the work with images [10]. This way is based on low-rank approximations of a matrix (matrix blocks) of DI and consists in the following.

For $n \times m$ -matrix \mathbf{F} ($n \geq m$) of DI its singular decomposition is built [10]:

$$\mathbf{F} = \mathbf{U}\mathbf{\Sigma}\mathbf{V}^T, \quad (1)$$

where \mathbf{U} , \mathbf{V} — orthogonal matrixes of sizes $n \times m$ and $m \times m$ accordingly, which columns are the left and right singular vectors of \mathbf{F} , $\mathbf{\Sigma} = \text{diag}(\sigma_1, \sigma_2, \dots, \sigma_m)$ — diagonal matrix of singular numbers, for which $\sigma_1 \geq \sigma_2 \geq \dots \geq \sigma_m \geq 0$. If $n \leq m$ then singular decomposition of a matrix \mathbf{F}^T is considered. Decomposition (1) of a matrix \mathbf{F} can be presented in the form of external products: $\mathbf{F} = \sum_{i=1}^m \sigma_i u_i v_i^T$, where $u_i, v_i, i = \overline{1, m}$, — columns of matrixes \mathbf{U} , \mathbf{V} accordingly.

Approximation of a matrix \mathbf{F} of a rank $k \leq m$ is called the matrix $\mathbf{F}_k = \sum_{i=1}^k \sigma_i u_i v_i^T$, that is nearest to \mathbf{F} (in sense of spectral matrix norm) by matrix of range k [10]. The substitution of \mathbf{F} to \mathbf{F}_k leads to image compression is greater, the less k .

Let's check a solvency of the offered approach of cloning detection in the conditions of compression of the cloned DI using low-rank approximations of a matrix of whole image.

During the computing experiment the DI from ES were exposed to cloning and then compressed using k -rank approximations with various values of k . As results of the experiment show, the offered approach remains well-founded up to $k = m/10$. We will notice that at $k < m/10$ there are obvious artifacts in DI.

The illustration of typical results of testing for the offered approach (detection of characteristic properties of the function that is interpolating \mathbf{G} matrix elements) for specific DI is presented in Fig. 2 (results are yielded for $k = 100$ and $k = 20$; for values $20 < k < 149$ qualitative picture is similar). It should be noted also obvious localization of a clone/prototype image areas on the projection of the plot of functions interpolating \mathbf{G} to the XOY plane (Fig. 2, c, e — the respective areas are specified by arrows).

Let's consider use of low-rank approximations during processing the separate 8×8 -blocks of a matrix of DI obtained by standard splitting (just as it performed in JPEG and JPEG2000). Such way of compression will be more preferable before use of low-rank approximation of all matrix in sense of computing complexity as here the costs of singular decomposition construction of the block won't depend on the size of initial DI matrix, and will be a constant concerning the size of input data. Computing complexity of DI compression process using low-rank approximations of blocks of its $n \times m$ -matrix will be defined by blocks quantity equal $O(nm)$.

Let's establish how the rank of blocks approximation influences on reliability of perception of compressed DI, that is quantitatively estimated standardly [4]: using the peak "signal noise" relation PSNR. The computational experiment has been made for this purpose, during which DI from ES were exposed to compression using k -rank approximations of 8×8 -blocks, where $k \in \{1, \dots, 7\}$ then PSNR value was calculated. Results are given in Fig. 3.

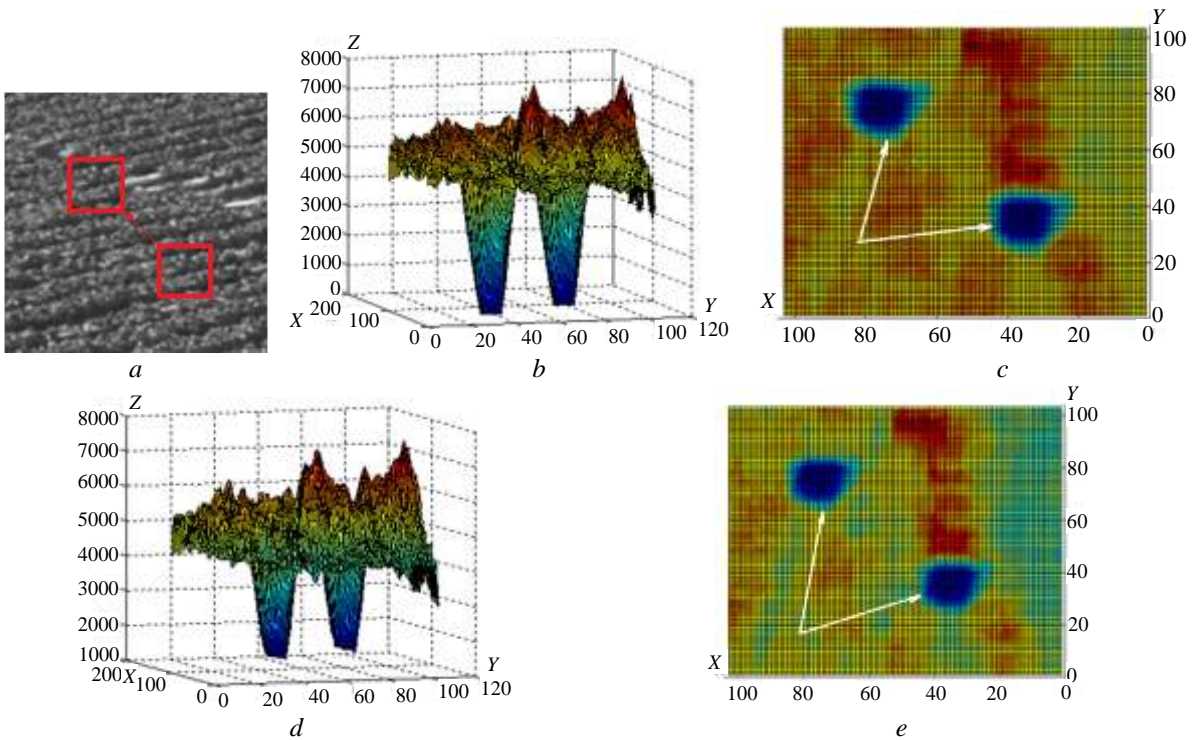


Fig. 2. Results of identification of areas of a clone/prototype in the conditions of the compression cloned DI with use low-rank approximations of his matrix: a —the part DI (the size of pixels) containing areas of a clone and a prototype, kept after cloning in a format without loss (TIFF); b —a function plot, interpolating elements of G matrix in case $k = 100$; c —projection of G to XOY-plane having $k = 100$; d —function plot, interpolating elements of G matrix in case $k = 20$; e —projection of G to XOY-plane having $k = 20$

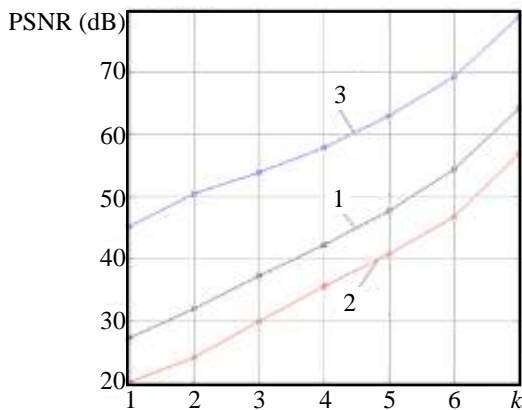


Fig. 3. Dependence of PSNR value on the approximation rank k of 8×8 -blocks of a DI matrix at its compression:
1 —average PSNR value of DI of ES;
2 —minimum PSNR value;
3 —the maximum PSNR value of all DI of ES

As computational experiment shows, already for $k = 3$ the average value of PSNR < 40 dB that can be expressed in appearance of artifacts on DI [11], however even at small value of rank of the used blocks approximations of DI the subjective ranging can not reveal any artifacts in compressed DI. The illustration to told is given in Fig. 4. Taking it into account is essentially possible the using of approximations of blocks of any rank $k \in \{1, \dots, 7\}$ to mask performed cloning. It leads to need for ensure (providing check) operability of the offered approach of cloning detection in conditions of use for compression of the cloned image of any rank $k \in \{1, \dots, 7\}$ blocks approximations.

When carrying out a computational experiment, it has been established by subjective estimation that characteristics of a function plot, that interpolate elements of G matrix, stated above were present for all DI, subjected to cloning with the subsequent compression using any rank of approximation blocks: $k = \overline{1, 7}$. Illustration of this is in Fig. 5, where DI was exposed to compression, presented in Fig. 2, a.

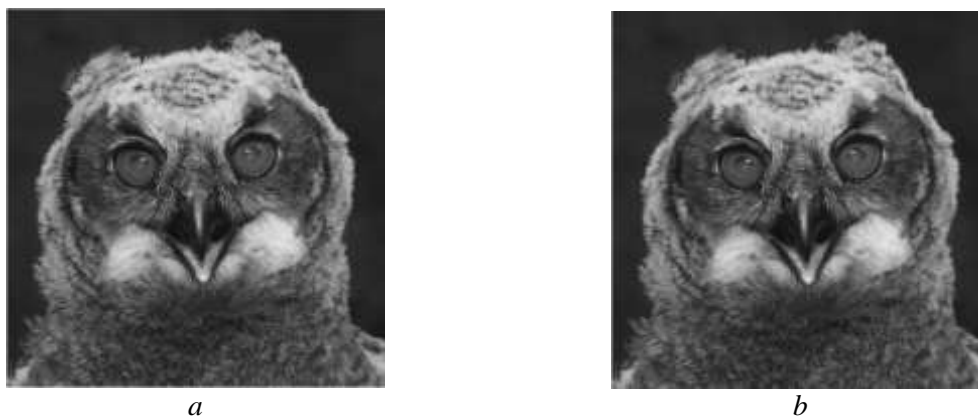


Fig. 4. Illustration of DI compression result using low-rank approximations of DI matrix blocks: a — initial DI; b — result of compression using 1-rank approximations of 8×8 -blocks of DI

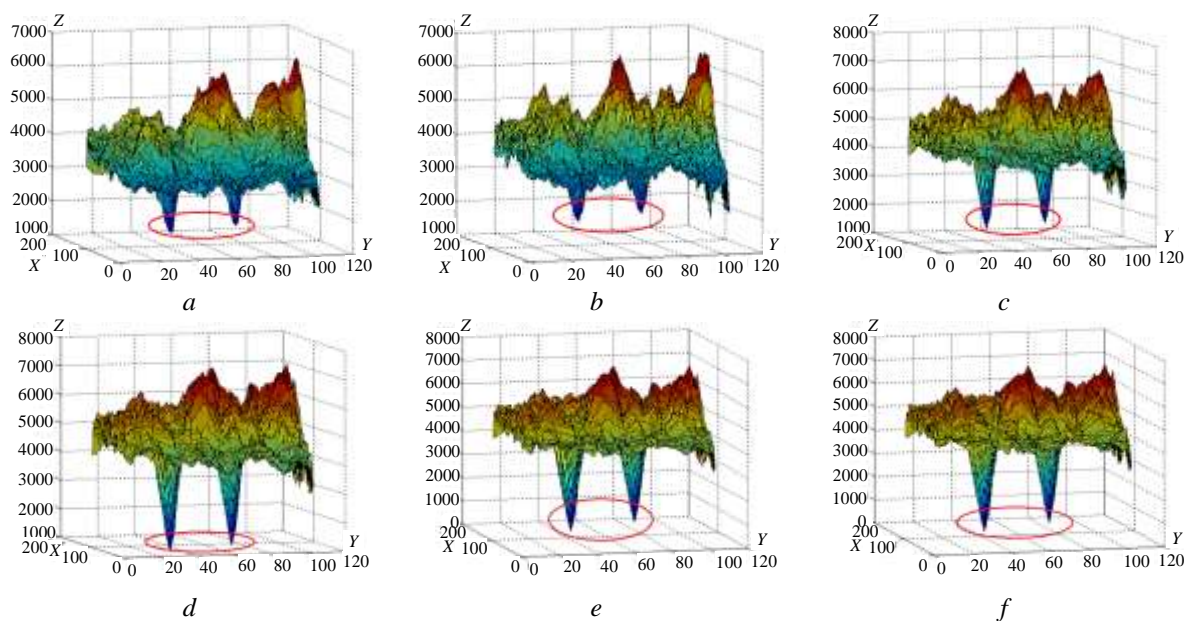


Fig. 5. Function plots, approximating the elements of DI matrix G , subjected to cloning with the subsequent compression having k -range approximations of 8×8 -blocks: a — $k = 1$; b — $k = 2$; c — $k = 3$; d — $k = 4$; e — $k = 5$; f — $k = 6$

Thus, the offered new approach to detect areas of a clone/prototype in DI in the conditions of lossy compression of the cloned image is well-founded in case for compression the low-rank approximations of matrix (matrix blocks) of DI are used.

Conclusions. In work the further development of new approach offered by authors earlier to the solution of a problem of a cloning/prototype image areas detection in the digital image in the conditions of his subsequent lossy saving is carried out.

The main object of the analysis is the matrix G which elements reflect the smallest difference of the corresponding block of the image matrix from any other incoincident with him. It is shown that the corresponding blocks of a clone/prototype image in matrix G correspond coincide by value its local minima, which generally can differ from value of a global minimum. The obtained conclusion has allowed to provide a solvency of the offered approach in conditions of compression of the cloned DI with any quality factor (compression ratio) when using for compression not only the JPEG standard,

but also other algorithms other than JPEG, in particular JPEG2000, algorithms based on low-rank approximations of an image matrix (matrix blocks).

Given the fact that the digital video sequence may be considered as a sequence of DI, there are no fundamental restrictions on the use of this method to identify a cloning in a digital video under additional attacks.

Література

1. Thajeel, S.A. State of the art of copy-move forgery detection techniques: A Review / S.A. Thajeel, G.B. Sulong // *International Journal of Computer Science*. — 2013. — Vol. 10, Issue 6. — PP. 174–183.
2. Kotkar, P.S. Detecting region duplication forgery in digital image using SIFT features / P.S. Kotkar, S.S. Shriramwar // *International Journal of Current Engineering and Technology*. — 2014. — Vol. 4, No. 3. — PP. 1437–1440.
3. Pan, X. Region duplication detection using image feature matching / X. Pan, S. Lyu // *IEEE Transactions on Information Forensics and Security*. — 2010. — Vol. 5, Issue 4. — PP. 857–867. DOI:10.1109/TIFS.2010.2078506
4. Copy-move forgery detection and localization by means of robust clustering with J-Linkage / I. Amerini, L. Ballan, R. Caldelli, *et al.* // *Signal Processing: Image Communication*. — 2013. — Vol. 28, Issue 6. — PP. 659–669.
5. Huang, H. Detection of copy-move forgery in digital images using SIFT algorithm / H. Huang, W. Guo, Y. Zhang // *Proceedings of the Pacific-Asia Workshop on Computational Intelligence and Industrial Application (PACIIA'08)*, 19–20 December 2008, Wuhan, China. — Los Alamitos: IEEE, 2008. — Vol. 2. — PP. 272–276.
6. Image copy-move forgery detection based on SURF / B. Xu, J. Wang, G. Liu, Y. Dai // *Proceedings of 2010 International Conference on Multimedia Information Networking and Security (MINES'2010)*, 4–6 November 2010, Nanjing, Jiangsu. — Los Alamitos: IEEE, 2010. — PP. 889–892.
7. A SIFT-based forensic method for copy-move attack detection and transformation recovery / I. Amerini, L. Ballan, R. Caldelli, *et al.* // *IEEE Transactions on Information Forensics and Security*. — 2011. — Vol. 6, Issue 3. — PP. 1099–1110.
8. Кобозева, А.А. Теоретические основы нового подхода к решению задачи выявления результатов клонирования в цифровом изображении, сохраненном в формате с потерями / А.А. Кобозева, С.Н. Григоренко // *Реєстрація, зберігання і обробка даних*. — 2015. — Т. 17, № 4. — С. 21–30.
9. NRCS Photo Gallery [Електронний ресурс] / United States Department of Agriculture. Washington, USA. — Режим доступу: <http://photogallery.nrcs.usda.gov> (Дата звернення: 26.07.2012).
10. Деммель, Д. Вычислительная линейная алгебра: теория и приложения / Д. Деммель; пер. с англ. Х.Д. Икрамова. — М.: Мир, 2001. — 430 с.
11. Коначович, Г.Ф. Компьютерная стеганография: теория и практика / Г.Ф. Коначович, А.Ю. Пузыренко. — К.: МК-Пресс, 2006. — 288 с.

References

1. Thajeel, S.A., & Sulong, G.B. (2013). State of the art of copy-move forgery detection techniques: A Review. *International Journal of Computer Science*, 10(6), 174–183.
2. Kotkar, P.S., & Shriramwar, S.S. (2014). Detecting region duplication forgery in digital image using SIFT features. *International Journal of Current Engineering and Technology*, 4(3), 1437–1440.
3. Pan, X., & Lyu, S. (2010). Region duplication detection using image feature matching. *IEEE Transactions on Information Forensics and Security*, 5(4), 857–867. DOI:10.1109/TIFS.2010.2078506
4. Amerini, I., Ballan, L., Caldelli, R., Del Bimbo, A., Del Tongo, L., & Serra, G. (2013). Copy-move forgery detection and localization by means of robust clustering with J-Linkage. *Signal Processing: Image Communication*, 28(6), 659–669. DOI:10.1016/j.image.2013.03.006
5. Huang, H., Guo, W., & Zhang, Y. (2008). Detection of copy-move forgery in digital images using SIFT algorithm. In Y. Zhang, H. Tan, Q. Luo (Eds.), *Proceedings of the Pacific-Asia Workshop on Computational Intelligence and Industrial Application (PACIIA'08)* (Vol. 2, pp. 272–276). Los Alamitos: IEEE. DOI:10.1109/PACIIA.2008.240

6. Xu, B., Wang, J., Liu, G., & Dai, Y. (2010). Image copy-move forgery detection based on SURF. In S. Gritzalis, S. Lian, X. Chen (Eds.), *Proceedings of the Second International Conference on Multimedia Information Networking and Security (MINES'2010)* (pp. 889–892). Los Alamitos: IEEE. DOI:10.1109/MINES.2010.189
7. Amerini, I., Ballan, L., Caldelli, R., Del Bimbo, A., & Serra, G. (2011). A SIFT-based forensic method for copy-move attack detection and transformation recovery. *IEEE Transactions on Information Forensics and Security*, 6(3), 1099–1110. DOI:10.1109/TIFS.2011.2129512
8. Kobozeva, A.A., & Grygorenko, S.N. (2015). Theoretical basis for a new approach to the problem of identifying the results of cloning in digital images stored in lossy formats. *Data Rec., Storage & Processing*, 17(4), 21–30.
9. USDA: United States Department of Agriculture (n.d.). *NRCS Photo Gallery*. Retrieved from <http://photogallery.nrcs.usda.gov/res/sites/photogallery/>
10. Demmel, J.W. (1997). *Applied Numerical Linear Algebra*. Philadelphia: SIAM.
11. Konahovich, G.F., & Puzyrenko, A.Yu. (2006). *Computer Steganography: Theory and Practice*. Kyiv: MK-Press.

Received May 31, 2016

Accepted July 10, 2016

UDC 004.7

S.A. Nesterenko, DSc, Prof.,
J.S. Nesterenko

Odessa National Polytechnic University, 1 Shevchenko Ave., 65044 Odessa, Ukraine; e-mail: sa_nesterenko@ukr.net

COSTS EVALUATION METHODIC OF ENERGY EFFICIENT COMPUTER NETWORK REENGINEERING

С.А. Нестеренко, Ю.С. Нестеренко. Методика вартісної оцінки енергоефективного реінжинірингу комп'ютерної мережі.

Одним з основних напрямів реінжинірингу сучасних комп'ютерних мереж є їх переведення на нову енергозберігаючу технологію IEEE 802.3az. Для прийняття аргументованого рішення щодо переведення на нову технологію необхідна методика, яка дозволяє мережним інженерам відповісти на питання відносно економічної доцільності проведення модернізації мережі. **Мета:** Метою роботи є розробка методики розрахунку економічної ефективності проведення енергоефективного реінжинірингу комп'ютерної мережі. **Матеріали і методи:** Методика використовує аналітичні моделі розрахунку споживчої потужності портом комп'ютерної мережі, яка працює за стандартом IEEE 802.3 та в енергоефективному режимі стандарту IEEE 802.3az. Для розрахунку часу передачі кадру в каналі зв'язку використовуються моделі масового обслуговування. Для визначення значень параметрів функціонування мережі запропоновано використовувати мультиагентний метод мережного моніторингу. **Результати:** Запропоновано методику, яка дозволяє розраховувати економічний ефект від переведення комп'ютерної мережі на енергозберігаючу технологію IEEE 802.3az. Для визначення параметрів функціонування мережі запропоновано використовувати SNMP-системи мережного моніторингу на базі агентів RMON MIB.

Ключові слова: стандарт IEEE 802.3az, аналітичні моделі, споживча потужність мережного порту, SNMP-менеджер, агент RMON MIB.

S.A. Nesterenko, J.S. Nesterenko. Costs evaluation methodic of energy efficient computer network reengineering. A key direction of modern computer networks reengineering is their transfer to a new energy-saving technology IEEE 802.3az. To make a reasoned decision about the transition to the new technology is needed a technique that allows network engineers to answer the question about the economic feasibility of a network upgrade. **Aim:** The aim of this research is development of methodic for calculating the cost-effectiveness of energy-efficient computer network reengineering. **Materials and Methods:** The methodic uses analytical models for calculating power consumption of a computer network port operating in IEEE 802.3 standard and energy-efficient mode of IEEE 802.3az standard. For frame transmission time calculation in the communication channel used the queuing model. To determine the values of the network operation parameters proposed to use multiagent network monitoring method. **Results:** The methodic allows calculating the economic impact of a computer network transfer to energy-saving technology IEEE 802.3az. To determine the network performance parameters proposed to use network SNMP monitoring systems based on RMON MIB agents.

Keywords: IEEE 802.3az standard, analytical models, network port power consumption, SNMP-manager, RMON MIB agent.

Introduction. The incoming of the IEEE 802.3az energy efficiency standards — Energy Efficient Ethernet (EEE) [1], which has a low power mode and the appearance of a large number of communication devices and network interface cards that support this standard, formed one of the main trends of reengineering of modern computer networks (CN) associated with the transition to new energy-saving IEEE 802.3az technology. In order to make a reasoned decision about the transition to the new technology requires a methodic that enables network engineers to answer the question about the economic feasibility of CN modernization.

Analysis of known publications on the field of EEE shows that most of them are devoted to study of the effectiveness of different switching modes from the active channel state (Active) to a state with low power consumption (Low Power Idle — LPI) [2...5] These works are used complex simulation or analytical models that required for calculating special modeling systems, and have rather theoretical than practical nature. There are a number of works devoted to the practical study of communication devices (CD) and network interface cards (NIC) of certain manufacturers [6...8]. However, in these studies there are no models and calculation methodic and the results are meaningful only for certain CD or NIC types.

The aim of this research is development of methodic for calculating the cost-effectiveness of energy-efficient computer network reengineering. The methodic and instrumental tools, allowing obtaining traffic parameters for real networks, which are used in the calculation models, was proposed.

DOI 10.15276/opu.2.49.2016.10.A

© 2016 The Authors. This is an open access article under the CC BY license (<http://creativecommons.org/licenses/by/4.0/>).

Materials and Methods. *The ownership cost of IEEE 802.3 standard communication networks.* Calculation of communication network power consumption is carried at the level of each its port. In this article a network communication ports defined as switch and router ports or network interface cards through which the subscribers are connected to the network. Obviously, any wired link contains two ports and power consumption in a channel is defined as the sum of consumption in each of its ports. Power consumed by the communication network is

$$P_C = \sum_{i=1}^N P_{CD_i} + \sum_{j=1}^M P_{NIC_j},$$

where P_C — power consumed by the communication network,

P_{CD_i} — power consumed by the i -th port of communication device,

P_{NIC_j} — power consumed by the j -th network interface card (subscriber port of CN),

N — number of ports in the communication network,

M — number of network interface cards in a communication network.

We will call wired channel IEEE 802.3 mode — as the standard operation mode. Then the power consumed by the port in the standard operation mode will be equal to [3]

$$P_i^S = [P_A U_i + P_P (1 - U_i)], \quad (1)$$

where P_A — power consumed by the port in the active state,

P_P — power consumed in pause state,

U_i — i -th port loading.

Expression (1) is a power consumption model of the port working at IEEE 802.3 standard operation mode.

The i -th port loading is defined as

$$U_i = \lambda_i T_{Ti},$$

where λ_i — the average intensity of incoming frames per port,

T_{Ti} — average frame transmission time via i -th port.

Given the assumption of simplest frames flow in a channel and exponential distribution of their service time the average frame transmission time via i -th port T_{Ti} may be expressed as

$$T_{Ti} = \frac{\lambda_i T_{TR_i}}{\lambda_i (1 - \lambda_i T_{TR_i})}, \quad T_{TP_i} = \frac{L_{S_i} + L_P}{V_{C_i}},$$

where T_{TR_i} — frame transaction time over physical channel of i -th port,

L_{S_i} — average size of the transmitted frames through the i -th port,

L_P — minimum pause size between frames equal to 96 bytes [1],

V_{C_i} — transmission rate over physical channel of i -th port.

The amount of energy Q_i^S consumed by i -th port in standard mode during time T is expressed as

$$Q_i^S = P_i^S T.$$

The amount of energy Q^S consumed by M -input CD operating in the standard mode during time T , can be written as

$$Q^S = T \sum_{i=1}^M P_i^S.$$

Maintenance cost of CD working in IEEE 802.3 standard mode during time T is equal to

$$C^S = Q^S C_{kW},$$

where C_{kW} — cost of 1 kW / hour of electricity.

If the communication network includes L CD, to which are connected N subscribers, the amount of energy consumed during time T working in standard mode Q_{CN}^S , expressed in the following form

$$Q_{CN}^S = \sum_{i=1}^L Q_{CD_i}^S + \sum_{j=1}^N Q_{NIC_j}^S,$$

where $Q_{CD_i}^S$ — amount of energy consumed by i -th CD operating in standard mode during time T ,

$Q_{NIC_j}^S$ — amount of energy consumed by the j -th NIC operating in standard mode during time T .

Cost of maintenance of the communication network operating in IEEE 802.3 standard mode C_{CN}^S during time T will be equal to

$$C_{CN}^S = Q_{CN}^S C_{kW}.$$

The ownership cost of IEEE 802.3az standard communications network. In IEEE 802.3az standard frame transmission time depends on in which channel state frame arrives [1]. Let us consider the situation of IEEE 802.3az standard implementations for 100 and 1000 Mbps/s. If the frame comes into an active state or when the channel is in transition to a low power state, the frame transmission time is minimum and equal to

$$T_T^{\min} = \frac{\lambda T_T}{\lambda(1-\lambda T_T)}.$$

If the frame comes in a low power state, the initially is a transition duration T_w to active state, and then performed the frame transmission. Obviously, in this case will be the maximum transmission time

$$T_T^{\max} = T_T^{\min} + T_w.$$

Then the average frame transmission time can be represented as

$$T_T^{\text{avr}} = T_T^{\min} P_1 + T_T^{\max} P_2,$$

where P_1 — probability of the next frame arrival at the time of previous frame transmission when the channel is active or in the time before the completion phase T_s , when the channel has not had time to switch to a low power state,

P_2 — probability of the opposite event.

Under the assumption that time intervals between the arrival of frames distributed over Poisson law probabilities P_1 and P_2 will be equal to

$$P_1 = T_T^{\min} (1 - e^{-\lambda T}), \quad P_2 = T_T^{\min} e^{-\lambda T}.$$

Loading the i -th switch port U_i operating in EEE mode can be written as

$$U_i = \lambda_i T_{T_i}^{\text{avr}}.$$

The power consumed by the i -th port in EEE mode will be equal

$$P_i^{\text{EEE}} = [P_A U_i + P_{LPI} (1 - U_i)], \quad (2)$$

where P_{LPI} — power consumption in a low power state LPI [1].

Expression (2) is the power consumption model of a network port working on standard IEEE 802.3az in EEE mode.

To verify the adequacy of the model were compared the data of port power consumption obtained using the model and experimental data given in [7]. Analysis shows that the error of calculation using the proposed model is not more than 8 % over the whole range of port loadings.

The amount of energy Q_i^{EEE} consumed by i -th port in EEE mode, during time T is expressed as

$$Q_i^{EEE} = P_i^{EEE} T.$$

The amount of energy Q_{CD}^{EEE} consumed by the N -input CD operating in EEE mode during time T , can be written as

$$Q_{CD}^{EEE} = \sum_{i=1}^N Q_i^{EEE}.$$

If the communication network includes L CD, to which is connected N subscribers, the amount of consumed energy during the time T working in EEE mode expressed in the form

$$Q_C^{EEE} = \sum_{i=1}^L Q_{CD_i}^{EEE} + \sum_{j=1}^N Q_{NIC_j}^{EEE},$$

where $Q_{CD_i}^{EEE}$ — amount of consumed energy by the i -th CD operating in the EEE mode during time T ,

$Q_{NIC_j}^{EEE}$ — amount of consumed energy by j -th NIC operating in EEE mode during time T .

Cost of maintenance of the communication network working in the IEEE 802.3az standard in EEE mode C_C^{EEE} during time T is equal to

$$C_C^{EEE} = Q_C^{EEE} C_{kW}.$$

Economic efficiency calculation of computer network EEE reengineering. The total cost savings C_T^{EEE} associated with the operation of upgraded network in EEE mode during period of time T is equal to

$$C_T^{EEE} = C_{kW} (Q_C^S - Q_C^{EEE}). \quad (3)$$

Payback term T_p of energy-efficient CN modernization, associated with buying L CD and N NIC operating in EEE standard, can be expressed as

$$T_p = \frac{\sum_{i=1}^L C_{CD_i}^{EEE} + \sum_{j=1}^N C_{NIC_j}^{EEE}}{[C_{kW} (Q_C^S - Q_C^{EEE})]}, \quad (4)$$

where $C_{CD_i}^{EEE}$ — cost of i -th CD operating in the EEE standard,

$C_{NIC_j}^{EEE}$ — cost of j -th NIC operating in EEE standard.

Obviously, the expression (3) and (4) can be used to calculate the cost-effectiveness and costs payback period of EEE modernization as a whole CN and any of it fragments.

Results. For the calculations of energy efficiency modernization in a real network it is necessary to determine the values of four parameters that are present in the models (1) and (2). These are the power consumed by the port in the active state P_A , the power consumed in the pause state P_P , the average intensity of transmission frames λ and the average frames size L_S . These parameters must be defined for each port of CN.

The values of power P_A and P_P are determined based on the passport data of the maximum P_{\max} and minimum P_{\min} power of CD or NIC consumption. Maximum power consumption corresponds to the situation when all CD ports loaded by 100% and the minimum – when ports loading is equal to 0%. Consequently, for the CD containing N ports P_A and P_P values are calculated for the port as a

$$P_A = \frac{P_{\max}}{N}, \quad P_P = \frac{P_{\min}}{N}.$$

It is obvious that the NIC value of P_A and P_P are defined as

$$P_A = P_{\max}, \quad P_P = P_{\min}.$$

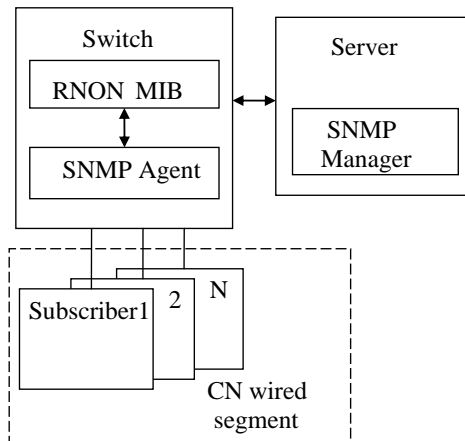


Fig. 1. The structure of a network monitoring SNMP-system

To carry out the measurement of values λ and L_S it suggested to use one of the standard network monitoring SNMP-systems [9]. Examples of such systems are Aggregate Network Manager, Zabbix, Nagios, etc. These systems operate under the agent-manager scheme [10]. Manager located on one of the network servers. As an SNMP-agents used RMON MIB agents, which are located at communication equipment (Fig. 1).

To calculate the average values of λ and L_S manager via SNMP protocol periodically polls the values of the corresponding table of the RMON MIB database for each CD port. To calculate the average frame rate is read out values of *Statistics* group, namely value of the parameter *etherStatsPkts*, which characterizes the total number of packets received at this port. Then the average frame rate value for the port is equal to

$$\lambda = \frac{K_{i+1} - K_i}{\Delta T},$$

where K_i, K_{i+1} — number of frames received by the port, respectively, at the beginning and end of the measurement period ΔT .

To calculate the average size of transmitted frames is read out values of *Statistics* group, namely value of the parameter *etherStatsOctet*, which characterizes the total number of bytes received at this port. Then, the average value of the transmitted frames size in the investigated port is equal to

$$L_S = \frac{B_{i+1} - B_i}{K_{i+1} - K_i},$$

where B_i, B_{i+1} — number of bytes received by port, respectively, at the beginning and the end of the measurement period ΔT .

Thus reading the values of only two parameters from the RMON MIB base for each port allows calculating the average values of the intensity and frame sizes for all CN ports. Using the built-in capabilities of network SNMP-monitors for data processing we can regulate the frequency of RMON MIB parameters poll and calculate the average values of λ and L_S for any work interval of CN.

Conclusion. In the paper presents simple analytical models for calculation the power port consumption operating in IEEE 802.3 standard mode and low-power mode EEE. Verification of obtained models shows that they have sufficient accuracy for engineering calculations of power consumption for the CN communication systems. The paper presents the analytical dependences allow to calculate the economic effect from the communications network transfer to the EEE technology. The methodic allows calculating the parameters of the real network which are used in the models of power consumption calculation. As an instrumental tool for collection of CN traffic parameters standard SNMP-system of network monitoring was suggested. The analytical dependences allowing on the basis of variables from the RMON MIB database calculate parameters for the models of port power consumption calculation was proposed. The developed methodic is an effective tool for network engineers in decision-making tasks of energy-efficient CN reengineering.

Література

1. IEEE Standard 802.3az-2010. Part 3: CSMA/CD Access Method and Physical Layer Specifications Amendment 5: Media Access Control Parameters, Physical Layers, and Management Parameters for Energy-Efficient Ethernet / Institute of Electrical and Electronics Engineers. — IEEE, 2010. — 272 P.

2. IEEE 802.3az: the road to Energy Efficient Ethernet / K. Christensen, P. Reviriego, B. Nordman, *et al.* // IEEE Communications Magazine. — 2010. — Vol. 48, Issue 11. — PP. 50–56.
3. Mathematical analysis of burst transmission scheme for IEEE 802.3az energy efficient Ethernet / K.J. Kim, S. Jin, N. Tian, B.D. Choi // Performance Evaluation. — 2013. — Vol. 70, Issue 5. — PP. 350–363.
4. Modeling and understanding burst transmission algorithms for Energy Efficient Ethernet / J. Meng, F. Ren, W. Jiang, C. Lin // Proceedings of 2013 IEEE/ACM 21st International Symposium on Quality of Service (IWQoS), 3–4 June 2013, Montreal, Canada. — Piscataway, NJ: IEEE, 2013. — PP. 1–10.
5. Optimal configuration of Energy-Efficient Ethernet / S. Herreria-Alonso, M. Rodriguez-Pérez, M. Fernández-Veiga, C. López-García // Computer Networks. — 2012. — Vol. 56, Issue 10. — PP. 2456–2467.
6. An Initial Evaluation of Energy Efficient Ethernet / P. Reviriego, K. Christensen, J. Rabanillo, J.A. Maestro // IEEE Communications Letters. — 2011. — Vol. 15, Issue 5. — PP. 578–580.
7. Performance evaluation of Energy Efficient Ethernet / P. Reviriego, J.A. Hernandez, D. Larrabeiti, J.A. Maestro // IEEE Communications Letters. — 2009. — Vol. 13, Issue 9. — PP. 697–699.
8. Characterizing 10 Gbps network interface energy consumption / R. Sohan, A. Rice, A.W. Moore, K. Mansley // Proceedings of 2010 IEEE 35th Conference on Local Computer Networks (LCN), 11–14 October 2010, Denver, Colorado, USA. — Piscataway, N.J.: IEEE, 2010. — PP. 268–271.
9. Stallings, W. High-speed networks and internets: Performance and quality of service / W. Stallings. — 2nd Ed. — Upper Saddle River, N.J.: Prentice Hall, 2002. — 715 p.
10. Olifer, N. Computer networks: Principles, technologies, and protocols for network design / N. Olifer, V. Olifer. — Hoboken, NJ: John Wiley & Sons, 2006. — 973 p.

References

1. Institute of Electrical and Electronics Engineers. (2010). *IEEE Standard 802.3az-2010. Part 3: CSMA/CD Access Method and Physical Layer Specifications Amendment 5: Media Access Control Parameters, Physical Layers, and Management Parameters for Energy-Efficient Ethernet*. Piscataway, N.J.: IEEE.
2. Christensen, K., Reviriego, P., Nordman, B., Bennett, M., Mostowfi, M., & Maestro, J.A. (2010). IEEE 802.3az: the road to Energy Efficient Ethernet. *IEEE Communications Magazine*, 48(11), 50–56. DOI:10.1109/MCOM.2010.5621967
3. Kim, K.J., Jin, S., Tian, N., & Choi, B.D. (2013). Mathematical analysis of burst transmission scheme for IEEE 802.3az Energy Efficient Ethernet. *Performance Evaluation*, 70(5), 350–363. DOI:10.1016/j.peva.2012.12.001
4. Meng, J., Ren, F., Jiang, W., & Lin, C. (2013). Modeling and understanding burst transmission algorithms for Energy Efficient Ethernet. In *Proceedings of 2013 IEEE/ACM 21st International Symposium on Quality of Service (IWQoS)* (pp. 1–10). Piscataway, NJ: IEEE. DOI:10.1109/IWQoS.2013.6550278
5. Herreria-Alonso, S., Rodriguez-Pérez, M., Fernández-Veiga, M., & López-García, C. (2012). Optimal configuration of Energy-Efficient Ethernet. *Computer Networks*, 56(10), 2456–2467. DOI:10.1016/j.comnet.2012.03.006
6. Reviriego, P., Christensen, K., Rabanillo, J., & Maestro, J.A. (2011). An Initial Evaluation of Energy Efficient Ethernet. *IEEE Communications Letters*, 15(5), PP. 578–580. DOI:10.1109/LCOMM.2011.040111.102259
7. Reviriego, P., Hernandez, J.A., Larrabeiti, D., & Maestro, J.A. (2009). Performance evaluation of Energy Efficient Ethernet. *IEEE Communications Letters*, 13(9), 697–699. DOI:10.1109/LCOMM.2009.090880
8. Sohan, R., Rice, A., Moore, A.W., & Mansley, K. (2010). Characterizing 10 Gbps network interface energy consumption. In *Proceedings of 2010 IEEE 35th Conference on Local Computer Networks (LCN)* (pp. 268–271). Piscataway, N.J.: IEEE. DOI:10.1109/LCN.2010.5735719
9. Stallings, W. (2002). *High-Speed Networks and Internets: Performance and Quality of Service* (2nd Ed.). Upper Saddle River, N.J.: Prentice Hall.
10. Olifer, N., & Olifer, V. (2006). *Computer Networks: Principles, Technologies, and Protocols for Network Design*. Hoboken, NJ: John Wiley & Sons.

Received July 5, 2016

Accepted July 26, 2016

UDC 004.056.55:004.932

O.V. Kostyrka, PhD

Cherkasy Institute of Fire Safety named after Heroes of Chernobyl of National University of Civil Protection of Ukraine,
8 Onoprienko Str., 18034 Cherkasy, Ukraine; e-mail: chaykaov@rambler.ru

THROUGHPUT INCREASE OF THE COVERT COMMUNICATION CHANNEL ORGANIZED BY THE STABLE STEGANOGRAPHY ALGORITHM USING SPATIAL DOMAIN OF THE IMAGE

O.V. Kostyrka. Підвищення пропускної спроможності прихованого каналу зв'язку, організованого стійким стеганографічним алгоритмом, що використовує просторову область зображення. При організації прихованого каналу зв'язку до стеганографічних алгоритмів, що використовуються, висувається ряд вимог, основними з яких є стійкість до атак проти вбудованого повідомлення, надійність сприйняття сформованого стеганоповідомлення, значна пропускна спроможність стеганографічного каналу зв'язку. **Мета:** Метою роботи є модифікація розробленого автором раніше стеганографічного методу, яка дозволить при збереженні стійкості до атак проти вбудованого повідомлення і надійності сприйняття стеганоповідомлення, що формується, властивих методу, збільшити пропускну спроможність відповідного прихованого каналу зв'язку. **Матеріали і методи:** Запропоновано дві модифікації стеганографічного методу, стійкого до атак проти вбудованого повідомлення, здійснюючого занурення і декодування інформації, яка пересилається (додаткової), в просторовій області зображення, що дозволяють збільшити пропускну спроможність прихованого каналу зв'язку. Використання просторової області зображення дозволяє уникнути накопичення додаткової обчислювальної похибки в процесі занурення/декодування додаткової інформації за рахунок «переходів» з просторової області зображення в область перетворення і назад, що позитивно позначається на ефективності декодування. Розглянуті наступні атаки проти вбудованого повідомлення: накладення на стеганоповідомлення різних шумів, фільтрація, стиск стеганоповідомлення із втратами, для чого використано формати JPEG і JPEG2000 з різними коефіцієнтами якості для збереження стеганоповідомлення. **Результати:** Показано, що алгоритмічні реалізації запропонованих модифікацій залишаються стійкими до збурюючих дій, в тому числі значних, забезпечують надійність сприйняття сформованих стеганоповідомлень, в два рази збільшують пропускну спроможність стеганографічного каналу зв'язку, що формується, в порівнянні з алгоритмом, який реалізує стеганографічний метод, взятий за основу. Всі висновки підтверджено результатами представницьких обчислювальних експериментів.

Ключові слова: стеганографічний алгоритм, цифрове зображення, пропускна спроможність прихованого каналу зв'язку, стійкість до атак проти вбудованого повідомлення, надійність сприйняття.

O.V. Kostyrka. **Throughput increase of the covert communication channel organized by the stable steganography algorithm using spatial domain of the image.** At the organization of a covert communication channel a number of requirements are imposed on used steganography algorithms among which one of the main are: resistance to attacks against the built-in message, reliability of perception of formed steganography message, significant throughput of a steganography communication channel. **Aim:** The aim of this research is to modify the steganography method, developed by the author earlier, which will allow to increase the throughput of the corresponding covert communication channel when saving resistance to attacks against the built-in message and perception reliability of the created steganography message, inherent to developed method. **Materials and Methods:** Modifications of a steganography method that is steady against attacks against the built-in message which is carrying out the inclusion and decoding of the sent (additional) information in spatial domain of the image allowing to increase the throughput of the organized communication channel are offered. Use of spatial domain of the image allows to avoid accumulation of an additional computational error during the inclusion/decoding of additional information due to “transitions” from spatial domain of the image to the area of conversion and back that positively affects the efficiency of decoding. Such methods are considered as attacks against the built-in message: imposing of different noise on a steganography message, filtering, lossy compression of a steganography message where the JPEG and JPEG2000 formats with different quality coefficients for saving of a steganography message are used. **Results:** It is shown that algorithmic implementations of the offered methods modifications remain steady against the perturbing influences, including considerable, provide reliability of perception of the created steganography message, increase the throughput of the created steganography communication channel in comparison with the algorithm implementing steganography method taken as a basis. All conclusions are confirmed with results of representative computational experiments.

Keywords: steganography algorithm, digital image, throughput of a steganography channel, resistance to attacks against the built-in message, reliability of perception.

Introduction. Information security — one of the main problems of modern society, and with rapid development of information technologies and computer systems its decision becomes more difficult. As is well-known [1,2], effective protection of information resources of any enterprise,

DOI 10.15276/opu.2.49.2016.11

© 2016 The Authors. This is an open access article under the CC BY license (<http://creativecommons.org/licenses/by/4.0/>).

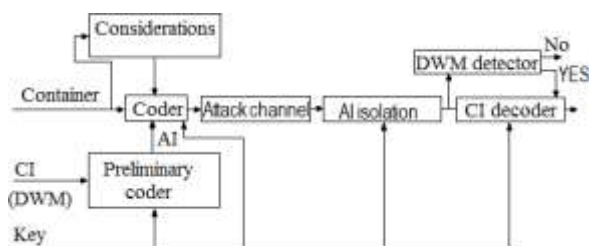


Fig. 1. Base elements of steganography system

establishment, etc., the states in general can be provided today only by means of complex system of information security, one of obligatory components of which is the steganographic system. Base elements of a steganosystem are presented in Fig. 1 [3].

At steganographing the confidential information (CI) or a digital watermark [3] (DWM) after preliminary coding, which result is the additional information (AI), as a rule, presented as the binary

sequence, enwraps into a container using steganographic algorithm which in the presented work the digital image (DI) is used. Result of inclusion of DI, or steganotransformation is the steganomessage (SM).

Efficiency of a steganosystem is determined by efficiency of the steganographic algorithm used by it. One of the main demands made to the modern steganomethods and algorithms implementing them used for the organization of the hidden communication channel are requirements of sufficient capacity of the organized channel [3], ensuring reliability of perception of the formed SM [3, 4], and also resistance to the attacks against the built-in message [3, 5...7] which purpose is distortion, up to destruction, of the sent AI. Such methods can act as the attacks: lossy saving of SM, imposing of various noise, SM filtration, etc.

A large number of works in the field of a steganography [8...12] is devoted to solution of a problem of ensuring resistance of steganomethods and methods to the attacks against the built-in message, however to speak about its final solution still early. So, the most of the existing stable methods carry out a steganotransformation in domain of a matrix DI transformation: frequency [6], discrete wavelet-transformation domain [13], domain of singular and spectral decomposition of the corresponding matrix [7], etc. The computational operations which are carried out upon DI transition from spatial domain to transformation one and back lead to accumulation of additional (in comparison with use of spatial domain of the image) computational error that has an adverse effect on efficiency of decoding of AI [14]. Besides, when using of DI transformation area for a steganotransformation the often uncommon problem is the organization of simultaneous ensuring of an algorithm stability and reliability of perception of the received SM that is obligatory for the hidden communication channel.

In [15...18] the base steganographic method implementing its polynomial algorithm (SA) SA_b and its modification, which resistance to the attacks against built-in message exceeds stability of modern analogs, at the same time providing reliability of SM perception. The area of steganotransformation and decoding of AI is the spatial domain of DI. A lack of the mentioned algorithms is the small capacity of the hidden communication channel which is organized at their use.

The aim of this research is to modify the developed steganomethod [15...17] that will allow with retention of resistance to the attacks against the built-in message and reliability of perception of the formed SM to increase the capacity of the corresponding hidden communication channel.

To accomplish the aims, such problems are solved in the work:

1. The choice of way/ways of dithering matrix of DI-container matrix block construction during steganotransformation process, that will allow to provide the increasing the quantity of various options of dithering of the container block at steganotransformation;
2. The efficiency analysis of algorithmic implementations of the offered modifications of a base method [17].

Materials and Methods. In this work color DI are used as containers (RGB-scheme), at the same time the inclusion of AI, being the binary sequence $p_1, p_2, \dots, p_t, p_i \in \{0,1\}, i = \overline{1,t}$, which is a result of sent CI coding, taking into account features of human vision [19], is carried out in a blue color component which formal representation is the $m \times m$ -matrix F . Corresponding $m \times m$ -matrix of SM is further defined as \overline{F} .

Efficiency of all steganomethods considered in the work will be determined with two components:

— resistance to the attacks against built-in message which is quantitatively estimated using correlation coefficient NC for AI [16]:

$$NC = \left(\sum_{i=1}^t p'_i \times \bar{p}'_i \right) / t,$$

where $p'_i = 1, \bar{p}'_i = 1$, if $p_i = 1, \bar{p}_i = 1$, at this $\bar{p}_1, \bar{p}_2, \dots, \bar{p}_t, \bar{p}_i \in \{0,1\}, i = \overline{1,t}$ — binary sequence, that is a decoding result AI, and $p'_i = -1, \bar{p}'_i = -1$, if $p_i = 0, \bar{p}_i = 0$;

— ensuring reliability of the formed SM perception which is quantitatively estimated using a PSNR differential indicator — the peak “signal noise” relation [16]:

$$PSNR = 10 \cdot \lg \left(255^2 / \left(\frac{1}{m^2} \sum_{i,j} (f_{ij} - \bar{f}_{ij})^2 \right) \right),$$

where $f_{ij}, \bar{f}_{ij}, i, j = \overline{1,m}$ — elements of F and \bar{F} matrices respectively.

For a base steganomethod [17] inclusion of 1 bit of AI was performed in the $l \times l$ -matrix F block obtained by its standard dividing [19], providing the maximum capacity (if steganotransformation covered all blocks of a container) of the corresponding hidden communication channel (CCC) $1/l^2$ bits/pixel. For this purpose, at inclusion of AI the two possible options of pixels of the block dithering, corresponding to included 0 and 1 were provided.

To provide the CCC increase in k times taking into account sufficient SA stability conditions to the attacks against the built-in message implemented in spatial domain of DI [15] it is needed to provide 2^k possible options of dithering of pixels of the block at steganotransformation.

Let's consider in detail a case when $k = 2$. Here, it is necessary to provide four various options of ditherings of the container block corresponding to inclusion the couples of bits: 00, 01, 10, 11.

Construction of a matrix of dithering of the $l \times l$ -container block at steganotransformation can be performed in various ways. In this work two options of construction of such matrices are presented, to each of which there corresponds the modification of a base steganomethod [17].

The main steps of the first of offered modifications further called $SA_M^{(1)}$ method look as follows.

Inclusion of AI.

1. Matrix F of DI-container to divide using standard way to $l \times l$ -blocks.
2. Construct matrices:

$$\Delta B^{(00)} \text{ with elements } b_{ij}^{(00)} = -\Delta b, i, j = \overline{1,l}, \Delta B^{(11)} \text{ with elements } b_{ij}^{(11)} = \Delta b, i, j = \overline{1,l},$$

$$\Delta B^{(01)} \text{ with elements } b_{ij}^{(01)} = \begin{cases} -\Delta b, i = \overline{1,l}, j = \overline{1, [l/2]} \\ \Delta b, i = \overline{1,l}, j = [l/2] + 1, l \end{cases}, \Delta B^{(10)} \text{ with elements}$$

$$b_{ij}^{(10)} = \begin{cases} \Delta b, i = \overline{1,l}, j = \overline{1, [l/2]} \\ -\Delta b, i = \overline{1,l}, j = [l/2] + 1, l \end{cases},$$

where Δb — dithering of one pixel during steganotransformation process, defined accounting potential attacks [15,16],

[•] — integer part of argument.

3. Let B — the next $l \times l$ -block of a container used for steganotransformation and chosen according to used secret key, and p_i, p_{i+1} — the next couple of AI bits, \bar{B} — corresponding block of \bar{F} matrix of SM.

$$\begin{array}{ll} \text{If} & p_i p_{i+1} = 11 \\ \text{then} & \bar{B} = B + \Delta B^{(11)}. \\ \text{If} & p_i p_{i+1} = 10 \end{array}$$

then $\overline{B} = B + \Delta B^{(10)}$.
 If $p_i p_{i+1} = 01$
 then $\overline{B} = B + \Delta B^{(01)}$
 If $p_i p_{i+1} = 00$
 then $\overline{B} = B + \Delta B^{(00)}$

Decoding of AI

1. Matrices of container F and possibly modified SM during transfer \overline{F} are divided using standard way to disjointed $l \times l$ -blocks.

2. Let \overline{B} — the next $l \times l$ -block of SM, used in transfer of AI (defined according to used secret key), of which the AI bits are decoded $\overline{p}_i, \overline{p}_{i+1}$, and B — corresponding container block.

2.1. Define $l \times l$ -matrix: $\overline{\Delta B} = \overline{B} - B$ with elements $\overline{b}_{ij}, i, j = \overline{1}, \overline{l}$.

2.2. Divide $\overline{\Delta B}$ to two $l \times [l/2]$ — submatrices: $\overline{\Delta B}^{(L)}$ with elements $\overline{b}_{ij}^{(L)}, i = \overline{1}, \overline{l}, j = \overline{1}, \overline{[l/2]}$, and $\overline{\Delta B}^{(R)}$ with elements $\overline{b}_{ij}^{(R)}, i = \overline{1}, \overline{l}, j = \overline{1}, \overline{[l/2]}$, where $\overline{b}_{ij}^{(L)} = \overline{b}_{ij}; \overline{b}_{ij}^{(R)} = \overline{b}_{i, j+[l/2]}$.

2.3. Determine the number of positive $k_p^{(L)}, k_p^{(R)}$ and negative $k_n^{(L)}, k_n^{(R)}$ elements in matrices $\overline{\Delta B}^{(L)}, \overline{\Delta B}^{(R)}$ accordingly.

If $k_p^{(L)} > k_n^{(L)}$,
 then $\overline{p}_i = 1$,
 else $\overline{p}_i = 0$.
 If $k_p^{(R)} > k_n^{(R)}$,
 then $\overline{p}_{i+1} = 1$,
 else $\overline{p}_{i+1} = 0$.

The way of construction of dithering matrixes of container blocks in $SA_M^{(1)}$ (at algorithmic implementation $l=8, \Delta b=9$ were used similarly to SA_B [16]) for steganotransformation has led to insignificant reduction of the PSNR value characterizing distortion of a DI container as a result of steganotransformation in comparison with SA_B (tab. 1). Taking into account that the developed methods are supposed to be used at the organization of the hidden communication channel, such degradation is undesirable. In this regard, one more modification is offered — the $SA_M^{(2)}$ method which also increases twice the capacity of the hidden communication channel, in comparison with SA_B , however revolts a container matrix less at AI inclusion. Main steps of $SA_M^{(2)}$ are the following

Inclusion of AI.

1. Matrix F of DI-container to divide using standard way to $l \times l$ -blocks.
2. Construct $l \times l$ -matrix ΔB , used during steganotransformation process of container block:

$$\Delta B = \begin{pmatrix} \Delta b & \Delta b & \dots & \Delta b \\ \Delta b & \Delta b & \dots & \Delta b \\ \dots & \dots & \dots & \dots \\ \Delta b & \Delta b & \dots & \Delta b \end{pmatrix}.$$

3. Let B — the next $l \times l$ -block of container used for steganotransformation according to secret key, and p_i, p_{i+1} — the next couple of bits of AI, \overline{B} — corresponding block of matrix \overline{F} of SM.

<i>If</i>	$p_i p_{i+1} = 11$
<i>then</i>	$\overline{B} = B + \Delta B.$
<i>If</i>	$p_i p_{i+1} = 10$
<i>then</i>	$\overline{B} = B + \frac{1}{2} \cdot \Delta B.$
<i>If</i>	$p_i p_{i+1} = 01$
<i>then</i>	$\overline{B} = B - \frac{1}{2} \cdot \Delta B.$
<i>If</i>	$p_i p_{i+1} = 00$
<i>then</i>	$\overline{B} = B - \Delta B$

Decoding of AI.

1. Construct a matrix $\Delta F = \overline{\overline{F}} - F$, where F and $\overline{\overline{F}}$ — matrices of container and of SM possibly modified during transfer respectively.

2. Divide matrix ΔF using standard way to disjointed $l \times l$ -blocks $\Delta B_p, t, p = \overline{1, [m/l]}$, where t, p correspond according to number of block arrow, column in ΔF .

3. For each block ΔB_p of matrix ΔF find arithmetical average of its elements s_p .

4. All obtained values $s_p, t, p = \overline{1, [m/l]}$, divide to two sets: $S_1 = \{s_p | s_p < 0\}$ and $S_2 = \{s_p | s_p > 0\}$.

5. Determine: T_1 and T_2 — medians of sets S_1 and S_2 respectively and $M_1 = \min S_1, M_2 = \max S_2$.

6. Divide matrices F and $\overline{\overline{F}}$ by standard way to disjointed $l \times l$ -blocks. Let $\overline{\overline{B}}$ — is the next block of SM, determining according to secret key, from which the bits are decoded $\overline{p_i}, \overline{p_{i+1}}$ AI, and B — corresponding to it container block.

6.1. Define matrix: $\overline{\overline{\Delta B}} = \overline{\overline{B}} - B$ with elements $\overline{b_{ij}}, i, j = \overline{1, l}$.

6.2. Determine the quantity of positive k_p and negative k_n elements in matrix $\overline{\overline{\Delta B}}$.

<i>If</i>	$k_p > k_n,$
<i>then</i>	$\overline{p_i} = 1,$

Determine the quantity $\overline{k_p}$ and $\overline{k_n}$ of positive elements of matrix $\overline{\overline{\Delta B}}$, for which their values are lower/greater than $(T_2 + M_2)/2$ respectively.

<i>If</i>	$\overline{k_p} > \overline{k_n},$
<i>then</i>	$\overline{p_{i+1}} = 0,$
<i>else</i>	$\overline{p_{i+1}} = 1,$
<i>else</i>	$\overline{p_i} = 0.$

Determine the quantity $\overline{k_n}$ and $\overline{k_p}$ of negative elements of matrix $\overline{\overline{\Delta B}}$, for which their values are greater/lower $(T_1 + M_1)/2$ respectively.

<i>If</i>	$\overline{k_n} > \overline{k_p},$
<i>then</i>	$\overline{p_{i+1}} = 1,$
<i>else</i>	$\overline{p_{i+1}} = 0.$

Results and Discussion. For the efficiency analysis of the developed modifications $SA_M^{(1)}$, $SA_M^{(2)}$ of base method the computational experiment has been made (in algorithmic implementation of a method $SA_M^{(2)}$ as well as $SA_M^{(1)}$, values $l=8, \Delta b=9$ were used). 400 DI of NRCS base [20] has been involved as containers. This base is traditional for testing of the algorithms work with DI. During the experiment the AI included into containers, at this CCC was 1/32 bits/pixel. At this stage of the experiment and average PSNR value on all used DI, characterizing distortion of DI container at the expense of steganotransformation was calculated. Results are given in Table 1. After that the SM were exposed to various attacks: imposing of various noise, filtration, lossy compression using JPEG and JPEG2000 standards with various QF quality coefficients after what there was decoding of AI from the dithered SM. Results of the experiment are given in Table 2.

Table 1

Average value of PSNR for algorithmic implementations of developed modifications and base steganomethods (dB)

SA_B	$SA_M^{(1)}$	$SA_M^{(2)}$
49	45	53

Table 2

Quantitative estimates of resistance to the attacks against the built-in message of algorithmic implementations of the developed modifications $SA_M^{(1)}$ and $SA_M^{(2)}$ and base steganomethods

The disturbing effects and their parameters		Values of NC		
		SA_B	$SA_M^{(1)}$	$SA_M^{(2)}$
Gaussian noise with zero mathematical expectation	$D = 0.0005$	0.994	0.973	0.961
	$D = 0.001$	0.993	0.966	0.960
	$D = 0.005$	0.988	0.955	0.940
	$D = 0.01$	0.962	0.941	0.922
	$D = 0.1$	0.524	0.510	0.499
Multiplicative noise	$D = 0.0001$	0.995	0.981	0.967
	$D = 0.001$	0.993	0.965	0.961
	$D = 0.01$	0.977	0.953	0.946
	$D = 0.08$	0.822	0.799	0.774
	$D = 0.5$	0.548	0.531	0.513
Averaging filter of size $p \times p$	$p = 3$	0.994	0.981	0.954
	$p = 5$	0.962	0.950	0.933
	$p = 7$	0.881	0.861	0.859
Gaussian filter of size $p \times p$ ($sig = 0.5$)	$p = 3$	0.997	0.988	0.964
	$p = 5$	0.997	0.988	0.964
	$p = 7$	0.997	0.988	0.964
Saving of SM in JPEG format with quality factor QF	$QF = 40$	0.969	0.947	0.905
	$QF = 60$	0.987	0.952	0.919
	$QF = 70$	0.988	0.959	0.928
	$QF = 80$	0.989	0.956	0.931
	$QF = 90$	0.991	0.974	0.961
Saving of SM in JPEG2000 format with quality factor QF	$QF = 40$	0.782	0.745	0.736
	$QF = 60$	0.947	0.937	0.904
	$QF = 70$	0.980	0.961	0.939
	$QF = 80$	0.990	0.974	0.946
	$QF = 90$	0.992	0.985	0.963
Poisson noise		0.9977	0.988	0.975
Median filter 3×3		0.997	0.988	0.964

Thus, the developed modifications provide reliability of perception of the formed SM (PSNR > 40 dB [4]), slightly concede to a base steganomethod [17] in resistance to the attacks against

the built-in message (the maximum deterioration were less than 7 % for $SA_M^{(2)}$ at compression of SM using JPEG format with $QF = 40, 60$), but provide increasing of the hidden communication channel capacity twice.

Conclusions. Two modifications of a steganographic method resistant against the attacks against the built-in message which is carrying out a steganotransformation in spatial area of the image container are offered in this work. Modifications result was: increase of the capacity of the corresponding hidden communication channels at insignificant reduction of stability in comparison with a base steganomethod, ensuring perception reliability of the formed steganomessages.

Література

1. Хорошко, В.А. Методы и средства защиты информации / В.А. Хорошко, А.А. Чекатков; ред. Ю.С. Ковтанюк. — К.: ЮНИОР, 2003. — 505 с.
2. Ленков, С.В. Методы и средства защиты информации: в 2 т. / С.В. Ленков, Д.А. Перегудов, В.А. Хорошко. — К.: Арий, 2008. — Т.2: Информационная безопасность. — 2008. — 344 с.
3. Стеганография, цифровые водяные знаки и стеганоанализ: монография / А.В. Аграновский, А.В. Балакин, В.Г. Грибунин, С.А. Сапожников. — М.: Вузовская книга, 2009. — 220 с.
4. Конахович, Г.Ф. Компьютерная стеганография: теория и практика / Г.Ф. Конахович, А.Ю. Пузыренко. — К.: МК-Пресс, 2006. — 288 с.
5. Al-Otum, H.M. A robust blind color image watermarking based on wavelet-tree bit host difference selection / H.M. Al-Otum, N.A. Samara // Signal Processing. — 2010. — Vol. 90, Issue 8. — PP. 2498–2512.
6. Wang, T.-Y. A novel robust color image digital watermarking algorithm based on discrete cosine transform / T.-Y. Wang, H.-W. Li // Journal of Computers. — 2013. — Vol. 8, No. 10. — PP. 2507–2511.
7. Harish, N.J. Hybrid robust watermarking technique based on DWT, DCT and SVD / N.J. Harish, B.B.S. Kumar, A. Kusagur // International Journal of Advanced Electrical and Electronics Engineering. — 2013. — Vol. 2, Issue 5. — PP. 137–143.
8. Fang, H. Robust watermarking scheme for multispectral images using discrete wavelet transform and tucker decomposition / H. Fang, Q. Zhou, K. Li // Journal of Computers. — 2013. — Vol. 8, No. 11. — PP. 2844–2850.
9. Qin, C. A novel digital watermarking algorithm in contourlet domain / C. Qin, X. Wen // Journal of Information & Computational Science. — 2014. — Vol. 11, No. 2. — PP. 519–526.
10. Yang, Q.T. A novel robust watermarking scheme based on neural network / Q.T. Yang, T.G. Gao, L. Fan // Proceedings of the 2010 International Conference on Intelligent Computing and Integrated Systems (ICISS), 22-24 October 2010, Guilin, China. — Piscataway, NJ: IEEE, 2010. — PP. 71–75.
11. A survey on image steganography and steganalysis / B. Li, J.H. He, J.W. Huang, Y.Q. Shi // Journal of Information Hiding and Multimedia Signal Processing. — 2011. — Vol. 2, No. 2. — PP. 142–172.
12. Fan, C.-H. A robust watermarking technique resistant JPEG compression / C.-H. Fan, H.-Y. Huang, W.-H. Hsu // Journal of Information Science and Engineering. — 2011. — Vol. 27, No. 1. — PP. 163–180.
13. Bazargani, M. Digital image watermarking in wavelet, contourlet and curvelet domains / M. Bazargani, H. Ebrahimi, R. Dianat // Journal of Basic and Applied Scientific Research. — 2012. — Vol. 2, Issue 11. — PP. 11296–11308.
14. Костырка, О.В. Анализ преимуществ пространственной области цифрового изображения-контейнера для стеганообразования / О.В. Костырка // Информатика та математичні методи в моделюванні. — 2013. — Т. 3, № 3. — С. 275–282.
15. Кобозева, А.А. Условия обеспечения устойчивости стеганоалгоритма при организации стеганообразования в пространственной области контейнера-изображения / А.А. Кобозева, О.В. Костырка // Інформаційна безпека. — 2013. — № 3(11). — С. 29–35.
16. Костырка, О.В. Стеганографічний алгоритм, стійкий до накладання шуму / О.В. Костырка // Безпека інформації. — 2014. — Т. 20, № 1. — С. 71–75.
17. Кобозева, А.А. Стеганообразование пространственной области изображения-контейнера, устойчивое к атакам против встроенного сообщения / А.А. Кобозева, Е.Ю. Лебедева, О.В. Костырка // Проблемы региональной энергетики. — 2014. — № 1(24). — С. 71–81.
18. Костырка, О.В. Модифікація стійкого до збурних дій стеганоперетворення просторової області зображення-контейнера / О.В. Костырка // Информатика та математичні методи в моделюванні. — 2016. — Т. 6, № 1. — С. 85–93.

19. Гонсалес, Р. Цифровая обработка изображений / Р. Гонсалес, Р. Вудс; пер. с англ. П.А. Чочиа. — М.: Техносфера, 2006. — 1070 с.
20. NRCS Photo Gallery [Электронный ресурс] / United States Department of Agriculture. Washington, USA. — Режим доступа: <http://photogallery.nrcs.usda.gov> (Дата звернення: 26.07.2012).

References

1. Khoroshko, V.A., & Chekatkov, A.A. (2003). *Methods and Tools for Information Security*. Kyiv: Junior.
2. Lenkov, S.V., Peregodov, D.A., & Khoroshko, V.A. (2008). *Methods and Means of Information Security. Vol. 2, The Information Security*. Kyiv: Ariy.
3. Agranovskij, A.V., Balakin, A.V., Gribunin, V.G., & Sapozhnikov, S.A. (2009). *Steganography, Digital Watermarking, and Steganalysis*. Moscow: Vuzovskaya Kniga.
4. Konahovich, G.F., & Puzyrenko, A.Yu. (2006). *Computer Steganography: Theory and Practice*. Kyiv: MK-Press.
5. Al-Otun, H.M., & Samara, N.A. (2010). A robust blind color image watermarking based on wavelet-tree bit host difference selection. *Signal Processing*, 90(8), 2498–2512. DOI:10.1016/j.sigpro.2010.02.017
6. Wang, T.-Y., & Li, H.-W. (2013). A novel robust color image digital watermarking algorithm based on discrete cosine transform. *Journal of Computers*, 8(10), 2507–2511. DOI:10.4304/jcp.8.10.2507-2511
7. Harish, N.J., Kumar, B.B.S., & Kusagur, A. (2013). Hybrid robust watermarking technique based on DWT, DCT and SVD. *International Journal of Advanced Electrical and Electronics Engineering*, 2(5), 137–143.
8. Fang, H., Zhou, Q., & Li, K. (2013). Robust watermarking scheme for multispectral images using discrete wavelet transform and tucker decomposition. *Journal of Computers*, 8(11), 2844–2850. DOI: 10.4304/jcp.8.11.2844-2850
9. Qin, C., & Wen, X. (2014). A novel digital watermarking algorithm in contourlet domain. *Journal of Information & Computational Science*, 11(2), 519–526. DOI:10.12733/jics20102841
10. Yang, Q.T., Gao, T.G., & Fan, L. (2010). A novel robust watermarking scheme based on neural network. In Z. Zhang (Ed.), *Proceedings of the 2010 International Conference on Intelligent Computing and Integrated Systems (ICISS'2010)* (pp. 71–75). Piscataway, NJ: IEEE. DOI:10.1109/ICISS.2010.5655017
11. Li, B., He, J.H., Huang, J.W., & Shi, Y.Q. (2011). A survey on image steganography and steganalysis. *Journal of Information Hiding and Multimedia Signal Processing*, 2(2), 142–172.
12. Fan, C.-H., Huang, H.Y., & Hsu, W.-H. (2011). A robust watermarking technique resistant JPEG compression. *Journal of Information Science and Engineering*, 27(1), 163–180.
13. Bazargani, M., Ebrahimi, H., & Dianat, R. (2012). Digital image watermarking in wavelet, contourlet and curvelet domains. *Journal of Basic and Applied Scientific Research*, 2(11), 11296–11308.
14. Kostyrka, O.V. (2013). Analysis on the benefits of spatial domain of cover image for steganography transformation. *Informatics and Mathematical Methods in Simulation*, 3(3), 275–282.
15. Kobozeva, A.A., & Kostyrka, O.V. (2013). Terms of ensuring the sustainability of the steganography algorithm during the organization of steganography transformation into a spatial domain of cover image. *Informative Safety*, 3, 29–35.
16. Kostyrka, O. (2014). Steganographic algorithm robust against noise imposition. *Ukrainian Scientific Journal of Information Security*, 20(1), 71–75.
17. Kobozeva, A., Lebedeva, E., & Kostyrka, O. (2014). Stego transformation of spatial domain of cover image robust against attacks on embedded message. *Problemele Energeticii Regionale*, 1, 71–81.
18. Kostyrka, O.V. (2016). Modification of sustainable steganography algorithm which robust against disturbance of steganography transformation into a spatial domain of cover image. *Informatics and Mathematical Methods in Simulation*, 6(1), 85–93.
19. Gonzalez, R.C., & Woods, R.E. (2008). *Digital Image Processing* (3rd Ed.). Upper Saddle River, N.J.: Prentice Hall.
20. USDA: United States Department of Agriculture (n.d.). *NRCS Photo Gallery*. Retrieved from <http://photogallery.nrcs.usda.gov/res/sites/photogallery/>

Received May 31, 2016

Accepted July 10, 2016

UDC 77.024.48.001.42:517.518.13

V.V. Zorilo, PhD,

Ye.Yu. Lebedeva, PhD, Assoc.Prof.,

M.O. Kozina, PhD,

D.S. Belush

Odessa National Polytechnic University, 1 Shevchenko Ave., 65044 Odessa, Ukraine; e-mail: mashak1989@rambler.ru

METHOD OF PHOTOMONTAGE DETECTION UNDER CONDITIONS OF LIMITATIONS ABSENCE FOR PHOTOS FALSIFICATION

В.В. Зоріло, О.Ю. Лебедева, М.О. Козіна, Д.С. Бєлуш. Метод виявлення фотомонтажу в умовах відсутності обмежень на використуванні при фальсифікації фотознімків. Поширене використання підроблених фотознімків в інформаційних війнах, судових справах, політиці, тощо потребує розробки нових ефективних методів виявлення фотомонтажу. Одним з них є метод виявлення фотомонтажу, заснований на аналізі сингулярних чисел блоків матриці цифрового зображення. **Мета:** Метою роботи є перевірка сфери застосування методу виявлення фотомонтажу, заснованого на аналізі сингулярних чисел блоків матриці цифрових зображень в умовах відсутності обмежень на ступінь їх стиснення. **Матеріали та методи:** В основі роботи розглянутого методу є виявлення відмінностей між зображеннями у випадку, коли вони мають різні ступені стиснення: значення матриці нульових сингулярних чисел блоків, що відповідають чужорідній частині зображення, вирізняють цю ділянку на фоні основного зображення, що дає змогу виявити фальсифікацію. Зазначений метод було досліджено за певних обмежень, що накладалися на використані тестові фотознімки. Проведено розширений експеримент з використанням зображень, для яких відсутні обмеження на ступінь стиснення. **Результати:** В результаті експерименту фальсифікацію було виявлено в 44.4 % випадків за умови збереження цифрового зображення після фотомонтажу в форматі без втрат, і в 53.3% випадків – при збереженні з втратами. Частіше фотомонтаж було виявлено тоді, коли різниця між коефіцієнтом якості Q основного зображення і заміщуючої ділянки була більше двох.

Ключові слова: фотомонтаж, перевірка цілісності цифрового зображення, метод виявлення фотомонтажу, матриця цифрового зображення, сингулярні числа.

V.V. Zorilo, Ye.Yu. Lebedeva, M.O. Kozina, D.S. Belush. Method of photomontage detection under conditions of limitations absence for photos falsification. The widespread using of fake pictures in information wars, lawsuits, politics, etc., needs to develop new detection methods of photomontage. One of them is a method of photomontage detection based on the analysis of singular values of matrix blocks of digital images. **Aim:** The aim of this research is to check the application area of photomontage detection method based on analysis of singular values of matrix blocks of digital images in the absence of restrictions on the degree of their compression. **Materials and Methods:** The basis of this method is the detection of the differences between the images when they have different degrees of compression: values of the zero singular values matrix of blocks corresponding to foreign part of image. We distinguish this area on the background of the main image, that allows to detect falsification. The mentioned method was investigated under certain restrictions imposed on the used test photos. An advanced experiment with images was held, for which there are no restrictions on the degree of compression. **Results:** The falsification was detected in 44.4% of cases in experimental study while saving the digital image after photomontage in lossless format, and in 53.3% of cases when saving the losses. Montage was detected most often when the difference between the quality factor Q of the main image and the replacing area was more than two.

Keywords: photomontage, digital image integrity checking, photomontage detection method, digital image matrix, singular numbers.

Introduction. Photomontage story begins long before the creation of modern graphic editors. With the first pictures people began to experiment — to combine the objects and scenes of different photos. Earlier to identify the photofake was easier by means of expert visual evaluation. Today, information technology in the area of computer graphic allows execute montage so that even experts are not able to detect it. Therefore, the development of photomontage detection methods that effective without expert is important and urgent today. In this paper as the montages we will understand the result and the process of images creating composed of several parts of different photos.

Scientists around the world work over photomontage detection. Note, the existing methods have their areas of application, its advantages and shortcomings.

Now actively the methods of digital image (DI) analysis are developing, grounded on the general approach to the analysis of the state and operation of information systems technology [1]. One is a method of photomontage detecting, based on the analysis of singular numbers of the matrix DI units.

DOI 10.15276/opu.2.49.2016.12

© 2016 The Authors. This is an open access article under the CC BY license (<http://creativecommons.org/licenses/by/4.0/>).

The work of this method is to identify the differences between the images when they have different degrees of compression. There are [2] formal differences established between DI in lossy and lossless format and DI in lossy formats with different quality factor.

Quality factor (Q) for lossy format JPEG determines the measure of photography compression. In this research it meets the standard of graphics editor Adobe Photoshop, according to which Q takes a value between 0...12 where more value Q corresponds to less compression of the image.

The mentioned method was investigated under certain limitations of used photos. In [2] it was justified the use of images with $Q \geq 8$ (for images compressed with a lower value of Q , the artifacts of compression appear that violate the stability of perception).

However, there are situations when images used in montages have low quality. In this regard, there is a need to clarify the application area of this method.

The aim of this research is to check the application area of photomontage detection method based on analysis of singular values of matrix blocks of digital images in the absence of restrictions on the degree of their compression.

Materials and Methods. The main instrument for the analysis of digital images for this method is the so-called zero singular numbers matrix of blocks (ZSNMB). Each element of this matrix corresponds to the block 8×8 matrix of digital image brightness, takes values from 0 to 8 and means number of zero singular numbers in the block [1, 2].

For DI in lossless format ZSNMB consists mostly of zeros. When compressing with the highest quality it is possible blotches of units, sometimes twos. With increasing DI compression the ZSNMB elements can take values from 0 to 8, which are caused by linear dependence row/columns of matrix [1]. Consider the example of this method (Fig. 1). In the image of the lake was inserted the boat with rowing.



Fig. 1. Photomontage (a) and ZSNMB of falsified DI (b)

As we can see, the ZSNMB value corresponding to foreign parts of images distinguish this area against the main image that allows you to detect the falsification.

Carry out an advanced experiment with images, for which there are no restrictions on the degree of compression. For the experiment there are 30 digital images in a lossless format of resource [3] used (traditional base of digital images when tested algorithms and methods).

In the image that saved before the montage in JPEG format with quality n (the main image), we insert a different part of the image (by replacing area) that has been saved in JPEG format with quality 1, 2, ..., $(n-1)$, where n takes the value from 1 to 10. The results are saved in lossless format (results typical for most photographic fakes are presented in Table 1) and in the lossy format JPEG with the same value of Q , as the main image (results typical for most received photo fakes are presented in Table 2).

Table 1

Results of the experiment with the saving of photomontage in lossless format

n	n	10	9	8	7	6	5	4	3	2	1
10	10	—	—	—	—	—	—	—	—	—	—
9	9	N	—	—	—	—	—	—	—	—	—
8	8	N	N	—	—	—	—	—	—	—	—
7	7	N	N	N	—	—	—	—	—	—	—
6	6	N	N	N	N	—	—	—	—	—	—
5	5	P	P	N	N	N	—	—	—	—	—
4	4	P	P	N	N	N	N	—	—	—	—
3	3	P	P	N	N	N	N	P	—	—	—
2	2	P	P	P	N	N	P	P	P	—	—
1	1	P	P	P	N	P	P	P	P	P	—

Table 2

Results of the experiment with saving of photomontage in the losses format

n	n	10	9	8	7	6	5	4	3	2	1
10	10	—	—	—	—	—	—	—	—	—	—
9	9	N	—	—	—	—	—	—	—	—	—
8	8	N	N	—	—	—	—	—	—	—	—
7	7	P	N	N	—	—	—	—	—	—	—
6	6	N	N	N	P	—	—	—	—	—	—
5	5	N	N	N	P	P	—	—	—	—	—
4	4	P	N	N	P	P	P	—	—	—	—
3	3	N	P	N	P	P	P	N	—	—	—
2	2	P	P	P	P	P	P	N	N	—	—
1	1	P	P	P	P	P	P	N	N	N	—

In these tables, we took the following notation: *N* (negative) — photomontage not found; *P* (positive) — photomontage found; “—” — experiment was not carried out.

Results and Discussion. In the experiment the falsification was detected in 44.4 % of cases when saving digital image after of photomontage in a lossless format, and in 53.3 % of cases — when saving the digital image with losses. More often montage was detected when the difference between the *Q* factor of the main image and replacing area was more than two. However, reveal a pattern that generally would make recommendations concerning area of application in this method is not possible.

Number of photomontage gaps if available — a very important indicator of the method effectiveness. The results showed that this method can not be recommended for widespread use to verify the integrity of digital images. However, it can be used in complex information security system or in combination with other methods of checking the integrity of digital images.

In the future the efficiency of this method we will research the impact of the block structure of digital images (background, contour) on properties its ZSNMB in the absence of restrictions on use for the photographs falsification. This, say the authors, will help monitor the uncharacteristic for integrated DI changes of singular numbers, which in turn will improve the process of fakes identifying.

This scientific work made it possible to critically assess the earlier developed method of detecting photomontage in conditions where there are no restrictions on use for the photographs falsification that are useful for the further development of an complex information security system.

Література

1. Кобозева, А.А. Основы общего подхода к решению проблемы обнаружения фальсификации цифрового сигнала / А.А. Кобозева // *Електромашинобудування та електрообладнання*. — 2009. — Вип. 72. — С. 35–41.
2. Зорило, В.В. Анализ особенностей сингулярных чисел матриц цифровых изображений при разных степенях сжатия для выявления фотомонтажа / В.В. Зорило, А.А. Кобозева // *Захист інформації*. — 2010. — Т. 12, № 3(48). — С. 34–40.
3. NRCS Photo Gallery [Электронный ресурс] / United States Department of Agriculture. Washington, USA. — Режим доступа: <http://photogallery.nrcs.usda.gov> (Дата звернення: 26.07.2012).

References

1. Kobozeva, A.A. (2009). Foundations of general approach to a problem of detection of digital signal forgery. *Electrical Machine-Building and Electrical Equipment*, 72, 35–41.
2. Zorilo, V.V., & Kobzeva, A.A. (2010). Analysis of features of singular values of the matrix of digital images at different compression ratios for the image forgery detection. *Ukrainian Information Security Research Journal*, 12(3), 34–40.
3. USDA: United States Department of Agriculture (n.d.). *NRCS Photo Gallery*. Retrieved from <http://photogallery.nrcs.usda.gov/res/sites/photogallery/>

Received June 7, 2016

Accepted July 22, 2016

ELECTRONICS. RADIO ENGINEERING. TELECOMMUNICATION FACILITIES

ЕЛЕКТРОНІКА. РАДІОТЕХНІКА.
ЗАСОБИ ТЕЛЕКОМУНІКАЦІЙ

UDC [681.2.084:537.533.3–033.65]:537.533

I.V. Yatsenko, PhD, Assoc.Prof.

Cherkasy State Technological University, 460 Shevchenko Blvd., 18006 Cherkasy, Ukraine; e-mail: irina.yatsenko.79@mail.ru

IMPROVEMENT OF SURFACE LAYERS PROPERTIES OF PRECISION ENGINEERING ELEMENTS OF OPTICAL CERAMICS BY PRELIMINARY ELECTRON-BEAM SURFACING

I.V. Яценко. Покращення властивостей поверхневих шарів елементів точного приладобудування з оптичних керамік шляхом попередньої електронно-променевої обробки їх поверхонь. Для запобігання руйнуванням елементів з оптичних керамік практичне значення має попередня електронно-променева обробка поверхонь на стадії виготовлення приладів на їх основі, яка дозволяє покращувати властивості поверхневих шарів елементів. **Мета:** Метою роботи є дослідження впливу параметрів попередньої електронно-променевої обробки елементів з оптичних керамік на попередження їх руйнувань, покращення властивостей поверхневих шарів і підвищення стійкості до зовнішніх термодій. **Матеріали і методи:** Для дослідження впливу параметрів електронного променя на властивості поверхневих шарів елементів з оптичної кераміки використовувались диски діаметром $3 \cdot 10^{-2} \dots 5 \cdot 10^{-2}$ м і товщиною $4 \cdot 10^{-3} \dots 6 \cdot 10^{-3}$ м, півсферичні обтічники діаметром $4 \cdot 10^{-2} \dots 8 \cdot 10^{-2}$ м. Для проведення досліджень термічної дії рухомого електронного променя на елементи з оптичної кераміки було використано електронно-променеве обладнання, що дозволяє реалізувати стрічковий електронний промінь шириною $5 \cdot 10^{-4} \dots 5 \cdot 10^{-3}$ м, довжиною $6 \cdot 10^{-2} \dots 8 \cdot 10^{-2}$ м, густиною теплової дії $F_n = 5 \cdot 10^6 \dots 9 \cdot 10^8$ Вт/м² і швидкістю переміщення $V = 5 \cdot 10^{-3} \dots 10^{-1}$ м/с. **Результати:** В результаті проведених експериментальних досліджень встановлено, що для розглядуваних діапазонів зміни параметрів електронного променя ($F_n = 10^6 \dots 1,6 \cdot 10^7$ Вт/м², $V = 10^{-3} \dots 10^{-1}$ м/с) мікротвердість поверхні елементів змінюється від 1.2...2.9 (для необроблених елементів) до 5.7...6.4 ГПа (для оброблених елементів). Покращення вказаних властивостей приводить до підвищення стійкості елементів до зовнішніх термодій. Збільшено у 1.3...1.7 рази критичні значення зовнішніх теплових потоків та час їх дії. Перевищення цих параметрів призводить до руйнування елементів та виходу з ладу приладів для досліджуваного діапазону зміни зовнішнього тиску $10^5 \dots 10^7$ Па. Підвищено гранично допустимі значення термопружних напружень з 50...140 до 160...370 МПа при температурах нагріву 300...1200 К.

Ключові слова: точне приладобудування, оптична кераміка, електронний промінь, мікроструктура, твердість, термопружні напруження.

I.V. Yatsenko. Improvement of surface layers properties of precision engineering elements of optical ceramics by preliminary electron-beam surfacing. To prevent destruction of the elements made of optical ceramics the practical importance has the preliminary electron-beam treatment of their surfaces during the manufacturing stage of devices based on them. This allows improving the properties of the surface layers of the elements, making them more resistant to external thermal and mechanical impacts. **Aim:** The aim of this research is to research the impact of parameters of preliminary electron-beam treatment of the elements made of optical ceramics to prevent their destruction, improvement of the surface layers properties and increasing of their resistance to external thermo-influences. **Materials and Methods:** The discs with diameter of $3 \cdot 10^{-2} \dots 5 \cdot 10^{-2}$ m and thickness of $4 \cdot 10^{-3} \dots 6 \cdot 10^{-3}$ m and hemispherical cowl with diameter of $4 \cdot 10^{-2} \dots 8 \cdot 10^{-2}$ m were used to research the impact of electron-beam parameters on surface layers properties of the elements made of optical ceramics. **Results:** After researches it was established that for studied range of electron beam parameters ($F_n = 10^6 \dots 1.6 \cdot 10^7$ W/m², $V = 10^{-3} \dots 10^{-1}$ m/s) the microhardness of the elements surface increases from 1.2...2.9 GPa (unprocessed elements) to 5.7...6.4 GPa (processed elements). It was defined, that improvement of these properties leads to improvement of elements resistance to external thermo-influences. The critical values of external heat streams and the time of their actions are increase in 1.3...1.7 times. The excess these parameters leads to the destruction of the elements and failure of the devices for the studied range of external pressure variation $10^5 \dots 10^7$ Pa. The maximum allowable values of thermal stresses in elements are raised from 50...140 to 160...370 MPa at the heating temperatures of 300...1200 K.

Keywords: precision engineering, optical ceramics, electron beam, microstructure, hardness, thermal stresses.

Introduction. The successes achieved over the past quarter century in the development of electron beam technology led to the creation of various electron-beam equipment for industrial, scientific, medical and military purposes.

DOI 10.15276/opu.2.49.2016.13

© 2016 The Authors. This is an open access article under the CC BY license (<http://creativecommons.org/licenses/by/4.0/>).

Modern instruments with elements of optical ceramics, (KO1, KO2, KO3, KO5, KO12 etc) for measurement and thermal testing of different physical objects (plates and discs as substrate filters of infrared devices, input protective window of laser sighting systems for surveillance in IR spectrum, hemispherical fairing of infrared homing devices and monitoring facilities etc. [1...6]) (Fig. 1) are subjected to intense external thermo-influences (high heating temperature and external pressure, shock thermo-influences in terms of shots and flight etc.).

In these conditions there is a significant change in the properties of the surface layers of the optical elements up to their destruction (cracking, chips and others. defects), leading to a significant deterioration in technical and operational characteristics of devices (reliability, service life, etc.) and their failure.

So important is the prevention of these undesirable effects at the design stage.

Experimental studies [7...14] show that to prevent the destruction of elements with optical ceramics the electron beam methods of pre-treatment of the working surfaces have practical importance. They can significantly improve (more than 2...3 times) properties of the surface layers of the elements (microhardness, thickness reinforced layers, etc.), which in turn affect the stability of materials for external thermo-influences.

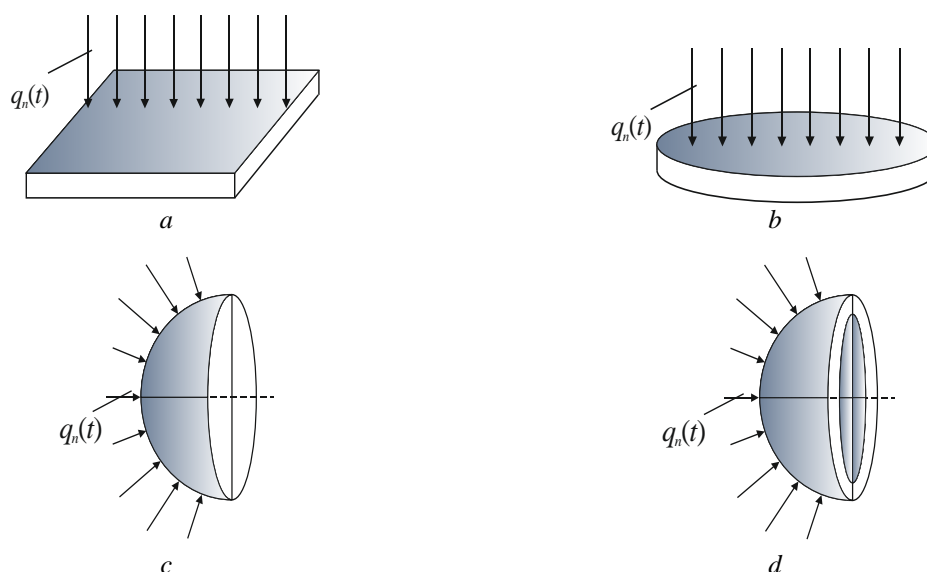


Fig. 1. General view of the optical elements of precision instrumentation which are subjected of external thermo-influences in conditions of operation of devices based on them, $q_n(t)$ — density of external thermo-influences, W/m^2 : a — plate; b — discs; c, d — hemispherical fairing

Currently, the process of prevention of possible destruction of elements of the precise instrument with optical ceramics under influence of external thermo-influences studied not enough. For example, not paid attention to the calculation the permissible ranges of parameters of the electron beam (density of thermo-influences, velocity), within which there would be a significant improvement of the properties of the surface layers of processed elements and would be missing their local destruction (cracks, bumps, depressions, chips etc).

Further study of the effects of external thermo-influences to elements of precise instrument with optical ceramic will help to improve their resistance to external heat loads and, ultimately, improve the technical and operational characteristics of the devices in their operation.

The aim of this research is to research the impact of parameters of preliminary electron-beam treatment of the elements made of optical ceramics to prevent their destruction, improvement of the surface layers properties and increasing of their resistance to external thermo-influences.

Materials and Methods. The discs with diameter of $3 \cdot 10^{-2} \dots 5 \cdot 10^{-2}$ m and thickness of $4 \cdot 10^{-3} \dots 6 \cdot 10^{-3}$ m and hemispherical cowl with diameter of $4 \cdot 10^{-2} \dots 8 \cdot 10^{-2}$ m were used to research

the impact of electron-beam parameters on surface layers properties of the elements made of optical ceramics (KO1, KO2, KO3, KO5, KO12) [10, 15].

For research the thermo-influences of moving electron beam to the optical elements with ceramics the specialized electron-beam equipment [10]. The main characteristics of strip electron beam were as follows: width — $5 \cdot 10^{-4} \dots 5 \cdot 10^{-3}$ m, length — $6 \cdot 10^{-2} \dots 8 \cdot 10^{-2}$ m, density of thermo-influences — $F_n = 5 \cdot 10^6 \dots 9 \cdot 10^8$ W/m² and velocity — $V = 5 \cdot 10^{-3} \dots 10^{-1}$ m/s.

The electron-beam equipment and its main elements. Equipment was established on the basis of universal vacuum installation UVN-74P3 (Fig. 2) [10]. The vacuum system consists of a vacuum chamber and a vacuum installation post UVN-74P3, oil vapor diffusion pump NP-400, vacuum pump AVZ-20, vacuum meters VIT-3 and VMB-8, vacuum sensors (thermocouple TP-1, ionization IP-1, magnetic blocking M-2) located in the vacuum volume. In a vacuum chamber of the installation the special technological equipment for electronic data processing was placed; there are quartz infrared preheating and final cooling oven, electron gun with Pierce optics to form the strip electron stream, the mechanism of movement of the optical elements. The following external devices provide the special technological equipment operations: high-voltage power source of electron gun based on unit UELI-1, control unit of a quartz oven on the base of thermal sensor — the thermostat RIF-101, an automated processing control system was developed.

For modeling the thermal effects on the studied optical elements under normal conditions ($T_0 = 293$ K, $P = 10^5$ Pa) and for finding the critical values of parameters (heat flow q_n^* and time of action t^*) controlled infrared heating has been used quartz lamps of type KNM-220-1000-1 with RIF-101 sensors for temperature control of surfaces elements in the range of 300...1900 K and heat flow that come to them.

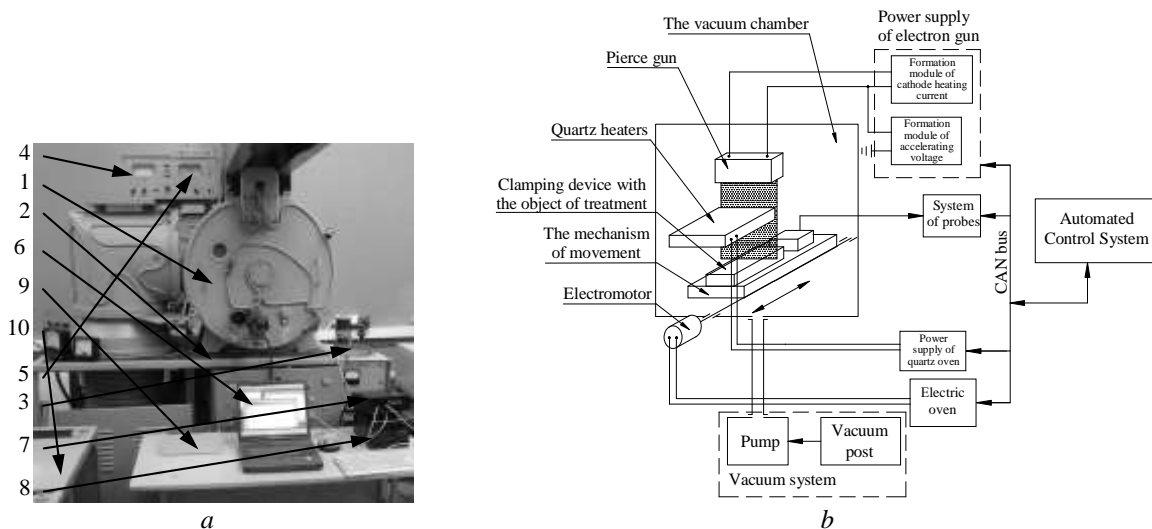


Fig. 2. Appearance (a) and general scheme (b) of equipment for the electronic processing of optical elements: 1 — vacuum chamber; 2 — electric drive mechanism for moving of the optical elements; 3 — temperature control system of optical elements based on thermostat RIF-101; 4 — vacuumeter VIT-3; 5 — vacuumeter VMB-8; 6 — PC for installation control; 7 — central unit of automatic control system; 8 — electric control unit; 9 — modules of temperature measuring in the area of processing and sensing of electron stream; 10 — power supply and control system of Pierce electron gun

For the modeling of high heating temperatures impact (1500 K) and external pressures (10^7 Pa) the specialized equipment was used, tests on which were held using methodic developed at SDP SE “Arsenal” (Kyiv) and Cherkasy State Technological University.

Installation for the study of optical elements at high temperatures (1500 K) and external pressures (up to $3 \cdot 10^7$ Pa). The installation is shown in Fig. 3 and designed for simultaneous testing of

three elements. Accuracy of working pressure in the installation is $\pm 5\%$. The installation consists of a device of permanent pressure and heating system, temperature control and temperature recording. Constant pressure device contains three test chambers which are connected to one unit. Unit of cameras is combined with the body of liquid filter which filling with water before testing. Heating of elements was made directly in chambers. When testing the device of constant pressure filled with an inert gas. All three elements are tested simultaneously. Products that cooled and cleaned of condensed particles in the liquid filter, entering to the valve of constant pressure controlled by compressed gas.

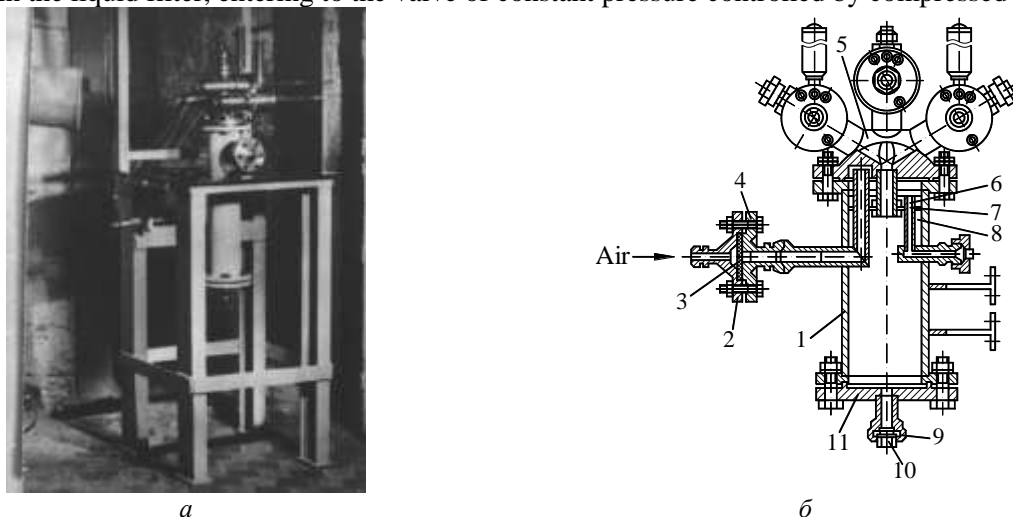


Fig. 3. Appearance of settings (a) and scheme of constant pressure device (b) 1 —filter housing; 2 —valve cap; 3 —membrane; 4 —valve body; 5 —unit of testing chambers; 6 —drain pipe; 7 —mechanical disk filter; 8 —water; 9 —nut; 10 —cap; 11 —filter cap

To determine the properties of the surface layers of the of optical elements before and after electron beam treatment (microhardness of surface (H_v , MPa), the quantities of residual thermo stressed (σ , MPa) and thickness of reinforced layers (Δ , m) we used known methods of physical and chemical analysis (micro identification by Vickers method, methods of optical microscopy and microprobe analysis, which includes the raster and scanning microscopy (SEM) and transmission electron microscopy (TEM), diffractometers DRON-0.5, DRON-2.0, DRON-3.0 with special consoles for measuring the microstresses in the surface layers, etc. [16...18]). Tensile strength of optical elements $\sigma^*(T)$ before and after electron-beam processing was found by the central annular bending method [10, 15].

In studies conducted to determine the above mentioned properties of the surface layers of optical elements and critical parameters of external influences the relative error does not exceed 5...10%.

Results. Experiments with electronic processing of elements with optical ceramics have shown that they can not be melted in a vacuum because of the high elasticity of vapor [5, 10]. Thus, pre-heating in vacuum of optical elements even up to 1300 K, leads to advanced evaporation of material, and when trying it melting the liquid phase is not formed.

This electronic processing of elements with optical ceramics without heating leads to increase their microhardness, streamline and strengthen the structure by forming the surface layers of compressive stresses and thereby to increase the strength of products to thermal shock effects, which they are exposed to in operation.

Electron microscopic analysis of images of surfaces and transverse thin sections of optical ceramics before and after processing shows that there is a noticeable change in the structure of the material in depth (up to 250...300 μm), which depending on the electron beam parameters (F_n , V).

As a result of experimental studies it was established that for studied range of electron beam parameters ($F_n = 10^6 \dots 1.6 \cdot 10^7 \text{ W/m}^2$, $V = 10^{-3} \dots 10^{-1} \text{ m/s}$) the microhardness of the elements surface increases from 1.2...2.9 GPa (unprocessed elements) to 5.7...6.4 GPa (processed elements). The increase in heat density F_n from 10^6 W/m^2 to $1.6 \cdot 10^7 \text{ W/m}^2$ leads to increasing of ceramics surface

microhardness in 1.5...1.7 times, and increase the velocity V from 10^{-3} to 10^{-1} m/s leads to decrease in microhardness of ceramic surface in 1.3...1.4 times (Fig. 4).

The results of studies of microhardness change on depth of elements with optical ceramics processed by electron beam, shown in Fig. 5. These data suggest that the microhardness of the material of all types of ceramics that were considered sufficiently decreases rapidly heading for its value for uncultivated material. The thickness of the hardened layer (Δ), where there are major structural changes and increased microhardness of the material for the electron beam parameters under consideration ranges from 70...90 μm to 210...230 μm in thickness of processed products $4...6 \cdot 10^{-3}$ m. The thickness of the hardened layer Δ depends greatly on the nature of ceramics as well as the parameters of the electron beam (Fig. 6): increase in heat density F_n from 10^6 W/m² to $2 \cdot 10^7$ W/m² leads to increased thickness of the hardened layer in 1.8...2.6 times, and increase the speed of the beam from $1.5 \cdot 10^{-3}$ m/s to $2 \cdot 10^{-2}$ m/s leads to decrease in thickness of hardened layer in 1.7...2.5 times.

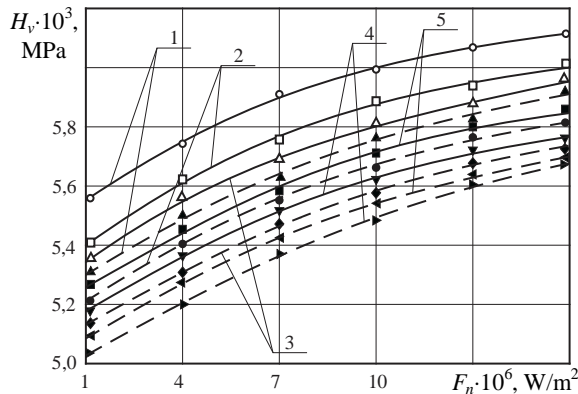


Fig. 4. Dependence of microhardness of the surface with optical ceramics KO12 (1), KO2 (2), KO1 (3), KO5 (4) and KO3 (5), which are processed by electronically beam on its thermal effects density: $V=7 \cdot 10^{-3}$ m/s (-----); $V=1,5 \cdot 10^{-2}$ m/s (- - - -); Δ , \circ , \square , \blacktriangle , \blacksquare , \blacklozenge , \blacktriangledown , \bullet , \blacktriangleright , \blacktriangleleft (experimental data)

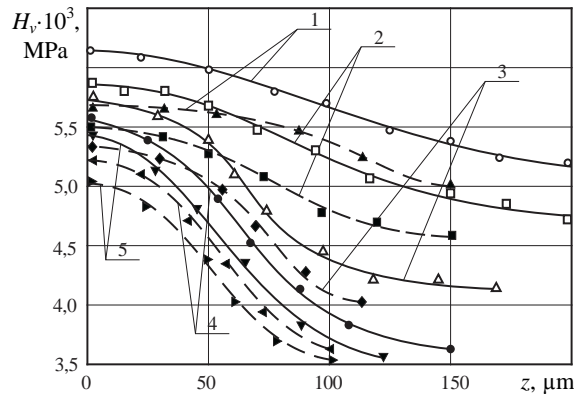


Fig. 5. Change of microhardness on depth of elements with optical ceramics KO12 (1), KO2 (2), KO1 (3) KO3 (4) and KO5 (5), which are processed by electron beam for different speeds of its movement ($F_n=1,5 \cdot 10^7$ W/m²): $V=7 \cdot 10^{-3}$ m/s (-----); $V=1,5 \cdot 10^{-2}$ m/s (- - - -); Δ , \circ , \square , \blacktriangle , \blacksquare , \blacklozenge , \blacktriangledown , \bullet , \blacktriangleright , \blacktriangleleft (experimental data)

It was established that the influence of the electron beam on the surface of the optical ceramics elements leads to a mosaic block increase and decrease the microstrains of crystal lattice. The value of mosaic blocks for optical elements that electron beam treated, compared to their condition before treatment increased in 3.9 times for items from the KO1, in 5.5 times for items from KO2, in 3.3 times for the elements of KO12, in 4.7 times for items from KO3 and in 7.7 times for items from KO5, and the value of microstrains reduced in 3.7 times for items from the KO1, in 5.4 times for items from KO2, in 4.2 times for items from KO12, in 5.5 times for items from KO3 and in 5.9 times for items from KO5.

It is shown that regardless of technological modes of processing (values F_n and V for the examined range of change) of elements with optical ceramics in all cases an increase in the size

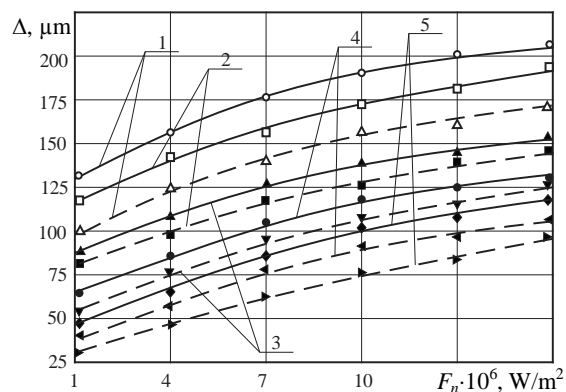


Fig. 6. Dependence the depth strengthening by electron beam the optical elements with ceramics KO12 (1), KO2 (2), KO1 (3) KO3 (4) and KO5 (5) from the values of its thermo-influences density: $V=7 \cdot 10^{-3}$ m/s (-----); $V=1,5 \cdot 10^{-2}$ m/s (- - - -); Δ , \circ , \square , \blacktriangle , \blacksquare , \blacklozenge , \blacktriangledown , \bullet , \blacktriangleright , \blacktriangleleft (experimental data)

of the mosaics blocks and reduce of microstrains their crystal lattice, that is, as a result of electronic processing we obtain a coarse surface layers with stress in the crystal lattice.

Analysis of the changes parameters of the elements crystal (after processing according to known methods of calculating these radiographs [18], based on the line analytical relationship between residual stresses acting on the surface element and change the period of the crystal lattice of the main components under consideration ceramics, showed the presence of compressive stresses in thin surface layers of the elements of depth 40...60 μm for the central part of the treated areas (plots size $4 \cdot 10^{-2} \dots 5 \cdot 10^{-2} \text{ m}$) in the considerable range of parameters of electron beam, for elements of optical ceramics KO1 — up to 30...40 MPa, for elements of optical ceramics KO2 — up to 60...70 MPa, for elements of optical ceramics KO3 — up to 25...30 MPa, for elements of optical ceramics KO5 — up to 55...65 MPa, for items from optical ceramics KO12 — up to 75...90 MPa.

As a result of studies it was found that after preliminary electron beam processing of optical elements there is increased the critical values of external heat flow q_n^* and the time of action t^* in 2...4 times (Fig. 7). The increase in external pressure up to 10^7 Pa , which can be implemented, for example, as the shock front at supersonic airflow with fairings infrared device in flight and shot [3, 10], resulting in increased value q_n^* and q_n^* only in 1.3...1.7 times (Fig. 8).

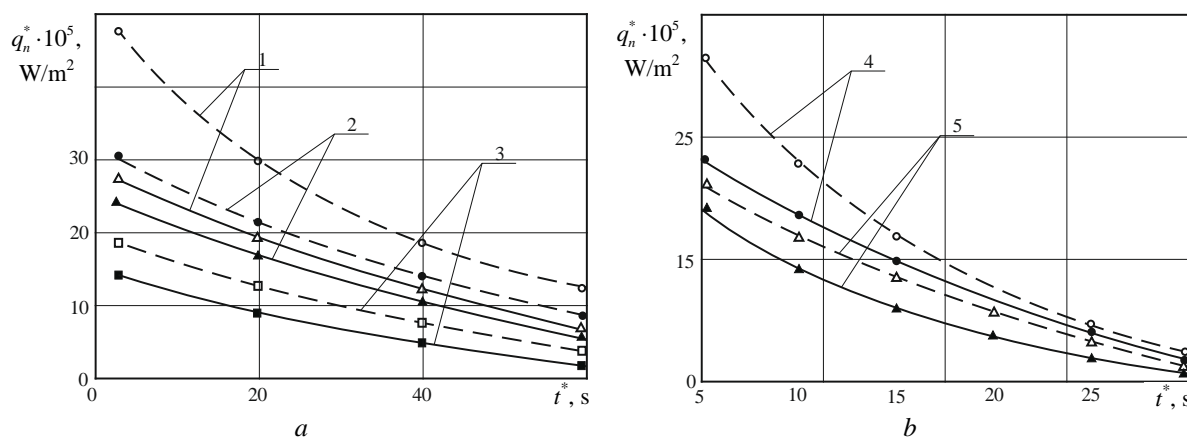


Fig. 7. Dependence of critical values of external heat flows q_n^* from the time of their effects t^* on treated and untreated optical elements by the electron beam (element thickness $H = 4 \cdot 10^{-3} \text{ m}$, $T_0 = 300 \text{ K}$, $P = 10^5 \text{ Pa}$):
untreated elements (—); treated elements ($F_n = 1,6 \cdot 10^7 \text{ W/m}^2$, $V = 10^{-3} \text{ m/s}$) (---);
a — elements with optical ceramics KO5 (1), KO1 (2) and KO12 (3);
b — elements with optical ceramics KO3 (4) and KO2 (5);
 Δ , \circ , \square , \blacktriangle , \blacksquare , \bullet (experimental data)

In addition, it was also shown that the maximum allowable value of thermoelastic stresses σ^* at various temperatures of heating T for the optical elements processed by electronic beam in 1.8...2.7 times higher than for unprocessed elements (Fig. 9).

Using the results obtained in the design and production of new and modernization of serial devices with the examined optical elements for measuring and thermal control objects of different physical nature (IR optical instruments, laser sighting systems, infrared homing devices and surveillance, laser medical devices based on optical fibers, etc.) will increase their basic technical and operational characteristics (reliability, resource and service life, etc.) during operation, taking into account the impact of external thermo actions. For example, during storage and transportation in terms of the emergence of high-temperature centers of fire (warehouse storage, combat zone, etc.), and application of products with infrared homing devices and monitoring in terms of shots and flight (drums exterior thermal and mechanical effects, etc.).

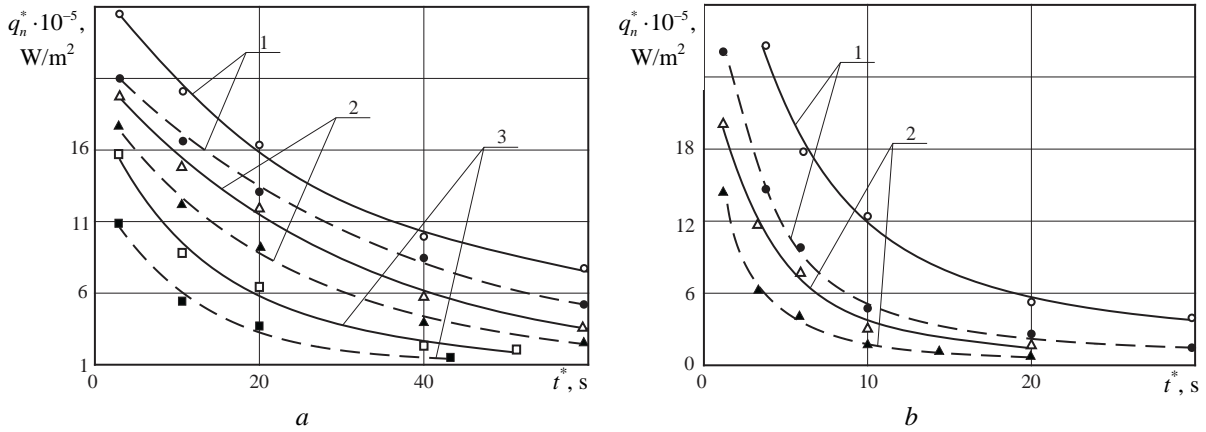


Fig. 8. Dependences of critical values of external heat flows q_n^* from the t^* time of their impact on processed by electron beam optical elements (element thickness $H = 6 \cdot 10^{-3}$ m, $F_n = 1,6 \cdot 10^7$ W/m², $V = 10^{-3}$ m/s): $P = 10^5$ Pa (—); $P = 10^7$ Pa (- - -); a — elements with optical ceramics KO5 (1), KO1 (2) and KO12 (3); b — elements with optical ceramics KO2 (4) and KO3 (5); Δ , \circ , \square , \blacktriangle , \blacksquare , \bullet (experimental data)

Conclusions. The study found that after pre-treatment of working surfaces of optical elements with ceramics (KO1, KO2, KO3, KO5, KO12) by moveable electron beam for studied range of electron beam parameters ($F_n = 10^6 \dots 1,6 \cdot 10^7$ W/m², $V = 10^{-3} \dots 10^{-1}$ m/s) the basic properties of the surface layers improve without local damage:

— The surface microhardness is increasing in 1.9...2.3 times;

— Compressive thermostatic stress of 25...90 MPa occur in the surface layers of thickness 40...60 μ m, which lead to the formation of reinforced layers with thick from 210 to 230 μ m.

It was defined, that improvement of these properties leads to improvement of elements resistance to external thermo-influences:

— The critical values of external heat flow and the time of their actions are increase in 2...4 times that lead to the destruction of the elements and failure of the devices; increasing in external pressure from 10^5 to 10^7 Pa reduces critical values in 1.5...1.9 times;

— The maximum allowable values of thermal stresses in elements are raised from 50...140 MPa to 160...370 MPa at the heating temperatures of 300...1200 K.

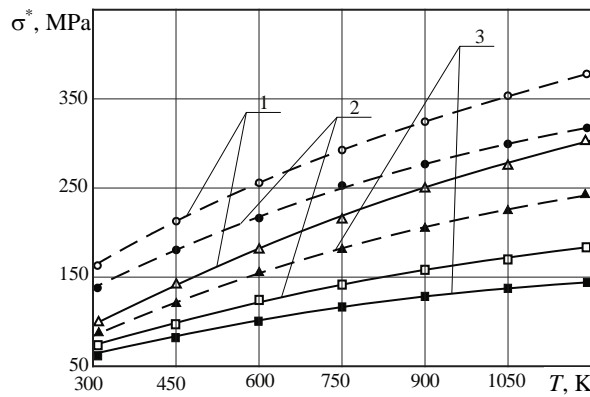


Fig. 9. The dependence of the maximum permissible thermoelastic stresses in the elements from optical ceramics KO1 (1), KO2 (2), KO3 (3) of the heating temperature ($P = 10^5$ Pa, the thickness of the element $H = 4 \cdot 10^{-3}$ m, $F_n = 1,6 \cdot 10^7$ W/m², $V = 10^{-3}$ m/s): unprocessed element (—); element processed by electron beam (- - -); Δ , \circ , \square , \blacktriangle , \blacksquare , \bullet (experimental data)

Література

1. Bessmertnyi, V.S. Plasma treatment of glasses (A review) / V.S. Bessmertnyi // Glass and Ceramics. — 2001. — Vol. 58, Issue 3–4. — PP. 121–124.
2. Тарасов, В.В. Инфракрасные системы «смотрящего типа»: монография / В.В. Тарасов, Ю.Г. Якушенко. — М.: ЛОГОС, 2004. — 443 с.

3. Тепловые процессы при электронной обработке оптических материалов и эксплуатации изделий на их основе: монография / В.А. Ващенко, Д.И. Котельников, Ю.Г. Лега и др. — К.: Наукова думка, 2006. — 368 с.
4. Anderberg, B. *Laser weapons: The dawn of a new military age* / B. Anderberg, M.L. Wolbarsht. — New York: Plenum Press, 1992. — 244 p.
5. Airborne laser sensors and integrated systems / R. Sabatini, M.A. Richardson, A. Gardi, S. Ramasamy // *Progress in Aerospace Sciences*. — 2015. — Vol. 79. — PP. 15–63.
6. Современные аспекты лазерной терапии: монография / М.Н. Бонусь, А.И. Гладкова, С.А. Горбатюк и др.; ред.: В.Д. Попов. — Черкассы: Вертикаль, 2011. — 607 с.
7. Канашевич, Г.В. Перспективи використання електронного променю в технології інтегральної оптики / Г.В. Канашевич, В.А. Ващенко, М.О. Бондаренко // *Вісник Черкаського інженерно-технологічного інституту*. — 2000. — № 2. — С. 189–193.
8. Спеціальні методи обробки оптичного скла. Технологія, техніка, економіка / М.П. Бочок, М.П. Бутко, В.А. Ващенко та ін.; за ред. Д.І. Котельніков. — Чернігів: ЧДТУ, 2002. — 152 с.
9. Получение функциональных слоев в оптическом стекле и керамике методом электронной обработки / Г.Н. Дубровская, Г.В. Канашевич, В.А. Ващенко и др. // *Сб. докл. Междунар. науч.-практ. симпозиума «Функциональные покрытия на стеклах» (FCG-1)*. — Харьков: НТЦ ХФТИ «Константа», 2003. — С. 135–137.
10. Основи електронної мікрообробки виробів з оптичних матеріалів: монографія / В.А. Ващенко, І.В. Яценко, Ю.Г. Лега, О.В. Кириченко. — К.: Наукова думка, 2011. — 560 с.
11. Influence of parameters by electronic ray on properties of superficial layers of optical elements of exact instrument-making / I. Yatsenko, V. Antoniuk, M. Bondarenko, V. Vashchenko // *Proceedings of Scientific-Technical Conference “Innovations in Engineering”*, 10-11 September 2015, Burgas, Bulgaria. — Sofia: Scientific-Technical Union of Mechanical Engineering, 2015. — PP. 64–66.
12. Определение критических значений параметров внешних термовоздействий на поверхность обтекателей ИК-приборов в условиях выстрела и полета / И.В. Яценко, В.С. Антонюк, В.А. Ващенко, В.В. Цыбулин // *Наноинженерия*. — 2015. — № 12. — С. 20–25.
13. Упреждение возможных разрушений оптических обтекателей ИК-приборов в условиях выстрела и полета / И.В. Яценко, В.С. Антонюк, В.А. Ващенко, В.В. Цыбулин // *Наноинженерия*. — 2015. — № 12. — С. 26–31.
14. Попередження можливих руйнувань оптичних елементів точного приладобудування в умовах зовнішніх термодій / І.В. Яценко, В.С. Антонюк, В.А. Ващенко, В.В. Цибулін // *Журнал нано- та електронної фізики*. — 2016. — Т. 8, № 1. — С. 01027-1 — 01027-6.
15. Yatsenko, I.V. Experimental and statistical models of impact determination of the electron beam parameters on surface layers properties of optical elements in precision instruments building / I.V. Yatsenko // *Пр. Одес. політехн. ун-ту*. — 2016. — Вип. 1(48). — С. 65–71.
16. Engel, L. *An atlas of metal damage: surface examination by scanning electron microscope* / L. Engel, H. Klingele. — 2nd Ed. — Herne: Flender Service, 2001. — 271 p.
17. Горелик, С.С. Рентгенографический и электронно-оптический анализ / С.С. Горелик, Ю.А. Скаков, Л.Н. Расторгуев. — М.: МИСИС, 2002. — 358 с.
18. Bauer, E. *Surface microscopy with low energy electrons* / E. Bauer. — New York: Springer, 2014. — 496 p.

References

1. Bessmertnyi, V.S. (2001). Plasma treatment of glasses (A review). *Glass and Ceramics*, 58(3–4), 121–124. DOI:10.1023/A:1010907701090
2. Tarasov, V.V., & Yakushenkov, Y.G. (2004). *Infrared Imaging Systems*. Moscow: Logos.
3. Vaschenko, V.A., Kotelnikov, D.I., Lega, Yu.G., Krasnov, D.M., Yatsenko, I.V., & Kirichenko, O.V. (2006). *Thermal Processes in the Electronic Processing of Optical Materials and Use of Products Based on Them*. Kyiv: Naukova Dumka.
4. Anderberg, B. & Wolbarsht, M.L. (1992). *Laser Weapons: The Dawn of a New Military Age*. New York: Plenum Press.
5. Sabatini, R., Richardson, M.A., Gardi, A., & Ramasamy, S. (2015). Airborne laser sensors and integrated systems. *Progress in Aerospace Sciences*, 79, 15–63. DOI:10.1016/j.paerosci.2015.07.002

6. Bonus', M.N., Gladkova, A.I., Gorbatyuk, S.A., Zubkova, E.V., Zubkova, S.T., Katyukova, L.D., ... Lobanov, G.F. (2011). *Modern Aspects of Laser Therapy*. Cherkasy: Vertikal'.
7. Kanashevich, G.V., Vaschenko, V.A., & Bondarenko, M.O. (2000). Prospects for the use of the electron beam in integrated optics technology. *Bulletin of Cherkasy Engineering and Technological Institute*, 2, 189–193.
8. Bochok, M.P., Butko, M.P., Vaschenko, V.A., Kanashevich, G.V., & Kotelnikov, D.I. (2002). *Special Techniques for Optical Glass Processing: Technology, Technique, and Economics*. Chernihiv: Chernihiv National University of Technology.
9. Dubrovskaya, G.N., Kanashevich, G.V., Vaschenko, V.A., Kotelnikov, D.I., & Yatsenko, I.V. (2003). Obtaining the functional layers in the optical glass and ceramic by electronic processing method. In *Proceedings of International Scientific and Technical Symposium on Functional Coatings on Glass (FCG-1)* (pp. 135–137). Kharkiv: Konstanta.
10. Vashchenko, V.A., Yatsenko, I.V., Lega, Yu.G., & Kirichenko, O.V. (2011). *The Basics of Electronic Microprocessing of Optical Materials*. Kyiv: Naukova Dumka.
11. Yatsenko, I., Antoniuk, V., Bondarenko, M., & Vashchenko, V. (2015). Influence of parameters by electronic ray on properties of superficial layers of optical elements of exact instrument-making. In *Proceedings of Scientific-Technical Conference on Innovations in Engineering* (pp. 64–66). Sofia: Scientific-Technical Union of Mechanical Engineering.
12. Yatsenko, I.V., Antonyuk, V.S., Vaschenko, V.A., & Tsybulin, V.V. (2015). Determination of critical values of parameters external thermo-influences on the surface of the fairings IR-devices in terms of shots and flight. *NanoEngineering*, 12, 20–25.
13. Yatsenko, I.V., Antonyuk, V.S., Vaschenko, V.A., & Tsybulin, V.V. (2015). Anticipation of possible destructions of the optical fairing IR-devices in the conditions of the shot and flight. *NanoEngineering*, 12, 26–31.
14. Yatsenko, I.V., Antonyuk, S.V., Vaschenko, V.A., & Tsybulin, V.V. (2016). Prevent potential destruction of the optical elements of precision instrumentation to external thermo-influences. *Journal of Nano- and Electronic Physics*, 8(1), 01027-1—01027-6. DOI:10.21272/jnep.8(1).01027
15. Yatsenko, I.V. (2015). Experimental and statistical models of impact determination of the electron beam parameters on surface layers properties of optical elements in precision instruments building. *Odes'kyi Politechnichniy Universytet. Pratsi*, 1, 65–71. DOI:10.15276/opu.1.48.2016.12
16. Engel, L., & Klingele, H. (2001). *An Atlas of Metal Damage: Surface Examination by Scanning Electron Microscope* (2nd Ed.). Herne: Flender Service.
17. Gorelik, S.S., Rastorguev, L.N., & Skakov, Yu.A. (2002). *Radiographic and Electro-Optical Analysis*. Moscow: MISIS.
18. Bauer, E. (2014). *Surface Microscopy with Low Energy Electrons*. New York: Springer.

Received May 26, 2016

Accepted July 10, 2016

FUNDAMENTAL AND APPLIED SCIENCES PROBLEMS

ПРОБЛЕМИ ФУНДАМЕНТАЛЬНИХ І ПРИКЛАДНИХ НАУК

UDC 539.3:517.518.12+624.044

O.B. Kozin¹, PhD, Assoc.Prof.,
O.B. Papkovskaya², PhD, Assoc.Prof.,
M.O. Kozina², PhD

¹ National University "Odesa Law Academy", 23 Fontans'ka Rd., 65009 Odessa, Ukraine; e-mail: kozindre@rambler.ru

² Odessa National Polytechnic University, 1 Shevchenko Ave., 65044 Odessa, Ukraine

MODELLING AND SOLUTION OF CONTACT PROBLEM FOR INFINITE PLATE AND CROSS-SHAPED EMBEDMENT

O.B. Kozin, O.B. Papkovskaya, M.O. Kozina. Моделювання і розв'язання контактної задачі для нескінченної пластини і хрестоподібного включення. Розробка ефективних методів визначення напружено-деформованого стану тонкостінних конструкцій з включеннями, підкріпленнями й іншими концентраторами напружень є важливим завданням як з теоретичної, так і з практичної точки зору, враховуючи їх велике практичне застосування. **Мета:** Метою дослідження є розробка аналітичного математичного методу вивчення напружено-деформованого стану нескінченної пластини з хрестоподібним включенням при вигині. **Матеріали і методи:** Метод граничних елементів є ефективним способом розв'язання крайових задач для систем диференціальних рівнянь. Методи, засновані на граничних інтегральних рівняннях, знаходять широке застосування в багатьох галузях науки і техніки, включаючи розрахунок пластин і оболонок. Одним із методів розв'язання численного класу інтегральних рівнянь і систем, що виникають на базі методу граничних інтегральних рівнянь, є аналітичний метод зведення цих рівнянь і систем до задач Рімана з подальшим їх розв'язанням. **Результати:** Отримано інтегральне рівняння для аналізу прогинів і аналізу напружено-деформованого стану тонкої пружної пластини з жорстким хрестоподібним включенням. Зведенням до задачі Рімана і її подальшим розв'язанням отримано точний розв'язок даної крайової задачі. Досліджено асимптотичну поведінку контактних зусиль на кінцях включення.

Ключові слова: крайова задача, ізотропна пластина, жорстке хрестоподібне включення, вигин, перетворення Мелліна, метод факторизації, задача Рімана.

O.B. Kozin, O.B. Papkovskaya, M.O. Kozina. Modelling and solution of contact problem for infinite plate and cross-shaped embedment. Development of efficient methods of determination of an intense-strained state of thin-walled constructional designs with inclusions, reinforcements and other stress raisers is an important problem both with theoretical, and from the practical point of view, considering their wide practical application. **Aim:** The aim of this research is to develop the analytical mathematical method of studying of an intense-strained state of infinite plate with cross-shaped embedment at a bend. **Materials and Methods:** The method of boundary elements is an efficient way of the boundary value problems solution for systems of differential equations. The methods based on boundary integral equations get wide application in many branches of science and technique, calculation of plates and shells. One of methods of solution of a numerous class of the integral equations and systems arising on the basis of a method of boundary integral equations is the analytical method of construction of these equations and systems to Riemann problems with their forthcoming decision. **Results:** The integral equation for the analysis of deflections and the analysis of an intense-strained state of a thin rigid plate with rigid cross-shaped embedment is received. The precise solution of this boundary value problem is received by reduction to a Riemann problem and its forthcoming solution. An asymptotical behavior of contact efforts at the ends of embedment is investigated.

Keywords: boundary problem, isotropic plate, rigid cross-shaped embedment, bend, Mellin transform, factorization method, Riemann problem.

Introduction. Development of efficient methods of determination of an intense-strained state of thin-walled constructional designs with inclusions, reinforcements and other stress raisers is an important problem both with theoretical, and from the practical point of view, considering their wide practical application. Plates, reinforced by a different inclusions and ribs, are widely used in practice as components of different constructions. In this study we proposed a method of analytical solution for boundary value problem of stress-strain state of the bending of an infinite plate with a rigid cross-shaped embedment. The exact solution of this boundary value problem is obtained by reduction to the Riemann problem and by its subsequent solution.

DOI 10.15276/opu.2.49.2016.14

© 2016 The Authors. This is an open access article under the CC BY license (<http://creativecommons.org/licenses/by/4.0/>).

The boundary element method is an effective way of solving boundary value problems for systems of differential equations. Methods based on the boundary integral equations, are a powerful tool in many fields of science and technology, including the calculation of plates and shells [1...5].

However, due to the singularity of the fundamental solutions, a problem associated with irregular borders (corners, edges, etc...) arises. So, the question to use of special techniques for solving the problems with non-smooth boundary is actual.

One of methods for solving numerous classes of integral equations and systems, arising on the basis of the method of boundary integral equations, is an analytical method of reducing these equations and systems to the Riemann problem with their subsequent solution [6...13].

This method was further developed in solving the problem of bending isotropic [6] and orthotropic plates [7, 8] with linear irregularities oriented arbitrarily.

Contact problem of bandpass orthotropic plate Kirchhoff model with a thin semi-infinite rigid reinforcement were studied and solved in [9] by present method, as well as with reinforcement in the form of elastic rib [10].

In [11], an exact solution of the antisymmetric contact problem of bending bandpass orthotropic semi-infinite plate and a rigid support was constructed by reduction to the Riemann problem. The asymptotic behavior of the contact forces at the end of this support has been investigated.

Exact solution of the boundary value problem of bending bandpass shallow shell, which is supported by intermediate thin semi-infinite rib, type Winkler foundation was obtained in [12]; and supported by intermediate thin semi-infinite rigid support, was obtained in [13].

The aim of this research is to develop the analytical mathematical method of studying of an intense-strained state of infinite plate with cross-shaped embedment at a bend. It is also necessary to investigate the asymptotic behavior of the contact forces at the ends of this embedment.

Materials and Methods. We consider the problem of the bending of an infinite plate $(-\infty < x, y < \infty)$, containing a cross-shaped, thin, absolutely rigid embedment $(|x| \leq a, y = 0; |y| \leq a, x = 0)$.

The force P applied to the embedment in point $x = 0, y = 0$. P is an applied transverse load. The plate is simply supported in $4N$ points

$$M_k = (b \cos(\pi k / (2N) + \pi / (4N)), b \sin(\pi k / (2N) + \pi / (4N))) = (x_k, y_k), \quad (b > a).$$

It is necessary to find the deflection of embedment W_0 and the contact forces of interactions $\psi_1(\xi), \psi_2(\xi)$ between embedment and plate.

Using the results of [6], we give mathematical formulation of the boundary problem described above. Equation, governing the deflection of mid-surface of plate $w(x, y)$ can be approximated as:

$$D\Delta^2 w(x, y) = \psi_1(x)\delta(y) + \psi_2(y)\delta(x) - \frac{P}{4N} \sum_{k=1}^{4N} \delta(x - x_k)\delta(y - y_k); \quad (1)$$

The boundary conditions are the following:

$$\frac{\partial^3 w(x, y)}{\partial x^i \partial y^{3-i}} \rightarrow 0, \quad i = \overline{0, 3} \quad \text{as} \quad x^2 + y^2 \rightarrow \infty; \quad (2)$$

Moreover:

$$w(x, 0) = W_0, \quad (|x| \leq a); \quad w(0, y) = W_0, \quad (|y| \leq a); \quad (3)$$

$$\int_{-a}^a \psi_1(\xi) d\xi + \int_{-a}^a \psi_2(\xi) d\xi = P, \quad (4)$$

where $\delta(x), \delta(y)$ — Dirac delta functions.

Using the fundamental solution of the biharmonic equation $\Phi(x, y) = (8\pi)^{-1}(x^2 + y^2) \ln(\sqrt{x^2 + y^2})$, we obtain the solution of equation (1), satisfying (2).

$$Dw(x, y) = \int_{-a}^a \psi_1(\xi)\Phi(x - \xi, y)d\xi + \int_{-a}^a \psi_2(\eta)\Phi(x, y - \eta)d\eta - \frac{P}{4N} \sum_{k=1}^{4N} \Phi\left(x - b \cos\left(\frac{\pi k}{2N} + \frac{\pi}{4N}\right), y - b \sin\left(\frac{\pi k}{2N} + \frac{\pi}{4N}\right)\right). \quad (5)$$

Substituting (5) in (3), we obtain a system of two integral equations for $\psi_1(\xi)$ and $\psi_2(\eta)$. Posed problem is symmetrical relative to the variables x and y .

Therefore $\psi_1(\xi) = \psi_2(\xi)$. $\psi_1(\xi)$ — is even, and eventually we come to an integral equation of the first kind with a smooth kernel:

$$\frac{1}{8\pi D} \int_0^a \psi_1(\xi)L(x, \xi)d\xi = W_0 + f(x), \quad 0 \leq x \leq a; \quad (6)$$

where $L(x, \xi) = (x - \xi)^2 \ln|x - \xi| + (x + \xi)^2 \ln(x + \xi) + (x^2 + \xi^2) \ln(x^2 + \xi^2)$;

$$f(x) = \frac{P}{4N} \sum_{k=1}^{4N} \Phi\left(x - b \cos\left(\frac{\pi k}{2N} + \frac{\pi}{4N}\right), b \sin\left(\frac{\pi k}{2N} + \frac{\pi}{4N}\right)\right).$$

Performing the differentiation (6) three times with respect to x and introducing the notation $\tau = a^{-1}\xi$, $t = a^{-1}x$, $\psi_1(\xi) = \psi(\tau)$, we come to a singular equation

$$-\frac{1}{4\pi D} \int_0^1 \psi(\tau)g\left(\frac{t}{\tau}\right)\frac{d\tau}{\tau} = f_3(t), \quad 0 \leq t \leq 1; \quad (7)$$

where $g(y) = \frac{1}{1-y} - \frac{1}{1+y} - \frac{6y}{1+y^2} + \frac{4y^3}{(1+y^2)^2}$, $f_3(t) = f'''(x)$

It is important to note that the solution of equation (7), when substituted into the left side of the equation (6), in general, can give a function that is different from $W_0 + f(x)$ on an even polynomial of the second order $A + Bx^2$. The necessary and sufficient conditions for the equality to zero of this polynomial will be equalities

$$\frac{1}{2\pi D} \int_0^a \psi_1(\xi)\xi^2 \ln|\xi|d\xi = W_0 + f(0); \quad \frac{1}{\pi D} \int_0^a \psi_1(\xi)(\ln|\xi| + 1)d\xi = f''(0). \quad (8)$$

The first is obtained by substituting of $x=0$ into (6). The second — by double differentiation of (d^2/dx^2) (6) with respect to x and subsequent substituting $x=0$ into result. To satisfy (8), we should be seeking $\psi(\tau)$ in such class of functions in which the homogeneous equation, corresponding (7), has two linearly independent solutions. As will show below, it is necessary to search $\psi(\tau)$ in class of functions with non-integrable singularity at the point $\tau=1$, and the corresponding integrals are understood in regularized sense [14].

We extend the definition of right-hand side of equation (7) as $1 \leq t < \infty$, using the unknown function $f_+(t)$. Introducing the notation

$$f_-(t) = \begin{cases} f_3(t), & (0 \leq t < 1); \\ 0, & (1 \leq t < \infty), \end{cases} \quad \psi_-(\tau) = \begin{cases} -(4\pi D)^{-1}\psi(\tau), & (0 \leq \tau < 1); \\ 0, & (1 \leq \tau < \infty), \end{cases}$$

let rewrite (7) in the form

$$\int_0^{\infty} \Psi_-(\tau) g\left(\frac{t}{\tau}\right) \frac{d\tau}{\tau} = f_-(t) + f_+(t), \quad (0 \leq t < \infty). \quad (9)$$

We applying Mellin transform to the (9)

$$M[f_{\pm}(t), \Psi_{\pm}(t)] = \int_0^{\infty} [f_{\pm}(t), \Psi_{\pm}(t)] t^{p-1} dt = [F^{\pm}(p), \Psi^-(p)], \quad p = \delta + it,$$

$$[f_{\pm}(t), \Psi_{\pm}(t)] = \frac{1}{2\pi i} \int_{\delta-i\infty}^{\delta+i\infty} [F^{\pm}(p), \Psi^-(p)] t^{-p} dp, \quad (0 \leq t < \infty).$$

Then we calculate $M[g] = G(p)$ using the formula 3.241 [15]. As a result, we have the Riemann problem

$$\Psi^-(p)G(p) = F^-(p) + F^+(p), \quad -\infty < \operatorname{Im} p < \infty, \quad (10)$$

where $G(p) = -\pi t g \frac{\pi p}{2} \left(1 - \frac{p-2}{\sin \frac{\pi p}{2}} \right)$, $(\max(\alpha, 0) < \operatorname{Re} p = \sigma < 1)$.

α is determined by the asymptotic behavior of function $\Psi_-(\tau) = O(\tau^{-\alpha})$ as $\tau \rightarrow 0$.

Problem (10) is solved by the factorization method [16] with the use of representations

$$-\pi t g \frac{\pi p}{2} = T^+(p)T^-(p), \quad T^+(p) = -\pi \frac{\Gamma\left(\frac{1-p}{2}\right)}{\Gamma\left(1-\frac{p}{2}\right)}, \quad T^-(p) = \frac{\Gamma\left(\frac{1+p}{2}\right)}{\Gamma\left(\frac{p}{2}\right)};$$

$$K(p) = 1 - \frac{p-2}{\sin \frac{\pi p}{2}} = K^+(p)K^-(p), \quad K^{\pm}(p) = \exp\left(\pm \frac{1}{2\pi i} \int_{\sigma-i\infty}^{\sigma+i\infty} \frac{\ln(K(s))}{s-p} ds\right);$$

$$G(p) = G^+(p)G^-(p), \quad G^{\pm}(p) = T^{\pm}(p)K^{\pm}(p);$$

$$H(p) = \frac{F^-(p)}{G^+(p)} = H^+(p) - H^-(p), \quad H^{\pm}(p) = \frac{1}{2\pi i} \int_{\sigma-i\infty}^{\sigma+i\infty} \frac{H(s)ds}{s-p}.$$

As a result, (10) is transformed into

$$\Psi^-(p)G^-(p) + H^-(p) = F^+(p) / G^+(p) + H^+(p) = Q(p). \quad (11)$$

To obtain two constants satisfying the conditions (8), it is necessary to have $Q(p) = c_0 + c_1 p$.

Results. Thus, exact solutions of equations (7) and (6) have the next form

$$\Psi(\tau) = 2\pi D \int_{\sigma-i\infty}^{\sigma+i\infty} (c_0 + c_1 p - H^-(p)) \frac{\tau^{-p}}{G^-(p)} dp, \quad (12)$$

where $\Psi_1(\xi) = \Psi(\xi a^{-1}) = 2\pi D [c_0 \varphi_0(\xi) + c_1 \varphi_1(\xi) + \varphi_*(\xi)]$;

$$\varphi_0(\xi) = \frac{i}{\pi} \int_{\sigma-i\infty}^{\sigma+i\infty} \frac{\xi^{-p}}{G^-(p)} dp;$$

$$\varphi_1(\xi) = \frac{i}{\pi} \int_{\sigma-i\infty}^{\sigma+i\infty} \frac{p \xi^{-p}}{G^-(p)} dp;$$

$$\varphi_*(\xi) = \frac{-i}{\pi} \int_{\sigma-i\infty}^{\sigma+i\infty} H^-(p) \frac{\xi^{-p}}{G^-(p)} dp.$$

Here the constants c_0, c_1, W_0 are found from the equations (8) and (4):

$$\begin{aligned} c_0 \int_0^a \varphi_0(\xi) \xi^2 \ln|\xi| d\xi + c_1 \int_0^a \varphi_1(\xi) \xi^2 \ln|\xi| d\xi + \int_0^a \varphi_*(\xi) \xi^2 \ln|\xi| d\xi &= W_0 + f(0); \\ c_0 \int_0^a \varphi_0(\xi) (\ln|\xi| + 1) d\xi + c_1 \int_0^a \varphi_1(\xi) (\ln|\xi| + 1) d\xi + \int_0^a \varphi_*(\xi) (\ln|\xi| + 1) d\xi &= \frac{f''(0)}{2}; \\ c_0 \int_0^a \varphi_0(\xi) d\xi + c_1 \int_0^a \varphi_1(\xi) d\xi + \int_0^a \varphi_*(\xi) d\xi &= \frac{P}{8\pi D}. \end{aligned}$$

Conclusions. Mathematical formulation of the boundary value problem is done. An integral equation for stress-strain analysis of thin supported elastic plate with rigid cross-shaped embedment is obtained. The exact solution of this boundary value problem is obtained by reduction to the Riemann problem and by its subsequent solution.

The behavior of the function $\psi_1(\xi)$ when $\xi \rightarrow a-0$ (defined by the asymptotic behavior $\Psi^-(p)$ at $|p| \rightarrow \infty$) is of great interest. Since $p[G(p)]^{-1} = O(p^{1/2})$ then, according to [17] $\psi_1(\xi) = O((a-\xi)^{-3/2})$, i.e., the contact forces have a non-integrable singularity at the ends of the cross-shaped embedment. This singularity coincides with the result in [9].

Література

1. Сурьянинов, Н.Г. Приложение численно-аналитического метода граничных элементов к расчету ортотропных пластин / Н.Г. Сурьянинов, И.В. Павленко // Пр. Одес. політехн. ун-ту. — 2014. — Вип. 1(43). — С. 18–27.
2. Усов, А.В. Математическое моделирование процессов контроля покрытий элементов конструкций на базе сингулярных интегральных уравнений / А.В. Усов, А.А. Батырев // Пробл. машиностроения. — 2010. — Т. 13, № 1. — С. 65–75.
3. Козин, А.Б. О решении краевых задач изгиба композитных пологих оболочек / А.Б. Козин, О.Б. Папковская // Сб. науч. тр. SWorld: матер. междунар. науч.-практ. конф. «Перспективные инновации в науке, образовании, производстве и транспорте '2013», 17–26 дек. 2013 г., Одесса. — 2013. — Т. 4: Физика и математика. — С. 33–37.
4. Козин, А.Б. Напряженно-деформируемое состояние оболочки с включением при изгибе / А.Б. Козин, О.Б. Папковская // Пр. Одес. політехн. ун-ту. — 2014. — Вип. 2(44). — С. 15–20.
5. Kozin, O.V. Analysis of stress-strain state of the spherical shallow shell with inclusion / O.V. Kozin, O.V. Papkovskaya // Пр. Одес. політехн. ун-ту. — 2016. — Вип. 1(48). — С. 24–29.
6. Козин, А.Б. Изгиб прямоугольной пластины с криволинейным концентратором напряжений / А.Б. Козин, О.Б. Папковская, Г.А. Козина // Пр. Одес. політехн. ун-ту. — 1997. — Вип. 1(3). — С. 290–292.
7. Папковская, О.Б. Математическая модель изгиба ортотропной пластины с криволинейной произвольно ориентированной неоднородностью / О.Б. Папковская, А.Б. Козин, Д. Камара // Пр. Одес. політехн. ун-ту. — 2008. — Вип. 1(29). — С. 237–241.
8. Красный, Ю.П. Метод решения задач изгиба пластин неоднородной структуры / Ю.П. Красный, А.Б. Козин, О.Б. Папковская // Наукові записки Міжнародного гуманітарного університету. — 2013. — Вип. 18. — С. 252–255.
9. Папковская, О.Б. Изгиб ортотропной упругой полосовой пластины при наличии жесткой промежуточной опоры / О.Б. Папковская, А.Б. Козин, Д. Камара // Пр. Одес. політехн. ун-ту. — 2005. — Вип. 1(23). — С. 180–184.

10. Папковская, О.Б. Построение и исследование разрывного решения задачи изгиба ортотропной полосовой пластины, подкрепленной упругой промежуточной опорой / О.Б. Папковская, А.Б. Козин, А.Б. Н'Диай // Пр. Одес. політехн. ун-ту. — 2003. — Вип. 2(20). — С. 176–179.
11. Папковская, О.Б. Построение и исследование решения задачи антисимметричного изгиба ортотропной полосовой пластины, подкрепленной жесткой опорой / О.Б. Папковская, А.Б. Козин, Д. Камара // Пр. Одес. політехн. ун-ту. — 2006. — Вип. 2(26). — С. 181–185.
12. Красный, Ю.П. Изгиб бесконечной пологой оболочки при наличии винклеровской полубесконечной опоры / Ю.П. Красный, А.Б. Козин, О.Б. Папковская // Науковий вісник Міжнародного гуманітарного університету. Серія: Інформаційні технології та управління проектами. — 2012. — № 4. — С. 29–31.
13. Kozin, O.V. Coque cylindrique surbaissee avec un support rigide intermediaire sous pression externe / O.V. Kozin, O.V. Papkovskaya, M.O. Kozina // Молодий вчений. — 2015. — № 12(27). — С. 77–80.
14. Гельфанд, И.М. Обобщенные функции и действия над ними / И.М. Гельфанд, Г.Е. Шилов. — М.: Добросвет, 2007. — 408 с.
15. Градштейн, И.С. Таблицы интегралов, сумм, рядов и произведений / И.С. Градштейн, И.М. Рыжик. — 5-е изд., стереотип. — М.: Наука, 1971. — 1108 с.
16. Попов, Г.Я. Контактные задачи для линейно-деформируемого основания / Г.Я. Попов. — К.: Вища школа, 1982. — 167 с.
17. Брычков, Ю.А. Интегральные преобразования обобщенных функций / Ю.А. Брычков, А.П. Прудников. — М.: Наука, 1977. — 287 с.

References

1. Suryaninov, N.G., & Pavlenko, I.V. (2014). Application of numerical-analytical boundary element method to the calculation of orthotropic plates. *Odes'kyi Politechnichnyi Universytet. Pratsi*, 1, 18–27. DOI:10.15276/opu.1.43.2014.04
2. Usov, A.V., & Batyrev, A.A. (2010). Mathematical modeling of controlling the coating process of the structural elements based on singular integral equations. *Journal of Mechanical Engineering*, 13(1), 65–75.
3. Kozin, A.B., & Papkovskaya, O.B. (2013). About solving boundary value problems of the bending composite shallow shells. In S.V. Kuprienko (Ed.), *Proceedings of International Science and Practical Conference on Perspective Innovations in Science, Education, Production and Transport '2013* (pp. 33–37). Odessa: KUPRIENKO.
4. Kozin, A.B., & Papkovskaya, O.B. (2014). Intensely deformed state of the shell with the inclusion in bending. *Odes'kyi Politechnichnyi Universytet. Pratsi*, 2, 15–20. DOI:10.15276/opu.2.44.2014.04
5. Kozin, O.B., & Papkovskaya, O.B. (2016). Analysis of stress-strain state of the spherical shallow shell with inclusion. *Odes'kyi Politechnichnyi Universytet. Pratsi*, 1, 24–29. DOI:10.15276/opu.1.48.2016.05
6. Kozin, A.B., Papkovskaya, O.B., & Kozina, G.A. (1997). Bending of rectangular plate with curvilinear strain concentrator. *Odes'kyi Politechnichnyi Universytet. Pratsi*, 1, 290–292.
7. Papkovskaya, O.B., Kozin, O.B., & Camara, D. (2008). Mathematical model of the flexion of orthotropic plate with curvilinear and arbitrarily oriented heterogeneity of structure. *Odes'kyi Politechnichnyi Universytet. Pratsi*, 1, 237–241.
8. Krasniy, J.P., Kozin, A.B., & Papkovsky, O.B. (2013). Problem-solving method for bending of an inhomogeneous structure plates. *Scientific Proceedings of International Humanitarian University*, 18, 252–255.
9. Papkovskaya, O.B., Kozin, O.B., & Camara, D. (2005). Bending in orthotropic elastic strip plate in the presence of a rigid intermediate support. *Odes'kyi Politechnichnyi Universytet. Pratsi*, 1, 180–184.
10. Papkovskaya, O.B., Kozin, O.B., & N'Diaye, A.B. (2003). Construction and research of the breaking solution for the problem of bending the orthotropic strip plate supported by an elastic intermediate bearing. *Odes'kyi Politechnichnyi Universytet. Pratsi*, 2, 176–179.
11. Papkovskaya, O.B., Kozin, O.B., & Camara, D. (2006). Construction and research of solution of anti-symmetric flexion task for an orthotropic strip plate supported by the rigid support. *Odes'kyi Politechnichnyi Universytet. Pratsi*, 2, 181–185.
12. Krasniy, J.P., Kozin, A.B., & Papkovsky, O.B. (2012). Bend infinite shallow shell if Winkler semi-infinite supports. *Herald of International Humanitarian University: Information Technologies and Project Management*, 4, 29–31.
13. Kozin, O.B., Papkovskaya, O.B., & Kozina, M.O. (2015). Coque cylindrique surbaissee avec un support rigide intermediaire sous pression externe. *Young Scientist*, 12, 77–80.

-
14. Gelfand, I.M., & Shilov, G.E. (2007). *Generalized Functions and Operations over Them*. Moscow: Dobrosvet.
 15. Gradshteyn, I.S., & Ryzhik, I.M. (1971). *Table of Integrals, Series, and Products* (5th Ed.). Moscow: Nauka.
 16. Popov, G.Ya. (1982). *Contact Problems for a Linearly Deformable Foundation*. Kyiv: Vyscha Shkola.
 17. Brychkov, Yu.A., & Prudnikov, A.P. (1977). *Integral Transforms of Generalized Functions*. Moscow: Nauka.

Received May 22, 2016

Accepted July 10, 2016

UDC 539.3+620.178.7

O.A. Mikulich, PhD, Assoc.Prof.,

V.I. Shvab'yuk, DSc, Prof.

Lutsk National Technical University, 75 Lvivska Str., 43018 Lutsk, Ukraine; e-mail: shyprao@gmail.com

INTERACTION OF WEAK SHOCK WAVES WITH RECTANGULAR MESHES IN PLATE

O.A. Mikulich, V.I. Shvab'yuk. Взаємодія слабких ударних хвиль з прямокутними отворами у пластинці. У машинобудуванні, будівництві та інших галузях виробництва значна частина процесів включає в себе наявність різноманітних динамічних навантажень, обумовлених технологічними і механічними впливами. Врахування впливів таких навантажень дає можливість точніше оцінити міцність елементів конструкцій чи деталей машин. **Мета:** Метою роботи є розробка алгоритму розрахунку динамічного напруженого стану пластинок з отворами за дії імпульсного навантаження у вигляді слабкої ударної хвилі. **Матеріали і методи:** Для розв'язання задачі використано інтегральне та дискретне перетворення Фур'є. Застосування перетворення Фур'є за часом дало можливість звести динамічну задачу плоского деформування до розв'язання скінченної кількості задач на усталені коливання при фіксованих значеннях циклічних частот. У області Фур'є-зображень для дослідження динамічної концентрації напружень використано метод граничних інтегральних рівнянь і апарат теорії функції комплексної змінної. **Результати:** На основі розробленої методики досліджено зміну розподілу динамічних кільцевих напружень з часом на межі прямокутного отвору. Побудовано часові зрізи полів розподілу напружень за дії імпульсного динамічного навантаження.

Ключові слова: пластинка, напружений стан, нестационарна задача.

O.A. Mikulich, V.I. Shvab'yuk. Interaction of weak shock waves with rectangular meshes in plate. In mechanical engineering, building and other industries a significant part of the process includes the presence of various dynamic loads due to technological and mechanical impacts. Consideration of such load effects allows more accurate assessment of the structural elements strength or machine parts. **Aim:** The aim is to develop an algorithm for calculating of dynamic stress state of plates with meshes for pulse loading in the form of a weak shock wave. **Materials and Methods:** An integral and discrete Fourier transform were used to solve the problem. An application of Fourier transform by time allowed reducing the dynamic problem of flat deformation to the solution of a finite number of problems for the established oscillations at fixed cyclic frequency values. In the area of Fourier-images the method of boundary integral equations and the apparatus of a complex variable function theory are used to study the dynamic stress concentration. **Results:** Based on the developed methodology the distribution change of the dynamic circle stress over time on the edge of a rectangular hole is studied. The time sections of stress distribution fields under the influence of pulse dynamic load is constructed.

Keywords: plate, stressed state, nonstationary problem.

Introduction. In engineering, construction and other industries a significant part of the technological processes is associated with dynamic loads. Such activity can be single within the operating cycle as a package pulses or vibration. Each of these loads types can be of shock nature.

Obviously, for the actions of such stresses, especially impulse, stress concentration significantly differs from those occurring under conditions of quasi-static deformation. Research of dynamic problems for bodies with meshes was based on Laplace transform. In [1] using the method in the area of images of series the distribution of dynamic stresses in the plate with rectangular meshes from the effects of the shock load applied to the border was investigated. In [2, 3] solving the problem is reduced to the singular and regular integral equations.

In [4, 5] solving of dynamic problems in the case of antiplane deformation is performed by finite differences method by time.

In [6, 7] to study the dynamic stress state of plates with stress concentrators at antiplane strain the Fourier transform is used.

In [8] the technique of research of dynamic stressed state of plates with meshes at the steady-state oscillations is developed. This technique is based on joint use of boundary integral equations method and the apparatus of the complex variable theory. The numerical realization of the offered technique was made on the basis of a method of mechanical quadratures and collocation. Such approach was efficient when calculating of dynamic stress concentration in the plates weakened by meshes of the irregular shape.

DOI 10.15276/opu.2.49.2016.15

© 2016 The Authors. This is an open access article under the CC BY license (<http://creativecommons.org/licenses/by/4.0/>).

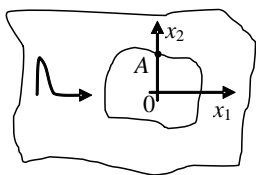


Fig. 1. Scheme of loading of a plate

The aim is to develop an algorithm for calculating of dynamic stress state of plates with meshes for pulse loading in the form of a weak shock wave. This algorithm should be based on boundary integral equations method and apparatus of the complex variable theory.

Materials and methods. Let us consider an infinite isotropic elastic plate, weakened by a hole of any form (fig. 1). We will designate by D the area which is occupied by a plate. Let L — its limiting contour. We will carry an elastic plate to the Cartesian system of coordinates Ox_1x_2 which we will place in its gravity center.

According to [3], the equation of the movement of an isotropic plate in movements is written as:

$$(c_1^2 - c_2^2)u_{i,jj} - c_2^2u_{j,ii} + b_j = \frac{\partial^2 u_j}{\partial t^2}, \quad (1)$$

where $\mathbf{u}(\mathbf{x}, t) = \{u_j(\mathbf{x}, t)\}$, $j = 1, 2$ — vector of arbitrary point movement $\mathbf{x} = \{x_1, x_2\}$;

$c_1 = \sqrt{(\lambda + \mu) / \rho}$, $c_2 = \sqrt{\mu / \rho}$ — speed expansion and shear of waves respectively;

λ, μ — Lamé constants;

$\mathbf{b} = \{b_j\}$ — vector of mass forces;

$(\cdot)_{,j}$ means for differentiation x_j ;

t — time.

Using Fourier transform [9] to an equation (1) for the time variable t

$$\tilde{f}(x, \omega) = \int_{-\infty}^{\infty} f(x, t)e^{-i\omega t} dt, \quad f(x, t) = \frac{1}{2\pi} \int_{-\infty}^{\infty} \tilde{f}(x, \omega)e^{i\omega t} d\omega \quad (2)$$

gets equation:

$$(c_1^2 - c_2^2)\tilde{u}_{i,jj} - c_2^2\tilde{u}_{j,ii} + \tilde{b}_j + \omega^2\tilde{u}_j = 0, \quad (3)$$

which is equivalent to the equation steady-state oscillations with cyclic frequency ω [3]. The use of Fourier integral transform gives the opportunity to conduct research in the field of images, thereby isolate the effect of the time factor.

Research of dynamic stress state we will conduct in case when plane shock wave waves to the mesh in the plate, that is similarly to [10] defined by the potential:

$$\varphi(\mathbf{x}, t) = \begin{cases} \varphi_0 f(\mathbf{x} / a - c_1 t / a), & t \geq 0 \\ 0, & t < 0 \end{cases} \quad \psi(\mathbf{x}, t) = 0, \quad (4)$$

where φ_0 — constant;

a — characteristic size.

Applying to the presentation (4) the integral Fourier transform (2), we get:

$$\tilde{\varphi}(\mathbf{x}, \omega) = \tilde{\varphi}_0 a \tilde{f}(\omega a / c_1) e^{-k_1 \mathbf{x}} / c_1 = \tilde{\varphi}_0(\omega) e^{-k_1 \mathbf{x}} \quad \tilde{\psi}(\mathbf{x}, \omega) = 0, \quad (5)$$

where $\tilde{\varphi}_0(\omega) = \tilde{\varphi}_0 \frac{a}{c_1} \tilde{f}\left(\frac{\omega a}{c_1}\right)$, $\tilde{f}(\omega) = \int_{-\infty}^{\infty} f(\tau) e^{-i\omega \tau} d\tau$.

Boundary conditions of the problem in the field of Fourier-images we will write as [3]:

$$\tilde{\sigma}_n|_L = \tilde{\sigma}(\mathbf{x}, \omega), \quad \tilde{\tau}_{sn}|_L = \tilde{\tau}(\mathbf{x}, \omega). \quad (6)$$

For the case of the first main problem the potential image of general solution for displacements we will choose as [10]:

$$\tilde{u}_i(\mathbf{x}, \omega) = \int_L p_j(\mathbf{x}^0, \omega) \cdot U_{ji}^*(\mathbf{x}, \mathbf{x}^0, \omega) ds, \quad (7)$$

where p_1, p_2 — unknown complex potential functions;
 L — border of plate area.

Integration along the border is held by the variables x_1^0, x_2^0 , and the $\mathbf{x}^0 = \{x_1^0, x_2^0\}$. Expressions for images of functions U_{ij}^* are chosen accounting the Sommerfeld conditions [10] as [3]:

$$U_{ij}^* = \frac{1}{2\pi\mu} (\psi \cdot \delta_{ij} - \chi \cdot r_i \cdot r_j), \quad (8)$$

where $\psi = K_0(k_2 r) + \frac{1}{k_2 r} \left(K_1(k_2 r) - \frac{c_2}{c_1} K_1(k_1 r) \right)$, $\chi = K_2(k_2 r) - \frac{c_2^2}{c_1^2} K_2(k_1 r)$;

$k_j = \frac{i\omega}{c_j}$, $j=1, 2$ — wave number;

$K_m(r)$, $m=0, 1, 2$ — modified Bessel functions of the third kind (or Macdonald functions);

$r = \sqrt{(x_1 - x_1^0)^2 + (x_2 - x_2^0)^2}$ — distance.

Satisfying the boundary conditions (6), we determine the unknown function on border p_1, p_2 , calculating the stresses in the plate by formulas [10]:

$$\begin{aligned} \tilde{\sigma}_n &= \frac{\sigma_{11} + \sigma_{22}}{2} + \frac{1}{2} \left(e^{-2i\alpha} \left(\frac{\sigma_{11} + \sigma_{22}}{2} + i\sigma_{12} \right) + e^{2i\alpha} \left(\frac{\sigma_{11} + \sigma_{22}}{2} - i\sigma_{12} \right) \right); \\ \tilde{\tau}_{sn} &= \frac{i}{2} \left(e^{2i\alpha} \left(\frac{\sigma_{11} + \sigma_{22}}{2} - i\sigma_{12} \right) - e^{-2i\alpha} \left(\frac{\sigma_{11} + \sigma_{22}}{2} + i\sigma_{12} \right) \right), \end{aligned} \quad (9)$$

where α — the angle between the normal line \vec{n} the plate and the axis Ox_1 .

Substituting dependences (7) taking into account the expressions for functions of influence (8) in formulas (9), we will obtain a representation like:

$$\tilde{\sigma}_n = \int_L f_1(z, \xi) q d\xi + \int_L f_2(z, \xi) \bar{q} d\bar{\xi}; \quad \tilde{\tau}_{sn} = \int_L g_1(z, \xi) q d\xi + \int_L g_2(z, \xi) \bar{q} d\bar{\xi}, \quad (10)$$

where $q = i \cdot p \cdot ds / d\xi$ — unknown complex functions;

$\xi = x_1^0 + ix_2^0$, $z = x_1 + ix_2$, $p = p_1 + ip_2$;

f_i, g_i , $i=1, 2$ — known function containing Bessel functions of the third kind:

$$f_1 = -\frac{i}{4\pi\mu r} \left((\bar{z} - \bar{\xi}) F - \left(\frac{dz}{d\bar{z}} \frac{(\bar{z} - \bar{\xi})^2}{z - \xi} G_2 + \frac{d\bar{z}}{dz} (z - \xi) G_1 \right) \right);$$

$$f_2 = \frac{i}{4\pi\mu r} \left((z - \xi) F - \left(\frac{dz}{d\bar{z}} (\bar{z} - \bar{\xi}) G_1 + \frac{d\bar{z}}{dz} \frac{(z - \xi)^2}{\bar{z} - \bar{\xi}} G_2 \right) \right);$$

$$g_1 = -\frac{1}{4\pi\mu r} \left(\frac{dz}{d\bar{z}} \frac{(\bar{z} - \bar{\xi})^2}{z - \xi} G_2 - \frac{d\bar{z}}{dz} (z - \xi) G_1 \right);$$

$$g_2 = \frac{1}{4\pi\mu r} \left(\frac{dz}{d\bar{z}} (\bar{z} - \bar{\xi}) G_1 - \frac{d\bar{z}}{dz} \frac{(z - \xi)^2}{\bar{z} - \bar{\xi}} G_2 \right),$$

$$F = \psi' - \chi' - \frac{\chi}{r}; \quad G_1 = \psi' - \frac{\chi'}{2}, \quad G_2 = \frac{\chi}{r} - \frac{\chi'}{2}.$$

The integrands $f_i, g_i, i=1, 2$ at small values of the argument are irregular. Let set their features, using the asymptotic expressions for the Bessel functions of the third kind [12]:

$$K_0(r) = \ln 2 - \ln 2 - \gamma + O(r^2); K_1(r) = \frac{1}{r} + \frac{1}{2} \left(-\ln 2 + \ln r + \gamma - \frac{1}{2} \right) + O(r^3); K_2(r) = \frac{2}{r^2} - \frac{1}{2} + O(r^2),$$

where γ — Euler's constant.

We obtain, that at $r \rightarrow 0$ functions ψ and χ have features of type:

$$\psi = -\frac{1}{2} \ln r(1 + \kappa) + O(r^2); \chi = -\frac{1}{2}(1 - \kappa) + O(r^2), \kappa = \left(\frac{c_1}{c_2} \right)^2.$$

Besides, functions F, G_1, G_2 have features of type:

$$F = -\frac{\kappa}{r} + O(r^2); G_1 = -\frac{1 + \kappa}{2r} + O(r^2); G_2 = -\frac{1 - \kappa}{2r} + O(r^2).$$

In the case of plane stressed state $\kappa = (1 - \nu) / 2$, ν — Poisson's ratio.

Considering the above mentioned features of integrand functions, the representation for definition of the functions $f_i, g_i, i=1, 2$ can be written as:

$$\begin{aligned} f_1 &= -\frac{i}{4\pi\mu} \left(\frac{\kappa}{z - \xi} + \frac{1}{2} \left((1 - \kappa) \frac{dz}{d\bar{z}} \frac{(\bar{z} - \bar{\xi})}{(z - \xi)^2} + \frac{d\bar{z}}{dz} \frac{1 + \kappa}{\bar{z} - \bar{\xi}} \right) \right) + f_1^R(z, \xi); \\ f_2 &= \frac{i}{4\pi\mu} \left(\frac{\kappa}{\bar{z} - \bar{\xi}} + \frac{1}{2} \left(\frac{dz}{d\bar{z}} \frac{1 + \kappa}{z - \xi} + (1 - \kappa) \frac{d\bar{z}}{dz} \frac{z - \xi}{(\bar{z} - \bar{\xi})^2} \right) \right) + f_2^R(z, \xi); \\ g_1 &= \frac{1}{8\pi\mu} \left((1 - \kappa) \frac{dz}{d\bar{z}} \frac{\bar{z} - \bar{\xi}}{(z - \xi)^2} - \frac{d\bar{z}}{dz} \frac{1 + \kappa}{\bar{z} - \bar{\xi}} \right) + g_1^R(z, \xi); \\ g_2 &= -\frac{1}{8\pi\mu} \left(\frac{dz}{d\bar{z}} \frac{1 + \kappa}{z - \xi} - (1 - \kappa) \frac{d\bar{z}}{dz} \frac{z - \xi}{(\bar{z} - \bar{\xi})^2} \right) + g_2^R(z, \xi), \end{aligned}$$

where the functions $f_i^R, g_i^R, i=1, 2$ are regular functions.

We apply the Sokhotski-Plemelj formula [10] at the boundary transition in dependences (10) with consideration of the obtained representations. As a result of these changes we obtain the system of integral equations to find the unknowns at functions border q, \bar{q} :

$$\begin{aligned} \operatorname{Re} \frac{q}{2} - \operatorname{Im} \left(A_1 \int_L \frac{q dt}{z - \xi} + \frac{dz}{d\bar{z}} \left(A_2 \int_L \frac{\bar{q} d\bar{\xi}}{z - \xi} + A_3 \int_L \frac{(\bar{z} - \bar{\xi}) q}{(z - \xi)^2} d\bar{\xi} \right) \right) + \int_L f_1^R(z, \xi) q d\xi + \int_L f_2^R(z, \xi) \bar{q} d\bar{\xi} &= \tilde{\sigma}; \\ \operatorname{Im} \frac{q}{2} - \operatorname{Re} \left(\frac{dz}{d\bar{z}} \left(A_2 \int_L \frac{\bar{q} d\bar{\xi}}{z - \xi} + A_3 \int_L \frac{\bar{z} - \bar{\xi}}{(z - \xi)^2} q d\bar{\xi} \right) \right) + \int_L g_1^R(z, \xi) q d\xi + \int_L g_2^R(z, \xi) \bar{q} d\bar{\xi} &= \tilde{\tau}; \end{aligned} \tag{11}$$

where $A_1 = \frac{1 + \nu}{4\pi\nu}, A_2 = \frac{3 - \nu}{4\pi}, A_3 = \frac{1 + \nu}{4\pi}$ — the constants defined for a case of flat stressed state;

$\tilde{\sigma}, \tilde{\tau}$ — known functions that are based on representation (5);

$f_i^R, g_i^R, i=1, 2$ — known regular functions.

Obtained system of integral equations (11) we solve numerically, using method of mechanical quadratures and collocation [12]. For integrals with Cauchy type feature we apply the clarified quadrature formulas [12]. We obtain a system of linear algebraic equations of the form:

$$\begin{aligned} \frac{q_s + \bar{q}_s}{4} + \sum_{n=1}^N f_1(z_s, \xi_n) q_n g'_n + \sum_{n=1}^N f_2(z_s, \xi_n) \bar{q}_n \bar{g}'_n &= \Phi_{1s}; \\ \frac{q_s - \bar{q}_s}{4i} + \sum_{n=1}^N g_1(z_s, \xi_n) q_n g'_n + \sum_{n=1}^N g_2(z_s, \xi_n) \bar{q}_n \bar{g}'_n &= \Phi_{2s}; \end{aligned} \quad (12)$$

where $\xi_n = g(\varphi_n)$, $z_s = g(\varphi_s)$, $\varphi_n = hn$, $\varphi_s = \varphi_n + \frac{h}{2}$, $h = \frac{2\pi}{N}$,

$g(\varphi)$ — parametric boundary setting L ;

$\Phi_{1s} = \tilde{\sigma}(\varphi_s)$, $\Phi_{2s} = \tilde{\tau}(\varphi_s)$;

N — number of nodal points.

The calculation of circular stresses in plate held numerically based on dependencies obtained from the formulas [10] by allocating irregular components and use of Sokhotski-Plemelj formula at the boundary transition:

$$\tilde{\sigma}_0 = \nu \operatorname{Re} \frac{q}{2} - \operatorname{Im} \left(A_1 \int_L \frac{qd\xi}{z-\xi} - \frac{dz}{d\bar{z}} \left(A_2 \int_L \frac{\bar{q}d\bar{\xi}}{z-\xi} + A_3 \int_L \frac{(\bar{z}-\bar{\xi})q}{(z-\xi)^2} d\xi \right) \right) + \int_L y_1^R(z, \xi) q d\xi + \int_L y_1^R(z, \xi) \bar{q} d\bar{\xi}; \quad (13)$$

where $y_1^R(z, \xi)$, $y_2^R(z, \xi)$ — functions that do not have features.

Definition of originals of obtained on the basis of formulas (13) stresses was conducted using inverse Fourier transform [9] according to dependences:

$$\sigma_0(\mathbf{x}, t) = \frac{1}{2\pi} \int_{-\infty}^{\infty} \tilde{\sigma}_0(\mathbf{x}, \omega) e^{i\omega t} d\omega, \quad (14)$$

which at numerical calculation of circular stresses can be implemented based on the discrete Fourier transform, which proved its effectiveness at researches of the dynamic stress condition at antiplane strain [6].

Results. Based on the proposed algorithm will explore the dynamic stress concentration in plate weakened by rectangular mesh with aspect ratio of 3.2. To describe the border of the plate mesh we use the presentation as a series used in the conformal reflection of a circle of radius a to given region [13]:

$$g(\varphi) = a \left(e^{-i\varphi} + \frac{e^{i\varphi}}{2} - \frac{e^{3i\varphi}}{8} - \frac{3e^{5i\varphi}}{80} - \frac{3e^{7i\varphi}}{896} + \frac{5e^{9i\varphi}}{768} + \frac{57e^{11i\varphi}}{11264} + \dots \right),$$

limiting the number of 11 members.

Numerical calculations we will perform for case of modulation of pulse by time in the form of a weak shock wave [6,7]:

$$f(\tau) = p_* \tau^{n_*} e^{-\alpha_* \tau}, \quad \tau > 0, \quad n_* \geq 0,$$

where $\tilde{f}(\omega) = p_*(n_*!) (\alpha_* + i\omega)^{-n_*-1}$.

In the calculations such values are taken, similar to [6, 7], $p_* = 185$; $n_* = 2$; $\alpha_* = 10$; $a = 1$. Research carried out for the interval of dimensionless time parameter $T \in [0, 8a/c_1]$.

As calculated by the formula (14) values of circular stresses σ_θ images in general are complex, then Fig. 1 shows the dependence of the changes over time of real and imaginary values of dynamic circular stresses: $\sigma_0^R = \operatorname{Re}(\sigma_0)$, $\sigma_0^I = \operatorname{Im}(\sigma_0)$, calculated at A point of a border. The calculation results shown in Figure 1 were made at a value of Poisson's ratio $\nu = 0.3$ and $N = 300$ of nodal points on the border of the plate.

Based on Fig. 1 it can be analyzed the distribution of weak shock waves in the plate, that come to the mesh border with time. Increasing of the values of dynamic stresses components σ_0^R and σ_0^I , that starts from $T = 0.22a/c_1$, corresponds to “coming” to “end” of mesh of disturbing impact $\varphi(\mathbf{x}, \tau)$.

Further growth of stresses in the plate is associated with the spreading of reflected and rereflected pulses from the edges of the mesh. Fig. 1 shows that the intensity of the shock wave rapidly decreases at reflection from the borders of the mesh. The main influence on the dynamic plastic stress state has the main wave and the first reflected wave from the right border.

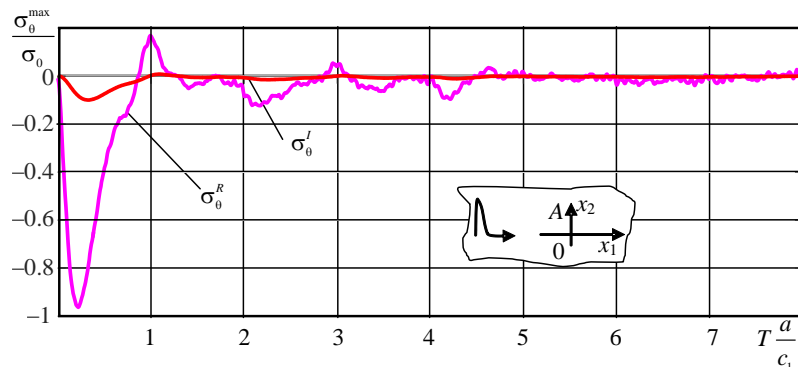


Fig. 1. Distribution of dynamic stresses in the plate with a rectangular mesh

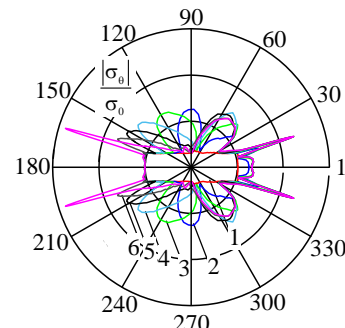


Fig. 2. Dynamic stresses distribution at the border of a circular mesh over time

For a detailed study of unsteady process at the plate over time we build time sections of dynamic stresses distribution along the border of the mesh. The calculation results are shown in Fig. 2 for the time interval $T \in [0; 1.2a/c_1]$ with step $\Delta T = 0.2a/c_1$ (curve 1...7).

Fig. 2 shows that under the influence of a weak shock wave the maximum dynamic stresses on the border of the mesh occur in the neighborhood of point A. Further distribution of stresses in the plate essentially depends on defragged waves from its mesh. Numerical calculations showed that the main shock of wave loading will reach the border of the mesh and reflect from it at $T = 0.2a/c_1$. Having $T = 1.6a/c_1$ the shock wave will reflect from the left side of the border. During the spread of reflected waves in a plate it is seen a significant increase of dynamic stress in angular points.

Having calculated the discrete time representation for movements that are similar to the formula (14) we can analyze a complete picture of unsteady flow wave process at the border of the mesh plate.

Conclusions. The use of integral Fourier transform over time and inverse discrete Fourier transform makes it possible to reduce the dynamic problem of plane deformation to solving the finite number of problems on steady-state oscillations at fixed values of cyclic frequencies. The advantage of the proposed approach is the setting for the incident wave for images area as (5), which makes it possible to calculate using the formula (14) the values of circular stresses for time moments $T_k \in [0, T]$, and not just half of them, as it does the calculations based on the discrete Fourier transform [9]. Thus the developed approach based on the method of boundary integral equations and the theory of functions of complex variables in field of Fourier-images makes it possible to calculate the time dependence of dynamic stresses in bodies with meshes for the actions of impulsive dynamic loads.

Література

1. Гузь, А.Н. Дифракция упругих волн / А.Н. Гузь, М.А. Черевко, В.Д. Кубенко. — К.: Наукова думка, 1978. — 307 с.
2. Banerjee, P.K. Boundary element methods in engineering science / P.K. Banerjee, R. Butterfield. — 2nd Ed. — London: McGraw-Hill, 1994. — 496 p.
3. Brebbia, C.A. Boundary element techniques in engineering / C.A. Brebbia, S. Walker. — London: Butterworth, 1980. — 210 p.
4. Mykhas'kiv, V.V. Interaction between rigid-disc inclusion and penny-shaped crack under elastic time-harmonic wave incidence / V.V. Mykhas'kiv, O.M. Khay // International Journal of Solids and Structures. — 2009. — Vol. 46, Issues 3-4. — PP. 602-616.

5. Саврук, М.П. Новый метод розв'язування динамічних задач теорії пружності та механіки руйнування / М.П. Саврук // Фізико-хімічна механіка матеріалів. — 2003. — № 4. — С. 7–11.
6. Пастернак, Я. Концентрація динамічних напружень біля тонких пружних включень за умов антиплоскої деформації / Я. Пастернак, Г. Сулим, Р. Пастернак // Фізико-математичне моделювання та інформаційні технології. — 2013. — Вип. 18. — С. 157–164.
7. Кунець, Я.І. Динамічна концентрація напружень в околі заглибленого тонкого прямолінійного включення низької жорсткості в умовах антиплоскої деформації / Я.І. Кунець, В.В. Матус, В.В. Пороховський // Математичні методи та фізико-механічні поля. — 2007. — Т. 50, № 1. — С. 136–139.
8. Shvabyuk, V. Stress state of plate with incisions under the action of oscillating concentrated forces / V. Shvabyuk, H. Sulym, O. Mikulich // *Acta Mechanica et Automatica*. — 2015. — Vol. 9, Issue 3. — PP. 140–144.
9. Director, S.W. Introduction to systems theory / S.W. Director, R.A. Rohrer. — Tokyo: McGraw-Hill, 1972. — 441 p.
10. Божидарник, В.В. Елементи теорії пружності / В.В. Божидарник, Г.Т. Сулим. — Львів: Світ, 1994. — 580 с.
11. Саврук, М.П. Двумерные задачи упругости для тел с трещинами / М.П. Саврук. — К.: Наукова думка, 1981. — 324 с.
12. Abramowitz, M. Handbook of mathematical functions with formulas, graphs, and mathematical tables / M. Abramowitz, I.A. Stegun. — Mansfield Centre, CT: Martino Publishing, 2014. — 1046 p.
13. Савин, Г.Н. Распределение напряжений около отверстий / Г.Н. Савин. — К.: Наукова думка, 1968. — 887 с.

References

1. Guz', A.N., Kubenko, V.D., & Cherevko, M.A. (1978). *Diffraction of Elastic Waves*. Kyiv: Naukova Dumka.
2. Banerjee, P.K., & Butterfield, R. (1994). *Boundary Element Methods in Engineering Science* (2nd Ed.). London: McGraw-Hill.
3. Brebbia, C.A., & Walker, S. (1980). *Boundary Element Techniques in Engineering*. London: Butterworth.
4. Mykhas'kiv, V.V., & Khay, O.M. (2009). Interaction between rigid-disc inclusion and penny-shaped crack under elastic time-harmonic wave incidence. *International Journal of Solids and Structures*, 46(3–4), 602–616. DOI:10.1016/j.ijsolstr.2008.09.005
5. Savruk, M.P. (2003). New method for the solution of dynamic problems of the theory of elasticity and fracture mechanics. *Materials Science*, 39(4), 465–471. DOI:10.1023/B:MASC.0000010922.84603.8d
6. Pasternak, I., Sulym, H., & Pasternak, R. (2013). Dynamic stress concentration at thin elastic inclusions under the antiplane deformation. *Physico-Mathematical Modelling and Informational Technologies*, 18, 157–164.
7. Kunets, Ya.I., Matus, V.V., & Porokhovs'kyu, V.V. (2007). Dynamic stress concentration in the vicinity of submerged thin plane inclusion of low rigidity under antiplane strain. *Mathematical Methods and Physicomechanical Fields*, 50(1), 136–139.
8. Shvabyuk, V., Sulym, H., & Mikulich, O. (2015). Stress state of plate with incisions under the action of oscillating concentrated forces. *Acta Mechanica et Automatica*, 9(3), 140–144. DOI:10.1515/ama-2015-0023
9. Director, S.W., & Rohrer, R.A. (1972). *Introduction to Systems Theory*. Tokyo: McGraw-Hill.
10. Bozhydarnyk, V.V., & Sulym, H.T. (1994). *Elements of the Theory of Elasticity*. Lviv: Svit.
11. Savruk, M.P. (1981). *Two-Dimensional Elasticity Problems for Bodies with Cracks*. Kyiv: Naukova Dumka.
12. Abramowitz, M., & Stegun, I.A. (2014). *Handbook of Mathematical Functions with Formulas, Graphs, and Mathematical Tables*. Mansfield Centre, CT: Martino Publishing.
13. Savin, G.N. (1970). *Stress Distribution around Holes*. Washington, D.C.: NASA.

Received May 13, 2016

Accepted June 25, 2016

CHEMISTRY. CHEMICAL ENGINEERING

XIMIA. XIMTEKHOLOGIA

UDC 661.842.092.4:631.842

M.A. Oliynyk,

A.B. Shestozub, PhD, Assoc.Prof.

Dniprodzerzhinsk State Technical University, 2 Dniprobudivska Str., 51918 Dniprodzerzhynsk, Ukraine; e-mail: olmyk@ua.fm

RESEARCH OF CALCIUM OXIDE HYDRATION IN CALCIUM NITRATE SOLUTIONS

M.A. Oliynyk, A.B. Shestozub. Дослідження процесу гідратації оксиду кальцію в розчинах кальцій нітрату. Мінеральні добрива – це один з важливих чинників інтенсифікації сільськогосподарства і збільшення кількості продуктів харчування. Обсяги виробництва і внутрішнього споживання мінеральних добрив в Україні свідчать про те, що використання азотних добрив тільки наближається до необхідної науково обгрунтованої кількості. Одним з найпоширеніших штучних мінеральних добрив є кальцієва селітра. **Мета:** Метою роботи є дослідження і теоретичне обгрунтування процесів, які відбуваються при приготуванні суспензій гідроксиду кальцію $\text{Ca}(\text{OH})_2$ в розчинах кальцій нітрату $\text{Ca}(\text{NO}_3)_2$. **Матеріали і методи:** В роботі використано технічний оксид кальцію (негашене вапно) ДСТУ Б В.2.7-90-99, розчини кальцієвої селітри концентрацій 15, 20, 25, 30, 35 і 40 % $\text{Ca}(\text{NO}_3)_2$. Вміст вапна при приготуванні суспензії у розчині змінювали (в перерахунку на оксид кальцію CaO) від 150 г/дм³ до максимально можливого. Кожний із цих розчинів насичували при температурі 40 °С вапном до максимально можливої концентрації. Придатними для використання в наступних експериментах і в технології отримання кальцієвої селітри вважалися ті розчини (суспензії), які протягом 12 годин не втрачали своєї рухливості (транспортальності). **Результати:** Результати експериментів показують, що при збільшенні концентрації нітрату кальцію у розчині в діапазоні 15...40 % кількість вапна, яку можна ввести в цей розчин без втрати ним транспортальності, зменшується. Подальше збільшення вище вказаної кількості вапна в розчинах зазначеної концентрації призводить до його загуснення, втрати рухливості (транспортальності). Розрахунки показали, що за присутності кальцієвої селітри розчинність $\text{Ca}(\text{OH})_2$ зменшується приблизно на порядок, що може привести до формування на поверхні оксиду кальцію CaO твердої фази $\text{Ca}(\text{OH})_2$, яка також може утворювати водневі зв'язки з компонентами розчину. Оскільки ймовірність утворення в розчині водневих зв'язків велика, то існує можливість утворення кластерів.

Ключові слова: кальцій нітрат, вапно, гідратація, концентрація, суспензія.

M.A. Oliynyk, A.B. Shestozub. Research of calcium oxide hydration in calcium nitrate solutions. Mineral fertilizers are one of the important factors of agriculture intensification and increasing of food products quantity. The volume of fertilizers production and its domestic consumption in Ukraine indicate that nitrogen fertilizer using only comes nearer to the required number of science-based. One of the most widespread artificial fertilizers is the calcium nitrate. **Aim:** The aim is to study and theoretically substantiate the processes occurring in the preparation of suspensions of calcium hydroxide $\text{Ca}(\text{OH})_2$ in solution of calcium nitrate $\text{Ca}(\text{NO}_3)_2$. **Materials and Methods:** The technical calcium oxide (quicklime) DSTU BV.2.7-90-99, solutions of calcium nitrate of 15, 20, 25, 30, 35 and 40 % $\text{Ca}(\text{NO}_3)_2$ concentrations were used in the work. The content of lime in the preparation of a suspension in the solution changed (in terms of calcium oxide CaO) from 150 g/dm³ to the maximum possible. Each of these solutions saturated at 40 °C in lime to maximum concentration. Suitable for use in these experiments and in the technology of calcium nitrate obtaining are considered the solutions (suspensions) that within 12 hours did not lose their mobility (transportability). **Results:** The experimental results show that increasing of the concentration of calcium nitrate in solution within the range 15...40 %, the amount of lime that you can put into the solution without loss of transportability decreases. Further increasing of lime quantity in solutions concentrations causes to its solidifying, loss of mobility (transportability). Calculations showed that in the presence of calcium nitrate the solubility of $\text{Ca}(\text{OH})_2$ is reduced nearly by order that can lead to the formation of calcium oxide CaO the solid phase $\text{Ca}(\text{OH})_2$ on the surface, which also can form hydrogen bonds with the components of the solution. As the probability of formation of hydrogen bonds in solutions is high, there is a possibility of formation of clusters.

Keywords: calcium nitrate, lime, hydration, concentration, suspension.

Introduction. Mineral fertilizers are one of the important factors of agriculture intensification and increasing of food products quantity. The volume of fertilizers production and its domestic consumption in Ukraine indicate that nitrogen fertilizer using only comes nearer to the required number of science-based.

One of the most widespread artificial fertilizers is the calcium nitrate. It is widely used, particularly as the basis of anti-ice mixes and corrosion inhibitors; as an additive in building mixtures; as the components of emulsion explosives, accumulating solutions in refrigeration and others.

DOI 10.15276/opus.2.49.2016.16

© 2016 The Authors. This is an open access article under the CC BY license (<http://creativecommons.org/licenses/by/4.0/>).

The chemical industry, including the production of mineral fertilizers is the branch which requires high material and energy expenses at a time when a major development trends now is resource saving. The actual is development of energy saving technologies of calcium nitrate production containing additional nutrients, primarily through improvement of prior preparation processes of calcium material acid treatment. Apart from entering into a ground the main nutrients (NPK), entering the Ca-compounds increases mobile forms of calcium, increases the microbiological and enzymatic activity of soil [1]. Using of calcium nitrate solution as a component of emulsion explosives reaches 15...30 % of the total mass [2]. Because of the wide scope of application a number of demands put forward this product: reduction of insoluble substances, enrichment solution of calcium nitrate and granular product with additional nutrients and reduce water absorption and caking, others.

In this regard, various approaches designed to improve the quality of calcium nitrate in solution and in granulated form, including the approach of pure calcium obtaining [3]. Chvertka [4] proposed decrease of suspended particles in calcium nitrate solution by flotation, and Obrestad [5] — treatment by flocculants.

In turn, Oliynyk [6] proposed energy-saving technology of calcium nitrate obtaining while increasing the concentration of lime in the initial suspension and the introduction of additional nutrients.

Note that a significant impact on quality of calcium saltpetre solution, including its contents, is method of introducing of initial reagents [7].

In modern calcium nitrate manufacturing various types of calcium processed with aqueous solutions of nitric acid suspended in the reaction system. When using quicklime the formation of different intermediate calcium compounds happened that will affect the suspension, and at the critical concentrations will lead to its thickening.

The aim is to study and theoretically substantiate the processes occurring in the preparation of suspensions of calcium hydroxide $\text{Ca}(\text{OH})_2$ in solution of calcium nitrate $\text{Ca}(\text{NO}_3)_2$.

Materials and Methods. The technical calcium oxide (quicklime) DSTU BV.2.7-90-99, solutions of calcium nitrate of 15, 20, 25, 30, 35 and 40 % $\text{Ca}(\text{NO}_3)_2$ concentrations were used in the work. The content of lime in the preparation of a suspension in the solution changed (in terms of calcium oxide CaO) from 150 g/dm^3 to the maximum possible.

Laboratory studies conducted on the installation, schematically shown in Fig. 1. Installation consists of cool reactor (working volume 1.75 dm^3) made of stainless steel grade 12Kh18N10T, electric motor with the paddle mixer and the possibility of speed control that mounted on a tripod of electric oven to maintain the temperature in the reactor.

The study was conducted as follows. In the reactor 2 was loaded with 1 dm^3 calcium nitrate indicated above. Each of these solutions saturated at 40 °C in lime to maximum concentration. Suitable for use in these experiments and in the technology of calcium nitrate obtaining are considered the solutions (suspensions) that within 12 hours did not lose their mobility (transportability).

Results and Discussion. The experimental results show that increasing of the concentration of calcium nitrate in solution within the range 15...40%, the amount of lime that you can put into the solution without loss of transportability decreases. Further increasing of lime quantity in solutions concentrations causes to its solidifying, loss of mobility (transportability). So, for a 15 %-solution of calcium nitrate $\text{Ca}(\text{NO}_3)_2$, the maximum possible concentration of lime in terms of calcium oxide is 350 g/dm^3 , for 20 %-solution — 320 g/dm^3 , for 25 %-solution —

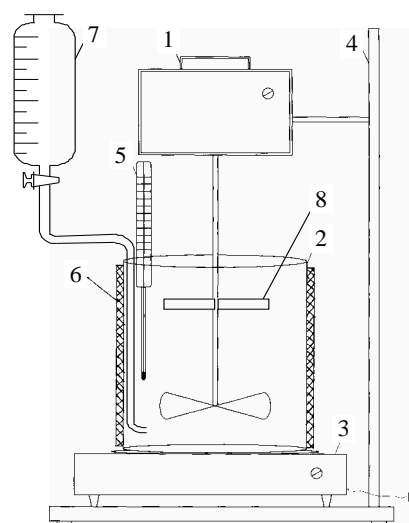


Fig. 1. Scheme of laboratory facility for the preparation of hydroxide suspensions: 1 — electric mixer with paddle; 2 — reactor; 3 — electric oven; 4 — tripod; 5 — thermometer; 6 — thermal insulation; 7 — graduated tank of nitric acid; 8 — additional paddles

295 g/dm³, for 30 %-solution — 275 g/dm³, for 35 %-solution — 240 g/dm³, and for 40 %-solution — 200 g/dm³, respectively (Fig. 2).

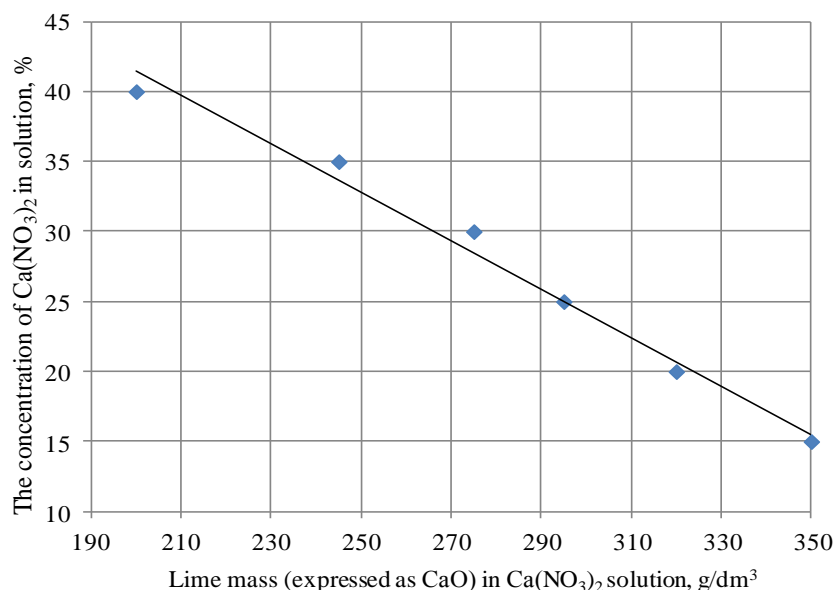


Fig. 2. Dependence of lime concentration in the transport solution on Ca(NO₃)₂ concentration

These lime concentrations can vary from deviation ± 3 g/dm³. Further increasing of lime quantity in solutions concentrations causes to its solidifying, loss of mobility (transportability). It is formed viscous gel-like mass, which is not subject of transportation with pipelines. Experimentally it was found that the dynamic viscosity of the obtained suspension shall not exceed 1.0...1.1 Pa·s. Increasing the viscosity of the suspension leads to difficulties in pumping and transportation with pipelines, and in some cases prevents these processes.

In subsequent studies used the 35 %-solution of calcium nitrate Ca(NO₃)₂ and determines the degree of conversion (hydration) of calcium oxide CaO therein.

Particular importance for the stage of preparation of suspensions in experimental studies is interaction time of reagents, which determines the degree of slaking of calcium oxide in 35 %-solution of calcium nitrate, productivity and size of equipment. Significant impact on the degree of conversion of calcium oxide has the intensity of mixing. The dependence of the degree of conversion of calcium oxide from Reynolds criterion Re and interaction time is shown in Fig. 3.

Thickening of suspension formed by adding calcium oxide in calcium nitrate solution of variable concentration is happening with different amounts of calcium oxide in solution. Moreover, increasing the concentration of calcium nitrate leads to a decrease of calcium oxide at which the thickening suspension happen. The experimental results are shown in Table 1.

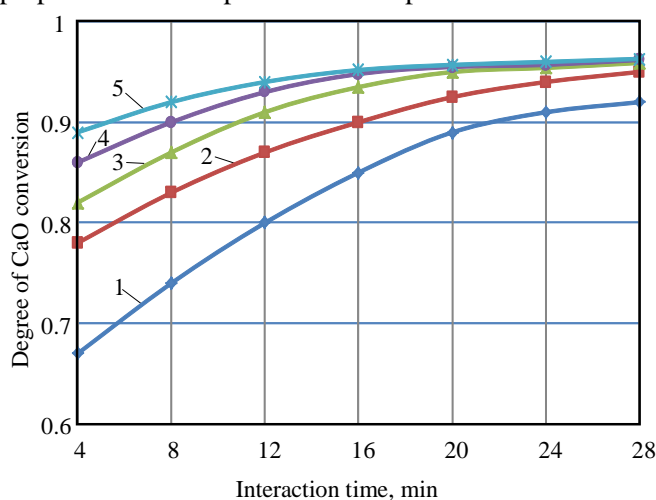


Fig. 3. The dependence of the degree of CaO conversion on the intensity of mixing and interaction time: 1 — Re = 1000; 2 — Re = 4000; 3 — Re = 7000; 4 — Re = 10000; 5 — Re = 13000

Table 1

The properties of the suspension at critical concentration of calcium oxide CaO

Components and some parameters of suspension	Values					
The concentration of the initial solution Ca(NO ₃) ₂ , %	15.0	20.0	25.0	30.0	35.0	40
The concentration of the initial solution Ca(NO ₃) ₂ , mol/dm ³	0.998	1.418	1.845	2.302	2.796	3.330
The density of the of the initial solution of Ca (NO ₃) ₂ , g/dm ³	1119.3	1163.6	1211.0	1259.0	1311.0	1366.0
Critical lime content expressed as CaO with thickening of the suspension, g/dm ³	350.0	300.0	295.0	275.0	243.0	200.0
Critical lime content expressed as CaO with thickening of the suspension, mol/dm ³	6.24	5.35	5.26	4.90	4.33	3.57
Water mass in the initial solution of Ca(NO ₃) ₂ , g	951.4	930.9	908.3	881.3	852.2	819.6
The mass of water required for complete hydration of CaO to Ca(OH) ₂ , g	112.5	96.4	94.8	88.4	78.1	64.3
Water mass remaining after hydration of CaO, g	838.9	834.5	813.5	792.9	774.1	755.3

Table 1 shows that the water mass required for complete hydration of calcium oxide CaO by the reactions

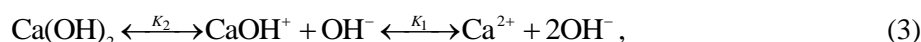


or



significantly less than the water mass which is present in suspension. So, impossible explain the thickening process by water flow in accordance with reactions (1) and (2). Thus there are other processes that are likely to occur at scheme outlined below.

Ionization of calcium hydroxide Ca(OH)₂ contained in the solution is as follows:



$$K_2 = \frac{[\text{CaOH}^+] \cdot [\text{OH}^-]}{[\text{Ca(OH)}_2]} \approx 1 \text{ (strong alkali)}, \quad K_1 = \frac{[\text{Ca}^{2+}] \cdot [\text{OH}^-]}{[\text{CaOH}^+]} = 5 \cdot 10^{-2}.$$

According to the scheme the material balance of calcium compounds can be represented by marking *C* as the total concentration of calcium compounds in the solution, as follows:

$$C = [\text{Ca(OH)}_2] + [\text{CaOH}^+] + [\text{Ca}^{2+}].$$

To calculate the equilibrium concentration of [CaOH⁺] in solution let make use of expressions for *K*₁ and *K*₂ taking *K*₂ = 1. Then [Ca(OH)₂] and [Ca²⁺] can be expressed via [CaOH⁺], and the material balance will take the following form:

$$C = \frac{[\text{CaOH}^+] \cdot [\text{OH}^-]}{K_2} + [\text{CaOH}^+] + \frac{K_1[\text{CaOH}^+]}{[\text{OH}^-]}.$$

Solving the equation with respect to [CaOH⁺], we obtain the expression

$$\frac{[\text{CaOH}^+]}{S} = \frac{K_1[\text{OH}^-]}{[\text{OH}^-]^2 + K_1[\text{OH}^-] + K_1K_2},$$

where *S* — solubility value, which will allow calculate the relative concentration of [CaOH⁺] when concentration of [OH⁻] changing.

Similarly equation for calculation of equilibrium concentrations of [Ca(OH)₂] and [Ca²⁺] have been obtained

$$\frac{[\text{Ca(OH)}_2]}{S} = \frac{[\text{OH}^-]^2}{[\text{OH}^-]^2 + K_1[\text{OH}^-] + K_1K_2},$$

$$\frac{[Ca^{2+}]}{S} = \frac{K_1 K_2}{[OH^-]^2 + K_1[OH^-] + K_1 K_2}$$

Fig. 4 shows the distribution of forms of existence of calcium compounds from solution pH when thickening.

As shown in Fig. 4, hydration of calcium oxide CaO is going partially according to reaction

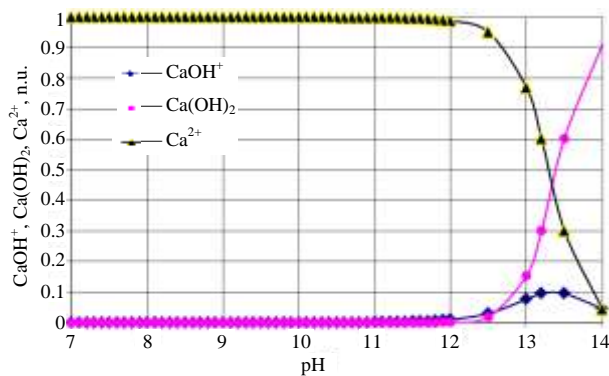
$$CaO + Ca^{2+} + H_2O = 2CaOH^+ \quad (4)$$


Fig. 4. Distribution of forms of existence of calcium compounds from solution pH upon reaching the thickening

This forms CaOH⁺ ion in which oxygen is in a state of unfilled orbitals that should promote the formation of hydrogen bonds and occur the clusters (Fig. 5); thus, solution become capsulate and as a result, suspension is thickening.

During calculations were conducted the values of basicity coefficients not taken into account, since for large values of ionic strength for a rough approximation you can accept their values as constant.

Solubility values S can be defined using the solubility constant K_{sp} $[Ca(OH)_2] = 5.47 \cdot 10^{-6}$. Calculations are performed without considering the degree of hydration of calcium oxide CaO and activity coefficients, taking an extra concentration C as the molar concentration of $Ca(NO_3)_2$ in solution:

$$K_{sp} = [Ca^{2+}] \cdot [OH^-]^2 = 5.47 \cdot 10^{-6}$$

Material balance of $Ca(OH)_2$ solution:

$$Ca(OH)_2 \leftrightarrow Ca^{2+} + 2OH^-, \quad (5)$$

$$[OH^-] = 2S; [Ca^{2+}] = S + C, \quad (6)$$

$$K_{sp} = (S + C) \cdot (2S)^2. \quad (7)$$

According the value of C given in Table 1, calculate the value of S , which are suitable for determining the relative concentration of $Ca(OH)_2$ using Eq. (5)...(7).

Calculations showed that in the presence of calcium nitrate the solubility of $Ca(OH)_2$ is reduced nearly by order that can lead to the formation of calcium oxide CaO the solid phase $Ca(OH)_2$ on the surface, which also can form hydrogen bonds with the components of the solution. As the probability of formation of hydrogen bonds in solutions is high, there is a possibility of formation of clusters (Fig. 6).

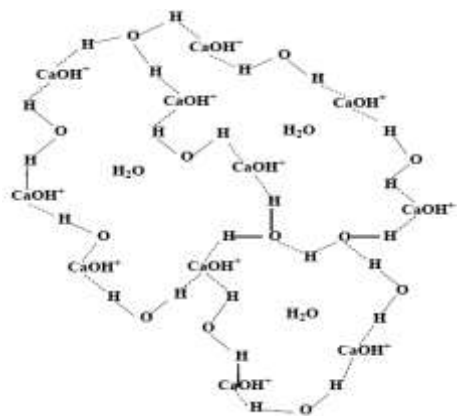


Fig. 5. Formation of clusters through hydrogen bonds

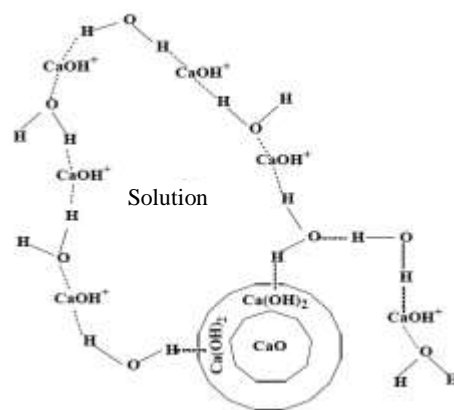


Fig. 6. The formation of $Ca(OH)_2$ membrane and clusters around CaO grain through hydrogen bonds

Conclusions. A number of experiments was held aimed at research and theoretical study of processes occurring in the preparation of suspensions of calcium hydroxide $\text{Ca}(\text{OH})_2$ in solution of calcium nitrate $\text{Ca}(\text{NO}_3)_2$. Experimentally determined the highest possible content of lime in a solution of calcium nitrate and the possibility of increasing the critical concentration of calcium oxide CaO for thickening of slurry. Theoretically grounded the calcium oxide hydration process and mechanism of slurry thickening.

Література

1. Лазарев, В.И. Влияние кальцийсодержащих соединений на микробиологическую активность и физико-химические свойства почвы / В.И. Лазарев, Н.Н. Трутаева // Достижения науки и техники АПК. — 2006. — № 10. — С. 7–9.
2. Пат. 41672 Україна, МПК C06B 31/00. Емульсійна вибухова речовина «Україніт-ПП-2Б» / Купрін О.В., Іщенко М.І., Савченко М.В., Купрін В.П.; патентовласник ТОВ «ІСТ-ФОРТ». — № u200902994; заявл. 30.03.2009; надр. 25.05.2009, Бюл. № 10.
3. Пат. 2239601 Российская Федерация, МПК C01F 11/36, C05C 5/04. Способ получения очищенного раствора нитрата кальция / Сеземин В.А., Абрамов О.Б., Захарова О.М.; патентообладатель ООО «Научно-инженерный центр». — № 2003133785/15; заявл. 20.11.2003; опубл. 10.11.2004.
4. Дослідження причин появи та методів зниження зважених часток в кальцієвій селітрі вітчизняного виробництва / Н.В. Чвертка, А.Б. Шестозуб, А.О. Багно та ін. // Зб. матеріалів 4-ї Української науково-техн. конф. «Сучасні проблеми технології неорганічних речовин», 14–16 жовтня 2008 р., Дніпродзержинськ, Україна. — Дніпродзержинськ: ДДТУ, 2008. — С. 149–150.
5. Пат. 220612 Польща, МПК C01F 11/36, C01F 11/38. Sposób oczyszczania roztworów lub stopów azotanu wapnia, oraz roztwór/stop azotanu wapnia / Obrestad T., Mutsaers P., Wallestad I.; YARA INTERNATIONAL ASA. — № 387815; заявл. 16.04.2009; надр. 30.11.2015.
6. Предпосылки создания энергосберегающей технологии производства модифицированной кальциевой селитры / Н.А. Олійник, А.Б. Шестозуб, Н.Д. Волошин и др. // Мат-лы XVII Междунар. заоч. науч.-практ. конф. «Технические науки — от теории к практике», 23 января 2013 г., Новосибирск, РФ. — Новосибирск: Изд. «СибАК», 2013. — Ч. 2. — С. 46–54.
7. Олійник, М.А. Дослідження впливу способу введення сировини на якість розчину кальцієвої селітри / М.А. Олійник, А.Б. Шестозуб, М.В. Зайцев // Зб. тез доповідей 5-ї Всеукраїнської наукової конференції студентів, аспірантів і молодих учених «Хімічні проблеми сьогодення», 14–17 березня, 2011 р., Донецьк, Україна. — Донецьк: Ноулідж, 2011. — С. 139.

References

1. Lazarev, V.I., & Trutaeva, N.N. (2006). Effect of calcium-containing compounds on microbial activity and physico-chemical properties of the soil. *Achievements of Science and Technology of AIC*, 10, 7–9.
2. “IST-FORT” LLC. (2009). “Ukrainit-PP-2B” Emulsion Explosive. Ukraine Patent: UA 41672.
3. “Nauchno-Inzhenerniy Tsentri” LLC. (2004). Purified calcium nitrate solution preparation method. Russian Federation Patent: RU 2239601.
4. Chvertka, N.V., Shestozub, A.B., Bagno, A.O., Voloshin, M.D., & Aleksanov, O.P. (2008). Study on reasons and methods to reduce the suspended particles of the domestically produced Calcium Nitrate. In *Proceedings of the 4th Ukrainian Scientific and Technical Conference on Modern Problems in Technology of Nonorganic Substances* (pp. 149–150). Dniprodzerzhynsk: Dniprodzerzhynsk State Technical University.
5. Yara International ASA. (2015). Sposób oczyszczania roztworów lub stopów azotanu wapnia, oraz roztwór/stop azotanu wapnia. Polish Patent: PL 220612.
6. Olinyk, N., Shestozub, A., Voloshin, N., Aleksanov, O., & Bagno, A. (2013). Background energy power generation modified calcium nitrate. In *Proceedings of the 17th International Scientific and Practical Conference “Engineering: From Theory to Practice”* (Vol. 2, pp. 46–54). Novosibirsk: SibAK.
7. Olinyk, M.A., Shestozub, A.B., & Zaitsev, M.V. (2011). Study of the effect of route of administration of the raw materials on the quality of Calcium Nitrate solution. In *Proceedings of the 5th All-Ukrainian Scientific Conference of Students, Aspirants, and Young Scientists “Today’s Chemical Problems”* (p. 139). Donetsk: Knowledge.

Received April 14, 2016

Accepted July 26, 2016

UDC 544.6.076.34–723.4:[547.361.2+546.81–31]

A.O. Maizelis, PhD,

B.I. Bairachniy, DSc, Prof.,

G.G. Tul'skiy, DSc, Prof.

National Technical University "Kharkiv Polytechnic Institute", 21 Frunze Str., 61002 Kharkiv, Ukraine; e-mail: a.maizelis@gmail.com

FORMATION OF THE ORGANIC-INORGANIC PROTON EXCHANGE MEMBRANE

A.O. Maizelis, B.I. Bairachniy, G.G. Tul'skiy. Формування органо-неорганічної протон-обмінної мембрани. Застосування електролізерів низькотемпературного розкладання води з твердою полімерною мембраною є перспективним для одержання водню з використанням відновлювальних джерел енергії. Однак висока вартість мембранних матеріалів перешкоджає масовому впровадженню таких електролізерів. Більшу частину досліджень, направлених на розробку методик формування мембран, альтернативних Nafion®, присвячено органічним матеріалам. **Мета:** Метою роботи є розробка методики формування конкурентоспроможної протон-провідної мембрани на основі полівінілового спирту (ПВС) і неорганічних гідратів. **Матеріали і методи:** Для одержання мембрани у 2...10 %-ий розчин ПВС додавали гідратований оксид олова, перемішували і пошарово наносили на інертну основу, від якої готову мембрану у подальшому відокремлювали. Для покращення її механічних властивостей використовували армуючу сітку. Гідратований оксид олова одержували взаємодією розчинів хлориду олова і гідроксиду амонію. **Результати:** Досліджено умови формування протон-обмінної мембрани на основі полівінілового спирту і гідратованого оксиду олова. Одержано серію мембран зі вмістом гідратованого оксиду олова 30, 50, 70, 80 і 90 %. Показано, що суцільна плівка мембрани товщиною понад 100 мкм може бути отримана, якщо зміст полівінілового, що дорівнює або перевищує 30 %. Показано, що необхідно проводити шшивку ПВС у одержаній плівці. Структура одержаної протон-провідної мембрани являє собою ланцюги ПВС, зшиті альдегідом, між якими розташовані глобули гідратованого оксиду олова. Провідність мембрани забезпечується як рухомістю протонів гідроксильної групи ПВС, так і за рахунок часткової дисоціації гідратованого оксиду на поверхні глобул з утворенням утворень $\text{H}_3\text{O}^+/\text{H}_2\text{O}$ і $\text{OH}^-/\text{H}_2\text{O}$.

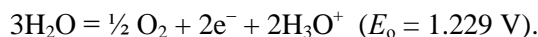
Ключові слова: протон-провідна мембрана, полівініловий спирт, гідратований оксид олова.

A.O. Maizelis, B.I. Bairachniy, G.G. Tul'skiy. Formation of the organic-inorganic proton exchange membrane. The use of electrolyzers for the low-temperature water electrolysis with the solid polymer membrane is perspective for production of hydrogen using renewable energy sources. However, the high cost of membrane materials obstructs the mass commissioning of such electrolyzers. Most of the researches devoted to the technologies of membranes formation, alternative to Nafion®, deal only with organic materials. **Aim:** The aim of this research is to develop the method for formation of the competitive proton exchange membrane based on polyvinyl alcohol (PVA) and inorganic hydrates. **Materials and Methods:** The hydrated oxide of tin was added to the 2...10 % PVA solution, mixed and applied to inert base layer by layer for formation of the membrane. Then the membrane was separated from the base. The reinforcing mesh was used to improve mechanical properties of the membrane. The hydrated tin oxide was prepared by reaction of tin chloride and ammonium hydroxide solutions. **Results:** The conditions of formation of proton-exchange membranes based on polyvinyl alcohol and hydrated oxide of tin were investigated. The series of membranes containing 30, 50, 70, 80 and 90 % of hydrated tin oxide are obtained. It is shown that a solid membrane film with the thickness over 100 μm can be obtained if the content of PVA exceeds 30 %. It is shown that it is necessary to crosslink the chains of PVA in the resulting film. The structure of the obtained proton exchange membrane consists of PVA chains crosslinked by aldehyde, between which the globules of hydrated tin oxide are situated. The membrane conductivity is provided by both proton mobility of hydroxyl group of PVA and $\text{H}_3\text{O}^+/\text{H}_2\text{O}$ and $\text{OH}^-/\text{H}_2\text{O}$ groups that are formed due to the partial dissociation of hydrated oxide on the surface of the globules.

Keywords: proton exchange membrane, polyvinyl alcohol, hydrated tin oxide.

Introduction. Recently, high interest is paid to finding the ways to improve the material for creation of hydrogen electrochemical generators with a solid polymer electrolyte. This generator (electrochemical cell) consists of two electrodes pressed against the proton exchange membrane (PEM), forming a membrane-electrode assembly. The distilled water serves as electrolyte.

The main chemical reaction on the anode is water oxidation that leads to formation of the hydronium ions and oxygen:

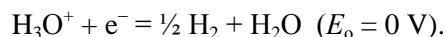


Oxygen is removed through the gas diffusion layer of the electrode. Hydronium ions pass through the proton exchange membrane, which is a solid electrolyte in electrochemical cell.

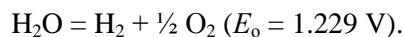
The main chemical reaction on the cathode is the reduction of hydronium that leads to the water release and hydrogen evaluation:

DOI 10.15276/opu.2.49.2016.17

© 2016 The Authors. This is an open access article under the CC BY license (<http://creativecommons.org/licenses/by/4.0/>).



Thus, the overall reaction is:



Due to the formation of protons, the media in the electrochemical cell (which is fed by deionized water) changes to acidic: the estimated concentration of protons at the standard load is about $1 \text{ mol}\cdot\text{dm}^{-3}$, i.e. pH is 1. This fact complicates both the selection of electrode materials and membranes.

The most expensive components of the cell with a solid electrolyte are proton exchange membrane and catalysts of electrode processes. The most used catalysts are platinum-group metals (platinum, palladium, iridium and ruthenium) in the form of nanoscale particles and their oxides. The most widely used solid electrolyte membrane is Nafion[®]. This membrane is a co-polymer of tetrafluoroethylene and co-monomer with side chains of perfluorinated vinyl ether ending by sulfo-group, so that proton is transferred from one sulfo-group to another one.

Among the requirements for the proton exchange membrane, that are used in water electrolysis, are high proton conductivity, low electron conductivity, low permeability of the gases (hydrogen and oxygen), high chemical stability in the acidic media, providing high speed electrode reactions, mechanical strength in the dry and humid condition, minor water transport across the membrane by diffusion and electroosmosis effects, as well as availability of materials and low production cost.

The high cost of Nafion[®] membranes has led to an active research for more reasonably priced membrane compositions. The similar perfluorinated membrane called MF-4SK was created in USSR. The number of another membranes were developed [2], but they are inferior to Nafion[®] membrane on the number of important characteristics. One of the developments is membrane based on polyvinyl alcohol (PVA) with addition of phenol-2,4-disulfonic acid [3]. PVA can conduct protons through a inherent system of hydrogen bonds. It also has high gas impermeability, which is one of the essential requirements for membranes (solid electrolytes) in electrochemical cells for hydrogen production and fuel cells. Additionally, the low cost of PVA led to the interest in practical application. However, the use of PVA is limited by its solubility in water and its insufficient proton conductivity.

On the other hand, it is known that some of the hydrated metal oxides (inorganic hydrates) of globular structure have proton conductivity. The composition of the globules inside is close to the metal oxide and the surface contains many high-active OH⁻-groups and water molecules, which provide proton conductivity [4]. For example, hydrated oxides of antimony and tin are used in sensors for hydrogen detection as a layer of a proton-conductive electrolyte. However, these precipitates are not mechanically stable hydrates and this prevents their use as membranes.

The aim of this research is to develop the method for formation of the competitive proton exchange membrane based on polyvinyl alcohol (PVA) and inorganic hydrates.

Materials and Methods. The tin chloride, ammonium hydroxide, polyvinyl alcohol and sodium sulfate ("chemically pure" qualification) were used in the work. The photographs were taken by a hardness measuring instrument PMT-3 and digital camera Canon PowerShot A1100IS. The PVA solution with concentration of 2...10 % was prepared by dissolving PVA in the heated to 50...70 °C distilled water during 2 hours and holding at room temperature until solution becomes clear.

The precipitate of hydrated tin oxide was obtained by the reaction between ammonium hydroxide and tin chloride (IV) solutions. The resulting precipitate was washed until the pH of filtrate becomes neutral. To prevent the loss of the hydrated water the prepared precipitate was stored in air at 100 % humidity.

Results and Discussion. The proton exchange membrane was formed by the method described in [5], by "brush" method using layering of PVA solution with addition of certain amount of hydrated tin oxide on an inert substrate. Free water was removed from each layer using heated (40...60 °C) air, preventing its complete drying, since the loss of the hydrated water significantly reduces the conductivity of the obtained membrane.

After applying the half of layers, the reinforcing mesh was stacked, and then the rest of the layers were applied. The use of reinforcing mesh improves the mechanical strength of the membrane.

The degree of swelling in hot water (50 °C) of the obtained membrane with PVA content 50 % was 640 % after 2 hours of exposing. The higher temperatures lead to slow dissolution, due to the solubility of PVA. To increase the heat resistance of membrane the crosslinking of PVA chains on the surface of the membrane was performed by treatment with aldehyde in the solution containing 2...5 wt. % of aldehyde, 20 wt. % of sulfuric acid and 20...25 wt. % of sodium sulphate at 60...70 °C during 25...30 minutes. The sulfuric acid acts as a catalyst, sodium sulfate reduces swelling degree of the membrane.

The series of membranes containing 30, 50, 70, 80 and 90 wt. % of hydrated oxide are marked as M30, M50, M70, M80 and M90, respectively. Samples containing 30...70 % of $\text{SnO}_2 \cdot n\text{H}_2\text{O}$ have a uniform structure for both thicknesses of 100 μm (Fig. 1, *a, b, c*) and 200 μm (Fig. 2, *a, b, c*).

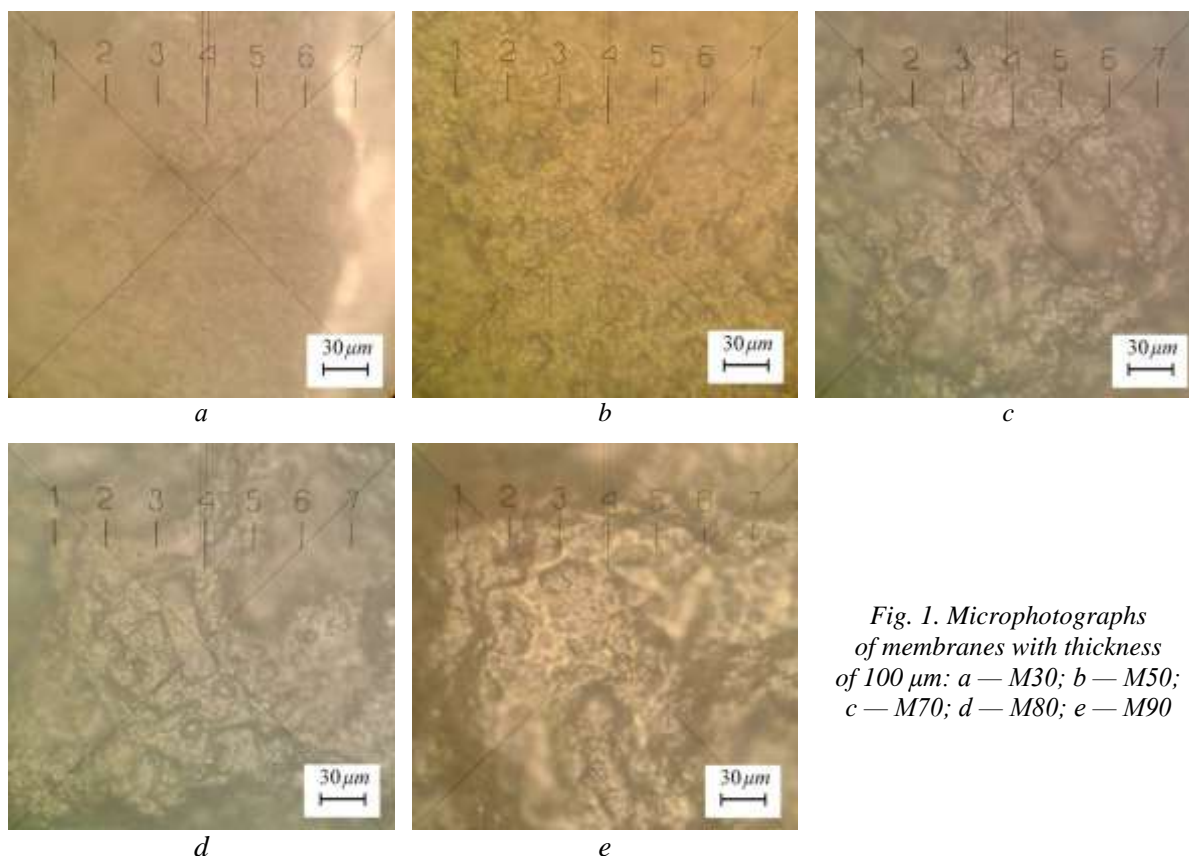
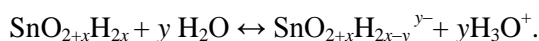


Fig. 1. Microphotographs of membranes with thickness of 100 μm : a – M30; b – M50; c – M70; d – M80; e – M90

With the further increase of $\text{SnO}_2 \cdot n\text{H}_2\text{O}$ content (Fig. 1, *d, e*, Fig. 2, *d, e*) the disadvantage of the PVA binder is critical for the film thickness higher than 100 μm : the cracks in the M80 membrane sample can be seen using microscope with a 400 times magnification, cracks in M90 membrane sample are visible with the naked eye.

The probable structure of proposed proton exchange membrane based on polyvinyl alcohol and addition of hydrated tin oxide is shown in Fig. 3, *a*. The chains of polyvinyl alcohol are crosslinked by aldehyde, which makes the polymer insoluble. There are the globular hydrated tin oxide and water molecules between PVA chains. This leads to the partial dissociation of $\text{SnO}_{2+x}\text{H}_{2x}$ producing hydronium ion:



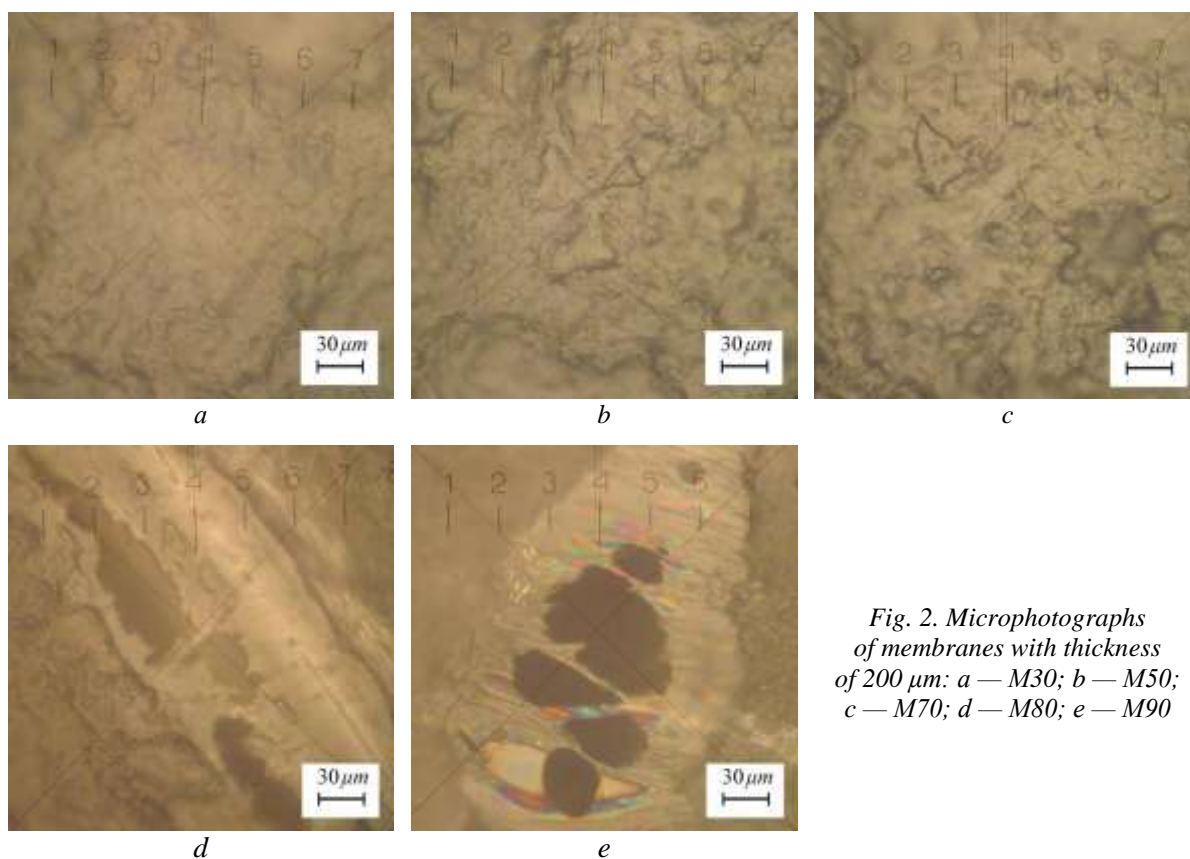


Fig. 2. Microphotographs of membranes with thickness of 200 μm : a – M30; b – M50; c – M70; d – M80; e – M90

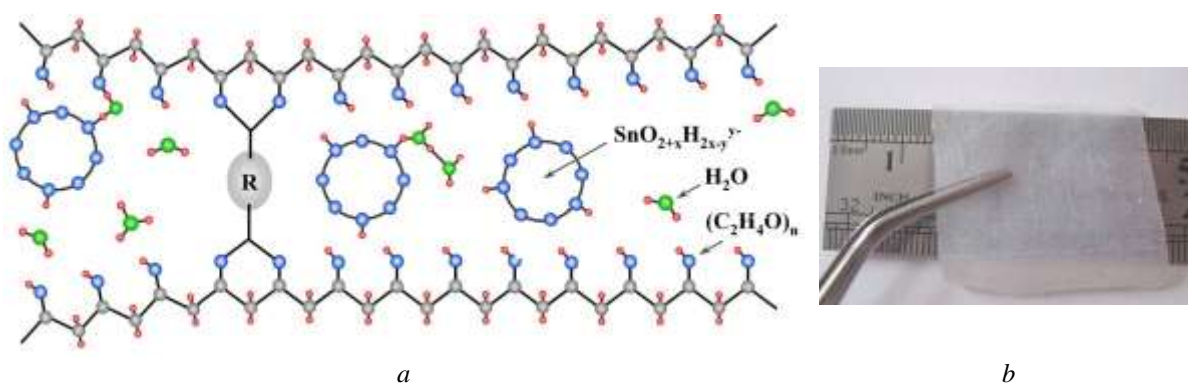


Fig. 3. Proton exchange membrane of polyvinyl alcohol and a hydrated tin oxide: a – the structure, b – exterior membrane M50

Thus $\text{H}_3\text{O}^+/\text{H}_2\text{O}$ and $\text{OH}^-/\text{H}_2\text{O}$ proton-containing groups are formed and the proton transfer process occurs by Grotthuss mechanism, which consists in proton overshoot between the proton exchange groups and their reorientation. Fig. 3, b shows a photograph of M50 membrane sample with 200 μm thickness.

Conclusions. Thus, a method of formation of the proton exchange membrane using reasonable materials, polyvinyl alcohol and hydrated tin oxide obtained from the tin chloride and ammonium hydroxide is proposed.

Література

1. PEM electrolysis for hydrogen production: Principles and applications / D.G. Bessarabov, H. Wang, H. Li, N. Zhao. — Boca Raton: CRC Press, 2016. — 389 p.
2. A comprehensive review on PEM water electrolysis / M. Carmo, D.L. Fritz, J. Mergel, D. Stolten // *International Journal of Hydrogen Energy*. — 2013. — Vol. 38, Issue 12. — PP. 4901–4934.
3. Charge and mass transport in the phenol-2,4-disulfonic acid-polyvinyl alcohol ion exchange membranes studied by pulsed field gradient NMR and impedance spectroscopy / V.I. Volkov, Yu.A. Dobrovolsky, M.S. Nurmiev, *et al.* // *Solid State Ionics*. — 2008. — Vol. 179, Issues 1–6. — PP. 148–153.
4. Ярославцев, А.Б. Протонная проводимость неорганических гидратов / А.Б. Ярославцев // *Успехи химии*. — 1994. — Т. 63, № 5. — С. 449–455.
5. Пат. 103734 Україна, МПК В01D 71/02 (2006.01), В01D 71/06 (2006.01), Н01М 2/14 (2006.01), С25В 1/04 (2006.01). Спосіб формування протон-провідної мембрани / Майзеліс А.О., Байрачний Б.І.; патентовласник НТУ «Харківський Політехнічний Інститут» (UA). — № u201506664; заявл. 06.07.2015; опубл. 25.12.2015, Бюл. № 24.

References

1. Bessarabov, D.G., Wang, H., Li, H., & Zhao, N. (2016). *PEM Electrolysis for Hydrogen Production: Principles and Applications*. Boca Raton: CRC Press.
2. Carmo, M., Fritz, D.L., Mergel, J., & Stolten, D. (2013). A comprehensive review on PEM water electrolysis. *International Journal of Hydrogen Energy*, 38(12), 4901–4934. DOI:10.1016/j.ijhydene.2013.01.151
3. Volkov, V.I., Dobrovolsky, Yu.A., Nurmiev, M.S., Sanginov, E.A., Volkov, E.V., & Pisareva, A.V. (2008). Charge and mass transport in the phenol-2,4-disulfonic acid-polyvinyl alcohol ion exchange membranes studied by pulsed field gradient NMR and impedance spectroscopy. *Solid State Ionics*, 179(1–6), 148–153. DOI:10.1016/j.ssi.2007.12.046
4. Yaroslavtsev, A.B. (1994). Proton conductivity of inorganic hydrates. *Russian Chemical Reviews*, 63(5), 429–435. DOI:10.1070/RC1994v063n05ABEH000095
5. National Technical University “Kharkiv Polytechnic Institute”. (2015). *A method of forming of a proton-conducting membranes*. Ukraine Patent: UA 103734.

Received May 10, 2016

Accepted July 15, 2016

UDC 661.842.091:661.333.002.84

E.O. Mikhailova¹, PhD, Assoc.Prof.,V.O. Panasenko², DSc, Prof.,N.B. Markova³, Senior Researcher¹ Simon Kuznets Kharkiv National University of Economics, 9-A Nauky Ave., 61166 Kharkiv, Ukraine; e-mail: eva.mikhaylova@mail.ru² State Research and Design Institute of Basic Chemistry (NIOCHIM), 25 Mironositskaya Str., 61002 Kharkiv, Ukraine³ National Technical University "Kharkiv Polytechnic Institute", 21 Bagaley Str., 61002 Kharkiv, Ukraine

CALCIUM CARBONATE SYNTHESIS WITH PRESCRIBED PROPERTIES BASED ON LIQUID WASTE OF SODA PRODUCTION

Е.О. Михайлова, В.О. Панасенко, Н.Б. Маркова. Синтез карбонату кальцію із заданими властивостями на основі рідних відходів содового виробництва. Перспективним напрямком у вирішенні екологічних проблем содової галузі є розробка мало-відходних ресурсозберігаючих технологій, які полягають у переробці цінних компонентів відходів з одержанням товарних продуктів. **Мета:** Метою роботи є встановлення оптимальних умов одержання карбонату кальцію із заданими властивостями з рідних відходів содового виробництва. **Матеріали і методи:** Хімічно осаджений карбонат кальцію застосовується як наповнювач і повинен мати певні фізико-хімічні властивості. Для одержання продукту необхідної якості процес осадження карбонату кальцію проводили з дистилерної рідини, що є відходом виробництва кальцинованої соди і містить значну кількість іонів кальцію, і надлишкового маточного розчину виробництва очищеного гідрокарбонату натрію, до складу якого входять карбонатні та гідрокарбонатні іони. **Результати:** Встановлено залежність насипної густини і питомої поверхні осадів карбонату кальцію і ступеня його осадження від таких технологічних параметрів: способу змішування вихідних розчинів, концентрації і мольного співвідношення реагентів, температури і часу протікання реакції. **Висновки:** Визначено оптимальний режим процесу осадження і розроблено принципову схему виробництва карбонату кальцію, якість якого відповідає сучасним вимогам щодо високої дисперсності, низької насипної густини і розвиненої питомої поверхні продукту.

Ключові карбонат кальцію, хімічне осадження, відходи содового виробництва

E.O. Mikhailova, V.O. Panasenko, N.B. Markova. Calcium carbonate synthesis with prescribed properties based on liquid waste of soda production. A promising direction in solving of environmental problems of soda industry is the development of low-waste resource-saving technologies, which consist in recycling of valuable waste components with obtaining the commercial products. **Aim:** The aim is to establish the optimal conditions for obtaining calcium carbonate with prescribed properties from liquid waste of soda production. **Materials and Methods:** Chemically deposited calcium carbonate is used as filler and should have certain physical and chemical properties. To obtain a product of prescribed quality the process of calcium carbonate deposition was performed of still waste liquid, that is the waste of calcium carbonate production and contain significant amount of calcium ions, and excessive production of the purified stock solution of sodium bicarbonate, which is composed of carbonate and hydrocarbonate ions. **Results:** The dependence of bulk density and specific surface area of calcium carbonate sediments and degree of deposition from such technological parameters are established: method of mixing the stock solutions, the concentration and molar ratio of reactants, temperature and reaction time. **Conclusions:** The optimal mode of deposition process is determined and the concept of production of calcium carbonate is developed. The quality of calcium carbonate meets the modern requirements of high dispersion, low bulk density and evolved specific surface of the product.

Keywords: calcium carbonate, chemical deposition, waste of sodium production.

Introduction. Soda production — one of the oldest in the world branches of chemical industry. In production, trade and in life under the name soda several products meet: ash soda — a waterless sodium carbonate Na_2CO_3 ; a purified sodium bicarbonate NaHCO_3 , often called as baking soda; caustic soda or sodium hydroxide NaOH ; crystal carbonate $\text{Na}_2\text{CO}_3 \cdot 10\text{H}_2\text{O}$ and $\text{Na}_2\text{CO}_3 \cdot \text{H}_2\text{O}$.

The soda ash which use is characterized by a wide range of modern industries in which technological process she plays the main role (Fig. 1) has the greatest value for economy. The leader in its use is the silicate industry. In chemical industry a significant amount of soda is spent in processes of water and brines purification, for synthesis of various salts, dyes, some mineral fertilizers. In metallurgy the sodium carbonate is applied to receive some nonferrous metals, for desulphurization of cast iron and enrichment of uranium ores. The soda ash plays a significant role for pulp-and-paper, petrochemical and coke-chemical branches. Besides, it is used in production of the purified sodium

DOI 10.15276/opu.2.49.2016.18

© 2016 The Authors. This is an open access article under the CC BY license (<http://creativecommons.org/licenses/by/4.0/>).

bicarbonate which, in turn, is used in food, rubber and medical industries, and also for production of the caustic soda, irreplaceable for purification of oil and metal sodium preparation [1].

From the moment of independence of Ukraine acquisition three soda plants worked in the territory: in Sloviansk (Donetsk region), Lysychansk (Luhansk region) and Krasnoperekopsk (Crimea). Feature of soda production is its high need for raw materials and large tonnage of waste. So, for production of one ton of soda ash the 1.5 t of table salt, 1.5 t of limestone, 1.7 t of conditional fuel are spent, and 8 t of waste are formed. Therefore, such positioning of the enterprises is explained by direct proximity to a source of raw materials, existence of the necessary territory for warehousing of waste, and also the convenient traffic intersection. In due time, the domestic manufacturers completely provided domestic market with necessary products of soda. Besides, domestic soda was one of the best and competitive in the European market and occupied about 2.5% of its volume.

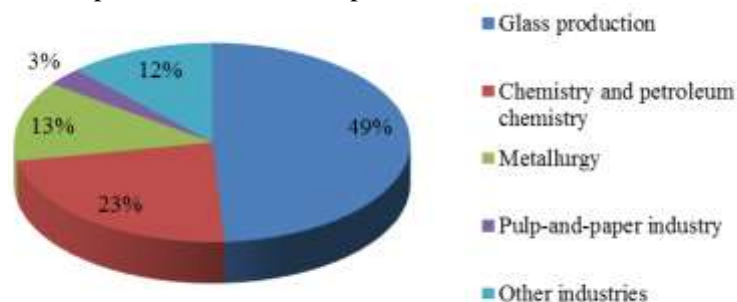


Fig. 1. Structure of soda ash consumption in Ukraine

Now need of Ukraine for soda ash is 300...350 thousand tons per year. On the place of the Sloviansk and Lysychansk enterprises there are only industrial platforms, and supply of soda from the Crimea to continental Ukraine became extremely unstable. Therefore, the domestic consumers who are using soda as raw materials are forced to import it from other countries.

In the emerged situation expedient and, the main thing, economically reasonable becomes creation in Ukraine of new production of soda ash. Dovgaliuk [2], the director of the state institute of NIOCHIM (Kharkiv), considers that the optimum place for placement of the soda enterprise is the platform of the former plant in Sloviansk. The reason of such choice consists in that unlike Lysychansk, necessary constructions have remained here — brine extraction facility, a chalk-pit and the sludge collector, that will allow to reduce costs of restoration of the plant.

Besides positive sides of revival of soda production in Ukraine, it is impossible to forget about ensuring ecological safety of this branch. In Ukraine, as well as in the majority of the countries of the world, soda ash is received by ammonia method Solvay which has a high level of the technological process organization and rather high economic efficiency. At the same time, shortcomings of this method are low extent of use of raw materials, high power consumption and existence of significant amount of waste in the form of liquid, solid and gaseous substances. If gas emissions contain components within maximum permissible norms, then they are released into atmosphere. At the same time, liquid and solid waste of production completely dumps in sludge collectors — “the white seas” which occupy more than 300...350 hectares of the land plots in regions of arrangement of the soda plants [1, 3].

Settlers-sludge collectors not only occupy considerable land areas, but also are sources of continuous impact on water objects and the soil. Slurry waters have high alkaline reaction of the environment (pH value is up to 12.0) and high mineralization due to the content of soluble ions (chlorides, sulfates, sodium, calcium, ammonium) that has high migratory ability. The arrangement of accumulators within settlements and in regions of large waterways worsens a sanitary and hygienic and ecological situation and threatens health of the population.

Processing of a wastage with receiving new products on its basis, which have wide application in the national economy, allows to reduce the amount of the wastage coming to the sludge collector and to lower anthropogenous load of soda production on the biosphere. Results of estimation of toxico-

logical impact of slimes and liquids of soda production on various test-objects (*Ceriodaphnia affinis*, *Paramecium caudatum*) received by Samutin [4] showed that this wastage refers to the IV class of hazard (are low-hazard for the environment) that is justification for the possible directions of their use.

Way of solution of ecological problems of soda enterprises are various and each of them deserves an attention and comprehensive study [5...8].

According to authors of article, the perspective direction of utilization of enterprises effluent for production of soda is obtaining a marketable product — chemically besieged calcium carbonate which finds wide application as an excipient for creation of various composites [9]. Production of chemically besieged calcium carbonate in Ukraine is also absent now.

The aim of the work is to establish the optimal conditions for obtaining calcium carbonate with prescribed properties from liquid waste of soda production.

Materials and Methods. As a part of almost all composites the excipients are widely used. They are various on chemical composition and origin natural and the synthetic materials and are entered into composition structures for reduction in cost or collimating of particular operational properties to them. One of the most widespread types of excipients is a fine-grained chalk (calcium carbonate). It finds application in production of dry structural blends, finishes, plasters, coating compositions, plastic, rubber, paper, cable production. Calcium carbonate is received in two ways:

- by refinement of breeds and sedimentary deposits (naturally occurring or natural calcium carbonate);
- by chemical deposition (chemically besieged calcium carbonate).

Particles of natural excipients, including with high level of micronization are, as a rule, significantly larger, than of the products obtained by deposition. They also concede on purity level, whiteness and content of the main substance that significantly limits the field of their application.

Obtaining of product by chemical deposition allows improving the quality of excipient (Table 1).

Table 1

The main rates of chemically besieged calcium carbonate quality

Rate	Value	
	1 st quality	2 nd quality
Whiteness, %, not less	93	No norm.
Containing, mas. %:		
— carbonates of Ca and Mg in terms of CaCO ₃ , not less	98.5	97
— the free alkali in terms of CaO, at most	0.03	0.05
— moisture, at most	0.5	1.5
— other impurities, at most	0.1	0.3
Bulk weight, g/cm ³ , at most	0.25	0.4
Specific surface area, m ² /g, not less	6...12	

Chemically besieged calcium carbonate is generally obtained by the “limy” way using calcium hydroxide suspension carbonization by gaseous carbonic oxide (IV) [10]. However, for a number of reasons, this method does not allow to obtain a product of necessary quality.

It is possible to receive calcium carbonate with necessary properties if to use the clear solutions containing well soluble salts of calcium as raw materials. From this point of view the technology of receiving besieged CaCO₃ based on wastage of the soda enterprises is of the considerable interest: the still waste liquid which is formed during the obtaining of soda ash, and also the excess mother solution obtained as a result of the cleared sodium bicarbonate manufacture process. These substances do not find further use in the next cycles and are pumped over in settlers stores.

The qualitative composition of a wastage according to production terms of the corresponding soda productions (Table 2) allows receiving a calcium carbonate deposit using the equations of reactions:

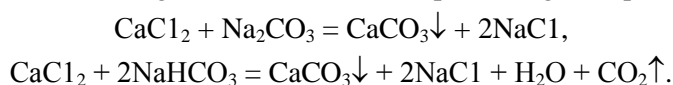


Table 2

Chemical composition of a wastage of soda production

The clarified still waste liquid			Excess mother solutions		
Composition	% mas.	g/dm ³	Composition	% mas.	g/dm ³
CaCl ₂	12.90	149.77	NaHCO ₃	12.95	145.25
NaCl	6.01	69.78	Na ₂ CO ₃	4.72	52.99
CaSO ₄	0.50	5.81	NaCl	0.47	5.26
MgCl ₂	0.21	2.44			
NH ₃	0.0034	0.040			

During an experiment the dependence of bulk weight and a specific surface area of depositions of calcium carbonate, and also its extent of sedimentation on the following technological parameters were studied by authors: way of mixture of initial solutions, concentration and molar ratio of reagents, temperature and time of reaction behavior.

The research of influence of the interfusing sequence of initial solutions was conducted by adding of the clarified still waste liquid to an excess mother solution (SWL→MS), dispensing of a mother solution to still waste liquid (MS→SWL) and at simultaneous interfusing of initial solutions (MS↓SWL↓).

Different concentration of CaCl₂, NaHCO₃, Na₂CO₃ substances in initial solutions it was created by their dilution at 1.25; 1.5; 1.75; 2; 2.25 times.

Dependence of the product quality on the molar charge ratio was established by creation of stoichiometric excess of one reagent concerning another. So, in the beginning, used the surplus of ions of Ca²⁺ equal to 1.2; 1.4; 1.6; 1.8; 2, and then — surplus of ions of HCO₃⁻ and CO₃²⁻.

Deposition of calcium carbonate was carried out in the range of temperatures from 70 to 90°C.

The lower temperature bound of process was chosen according to solubility polytherm in the Na₂CO₃ — NaHCO₃ — H₂O system, and also taking into account a possibility of future technology implementation of obtaining of chemically besieged calcium carbonate in the conditions of already existing productions of the corresponding soda products.

The analysed time of reaction behavior was from 1 to 10 minutes that corresponds to results of the state-of-the-art review of references.

For carrying out researches the experimental assembly (Fig. 2) was created. Deposition of CaCO₃ was carried out in the reactor-precipitant 3, where in the given temperature mode the initial solutions entering from tanks 1 and 2 mixed up at continuous hashing of a reaction mixture (Re=16000, 500 rpm). Dispensing of reagents was controlled using flowmeters 7. The obtained deposit was filtered by a vacuum filter 4 from a mother solution, in the same place was washed using hot distilled water from chlorine ions, and then dried up at a temperature of 105...110 °C in a drying chamber up to the constant weight. Further, the qualitative and quantitative analysis of obtained filtrate and deposition of calcium carbonate was carried out.

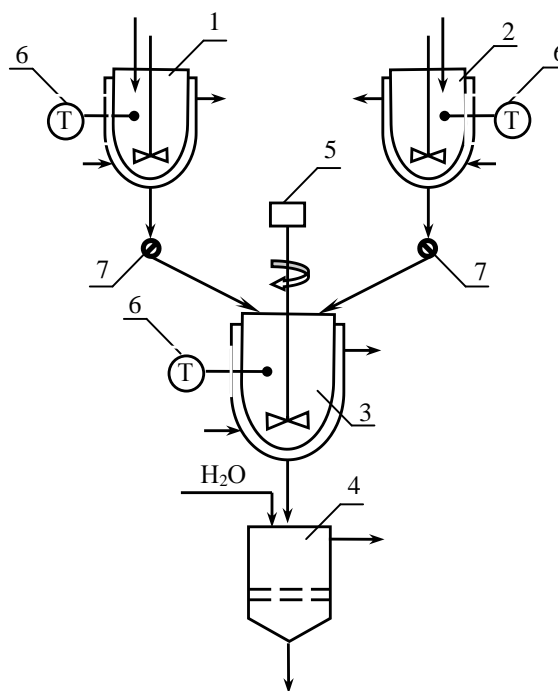


Fig. 2. Scheme of the experimental assembly: 1, 2 — temperature-controlled collections of initial solutions; 3 — temperature-controlled reactor-precipitant; 4 — vacuum filter; 5 — tachometer; 6 — mercurial thermometer; 7 — flowmeter

Results. The analysis of the experimental data of dependence of calcium carbonate properties on concentration of reagents showed that a dilution of initial solutions leads to receiving of CaCO_3 depositions with high bulk weight and undeveloped specific surface area. It is possible to reach increase in concentration of solutions by evaporation that demands the considerable energy cost. Therefore, the solution of use of initial solutions with concentration with which they are formed in the corresponding productions is optimum.

During researches it was established that the molar charge ratio slightly influences on quality of the received calcium carbonate. Besides, the amounts of an excess mother solution which are formed in production of the cleared sodium bicarbonate it is, much less, than it is necessary for complete utilization of the corresponding amounts of the clarified still waste liquid of soda ash production. Thus, it is possible to receive a product with necessary physical and chemical properties in the conditions of a stoichiometric relationship of initial reagents that will allow using more rationally the corresponding wastage as raw materials.

Researches results of bulk weight dependence of calcium carbonate from a way of mixture of initial solutions showed (Fig. 3) that for receiving of deposit with bulk weight at least 0.4 g/cm^3 , simultaneous adding of reagents to the reactor precipitant is the most acceptable. Other consequence of solutions interfusing leads to increase in bulk weight. Also it was established that in the conditions of elevated temperatures the calcium carbonate deposit with smaller value of bulk weight is formed. Increase in time of a precipitation process, on the contrary, promotes receiving a product with higher rate of bulk weight.

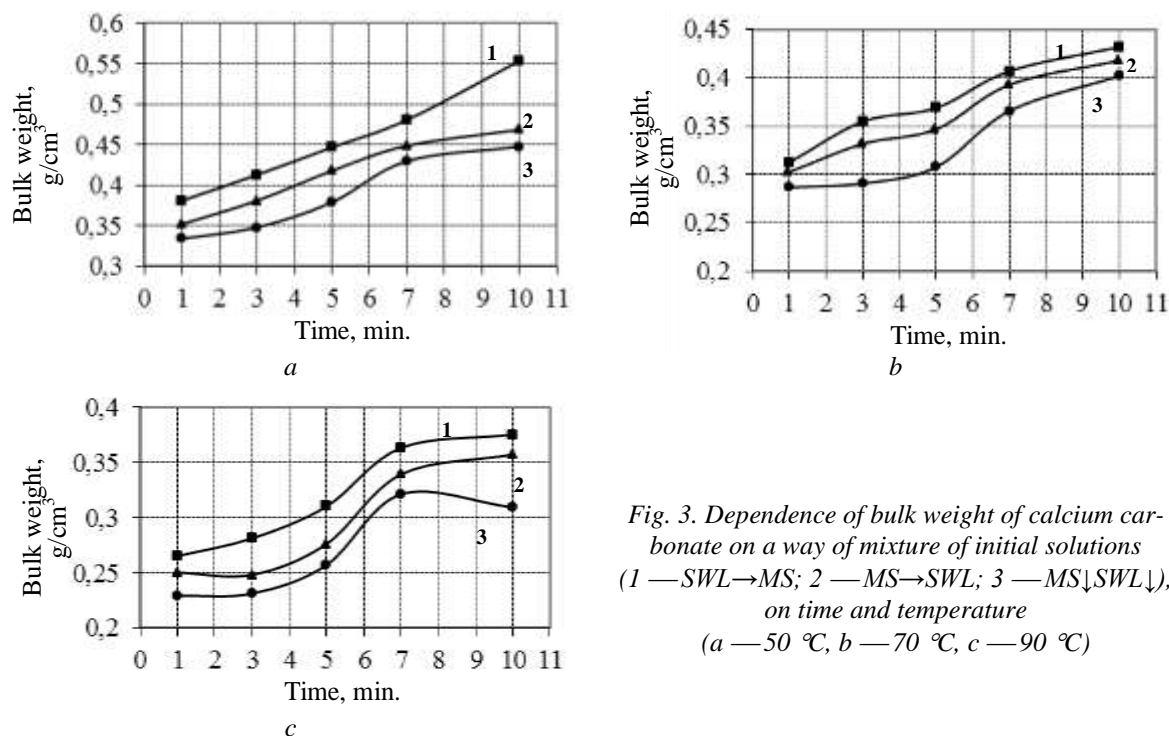


Fig. 3. Dependence of bulk weight of calcium carbonate on a way of mixture of initial solutions (1 — $\text{SWL} \rightarrow \text{MS}$; 2 — $\text{MS} \rightarrow \text{SWL}$; 3 — $\text{MS} \downarrow \text{SWL} \downarrow$), on time and temperature (a — $50 \text{ }^\circ\text{C}$, b — $70 \text{ }^\circ\text{C}$, c — $90 \text{ }^\circ\text{C}$)

Researches of temperature effect and time of precipitation process in the conditions of simultaneous interfusing of initial solutions on a specific surface area of exemplars of calcium carbonate showed the exacting nature of the obtained dependences (Fig. 4).

It can be explained with the fact that at the beginning of precipitation process a large number of shallow particles of calcium carbonate is formed that it leads increase of a specific surface area. And, the process temperature is higher, the quicker there is an achievement of the maximal value. By results of the experimental data it is possible to draw a conclusion that it is possible to obtain calcium carbonate with necessary value of specific surface area at any temperature, however time of precipitation process should

not exceed 5 minutes. It was established that in all area of the studied temperatures the functions of specific surface area curves have an extremum (point of a global maximum).

One of the key technological parameters influencing on effectiveness of raw materials use is extent of its sedimentation. The dependence of sedimentation extent of calcium ions on time and temperature of process at simultaneous mixture of still waste liquid with excess mother solution (Fig. 5) is established by authors during the experiment. Results of researches demonstrate increase in the given rate at increase of (behavior) process temperature that it is possible to explain with decrease of calcium carbonate solubility in these conditions. It is known that sodium chloride in which solution there is a sludging, increases solubility of calcium carbonate. However, according to the equation of "salt" effect it is established, that both in clear solvent (water), and in sodium chloride solution solubility of calcium carbonate decreases with increase of temperature.

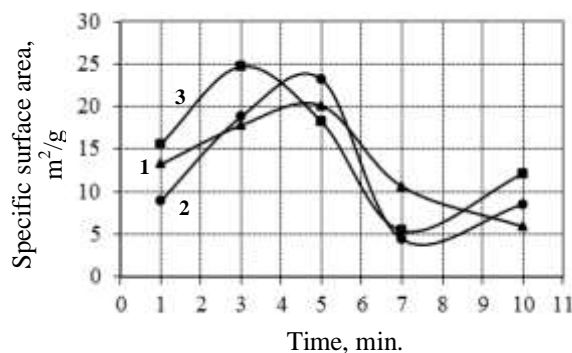


Fig. 4. Dependence of a specific surface area of calcium carbonate on time and temperature (1 — 50 °C, 2 — 70 °C, 3 — 90 °C)

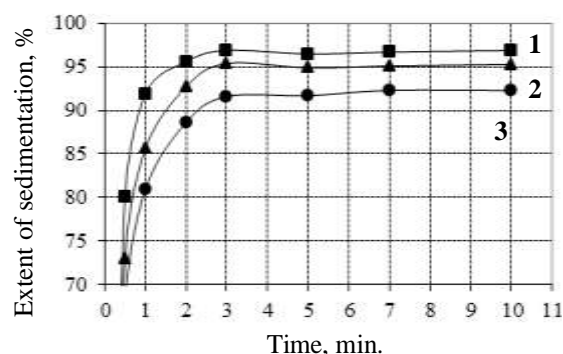


Fig. 5. Dependence of sedimentation extent of calcium carbonate on time and temperature (1 — 90 °C, 2 — 70 °C, 3 — 50 °C)

Conclusions. By results of the conducted researches the optimum process conditions of calcium carbonate deposition is defined. It is established that to receive the product meeting requirements to this excipient it is possible at simultaneous interfusing of the clarified still waste liquid and an excess mother solution in the conditions of a stoichiometric ratio of reactants at a temperature of 80...85 °C within no more than 3 minutes. In this case bulk weight of a product will make at least 0.24 g/cm³, its specific surface area — not less than 23 m²/g, and extent of sedimentation — not less than 96.5 %.

Authors also developed the concept scheme of chemically besieged calcium carbonate production which provides predefining of still waste liquid from solids, interfusing of initial solutions in the given technological mode, filtration and washing of the obtained deposit till complete removal of chlorine ions, and then drying, crushing, sieving and casing of a finished stock. The offered way gives the possibility to obtain no more than 5 thousand tons of synthetic calcium carbonate a year that it is not enough for requirements of domestic market of Ukraine. The outputs are limited to the actual number of the waste which is formed in production of the cleared sodium bicarbonate. To increase the efficiency of technology of Mikhaylova, etc. [11] it was offered to use solution of soda ash as precipitant instead of mother solutions or along with them.

Thus, the offered way of receiving chemically besieged calcium carbonate based on effluent of soda production promotes not only utilization of valuable components of this waste and decrease of dumping of highly mineralized solutions into sludge collectors, but also receiving the qualitative product which have found wide application in various industries which consumption steadily increases over the last few years.

Література

1. Ткач, Г.А. Производство соды по малоотходной технологии: монография / Г.А. Ткач, В.П. Шаповров, В.М. Титов. — Харьков: ХГПУ, 1998. — 429 с.

2. Украина будет с содой [Электронный ресурс] / И. Довгалюк // Государственное учреждение Государственный научно-исследовательский и проектный институт основной химии. — 2016. — Режим доступа: <http://niochim.kharkov.ua/?q=ru/news/ukraine-budet-s-sodoi> (Дата звернення: 15.03.2016).
3. Steinhäuser, G. Cleaner production in the Solvay Process: general strategies and recent developments / G. Steinhäuser // *Journal of Cleaner Production*. — 2008. — Vol. 16, Issue 7. — PP. 833–841.
4. Санитарно-гигиеническая оценка отходов содового производства / Н.М. Самутин, Я.И. Вайсман, Л.В. Рудакова [и др.] // *Гигиена и санитария*. — 2013. — № 2. — С. 30–33.
5. Манойло, Е.В. Применение отходов содового производства / Е.В. Манойло, Ю.А. Манойло, В.Ф. Моисеев // *Восточно-Европейский журнал передовых технологий*. — 2010. — № 6/6 (48). — С. 13–17.
6. Gur, N. Utilization of soda ash plant solid wastes in manufacture of cement / N. Gur, Y. Aktas, E. Oztekin // *Elixir Cement and Concrete Composites*. — 2012. — Vol. 47. — PP. 8866–8873.
7. Магеря, Я.О. Применение выпарных аппаратов при получении хлорида кальция из отходов содового производства / Я.О. Магеря, В.П. Михайличенко, С.А. Гринь // *Восточно-Европейский журнал передовых технологий*. — 2013. — № 1/6 (61). — С. 10–13.
8. Utilization of distiller waste from ammonia-soda processing / T. Kasikowski, R. Buczkowski, B. Dejewski, *et al.* // *Journal of Cleaner Production*. — 2004. — Vol. 12, Issue 7. — PP. 759–769.
9. Białowicz, K. Precipitation of calcium carbonate in the presence of urea at 293 K and 343 K / K. Białowicz, U. Kielkowska // *Polish Journal of Chemical Technology*. — 2014. — Vol. 16, Issue 2. — PP. 95–98. DOI:10.2478/pjct-2014-0037
10. Курта, С.А. Наповнювачі – синтез, властивості та використання / С.А. Курта. — Івано-Франківськ: Прикарпат. нац. ун-т ім. Василя Стефаника, 2012. — 295 с.
11. Спосіб утилізації рідинних відходів виробництва кальцинованої соди / Є.О. Михайлова, Н.Б. Маркова, І.В. Багрова [та ін.] // *Збірник наукових праць ДУ «НІОХІМ»: Хімія і технологія виробництв основної хімічної промисловості*. — 2013. — Т. 77. — С. 76–81.

References

1. Tkach, G.A., Shaporev, V.P., & Titov, V.M. (1998). *Production of Sodium Carbonate by a Low-Waste Technology*. Kharkiv: H.S. Skovoroda Kharkiv National Pedagogical University.
2. Dovgaliuk, I. (2016). Ukraine will be with Soda. *State Research and Design Institute of Basic Chemistry*. Retrieved from <http://niochim.kharkov.ua/?q=en/news/ukraine-will-be-soda>
3. Steinhäuser, G. (2008). Cleaner production in the Solvay Process: general strategies and recent developments. *Journal of Cleaner Production*, 16(7), 833–841. DOI:10.1016/j.jclepro.2007.04.005
4. Samutin, N.M., Vaisman, Ya.I., Rudakova, L.V., Kalinina, E.V., Glushankova, I.S., & Batrakova, G.M. (2013). Sanitary and hygienic assessment of waste of soda production, *Hygiene and Sanitation*, 2, 30–33.
5. Manoilo, E., Manoilo, Yu., & Moiseev, V. (2010). Application of wastes of soda production. *Eastern-European Journal of Enterprise Technologies*, 6(6), 13–17.
6. Gur, N., Aktas, Y., & Oztekin, E. (2012). Utilization of soda ash plant solid wastes in manufacture of cement. *Elixir Cement and Concrete Composites*, 47, 8866–8873.
7. Magerya, Y., Mihaylichenko, V., & Grin, S. (2013). Application of evaporator getting the calcium chloride from waste soda production. *Eastern-European Journal of Enterprise Technologies*, 1(6), 10–13.
8. Kasikowski, T., Buczkowski, R., Dejewski, B., Peszyńska-Białczyk, K., Lemanowska, E., & Igliński, B. (2004). Utilization of distiller waste from ammonia-soda processing. *Journal of Cleaner Production*, 12(7), 759–769. DOI:10.1016/S0959-6526(03)00120-3
9. Białowicz, K., & Kielkowska, U. (2014). Precipitation of calcium carbonate in the presence of urea at 293 K and 343 K. *Polish Journal of Chemical Technology*, 16(2), 95–98. DOI:10.2478/pjct-2014-0037
10. Kurta, S.A. (2012). *Fillers – Synthesis, Properties, and Application*. Ivano-Frankivsk: Vasyl Stefanyk Precarpathian National University.
11. Mikhailova, E.O., Markova, N.B., Bagrova, I.V., Gavrish, Y.G., & Panasenکو, V.A. (2013). A method of utilization of soda ash plant effluent. *NIOCHIM Collected Works*, 77, 76–81.

Received May 24, 2016

Accepted July 17, 2016